NMR Spectroscopic Exploration of Tin-Catalysed Biomass Conversion

Elliot, Samuel Gilbert

Publication date:
2019

Document Version
Publisher's PDF, also known as Version of record

NMR Spectroscopic Exploration of Tin-Catalysed Biomass Conversion

Ph.D. Thesis 2019

Samuel Gilbert Elliot

supervised by
Prof. Robert Madsen
Dr. Sebastian Meier

"The Stone Age did not end for lack of stone, and the Oil Age will end long before the world runs out of oil."

Sheikh Ahmed Zaki Yamani, Saudi Arabian Oil Minister (1962-1986)

Preface

This dissertation summarises work from my PhD project which was performed at the Technical University of Denmark (DTU) from May 2016 to April 2019. The dissertation was completed as part of the Cat2BioChem project, a collaborative project between DTU, and the companies Haldor Topsøe and Perstorp, which was funded by the Innovation Fund Denmark (case number 5150-00023B). The work in this thesis was performed primarily at the Department of Chemistry (DTU), partly at the New Business R&D department at Haldor Topsøe and during a one month research stay at the Innovation department of Perstorp. My PhD project was initially supervised by Assoc. Prof. Peter Fristrup, who transferred to the private sector to seek new challenges. My project was subsequently supervised by Prof. Robert Madsen. The project was co-supervised throughout by Senior Research Scientist Sebastian Meier.

This thesis is divided into 11 Chapters. The first three chapters provide the background and motivation for this project. The first chapter introduces petrochemicals, the motivation for transitioning towards biobased chemicals and which chemicals to target. In the second chapter, the Sn-Beta catalysed conversion of carbohydrates to α-hydroxy esters is introduced, leading to the aim and outline of the project in chapter 3. Chapter 4 details the experimental methods used in this thesis. Chapters 5 to 10 present the main results produced in the course of this PhD project. Chapter 5 focusses on identification of reaction products. Chapter 6 regards development of quantitative NMR methods, which are employed in Chapters 7-10. In Chapter 7, general operational conditions are optimised with focus on production of double dehydration products (DPM and THM). Further optimisation is performed in Chapter 8, with focus on addition of alkali salts; the correlation between alkali anion and selectivity as well as alkali concentration, catalyst active site and selectivity are examined. Chapter 9 explores the reaction mechanisms of newly identified products through the use of isotopically labelled carbohydrates. In Chapter 10, applications of DPM and MVG are touched upon with focus on polymer applications. Finally, in Chapter 11 an overall conclusion on project and results is given.

Unless otherwise stated, the work presented in chapters 5 to 10 was performed by me and is largely based on my published articles, which have been reproduced in the appendix for the convenience of the reader.

Acknowledgements

I would like to start by thanking my former supervisor Peter Fristrup for hiring me for this position, and to Robert Madsen for taking over as my supervisor when Peter left. A very special thanks goes to Sebastian Meier, I have learnt a lot from your NMR expertise, but even more so his enthusiasm, engagement, honest interest and humour, along with a constant focus on my well-being, has been truly priceless for me during the past three years.

Thank you to my two co-PhD students in the Cat2BioChem project, Irene Tosi and Bo Jessen, who have accompanied me on this long journey. The constant collaboration in different aspects of this project has been highly beneficial.

I would like to express my great appreciation to our two industry collaborators, for adding a perspective to this project that goes far beyond the laboratory. The "real life" perspective has been and is a great motivator for me. I wish to acknowledge Stefan, Oleg, Pia and the rest of the Perstorp team, it was a fantastic experience visiting you in Sweden, and I am very thankful for how well you took care of us. To my colleagues at Haldor Topsøe, my second workplace, thank you for making me feel like part of your team, I have enjoyed every Wednesday morning breakfast with you over the years. In particular I would like to express my gratitude to Esben Taarning, Søren Tolborg, Irantzu Sádaba and Juan Martinez for taking the time to provide sparring and advice, your assistance has been invaluable in producing high quality research.

To the former members of the Fristrup group and in particular Rita, Daniel, Mathias, Allan and Lasse, sharing an office and a lab with you was both entertaining and enlightening. Also to my other colleges at DTU and the members of Robert Madsens group, your friendship and company has been and is greatly appreciated.

Finally I wish convey my sincerest thanks to all my Friends and Family, that have stood by me throughout the years. Thanks you to my good friends Kasper, Andreas, Thomas, Nina and Claes for your support and friendship, and for taking the initiative to see me when I have been too preoccupied to do it. I wish to express my greatest appreciation and deepest thanks to my girlfriend Thea, for the constant loving, supportive and overbearing companionship, through all the ups and downs over the past three years and particularly during stress and challenges of the past half year.

Abstract

In the pursuit to replace fossil resources with more sustainable alternatives, the chemocatalytic conversion of carbohydrates provides an important method for producing new functional chemicals. This PhD project focussed on the use of a Sn-Beta zeolite catalyst for the conversion of glucose, xylose and glycolaldehyde in methanol, to form α-hydroxy esters, such as methyl lactate and methyl vinyl glycolate (MVG), with interesting potential for applications as building blocks for polymer production.

The studies primarily used NMR spectroscopy to reveal previously unexamined chemical details. Several previously unreported products were identified in the conversion of xylose, glucose and glycolaldehyde, respectively, leading to vast improvements in carbon balances, which aided in the understanding of the reaction process. Two new key products that were identified are methyl 2,5-dihydroxy-3-pentenoate (DPM) and methyl 2,4,5-trihydroxy-3-pentanoate (THM). These products possess multiple different functional groups, making them extremely versatile for upgrading of the monomer or functionalisation of polymers.

NMR methods suitable for quantification of these products in complex mixtures without prior purification were developed. These methods included the adaptation of protocols used in biocatalysis for compound identification, and the development of methods for reducing analysis time of chemocatalytic product mixtures to 5 min, even for highly accurate quantifications of minor by-products.

The effects of different reaction conditions were assessed to optimise the formation of new chemicals from abundant pentoses and hexose, respectively. Tested parameters included substrate stereochemistry, reaction concentration, catalyst to substrate ratios, catalyst metal and framework, temperature and solvent. The highest yields were obtained with 8.3-23 wt% substrate and a 1:2 catalyst to substrate ratio at 160 °C in ethanol. Under these conditions, THM and DPM yields of up to 19.4% and 42% were obtained, respectively.

The presence of alkali metal salt has been known to modify Sn-Beta reaction selectivity. Here, the influence of alkali salts was assessed to obtain more detailed understanding of their effect on the reaction. Alkali salts were observed to facilitate retro-aldol reactions and to suppress other pathways including dehydration. The trends for product yields correlated with initial rate trends, indicating that reaction selectivity is under kinetic control. It was further demonstrated that the effect is proportional to the alkali salt to tin active site ratio, and that trends can be correlated to a double dissociation model. This model indicates that the catalyst may be modified between three states with either no, one or two alkali substituted. Alkali was observed to have equivalent effects on epimerisation by 1,2-carbon shift and retro-aldol cleavage, supporting that the presence of alkali salts reduces the energy barrier for carbon-carbon bond cleavage.

Focus on mechanistic pathways and the transition of substrates through the catalytic system were studied further by using both ^{2}H and ^{13}C isotopically labelled carbohydrate substrates. From these experiments, it was deduced that incorporation of hydrogen by

tautomerisation occurs stereoselectively. Furthermore, competition between tautomerisation and dehydration is determining for selectivity between single and double dehydration products. In addition, reactions are occurring in a reaction cascade with minimal release of intermediates. Finally, Sn-Beta was shown to catalyse a 5,1-hydride shift in pentoses.

In the final part of the PhD project, application properties of xylose derived DPM and glycolaldehyde derived MVG were assessed. DPM was successfully tested in polyesterification reactions, forming a copolymer with ethyl 6-hydroxy-hexanoate. The unused functionality from DPM in the copolymer could also be modified. Meanwhile, having already shown that MVG could be polymerised, MVG was tested for storage stability and further applications in polymer blends. During storage, MVG underwent slow oxidation, which could be slightly hindered by cold storage. Preliminary tests in polymer blends showed interesting opportunities for modifying blend properties, which require further examination.

Overall, this project has provided more detail on the Sn-Beta catalysed conversion of carbohydrates through examination of detailed product distributions and atomic tracking. Currently, MVG and DPM are of greatest interest due superior product yields compared to other observed products, and due to multiple functionality providing high versatility for future applications.

Resumé

I jagten på at erstatte fossile ressourcer med bæredygtige alternativer udgør den kemokatalytiske omdannelse af kulhydrat en vigtig metode til fremstilling af nye funktionelle kemikalier. Dette ph.d. projekt fokuserer på brug af en Sn-Beta zeolit katalysator til omdannelse af glukose, xylose og glykolaldehyd til en række α-hydroxy estere, såsom methyl laktat og methyl vinyl glykolat (MVG), med potentiale for anvendelse som byggesten til produktion af polymere.

Studiet har primært anvendt NMR spektroskopi til at afsløre hidtil uudforskede kemiske detaljer. Adskillige hidtil urapporterede produkter er blevet identificeret fra omdannelsen af glukose, xylose og glykolaldehyd. Dette har resulteret i markante forbedringer til karbonbalancer, som forbedrer forståelsen af reaktionsprocessen. To nøgleprodukter er blevet identificeret, hhv. methyl 2,5-dihydroxy-3-pentenoat (DPM) og methyl 2,4,5-trihydroxy-3-pentanoat (THM). Disse to produkter indeholder adskillige funktionelle grupper, hvilket gør dem aldeles alsidige for modificering som monomere eller funktionalisering som polymere.

NMR-metoder, til kvantificering af ovenstående produkter direkte fra komplekse reaktionsblandinger uden forudgående oprensning, er blevet udviklet. Disse metoder indbefatter tilpasning af protokoller anvendt til produktidentifikation i biokatalyse samt en reducering af analysetiden for kemokatalytiske produktblandinger til 5 minutter selv for meget nøjagtig kvantificering af mindre biprodukter.

Virkningen af forskellige reaktionsparametre er blevet undersøgt for at optimere dannelsen af nye kemikalier fra hyppigt forekommende pentoser og hexoser. De testede parametre inkluderer substratstereokemi, reaktionskoncentration, katalysator til substratforhold, katalysatormetal og -struktur, temperatur og opløsningsmiddel. De højeste udbytter blev opnået med 8,3-23 wt% substrat og et katalysator til substratforhold på 1:2 ved 160 °C i ethanol. Under disse betingelser opnåedes udbytter på op til 19,4% og 42% af hhv. THM og DPM.

Alkalisalte er kendt for at modificere reaktionsselektiviteten af Sn-Beta. I denne undersøgelse blev indflydelsen af alkalisalte vurderet for at opnå en mere detaljeret forståelse af deres påvirkning på reaktionen. Det blev observeret, at alkalisalte fremmer retro-aldol reaktioner, samtidigt med at de undertrykker andre reaktionsveje herunder dehydrering til DPM/THM. Endvidere blev en korrelation mellem tendenserne for produktudbytter og reaktionshastigheder observeret, hvilket indikerer, at reaktionsselektiviteten er under kinetisk kontrol. Ligeledes blev det demonstreret, at de observerede effekter var proportionale til forholdet imellem alkalisalt og tin *active sites* samt, at tendenserne kan korreleres til en dobbelt dissociationsmodel. Modellen antyder, at katalysatoren kan skifte imellem tre tilstande; enten med ingen, en eller to alkali per tin *active site*. Alkalisaltene udviste ækvivalente effekter på epimerisering ved et 1,2-karbonskift og på retro-aldolkløvning. Dette underbygger teorien om, at alkalisalte er med til at reducere energibarrieren for kløvning af karbon-karbonbindinger.

De reaktionsmekanistiske veje og omdannelse af substrater igennem det katalytiske

system er blevet studeret nærmere ved anvendelse af både ^{2}H og ^{13}C isotop-mærkede kulhydrater. Disse eksperimenter viste, at inkorporering af hydrogen ved tautomerisering sker stereoselektivt, samt at konkurrencen imellem tautomerisering og dehydrering er afgørende for at bestemme selektivitet mellem enkelt- og dobbeltdehydreringsprodukter. Alle reaktioner forløber i en kaskade med minimal frigivelse af mellemprodukter.

I den sidste del af ph.d. projektet blev anvendelsesegenskaberne af DPM, som er produceret fra xylose, og MVG, som er produceret fra glykolaldehyd, vurderet. DPM blev med succes polymeriseret med ethyl 6-hydroxy-hexanoat ved polyesterificering. De ubrugte funktionelle grupper fra DPM i polymeren kunne efterfølgende modificeres og derved ændre polymerens egenskaber. I mellemtiden blev MVGs, der tidligere har vist sig at kunne polymeriseres, opbevaringsstabilitet og dens brug i polymerblandinger testet. Under opbevaring undergår MVG langsomt oxidering, hvilket kan bremses til en hvis grad ved at opbevare prøven koldt. Foreløbig afprøvning af MVG i polymerblandinger viser interessante muligheder for at påvirke blandingens egenskaber, hvilket kræver yderligere undersøgelse.

Samlet set har dette projekt bidraget med yderligere detaljer om Sn-Beta katalyseret omdannelse af kulhydrater igennem undersøgelse af produktfordelinger og sporing af atomer. På grund af opnåelse af højere udbytter end andre observerede produkter og adskillig funktionalitet, der gør dem særdeles alsidige, er MVG og DPM foreløbigt de mest interessante produkter i disse reaktioner.

List of Abbreviations

1D-NMR	One dimensional NMR
2D-NMR	Two dimensional NMR
3DG	3-deoxy glucosone
3DX	3-deoxy xylosone
B.P.	Boiling point
Beta	Beta polymorph structure zeolite structure
CAL-B	Candida Antarctica Lipase B
COSY	Correlation spectroscopy
DFT	Density function theory
DHL	3-deoxy-hexono-γ-lactone
DHM	3-deoxy-hexonic acid methyl ester
DMPM	2,5-dihydroxy-4-methoxy-pentanoic acid methyl ester
DMSO	Dimethylsulphoxide
$DMSO_2$	Dimethylsulphone
DPA	2,5-dihydroxy-3-pentenoic acid
DPE	Ethyl 2,5-dihydroxy-3-pentenoate
DPM	Methyl 2,5-dihydroxy-3-pentenoate
DPL	3-deoxy-pentono-γ-lactone
E6-HH	Ethyl 6-hydroxy-hexanoate
ECC	3,4-epoxycyclohexylmethyl 3',4'-epoxycyclohexane-carboxylate
epoxy-MVG	Methyl 2-hydroxy-3,4-epoxy-butanoate
ERY	Erythrulose
F	Furfural
FA-DMA	Formaldehyde dimethyl acetal
FDA	Food drug administration (USA)
F-DMA	Furfural dimethyl acetal
FT-IR	Fourier-transform infrared spectroscopy
GA	Glycolaldehyde
GA-DMA	Glycolaldehyde dimethyl acetal
GA-HA	Glycolaldehyde hemi-acetal
GC-FID	Gas chromatography – flame ionization detection
GC-MS	Gas chromatography – mass spectrometry
H2BC	Heteronuclear 2 bond correlation
HBL	2-hydroxy butyro-γ-lactone
HDDA	1,6-hexandiol diacrylate
HDO-VG	1,6-hexandiol di(2-vinyl-glycolate)
HMBC	Heteronuclear multiple bond correlation
HMF	5-(hydroxymethyl)furfural
HMF-DMA	5-(hydroxymethyl)furfural dimethylacetal
HPLC	High performance liquid chromatography
HSQC	Heteronuclear single quantum coherence
HT	Hydrothermal synthesis
IS	Internal standard
LA	Lactic acid
MAS-NMR	Magic-angle spinning solid-state NMR spectroscopy
MCM-41	Mobil Composition of Matter No. 41 framework
MDHB	Methyl 2,3-dihydroxy butanoate
Me	Methyl
MF	Methyl formate
MFI	Zeolite Socony Mobil–5 (ZSM-5) zeolite framework

MGA-DMA	2-methyoxy glycolaldehyde dimethyl acetal
MHHB	Methyl 2,4-dihydroxy butanoate
MHIB	Methyl 2-hydroxy isobutanoate
ML	Methyl lactate
MLA	Methyl levulinate
MMF	5-(methoxymethyl)furfural
MMF-DMA	5-(methoxymethyl)furfural dimethylacetal
MMHB	Methyl 4-methoxy-2-hydroxy-butyrate
MMVG	3-methoxy MVG (methyl 2-hydroxy-3-methylbut-3-enoate)
MPVO	Meerwein-Ponndorf-Verley-Oppenauer
MVG	Methyl vinyl glycolate
MVG-sat	Methyl 2-hydroxy butanoate
NMR	Nucelar magnetic resonance (spectroscopy)
OxoB-HA	Methyl 2-oxobutanoate hemi-acetal
PE	Polyethylene
PET	Polyethylene terephthalate
PLA	Poly(lactic acid)/polylactide
PT	Post-treatment synthesis
PTFE	Polytetrafluorethylen
PUR	Polyurethane
PVA	Polyvinyl acetate
qNMR	Quantitative NMR
RT	Room temperature
Sn-Beta	Tin zeotype of beta polymorph structure
TFAA	Triflouroacetic anhydride
THA	2,4,5-trihydroxy-3-pentanoic acid
THE	Ethyl 2,4,5-trihydroxy-3-pentanoate
THM	Methyl 2,4,5-trihydroxy-3-pentanoate
THO	Threose
TMPO	Trimethylolpropane oxetane
TOCSY	Total correlation spectroscopy
TPD	Temperature Programmed Desorption
TPM	Methyl 2,4,5-trihydroxy pentenoate
UL	Uniformly labelled
UV	Ultra violet
VGA	Vinyl glycolic acid
XRD	X-ray diffraction

Contents

Appendix

Part I

Introduction

1 Transitioning from Petrochemicals to Biochemicals

The introduction is divided into two chapters. The goal of the first chapter is to narrow down the replacement of fossil resources to a specific area that may be constructively targeted and developed towards commercial implementation of a specific chemical product. This section encompasses the motivations for transition away from from fossil resources (Section 1.1), and how the petrochemical industry provides an ideal area for implementation of biomass (Section 1.2 and 1.3), as well as an introduction to plastic (Section 1.4), and issues leading to a market opening for new biobased plastics (Section 1.4.1 and 1.4.2). These sections lead to discussion of the α-hydroxy acid lactic acid as a versatile target with many opportunities (Section 1.5), which will be detailed further in Chapter 2.

1.1 Fossil Resources

There are three main driving forces leading to the development of alternatives to use of fossil resources: environmental, economical and political drivers.

Environmental sustainability is one of the main reasons for transition away from fossil resources. The world is generally viewed as a closed ecological cycle that slowly changes over time. This allows plants and animals to evolve and adapt to their environments, a process that occurs over several generations, and allows a form of balance to be maintained. When a large outside force, namely us humans, impose large changes over short time it causes a problem as there is insufficient time for the ecosystem to adapt.

As shown in figure 1.1, there has been a large overall increase in the emission of CO_2 over the past 70 years.[1] This increase has largely been attributed to the combustion of fossil resources, which takes large underground carbon deposits and reintroduces them into

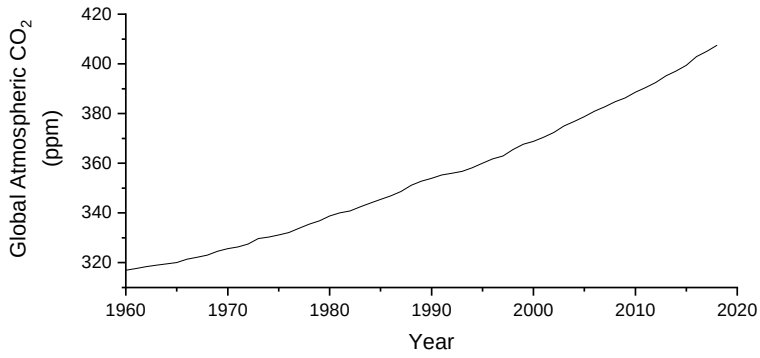

Figure 1.1: Global annual atmospheric CO_2 levels from 1960 to 2015.[1]

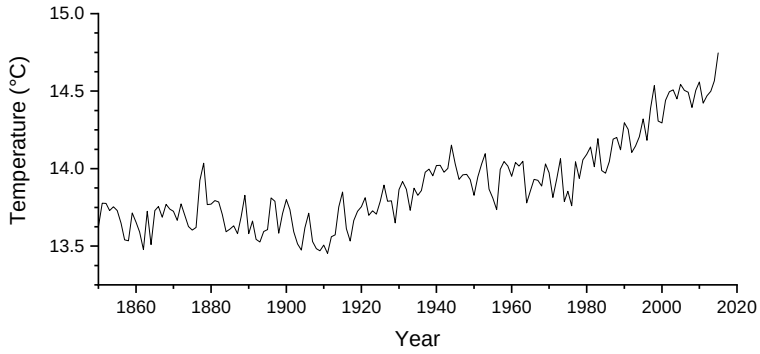

Figure 1.2: Global annual temperatures from 1850 to 2015.[2]

the atmosphere.[3] CO_2 is a greenhouse gas, and the increased levels have been correlated to increasing global temperatures (figure 1.2). The current increase in temperature already exhibits clear ecological consequences.[4] For this reason, political initiatives have been accelerating the development of replacement technologies for fossil resources.

The second is an economical driver. Fossil resources are considered a finite resource, therefore, when the consumption exceeds rate of production, as is the current case, stockpiles will inevitably run out. Naturally, this is not expected to happen suddenly and stockpiles are unlikely to deplete completely. Instead, the production is expected to peak and then decline, a concept referred to as peak oil.[5] The peak oil trend describes the effect of dwindling resource stockpiles on the consumption rate. Dwindling stockpiles result in oil becoming progressively more difficult and thereby more expensive to acquire, leading to increasing oil prices. An increase in price opens the market for increased competition, and with increased competition some stockpiles will become unprofitable to extract. Providing that these alternatives are sustainable, the fossil resources will inevitably become unprofitable.

The final is a political driver. The taxation of fossil based resources and emissions from industry provides an additional politically created economic driver based on environmental factors. In addition oil deposits are not evenly distributed geographically. With a global infrastructure that is highly reliant on fossil resources, this places countries with large production of fossil resources at a political advantage. An example of this was the oil crisis of 1973, where the Organization of Arab Petroleum Exporting Countries (OPEC) placed an oil embargo, as a political force of hand. As a result oil prices quadrupled in only one year, giving a wakeup call to all nations reliant on international oil supplies.[6,7]

In summary, transitioning from fossil resources to renewable resources would provide alleviation of negative environmental effects, higher infrastructure stability and a future secure economical investment.

1.2 Changing from Petrochemicals to Biochemicals

Fossil resources are characterised as complex mixtures of hydrocarbons. These hydrocarbons possess a large amount of stored chemical energy and are therefore well suited as

fuels or for energy production. In the US the total annual crude oil consumption is approximately one billion metric tons, with the majority of this oil being used for the production of fuel and energy (~85%).[8–10] Meanwhile, up to 10% of oil is used for the production of chemicals. These distributions are considered roughly equivalent to estimated global values.[9,11]

The key element of oil is the carbon backbone and the only readily available renewable source of carbon is biomass. Biomass generally contains a higher amount of oxygen per carbon than oil, resulting in oil containing approximately twice as much carbon per mass. Therefore, for biomass to be able to replace the entire US oil industry, the production of biomass for non-food purposes would need to reach approximately 2 billion tons per year. In comparison, the annual production of biomass for non food purposes (biofuel, heat, electricity) is currently approximately 190 million tons, just 10% of the required amount. The production may be up-scaled and according to the US department of energy, the maximum sustainable production of biomass is projected to be at least 1.2 billion tons.[8] Thus the maximum predicted substitution potential for oil with biomass is only 60%.

Based on these projections it is not possible to replace the entire petroleum industry by biomass. However, the energy and transportation sectors can draw from alternatives that are not related to chemical production, such as wind, solar, geothermal and nuclear power. As a result, if biomass resources are solely targeted towards the replacement of oil consumed by the petrochemical industry, where the carbon source is a necessity, only 200 million tons of biomass would be required, which is already within the biomass production capacity. Despite the small segment size, chemical production accounts for almost 50% of the income generated from crude oil,[12] providing a high value added business case for biomass, with more economical flexibility than the fuels and energy sector.

In summary, the chemical industry provides a high-value added market, where biomass may be used on a sustainable scale.

1.3 Targeting Chemicals from Biomass

When seeking to replace oil with biomass for chemical production, the difference in chemical composition is important, as the initial chemical composition dictates the amount of modification required to obtain the desired target chemical. The greatest difference between oil and biomass is in the degree of oxidation. The degree of oxidation may be expressed by the H/C ratio (Equation 1.1), which ranges from 4 for methane to -4 for carbon dioxide.

$$H/C = \frac{n(H) - 2n(O)}{n(C)} \tag{1.1}$$

Within biomass, carbohydrates form the most abundant product group. An estimated 75-95% of the annual renewable biomass produced is in the form of carbohydrates, making carbohydrates the worlds most abundant renewable chemical feedstock.[13,14] As a result, carbohydrates are a key chemical feedstock for substitution of oil in the future.

Carbohydrates have a H/C value of 0 forming an ideal position to access several chemicals in a mid range of oxidation states (figure 1.3). In comparison, crude oil has a H/C ratio of around 2 a relatively low oxidation state.[8] The presence of oxygen, which is a

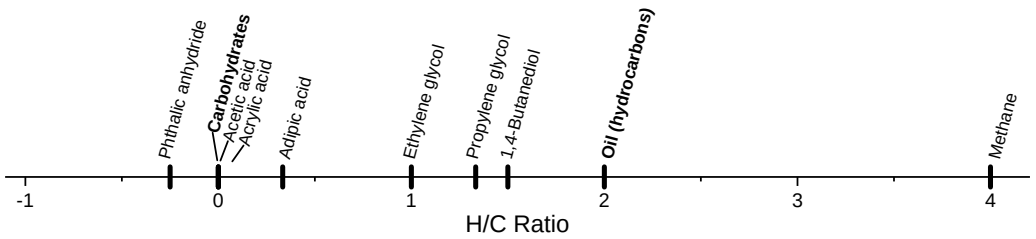

Figure 1.3: H/C ratios of target chemicals commonly produced from petrochemical platform molecules.

disadvantage for energy utilisation, gives carbohydrates their high inherent functionality and multiple handles that may be exploited for the production of diverse multifunctional chemicals. Figure 1.3 shows that compounds such as acids, currently produced from oil, are closer to carbohydrates in oxidation state and therefore have the potential to be produced with a higher atom efficiency than from oil. These compounds provide key opportunities to develop competitive carbohydrate-based synthesis routes, in a so called drop-in strategy.

Many of these compounds are used in plastic formulations, entitling a closer look at the plastic industry: acrylic acid is used for production of polyacrylates,[15] phthalic anhydride is used as a plasticiser, and in polyester and alkyd resins,[16] acetic acid is mainly used for production of vinyl acetate, the monomer of polyvinyl acetate (PVA),[17,18] and adipic acid is a precursor for nylon.[19]

1.4 Plastic

The use of plastic has facilitated the advancement and development of societies across the globe during the past century. Plastics provide versatile materials which are cost-effective, require little energy to produce and are lightweight and biocompatible.[20,21] The majority of plastic is currently produced from oil, constituting around 50% of the resources consumed by the petrochemical industry, and amounting to roughly 6% of the world oil production (4% of oil and natural gas).[21,22]

Besides the concerns regarding use of fossil resources covered in Section 1.1, there are also growing concerns regarding end-of-life handling of plastic.[23] Approximately 50% of plastic is used in single-use applications such as packaging, resulting in a large amount of waste generation.[21] As most of these types of plastic are not biodegradable,[24] proper disposal using recycling, incineration or landfills is vital to avoid environmental and ecological consequences.[20,21,25]

1.4.1 Plastic Pollution of Oceans

The first reports of plastic pollution in scientific literature appeared in the 1970s and since then the issue has only escilated. In 2010, 4.8 to 12.7 million metric tons of plastic were estimated to have entered the ocean (1.7-4.6% of the total plastic waste).[23] Considering

that the majority of these plastics require decades if not centuries or millennia to degrade, the accumulation of plastic debris in the ocean is of critical concern.

Larger plastic waste (or fragments thereof) are a suffocation risk to animals, either by strangulation or swallowing. Entanglement can also result in drowning for many marine animals. Plastic in oceans is mainly decomposed by UV radiation,[26] resulting in smaller and smaller pieces of plastic, the smallest of which are referred to as microplastic.

Microplastic is almost impossible to remove by physical methods due to the small particle size. These microscopic pieces of plastic may be consumed by fish, animal, algae or other microorganisms. As evidence of this, investigations have observed coloured pieces of plastic in ocean-dwelling micro-organisms.[27] As of now, the consequences of microplastic are not completely clear, but the accumulation of microplastic in the food chain and into our own food can be a reality.[28]

As most plastic types are very robust, the time-scale for the complete degradation of microplastic to monomeric forms is very long.[26] Therefore, the use of biodegradable plastics is of great interest. These are new plastic types that can be degraded by biological processes on a much shorter time-scale than other methods and should therefore be able to help reduce accumulation of plastic and microplastic. It should be noted that such degradation is highly dependent on the micro-organisms present and therefore the described biodegradability will vary depending on the local environment.

1.4.2 Bioplastics

Bioplastic is a term generally referring to plastics that are biobased and does not necessitate biodegradability. Bioplastics currently make up only 2% of the total plastic market and only 23.2% of these bioplastics are also biodegradable.[29] Bioplastics have a projected potential to substitute 90% of the fossil-based plastics.[30] It is also possible that development of new bioplastics could further improve that potential.

Within the 2% bioplastic market share, the five main bioplastics, by production capacity and listed in descending order, are PUR (10-100% biobased), PET (20% biobased), Starch blends (25-100% biobased), PLA (100% biobased) and PE (100% biobased), making up 84% of the total bioplastic production capacity.[29] Amongst these, only PLA (polylactide) is both 100% biobased and biodegradable, accounting for 5.1% of total bioplastic production capacity. PLA is an excellent example of employing an emerging strategy for innovation, introducing a completely new polymer to the market with new properties that existing plastic are unable to compete with.

1.5 Targeting Biochemicals from Carbohydrates

When assessing opportunities, it is important to look at reactions that carbohydrates are naturally poised to undergo. A good indicator of this perspective is to look at biological systems, which have evolved to be highly efficient. Chemicals currently produced from fermentation processes include lactic acid, succinic acid, 3-hydroxy propanoic acid, itaconic acid, glutamic acid.[13] Of these, lactic acid is of particular interest as lactic acid has a H/C ratio of 0, eliminating the need for redox reactions and a redox acceptor, when converting carbohydrates. Furthermore, chemicals accessible from lactic acid include acrylic

acid, propylene glycol and lactide.[8,13]

Acrylic acid and propylene glycol are both currently produced from oil and therefore provide a drop-in market opportunity for biomass processes. Acrylic acid provides a particularly good opportunity as it has a H/C ratio of 0, identical to lactic acid and carbohydrates (Figure 1.3). Lactide is the precursor for production of polylactide (PLA), mentioned in Section 1.4.2, a product following an emerging market strategy.[22,29]

The multiple strategies available for further upgrading of lactic acid, makes the production og lactic acid from glucose a robust target for further development.

2 | α-Hydroxy Acids for Biopolymers

The following section focuses on the Sn-Beta catalysed reaction of glucose to lactic acid. The description involves insight into lactic acid, zeolites and Sn-Beta, and leading to selection of this reaction as a high-potential target for development towards industrialisation. The concept of NMR analysis and its use in chemocatalysis will also be introduced. This description will finally lead to the aim and outline of the current PhD project.

2.1 Lactic Acid

Lactic acid (2-hydroxypropanoic acid) is a simple naturally occurring organic acid found many places in nature.[31,32] It was first discovered in 1780 by the Swedish chemist Scheele, who discovered lactic acid in sour milk.[31–33] Later, in 1881, the controlled fermentation and first commercialisation was developed by French scientist Frémy.[31,32,34] Lactic acid is the simplest form of a chiral α-hydroxy acid. It is a bifunctional molecule possessing both alcohol and carboxylic acid functionality, making it extremely versatile with a high functionality per carbon (1.5).

2.1.1 Applications

Lactic acid has many beneficial properties leading to a multitude of applications. The compound is generally regarded as safe, by the FDA and other regulatory agencies,[31,33] allowing for applications involving direct consumption and prolonged skin contact. Such applications include food production, where lactic acid can be used as an acidulant, pH

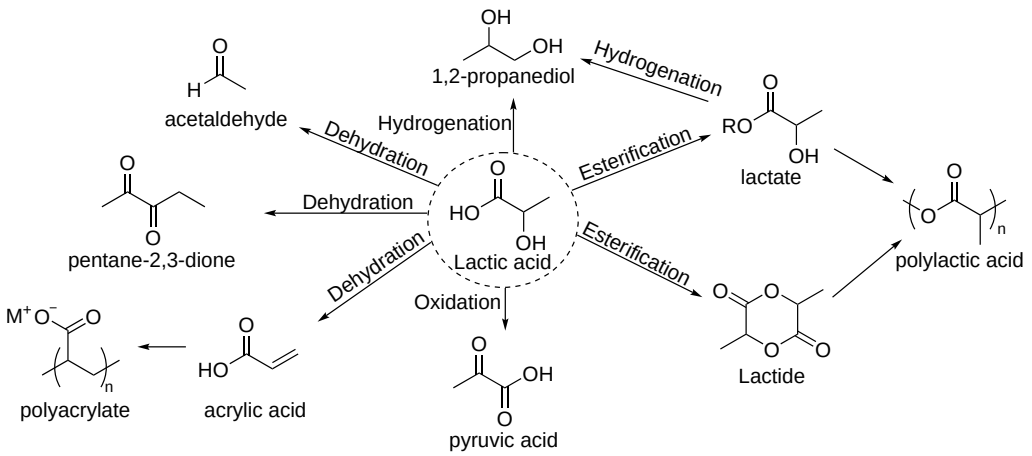

Figure 2.1: Select products available from lactic acid.

buffering agent, emulsifying agent and flavouring agent. These properties are used in processed foods such as bread, sweets, dairy products and alcoholic beverages.[32–34] The salts of lactic acid, as well as lactic acid itself may be used in solution for disinfection and preservation of raw meats, and the sodium salt is even used for medical applications such as dialysis.[33] On the other hand, lactic acid esters (and lactic acid) have many uses in cosmetic applications, for example as solvents, exfoliants and pH regulators.[35]

Chemically, lactic acid is used as a platform molecule (precursor) for the production of many important small molecules, such as propylene glycol and acrylic acid (Figure 2.1, leading to larger compounds such as acrylic polymers and polyesters.[36–38]. The homo-polymer of lactic acid is called polylactic acid (PLA). PLA is a biodegradable and biocompatible polyester,[39] which upon degradation reforms lactic acid. Theses properties are exploited for medical applications such as stitches, controlled drug release and prostheses,[33] as well as biodegradable packaging and labelling.[36] Lactic acid can be polymerised by refluxing, but the resulting polymer tends to be of low molecular weight.[40](Zhao et al. 2004) The major industrial method of PLA production is catalytic ring-opening polymerisation.[40]

2.1.2 Production

Lactic acid is primarily produced biocatalytically by fermentation of glucose.[13,34] The enzymes involved in these processes are highly selective and some micro-organisms are able to produce lactic acid enantioselectivly.[31,34,41] Fermentation processes require close regulation of fermentation conditions including pH, temperature and micro-organism nutritions. The additives employed for the fermentation process can significantly affect the requirements for the subsequent purification.[31,34] The purification phase of lactic acid production is considered the most expensive part of the process, and the main source of the high price for lactic acid.[42]

Typically, lactic acid is precipitated as its calcium salt, and subsequently rehydrated, leading to the formation of a stoichiometric amount of calcium and sulphuric acid waste.[13,34,41] Purification methods also include crystallisation of calcium lactate, extraction of lactic acid with a solvent such as isopropyl ether and high vacuum distillation.[41,42] However, many of these methods are made difficult by the low vapour pressure, self esterfication, and high solubility in water, which are further complicated by impurities from fermentation, such as dextrins, proteins, inorganic salts, and unfermented sugars.[42] The recommended purification method is conversion of calcium lactate into methyl lactate, followed by purification by distillation and (depending on the end application) re-hydrolysis of the ester.[41,42]

Recent research has shown the potential for production of lactic acid by chemocatalytic conversion of glucose by Sn-Beta.[43] The Sn-Beta catalyst employed in this process is a solid acid zeolite catalysts, mimicking the industrial methods employed for catalytic upgrading of oil. Although less selective than highly evolved enzymes, zeolites are more robust, allowing the use of a broader range of reaction conditions and solvents. Furthermore, the solid catalysts allow for establishment of heterogeneous flow processes, leading to lower predicted production costs than fermentation.[44]

2.2 Zeolites and Zeotypes

Zeolites are aluminosilicates which are well known as solid acid catalysts in several industrial applications, including the use of acidic zeolite Y for fluid catalytic cracking in oil refinery.[45] Zeolites were first classified in 1756 by Axel Fredrik Cronstedt, who, upon heating a zeolite, found that steam was formed from the stone, and therefore named them zeolites from the greek zeo, to boil, and lithe, stone. They are known for their crystalline structures which exist in many forms, each classified by a three letter code. The Structure Commission of the International Zeolite Association has currently registered 245 different structures (2019). Most of these structures are produced synthetically, although many are naturally occurring.

Many aspects of zeolites catalytic function resembles enzymes. Like enzymes, the majority of the molecular structure is not actively involved in catalysis, but forms a three-dimensional crystalline structure. This structure forms uniform pores and channels through the material on the scale of Ångstrøms, which enables shape selectivity. The shape selectivity can function by three methods: By limiting the diffusion of large or bulky molecules into the pores (reactant selectivity), by sterically hindering the formation of specific transition states (transition-state selectivity) or by preventing products from diffusing out of the pores (product selectivity). Although zeolite shape selectivity is not as specific as enzymatic shape selectivity, it provides a great advantage over homogeneous and surface-based heterogeneous catalysts.

The catalytic activity of zeolites, similar to some enzymes, originates from a metal atom substituted into the three-dimensional framework, typically in low abundance. In a zeolite the metal and silicon atoms are tetrahedrally coordinated to oxygen. For silicon, this coordination results in a neutral charge balance, but for aluminium, which belongs to the group 13 elements, a surplus negative charge is produced. A proton is therefore necessary to counterbalance the negative charge giving the catalyst its Brønsted acidic character (Figure 2.2). The aluminium atom of a zeolite may be substituted by a different metal atom, changing the catalytic properties of the zeolite. Commonly used metals include transition metals and tin, as with Sn-Beta. When for instance aluminium is substituted by tin, a neutral charge balance is obtained, thus eliminating the Brønsted acidic character of the catalyst (Figure 2.2). Instead, the resulting tin zeolite exhibits strong Lewis acid character.

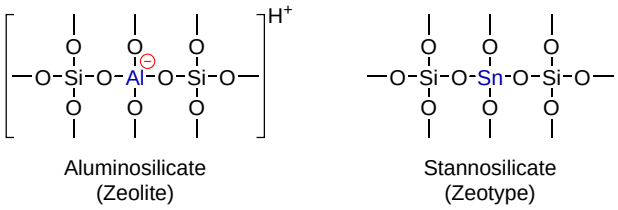

Figure 2.2: Molecular representation of a zeolite with aluminium or substituted with tin.

2.3 The Active Site of Sn-Beta

A lot of effort from different research groups has gone into the elucidation of the chemical structure of the Sn-Beta active site. The primary methods used have been FT-IR with probe molecules and MAS-NMR combined with DFT calculations to interpret the resulting spectra.[46–53]

FT-IR using acetonitrile was performed on dehydrated Sn-Beta samples resulting in two distinct peaks at 2316 and 2308 cm^{-1}.[48,49,54] By combination with DFT these peaks were assigned to tetrahedrally coordinated tin in a closed form (2308 cm^{-1}), coordinating to four framework OSi groups, and a partially hydrolyzed open form (2316 cm^{-1}), where OSi group has been hydrolyzed to OH (Figure 2.3). From the strength of acetonitrile absorption, the open form was determined to be a stronger Lewis Acid, and was also more active in both Bayer-Villiger oxidation and Meerwein–Ponndorf–Verley reduction reactions.[48,51,55]

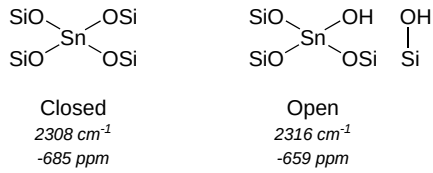

Figure 2.3: Proposed structure of the open and closed active sites of tin.

Studies with tin MAS-NMR corroborated these results by showing peaks at -424 ppm and -443 ppm, which were assigned to the open and closed sites, respectively. In addition, MAS-NMR could be used for analysis of hydrated samples, which should more closely resemble the tin active site in a reaction solution. These samples showed two peaks between -650 and -750 ppm, instead.[54]

The peaks observed were not well defined and DFT calculations have since proposed that hydrogen bonding and the solvent have a role to play in catalytic activity.[52] Wolf and co-workers assigned the two primary MAS-NMR peaks to a closed hydrogen bonded site (-685 ppm) and an open hydrogen bonded site (-659 ppm) (Figure 2.3).[47] From improvements in NMR methodology, it has become increasingly apparent that the Sn-Beta active site is far more complex than first assumed,[46,52] and the lack of incorporation of the structural position of tin may also play an important and yet undetermined role.

2.4 Sn-Beta to Methyl Lactate

The chemocatalytic conversion of carbohydrates to lactic acid was first demonstrated using a homogeneous tin catalyst and the triose glyceraldhyde in methanol, forming methyl lactate.[56] The process has since then been expanded to include a heterogeneous Sn-Beta zeolite catalyst, which was able to obtain similar yields, while enabling efficient removal of the catalyst by filtration or precipitation.[57] Subsequently, the substrate portfolio was expanded to include the hexose sugars.[43] Reaction at 160 °C resulted in reasonable yields of alkyl lactate from glucose, fructose and sucrose, (43%, 44% and 64%, respectively).[43]

In 2012 the substrate and product scope of the Sn-Beta catalysed carbohydrate conversion was expanded further. Use of xylose and other pentoses was demonstrated, forming around 40% methyl lactate, while use of glycolaldhyde was only able to form 16% methyl lactate.[58] A mixture of hexoses and pentoses, emulating depolymerised hemi-cellulose, was also tested, showing yields comparable to linear combinations of conversion of the pure carbohydrates (42.5%).[58]

With future prospects of up-scaling the reaction, studies transitioned towards the use of a Sn-Beta synthesis by a scalable post-treatment method (PT), where tin is substituted into an existing dealuminated zeolite framework, instead of the previously employed hydrothermal synthesis (HT).[59] Unfortunately the new PT catalyst suffered from lower lactate yields than the HT.[60] A major breakthrough was the discovery of the "alkali effect", by which the addition of millimolar amounts of basic alkali salts lead to an increase of methyl lactate formation from 20% up to 72% from sucrose (using potassium carbonate and PT Sn-Beta).[60]

2.4.1 Mechanism

The reaction mechanism for the conversion of carbohydrates to lactic acid is characterised by Lewis and Brønsted acid catalysed reactions. At present six mechanistic steps have been proposed and substantiated (Figure 2.4). The majority of the mechanism is based on initial research into triose conversion to alkyl lactate by tin chloride, but was expanded to include Sn-Beta.[56,57] The investigation showed five mechanistic steps starting from trioses: 1) isomersation of aldose to ketose, 2) α-dehydration to enol-pyruvaldehyde, 3) tautermerisation to pyruvic aldehyde, 4) solvolysis from aldehyde to hemi-acetal, and 5) 1,2-hydride shift.[56]

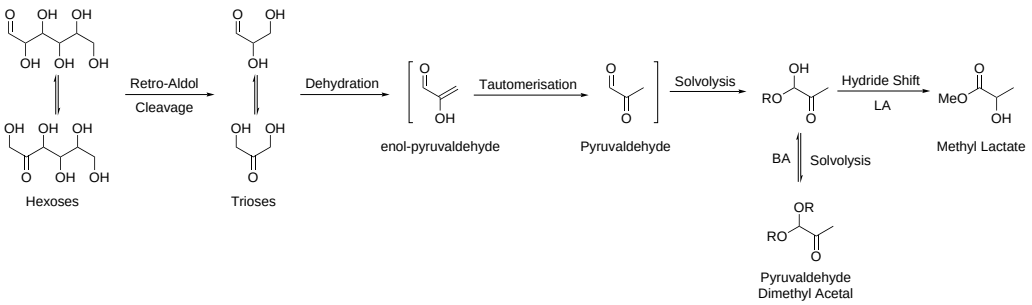

Figure 2.4: Pathway to the formation of alkyl lactate from carbohydrates

The first reaction step is a rapid isomerisation between dihydroxyacetone and glyceraldehyde. The yields reported for trioses show no distinction between use of aldose or ketose, leading to the conclusion that isomerisation occurs easily and rapidly so as not to be limiting for further reaction.[56] Transition towards methyl lactate is inititated by dehydration of the C3 hydroxyl group, leading to the formation of enol-pyruvaldehyde.[56] Enol-pyruvaldehyde is proposed based on its formation as an intermediate in dehydration of trioses in the methylglyoxal synthetase reaction.[61]

Enol-pyruvaldehyde is subsequently tautomerised to the thermodynamically more stable pyruvaldehyde, which is likely to undergo immediate solvolysis to the corresponding hemi-acetal. The formation of this alde-keto intermediate has been substantiated through observation of pyruvaldehyde acetals in the reaction.[56,62]

The final step involves a MPVO type reaction leading to formation of the final α-hydroxy ester. Conversion of dihydroxyacetone conducted in deuterated solvents, to observe solvent incorporation of protons, showed no solvent proton incorporation in the C2 position of methyl lactate, substantiating an intramolecular hydrid shift in the final step.[63] Reactions in deuterated methanol also showed incorporation of a single deuterium in the C3 methyl group of both pyruvaldehyde and alkyl lactate when starting from trioses, while no such incorporation was observed when starting from pyruvaldehyde, indicating that tautermeristaion is irreversible.[56,63]

Reactions starting from pyruvaldehyde showed formation of high amounts of methyl lactate, confirming its role as a reaction intermediate.[56] The pyruvaldehyde dimethyl actetal was found to be formed in high ammounts by Brønsted acidic catalysts, while Lewis acid catalysts promoted formation of alkyl lactate.[57,62]

The progression to use of larger carbohydrates lead to identification of an additional reaction, retro-aldol cleavage.[43] The ability of β-hydroxy carbonyls to undergo retro-aldol cleavage is well known from biological processes, including the glycolytic metabolic pathway.[64,65]

Detailed studies on Sn-Beta with carbohydrates shows that isomerisation occurs by a 1,2-hydride shift mechanism catalysed by the simultaneous coordination of carbonyl and alcohol.[54,66] However, isomerisation is also in competition with epimerisation, which occurs by 1,2-carbon shift following a Bilik type reaction mechanism.[54,67]

2.4.2 Alkali Modification of the Active Site

The addition of alkali ions has been observed to have a considerable effect on the reaction selectivity of Sn-Beta,[60] signifying that alkali salts may be modifying the catalyst active site. FT-IR experiments have shown a decrease in silanol signals upon addition of alkali. It was therefore proposed that the exchange of alkali primarily occurs at the silanol group of open sites, rather than at the stannol group.[49] DFT calculations show that reactions such as isomerisation have the lowest energy barrier when coordinated both to the silanol and tin, while epimeristion is favoured when the sugar is bi-dentatly coordinated to the tin.[68] It is thefore hypothesised that alkali salts inhibit the coordination of a silanol group leading to more bidentate coordiantion to tin.[54,68]

2.5 Methyl Vinyl Glycolate

Methyl vinyl glycolate (MVG) was recently identified in the Sn-Beta catalysed conversion of carbohydrates.[58,69–71] It is of high interest, because it is a simple α-hydroxy ester, like methyl lactate, allowing it to undergo polyesterfication reactions.[69,70] However, MVG also contains a double bond allowing for additional modification either before or after polymerisation. Such properties are of great interest during polymer formulation as they enable tuning of polymer properties, thus increasing the versatility of the

building block. Dusselier and co-workers have previously demonstrated this capability, by co-polymerisation of MVG with methyl lactate and post-modification of the resulting co-polymer.[69]

2.5.1 Mechanism

The formation of MVG is proposed to occur by a pathway analogous to that of methyl lactate, starting from tetroses. The tetroses may be employed directly or formed either by aldol condensation of glycolaldehyde or retro-aldol cleavage of glucose.[69,70] Under catalytic conversion of tetroses with tin three additional products were observed: methyl 4-methoxy-2-hydroxy butanoate (MMHB), methyl 2,4-dihydroxy butanoate(MHHB) and 2-hydroxy butyro-gamma-lactone (HBL). These form two competing pathways to the formation of MVG (Figure 2.5).

The first competition occurs after the initial dehydration of tetrose to an enol form. At this stage, the substrate may tautomerise to follow a pathway identical to the formation of methyl lactate, leading to formation of HBL and MHHB, which are in equilibrium. The enol may instead dehydrate further, in this case forming a highly conjugated unsaturated aldo-keto intermediate. After solvolysis, the double dehydrated intermediate may undergo a hydride shift to form the final MVG, or instead undergo conjugated addition prior to a hydride shift to form MHHB instead.

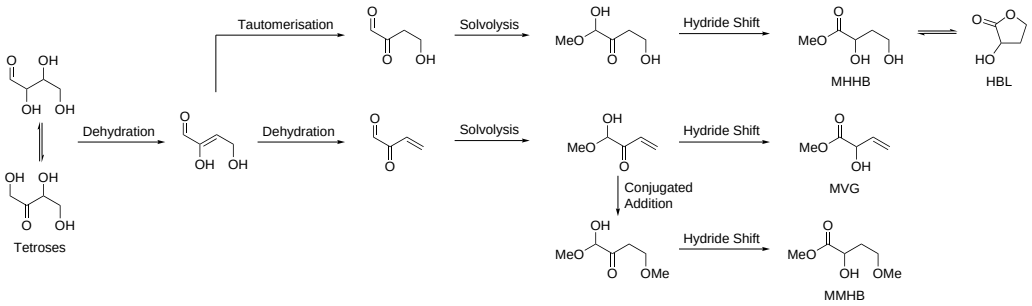

Figure 2.5: Pathway to the formation of MVG, MMHB and HBL/MHHB from tetroses.

2.6 Nuclear Magnetic Resonance Spectroscopy in Chemocatalysis

Nuclear magnetic resonance (NMR) spectroscopy is a tool for the measurement of magnetically distinct atoms. Many atomic nuclei can be detected by NMR, but the most commonly used in organic chemistry applications are naturally hydrogen and carbon. NMR is able to provide information about the local electronic environment of an atom, thereby discerning structural information such as bonding and sterochemistry.

2.6.1 Nuclear Spin

Only atoms with an uneven number of protons and/or neutrons are detectable by NMR. Therefore, hydrogen is detectable as its most abundant isotope (^{1}H), while carbon is only detectable as the less abundant ^{13}C (1.1% natural abundance) isotope, as ^{12}C has an even number of protons and neutrons.

NMR active nuclei all possess an intrinsic quantum mechanical property called spin. Nuclei with non-zero spin produce a magnetic field and have a magnetic moment. For nuclei, spin is quantified. Nuclei such as ^{1}H and ^{13}C have two possible spin eigenstates. Without an external magnetic field, there is no difference in energy between these states. However, when exposed to a strong external magnetic field, the energy levels are split forming a low and a high energy state. Thus, macroscopic samples are magnetised by increased population of the low energy state.

When exposed to a magnetic field, magnetic moments oscillate around the magnetic field with the so-called Lamour frequency. After excitation with a radio-frequency pulse, this oscillation induces a measurable current in a coil in the NMR instrument, which is used to produce the NMR spectrum. The oscillation is described by a frequency and an amplitude. The amplitude is determined by the type and amount of nuclei and is independent of their chemical or molecular environments. This property enables NMR to perform quantitative measurements of atoms, for example all hydrogens give the same instrument response if a suitable experiment is used. The Lamour frequency is dependent on the type of NMR active atomic nuclei and the local magnetic field. This magnetic field, that the nuclei experience, is modulated by electronic shielding from surrounding electrons, which is what leads to the ability to differentiate atoms in different molecular environments by NMR spectroscopy.

2.6.2 Application of NMR

NMR experiments are available that can provide information about the way atoms are bound to each other, and how many hydrogen atoms are bound to a carbon (Figure 2.6). When combined with the chemical shift, which senses the electronic environment, the positions of double bonds and of oxygen atoms may be deduced. This is particularly useful in the analysis of carbohydrates and carbohydrate dehydration, isomerisation and cleavage products, where oxygen is the only heteroatom. The extensive stereo-chemistry of these compounds can be distinguished by NMR, as atoms in diastereomers includ-

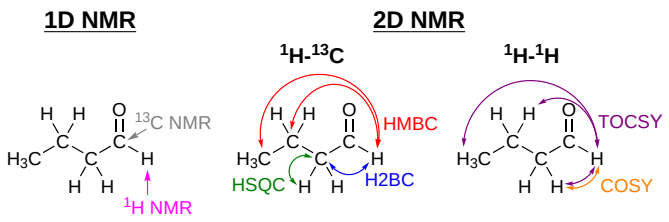

Figure 2.6: Illustration of select NMR experiments, both one and two dimensional, hetero- and homonuclear, and the correlations each experiment is able to detect.

ing *cis/trans* isomers have different electronic environments and thereby possess different chemical shifts. The techniques are also applicable on unpurified reaction mixtures. Such application is naturally dependent on sufficient spectral resolution to avoid signal overlapping.

All atoms produce the same amount of signal independent of the molecule they are part of. As a result, the signal area in a 1D-NMR experiment corresponds to the molar ratios of each atom in each substrate, provided that care is taken to warrant quantitative data acquisition (complete relaxation between accumulated scans, no signal enhancement by bonded atoms and homogeneous excitation). Therefore, if the molar quantity of one atom is known, e.g. by addition of a known amount of a standard, the quantity of any molecule in the sample may be determined, even if the complete structure is undetermined or authentic standards are not available.

2.6.3 Advances in NMR Analysis of Complex Mixtures

Both 1D and 2D NMR techniques have previously been used extensively in organic and natural product chemistry. However, these techniques have primarily focussed on the identification of purified products, where high purity was considered essential for accurate identification.[72] The past two decades have seen extensive advances in application of NMR spectroscopy for analysis of biocatalytic intermediates and products (i.e. metabolites) in complex mixtures. These advances have been fuelled by improvements in instrumentation, including stronger magnetic fields and higher sensitivity probes.[72,73]

NMR spectroscopy offers advantages for compounds that are difficult to ionize or require derivatisation for MS and is unbiased, detecting all compounds present without targeted optimisation.[72,73] Hence, analysis of complex metabolic mixtures expanded to other 2D methods and other systems, including analyses in compartments such as *in vivo* analysis of metabolic processes. While biocatalysis has adapted advanced NMR spectroscopic methods alongside synergistic chromatographic mass spectrometry methods, chemocatalysis has been much slower to adapt to the opportunities provided by ultra-high resolution methods. Throughout this thesis work, chemocatalytic biomass conversion was hypothesized to benefit from advanced NMR spectroscopic methods to provide detailed insight into chemocatalytic processes, including for instance the detection of short-lived intermediates *in situ* and the identification of new reaction products.

3 | Aim and Outline of the Study

The overall objective of this dissertation of is to explore the formation of four chemical building blocks with potential for industrialisation by chemocatalytic conversion of carbohydrates. These compounds are methyl lactate (ML), methyl vinyl glycolate (MVG), methyl *trans*-2,5-dihydroxy-3-pentenoate (DPM), methyl *trans*-2,5,6-trihydroxy-3-hexenoate (THM) and other simple esters hereof (Figure 3.1). These chemicals show high potential for future applications as functionalised polymer building blocks, which will be explored further in this work. As previously discussed, it is a requirement that the starting material is bio-renewable and industrially scalable, therefore various abundant carbohydrates have been selected for this endeavour. The main goal will be to improve the understanding of the reaction mechanism through detailed analysis of product distributions, utilisation of isotope labelled substrates and a general parameter/additive screening approach. These studies should also lead to a better understanding of selectivity control, in order to warrant the efficient use of substrate feedstocks.

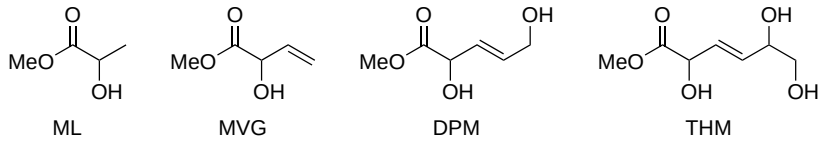

Figure 3.1: Target molecules for further developments towards industrial application.

Part II

Experimental

4 | Experimental

4.1 Standard Reaction Conditions

In a typical experiment, 360 mg substrate, 180 mg Sn-Beta, 5 mL methanol (4.0 g) and 50 mg internal standard was added to a 5 mL glas microwave reaction vial. The vial was heated in a Biotage Initiator+ microwave reactor to 160 °C under stirring (600 rpm) for 2 hours, then the reaction vessel was rapidly cooled to room temperature and the catalyst was removed by filtration through a 0.4 μL syringe filter. Analysis was performed by GC-FID and HPLC on aliquots of the unmodified sample. For analysis by NMR, 500 μL sample aliquots were added to an NMR vial together with 50 μL of d4-methanol as lock substance.

Perturbation experiments followed the standard reaction procedure with the exception of the perturbation. In reactions involving alkali-containing solutions, the alkali metal source was dissolved directly in methanol in the desired concentration, before addition to the reaction vial. In reactions with solvents other than methanol, the reaction volume was kept constant while varying the solvent.

Rate experiments were conducted in accordance with the standard reaction procedure while reducing the catalyst amount to 90 mg.

Reactions with isotope-labelled substrates were conducted in 500 μL glass reaction vials. Reactions were typically conducted with 18 mg Sn-Beta (Si/Sn=200, hydrothermally synthesized), 36 mg labelled substrate, 500 μL methanol and 5 mg internal standard.

4.2 Catalysts

Post-treatment (PT) synthesised Sn-Beta was prepared according to a modification of the procedure described by Hammond *et al*,[59] and provided by Dr Søren Tolborg (Haldor Topsøe), with the exception of the Sn-Beta (PT) catalyst employed for the experiments in Section 8.3 which were prepared by PhD student Irene Tosi (Department of Chemistry, DTU).

The Sn-Beta (HT) catalyst employed in Section 7.2 was also prepared by PhD student Irene Tosi, while all additional catalysts synthesised via hydrothermal synthesis (HT)[74–76] were prepared by Dr Søren Tolborg (Haldor Topsøe), as were the Sn-MFI,[77] Sn-MCM-41[78] and Sn-SBA-15[79] catalysts.

4.3 NMR Analysis

1D and 2D NMR was used for analysis of the catalytic experiments. NMR samples were prepared by rapid cooling of the reaction vessel to room temperature. The Sn-Beta catalyst was removed by filtration through a 0.4 μL syringe filter. 500 μL sample aliquots were added to an NMR vial together with 50 μL of d4-methanol as lock substance.

The spectra were recorded on a Bruker (Fällanden, Switzerland) Avance III 800 MHz spectrometer equipped with a TCI Z-gradient CryoProbe, an 18.7 T magnet and a sample changer. A pulse sequence with ^{1}H irradiation only applied during signal acquisition was used to minimize distortions of signal integrals by the nuclear Overhauser effect for 1D ^{13}C NMR spectra.

4.3.1 Compound Identification

Standard DQF-COSY, TOCSY, ^{1}H-^{13}C HMBC, standard and edited ^{1}H-^{13}C HSQC, as well as ^{1}H-^{13}C HSQC-TOCSY experiments were employed for compound identification in samples following solvent evaporation overnight in a fume hood and re-dissolution in deuterated solvents.

4.4 Other Analysis Methods

Unless otherwise stated, the quantifications listed, were determined or confirmed by NMR. GC-FID/MS and HPLC were used to supplement or validate NMR quantifications.

GC-FID was performed with a 7890A Series GC system (Agilent Technologies) with a SolGel-WAX column (Phenomenex). Quantification of methyl lactate (ML), methyl vinyl glycolate (MVG), glycolaldehyde dimethylacetal (GA-DMA) and methyl 4-methoxy-2-hydroxybutanoate (MMHB) were performed after calibration with referencing standards. Quantification of DPM and THM (see Chapter 5) were also performed by calibration, after synthesis and purification of referencing samples of each compound.

GC-MS was performed on an Agilent 6890 with a Phenomenex Zebron ZB-5 column equipped with an Agilent 5973 mass selective detector, and used in product identification.

HPLC analysis was performed on a Agilent 1200 series HPLC. An Aminex HPX-87H (BioRad) column (0.004 M H_2SO_4, 0.6 mL min^{-1}, 65 °C) and a refractive index and diode array detector was used for quantification of furanic compounds. Hydrolysis under the acidic conditions in the column enabled quantification as 5-(hydroxymethyl)furfural (HMF), 5-(methoxymethyl)furfural (MMF) and furfural using the appropriate standards. Sugar conversion as well as an estimation of the remaining methyl sugars were quantified using a Carbohydrate (Zorbax) column (60 wt% acetonitrile/water, 0.5 mL min^{-1}, 30 °C). The response factor used for the combined methylated sugar yields were based on averages of commercially available methyl sugars.

4.5 Stability Testing

Stability of MVG was tested by exposing freshly distilled samples of MVG to different conditions. 10 g of freshly distilled MVG was added to each of eight brown and two colourless 25 mL GL25 borosilicate glass flasks and the flasks were sealed with a GL25 screw cap with a PTFE coated silicon seal. Prior to sealing, nitrogen atmosphere was formed on four of the brown flasks, by flushing nitrogen into the flask for 2 min and thereafter sealing the flask while maintaining a flow of nitrogen across the opening. Four brown flasks were stored in a fridge at 5 °C, and four flasks were stored in a dark cupboard at room temperature, two with nitrogen atmosphere and two without in each location. The final two clear flasks were stored in a glass fronted cupboard facing a window, resulting in two identical flasks in each of the three locations. One set of flasks was removed for testing after 59 days in storage, and the second set of flasks was removed after 150 days in storage. Analysis was performed by GC-FID and HPLC on aliquots of the unmodified samples, and by ^{13}C NMR on a sample diluted 50 vol% with deuterated methanol.

4.6 Coating Formulation

Radiation curing blends were made using 99 wt% monomer and 1 wt% IRGACURE 500 photoinitiator (50 wt% Benzophenone and 50 wt% 1-Hydroxy-cyclohexyl-phenyl-ketone). The monomer was either HDDA or HDO-VG (Figure 10.6 on page 78) in pure form or in a 1:1 weight ratio with TP30 (bisphenol A epoxy diacrylate in 30% tripropylene glycol diacrylate). After stirring until homogeneous, a 6-12 μm film was applied to an aluminium plate and cured by running repeatedly under a UV lamp by a conveyor belt. The curing was deemed complete when a cotton bud pulled over the surface, left no mark in the film.

Cationic curing blends were made using 99 wt% monomer and 1 wt% IRGACURE 250 photoinitiator (4-Isobutylphenyl-4'-methylphenyliodonium hexafluorophosphate). The primary monomer was ECC with upto 10 wt% of epoxy-MVG (Figure 10.7 on page 78) or 10 wt% epoxy-MVG and 10 wt% TMPO (Trimethylolpropane oxetane). After stirring until homogeneous, a 12 μm film was applied to an aluminium plate and cured by running repeatedly under a UV lamp by a conveyor belt. The curing was deemed complete when a cotton bud pulled over the surface, left no mark in the film.

4.6.1 Coating Evaluation

Coatings for evaluation were made by a thin film of polymer blend on aluminium and glass plates and cured by running under a UV lamp by a conveyor belt (UV curing) or drying in the fume-hood (thermal curing). The curing was deemed complete when a cotton bud that was pulled over the surface left no mark in the film.

Hardness was evaluated by using the König hardness test (pendulum hardness), where a bar with two points was placed on the film, and a pendulum rocked back and forth. The harder a film, the less resistance the pendulum experiences and more swings are obtained.

Film flexibility was tested by the Ericson hardness method, where a rounded piston bends the coated aluminium plate until cracking of the film is observed.

Chemical resistance of a film was tested by soaking a cotton bud in methyl ethyl ketone, and then swiping the cotton bud back an forth over the same area of the film, with 0.5 kg of force. The test was stopped when dissolution of the film was observed.

Part III

Results, Discussion and Conclusion

5 | Identification of New Reaction Products[†]

A complete picture of the products formed in a reaction provides important insight into the reaction process. The information gained allows for the development of substantiated hypothesis concerning the reactions taking place, and in turn testing these hypothesis by evaluation of changes to product distributions. Eventually, the knowledge gained may be employed to perform targeted optimisation of selectivity towards desired products.

The conversion of glucose by Sn-Beta has been prone to low overall carbon balances, despite high conversions.[43] Gradual expansion of the reaction product portfolio has assisted in improving this balance and known reaction products now included methyl vinyl glycolate (MVG), methyl 4-methoxy-2-hydroxy-butyrate (MMHB), 2-hydroxy-butyro-γ-lactone (HBL), glycolaldehyde dimethyl acetal (GA-DMA), 5-(hydroxymethyl)furfural (HMF) and methyl lactate (ML), with methyl lactate forming the major product.[43,58,60,70,71] The proton and carbon chemical shifts of these products were assigned and are displayed in Figure 5.1. High carbon balances remain elusive and have so far only been achievable in reactions with high yields of methyl lactate.[60]

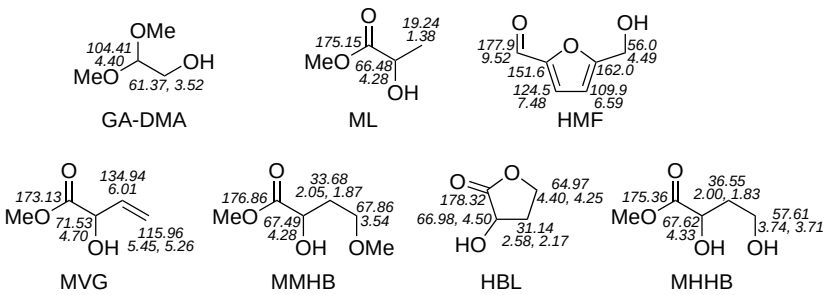

Figure 5.1: Structures of known products in the conversion of trioses, tetroses and hexoses. Abbreviations: Glycolaldehyde dimethyl acetal (GA-DMA), methyl lactate (ML), 5-(hydroxymethyl)furfural (HMF), methyl vinyl glycolate (MVG), methyl 4-methoxy-2-hydroxy-butyrate (MMHB) and 2-hydroxy-butyro-γ-lactone (HBL)

The persistent low carbon balance lead our efforts to further expand the reaction product portfolio. This portfolio has since acted as a tool in other experiments by which a more complete understanding of the reaction product distributions are obtained. By employing high resolution NMR techniques it has been possible to identify and assign several new products formed in the conversion of hexoses and pentoses by Sn-Beta in methanol.

[†]This chapter is adapted from Tolborg *et al.*, *Green Chem.*, 2016, **18**, 3360–3369.; Elliot *et al.*, *RSC Adv.*, 2017, **7**, 985–996.; and Elliot *et al.*, *ChemSusChem*, 2017, **10**, 2990–2996.

5.1 Identification of new C6 products

In a reaction starting from glucose in methanol solvent 11 products were identified, in addition to the aforementioned products and not including stereoisomers (Figure 5.2). Although the Sn-Beta catalyst is a Lewis acid, it still possesses some Brønsted acidity. This is evident from the observation of products typically found in the Brønsted acid catalysed deyhydration of fructose to HMF.[83] With the exception of methyl levulinate (MLA) and methyl formate (MF), these products are characterised by a central furan ring (Figure 5.2).

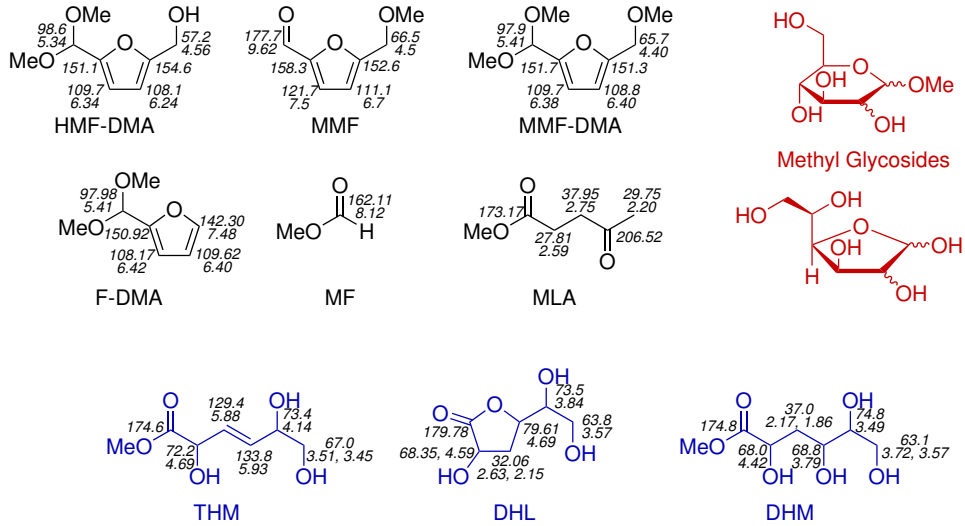

Figure 5.2: Structures of new products identified in the conversion of hexoses by Sn-Beta in methanol. Furanic compounds include 5-(hydroxymethyl)furfural dimethyl acetal (HMF-DMA), 5-(methoxymethyl)furfural (MMF), and the corresponding dimethyl acetal (MMF-DMA), furfural dimethyl acetal (F-DMA) and methyl levulinate (MLA). Methyl glycosides are displayed in a general stereochemical form, as are *trans*-2,5,6-trihydroxy-3-hexenoic acid methyl ester (THM), 3-deoxy-hexono-γ-lactone (DHL) and 3-deoxy-gluconic acid methyl ester (DGM).

Methyl glycosides, the methyl acetals of ring closed carbohydrates, are formed by Brønsted acid catalysed solvolysis of carbohydrates. They constitute one of the most abundant compound groups and may exist in as many forms as there are corresponding carbohydrates. With glucose as the starting substrate, methyl glycosides are primarily formed as methyl glucopyranoside and methyl mannopyranoside. The furanoside forms of methyl glycosides are only observed in small amounts and are not observed at long reaction times, indicative of their lower stability under the reaction conditions.

The most interesting compounds discovered were *trans*-2,5,6-trihydroxy-3-hexenoic acid methyl ester (THM), 3-deoxy-hexonic acid methyl ester (DHM) and 3-deoxy-hexono-γ-lactones (DHL) consisting of 3-deoxy-glucono-γ-lactone and 3-deoxy-mannono-γ-lactone, the six carbon analouges to MVG, MHHB and HBL, respectivly. As their names indicate, these compounds are the mono-dehydrated (DHL/DHM) and the double

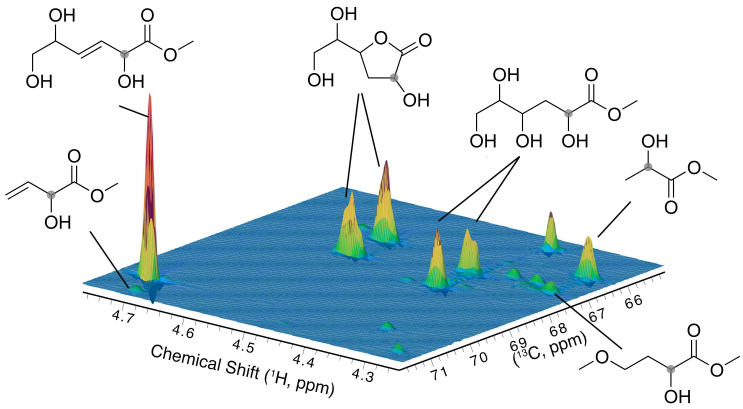

Figure 5.3: ^{1}H–^{13}C spectral region of secondary alcohol CH-groups (indicated by small spheres) adjacent to carboxylic groups, showing the signals of both known and new α-hydroxy esters formed from conversion of glucose.[80]

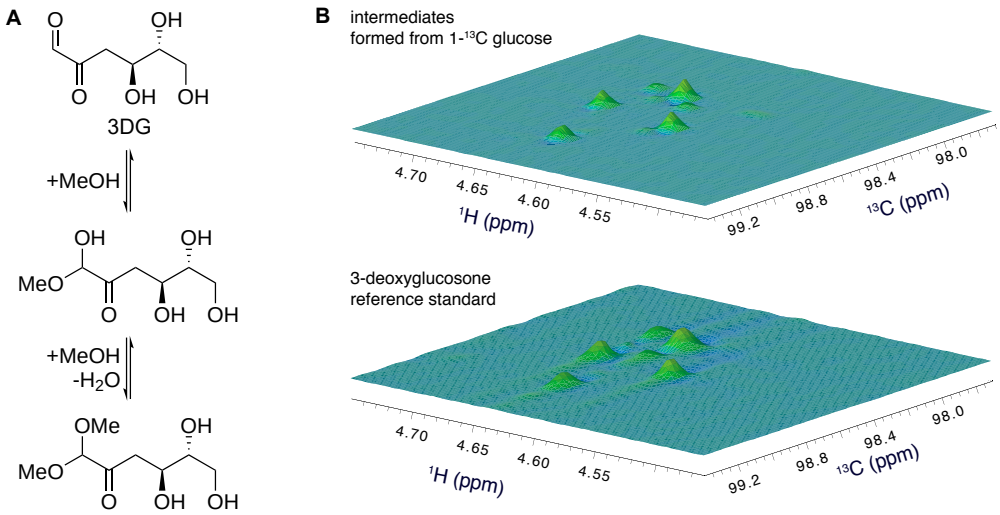

Figure 5.4: Different forms of 3-deoxyglucosone in methanol solution (A), and a comparison of the ^{1}H–^{13}C spectral regions of acetal and hemi-acetals in a 3-deoxyglucosone reference standard, with that of a reaction mixture formed from conversion of glucose by Sn-Beta in methanol (B).

dehydrated (THM) forms of a gluconic acid base unit. Like MVG, MMHB and methyl lactate, these compounds are α-hydroxy esters with the characteristic secondary alcohol groups distinguishable in ^{1}H–^{13}C HSQC (Figure 5.3).

In addition to these products, a reaction intermediate was detected in the form of 3-deoxy-glucosone (3DG) (Figure 5.4A), a six carbon equivalent to methyl glyoxal formed in the pathway to methyl lactate. Due to low abundance of the pathway intermediate, a comparison of the compound with a reference standard was performed to confirm the presence of the compound (5.4B).

Under full conversion, low methyl lactate selectivity conditions (360 mg glucose, 4 g methanol, 180 mg Sn-Beta (PT), 160 °C, 6 hours) the addition of the aforementioned products to the product spectrum was able to raise the carbon balance from 27% to 68%.

5.2 Identification of new C5 products

Following the successful identification of new C6 products, a clear pattern of dehydration products emerge. A homologous series of ester products of different chain lengths is expected, depending on the carbon backbone of the starting material, in accordance with observation of methyl lactate from trioses, MVG, MHHB and HBL from tetroses, THM, DHM and DHL from hexoses (Figure 5.5). There should therefore be equivalent versions of these esters when starting from pentoses.[81,84]

In a reaction mixture formed from xylose substrate, it was possible to identify *trans*-2,5-dihydroxy-3-pentenoic acid methyl ester (DPM), 3-deoxy-pentono-γ-lactone (DPL) and 2,4,5-trihydroxy-3-pentanoic acid methyl ester (TPM), thus completing the ester series (Figure 5.5). Concurrent research by Chen *et al.* identified the acid analogues

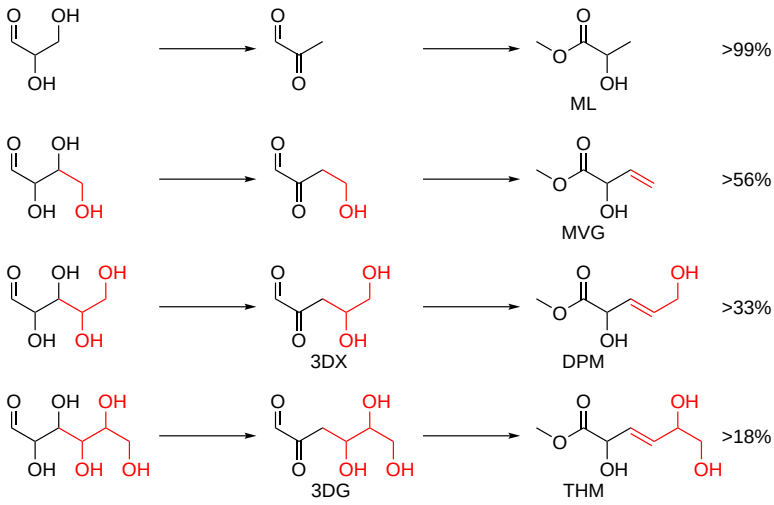

Figure 5.5: Expected series of homologous α-hydroxy ester products formed from C_3–C_6 sugars catalysed by Sn-Beta and their corresponding maximum reported yields.[43,57,80,81] The reaction is applicable both to aldoses and ketoses.

of these compounds in water.[84] In addition, the five carbon equivalent of MMHB was also detected, 2,5-dihydroxy-4-methoxy-pentanoic acid methyl ester (DMPM), despite its absence in the hexose product mixture. Analogously, C5 equivalents of the furanic product groups were observed as furfural dimethylacetal (F-DMA) and furfural (F), and pentose equivalents of methyl glycoside products were also detected (Figure 5.6).

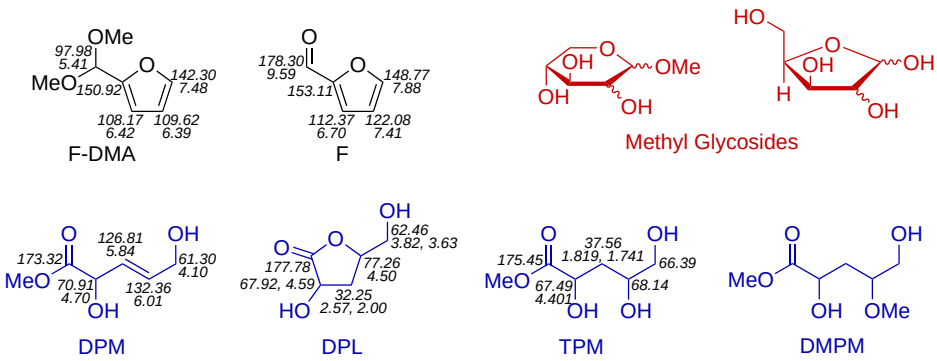

Figure 5.6: Products formed in the catalytic conversion of pentoses by Sn-Beta in methanol.

5.2.1 *Cis* and *Trans*-DPM

After optimising the formation of DPM through solvent variation (see section 7.2), an additional stereoisomer of DPM was identified (Figure 5.7B). The *cis* form of DPM was distinguished from the predominant *trans* form by measuring the $^{3}J_{H^1H}$ coupling across the double bond, which was 11 Hz, a typical value for a *cis* coupling. In addition to the open chain form of *cis*-DPM a cyclic form was also detected, albeit only in trace amounts.

5.3 Reaction Pathway

Based on all the previously shown products, an overview of the reaction system may be made, here for the pentose reaction system (Figure 5.8). The pentose system has an analytical advantage over the hexose system, due to the reduced number of products and stereo-isomers formed. This is of particular advantage when performing analysis by NMR, as NMR will detect each diastereo-isomer as a separate product, creating a more complex spectrum and reducing signal intensities. The pentose system produces products within all the same product groups as the hexose system, and it is therefore possible to draw parallels between selectivity and mechanistic effects observed for pentose ad hexose systems.

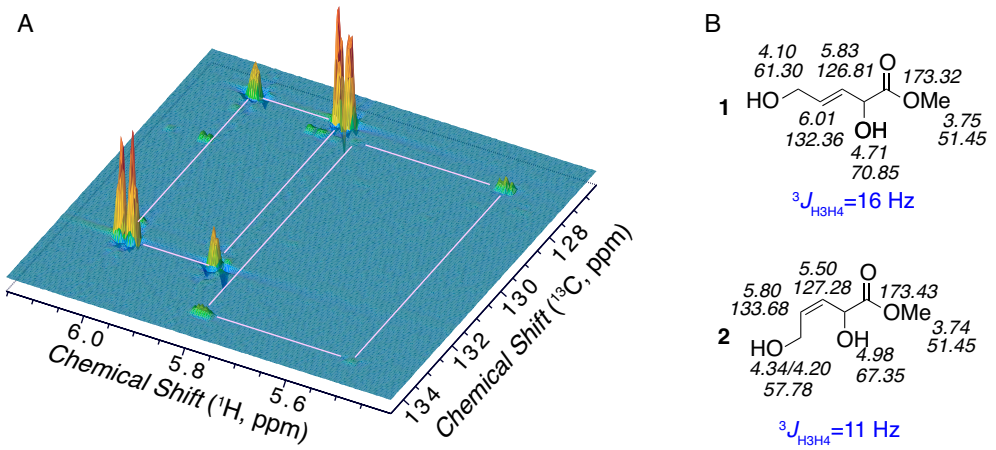

Figure 5.7: A) ^{1}H-^{13}C HSQC spectral region displaying the olefinic signals of *trans*-DPM and *cis*-DPM in a reaction mixture. $^2J_{CH}$ correlations across the double bond are indicated by thin white lines. B) Chemical shift assignments of *trans*-DPM (**1**) and *cis*-DPM (**2**).[82]

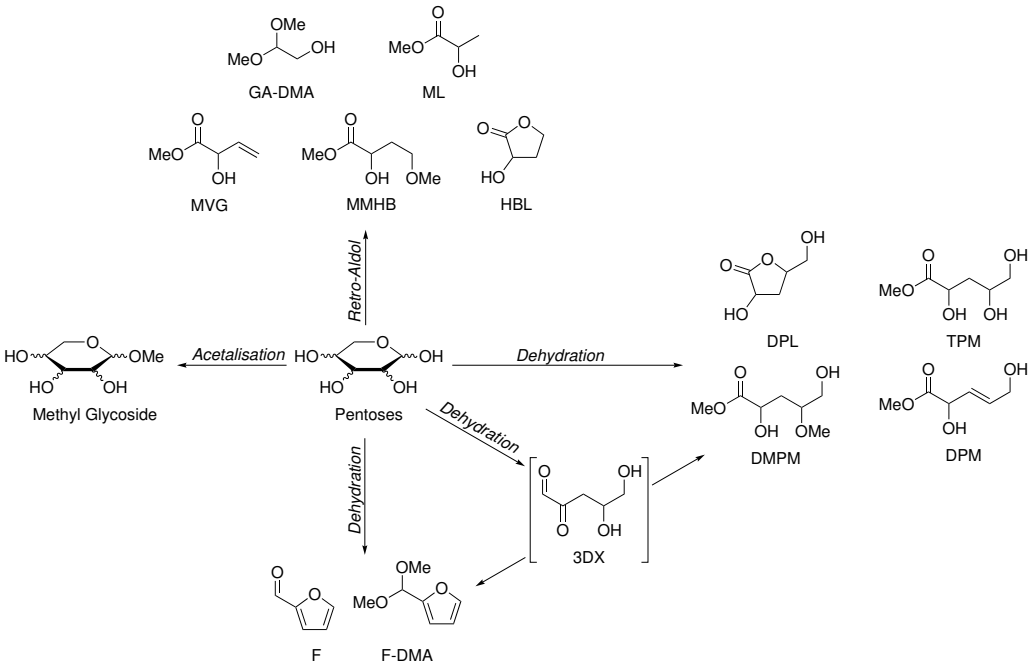

Figure 5.8: Map of reaction pathways in the catalytic conversion of pentoses by Sn-Beta, based on known products and intermediates. Reactions are applicable for both aldoses and ketose, and are analogous to the hexose system.

5.4 Deconstruction-Reconstruction Approach to Biomass Conversion

As an alternative method to production of chemicals directly from glucose or xylose, an intermediary building block produced from carbohydrates may be selected instead. Glycolaldehyde provides one such option, which may be produced as a by-product from bio-oil.[85] Although yet to reach industrial implementation, thermal cracking of sugar is able to obtain over 50% yield of glycolaldehyde.[86,87] Breaking down mixtures of sugars to smaller fragments provides the advantage of homogenizing the feed composition and stereochemistry, while maintaining functionality. If a system with suitable reaction control is available, then smaller building blocks may be used to form a large variety of larger compounds. This method of construction resembles, proposed origin of life chemistry.[88]

Conversion of glycolaldehyde by Sn-Beta in methanol does not follow the series of homologous α-hydroxy ester products shown in Figure 5.5 on page 32, as it does not posses a γ-hydroxy group for dehydration. Instead, glycolaldehyde predominantly undergoes aldol condensation to C4 and C6 sugars (Figure 5.9). Hexoses subsequently undergo retro-aldol cleavage forming trioses and ultimately methyl lactate, while tetroses lead directly to formation of MVG or other C4 products, hence C4 products are predominantly observed.[58,69–71]

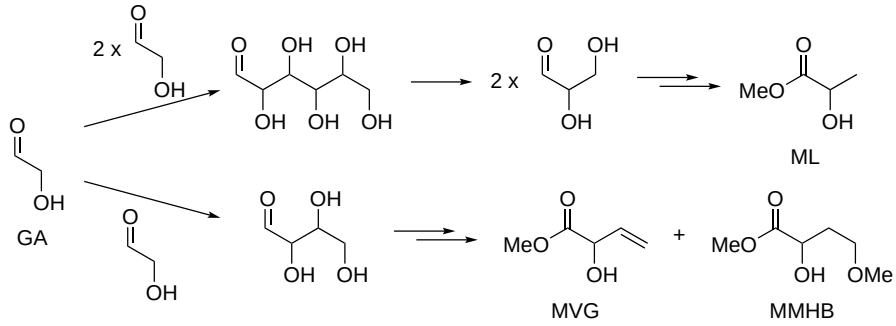

Figure 5.9: Pathways for formation of methyl lactate, MVG and MMHB from aldol condensation of glycolaldehyde.

Under standard reaction conditions (400 mg glycolaldehyde, 200 mg Sn-Beta (PT), 5 mL methanol, 160 °C), 43% MVG was obtained after 2 hours of reaction, and upto 47% was obtained after 24 hours (Table 5.1), showing a 1.5 fold increase compared to previously reported values (30 %).[58] Although several co-products of this reaction have already been documented,[58,69,71] full elucidation of the carbon balance was sought, thereby aiding further reaction development and optimization. Using high resolution 2D-NMR to analyse the aforementioned reactions, 21 reaction products were identified and assigned (Figure 5.10). Implementation of these products contributed about 10% addition carbon to the carbon balance increasing the total balance to 82-83% (Table 5.1). However further studies will be necessary to obtain a complete understanding of the pathways involved in the formation of these by-products.

Table 5.1: Product distribution from Sn-Beta catalysed conversion of glycolaldehyde in methanol.

Time	GA[a]	Glycosides[b]	MGA-DMA	HBL[c]	ML	MVG[d]	MMHB	MVG-sat	Others[e]	Total
2 h	7.5	1.1	2.4	7.9	1.3	45.0	11.9	1.0	5.0	83%
24 h	0	0	1.6	6.7	2.3	47.7	13.9	2.7	6.2	82%

All yields are in mol% carbon. a) GA-DMA and GA-HA. b) methyl β-ERY and α-THO glycoside. c) MHHB and HBL. d) MVG and VGA. e) MF, MG, FA-DMA, MDHB, MMVG, OxoB-HA and MHIB, all present in under 2% yield.

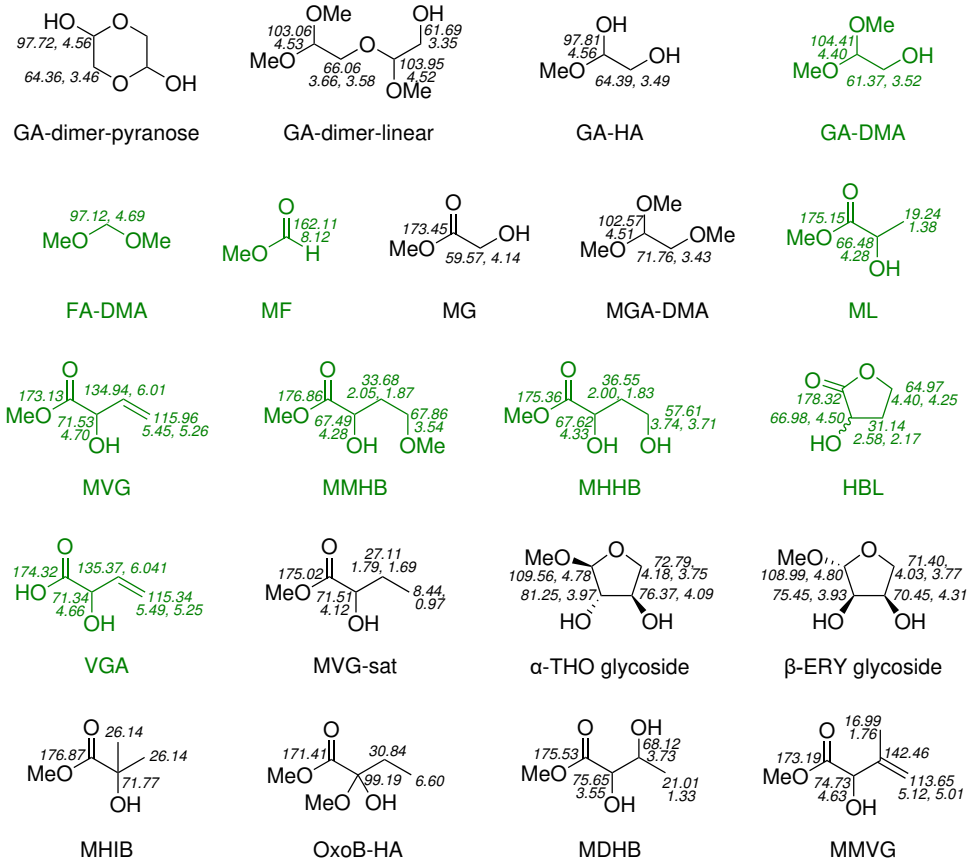

Figure 5.10: NMR assignment of major products identified in the catalytic conversion of glycolaldehyde by Sn-Beta in methanol.

6 | Quantitative Analysis of Complex Mixtures[†]

In Chapter 5, traditional NMR methods together with high resolution spectra were employed to identify new reaction products directly in the complex reaction mixture. This chapter transitions to application of NMR for quantification. The chapter will cover the selection of suitable internal quantification standards for the reaction system, which may be employed in the usual 1D-NMR quantification methods. The standards will also be employed in the development of a faster and more accurate 2D-NMR quantification method, which will also be presented herein.

6.1 Selection of an Internal Standard

In order to use NMR quantitatively, it is advisable to employ an internal referencing standard. Based on common NMR standards from literature, 6 compounds (Figure 6.1) were selected for testing as internal standards, and evaluated against the following four requirements: 1) The compound must be unreactive under operando conditions, which excludes certain functional groups such as acids and esters. 2) Low volatility is desirable to enable reliable and reproducible sample preparation. 3) High solubility/miscibility in methanol and other polar protic solvents is necessary to avoid inhomogeneities leading to unreliable quantification. 4) The compounds should have a low complexity in ^{1}H and ^{13}C NMR, producing few ^{1}H and ^{13}C NMR signals with high intensities at low concentrations, which is typically achieved by using small molecules with high degrees of symmetry.

The selected compounds are all either high boiling liquids or solids, facilitating easy handling during sample preparation (Table 6.1) and preventing product loss. In addi-

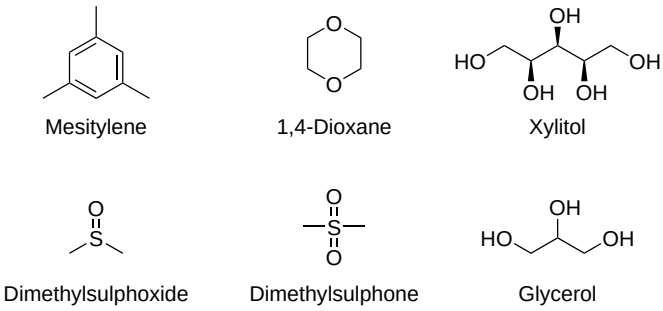

Figure 6.1: Structures of compounds selected for evaluation as internal standards in the catalytic conversion of carbohydrates by Sn-Beta in methanol.[89]

[†]This chapter is adapted from Elliot *et al.*, *Top. Catal.*, 2019, doi:10.1007/s11244-019-01131-y.

tion to the evaluated parameters, glycerol was observed to be highly viscous complicating sample preparation and accurate addition to samples. The only problematic compound based on the data from Table 6.1 is xylitol. Xylitol is the only compound with low solubility in methanol, which is the standard reaction solvent, therefore xylitol is unsuitable as an standard for our application. Fortunately, all the other substrates showed good miscibility or solubility at high concentrations in methanol and the other tested solvents.

As expected for common NMR standards, the compound structures are simple and often have high degrees of symmetry, thereby producing few NMR signals (Table 6.1). 1,4-dioxane, dimethylsulphoxide (DMSO) and dimethylsulphone ($DMSO_2$) have multiple identical atoms and produce only a single signal in both carbon and proton NMR, respectivly (Table 6.1). This leads to minimal spectrum congestion and high signal intensity for a given amount of standard, allowing for addition of smaller amounts of standard and thereby minimising the influence of the addition.

Table 6.1: Overview of selected internal standards and their performance on conditions 2 to 4.[89]

Entry	Compound	B.P.[a]	Solubility				NMR signals	
		°C	H_2O	MeOH	$CHCl_3$	DMSO	^{13}C	$^{1}H^{a}$
1	*Mesitylene*	164	N	Y	Y	Y	137.2, 126.4, 19.9	6.76, 2.24
2	*1,4-Dioxane*	101	Y	Y	Y	Y	66.7	3.67
3	*Dimethylsulphoxide*	189	Y	Y	Y	-	39.0	2.66
4	*Dimethylsulphone*	107[b]	>1M	420 mM	850 mM	>1 M	41.1	3.01
5	*Glycerol*	290	Y	Y	Y	Y	72.6, 63.2	3.67, 3.60, 3.54
6	*Xylitol*	94[b]	$\geq$ 1 M	< 50 mM	< 50 mM	$\geq$ 250 mM	N.A.	N.A.

[a]Considering only protons attached to carbon. [b]Melting point.

A test reaction was selected to evaluate the stability of the internal standards under reaction conditions. The test was based on the standard conditions employed for Sn-Beta catalysed conversion of xylose (8 wt% xylose and 2 wt% Sn-Beta (PT) in methanol reacted at 160 °C).[43,81] The compound stability was evaluated by analysis of the reaction mixture at different time intervals (Figure 6.2). Under typical full conversion conditions, under 2 hours, all substrates show comparable stability. However, at elevated reaction times, DMSO shows significant and progressive decomposition. Thus from a performance perspective, among the tested compounds mesitylene, 1,4-dioxane and $DMSO_2$ show the greatest potential as internal standards.

Although analytical standards are generally used in such small quantities that safety hazards are greatly reduced, it should be noted that DMSO, $DMSO_2$, glycerol and xylitol are all considered benign and have no hazards associated with their use. In contrast, 1,4-dioxane is suspected of being carcinogenic and mesitylene has high toxicity to humans and aquatic lifeforms. In summary, the most promising compound tested was $DMSO_2$. It is a safe, easy-to-handle solid with good solubility in polar solvents, and the two identical methyl groups contained in the compound produce a high intensity, uncluttered signal in the NMR spectrum.

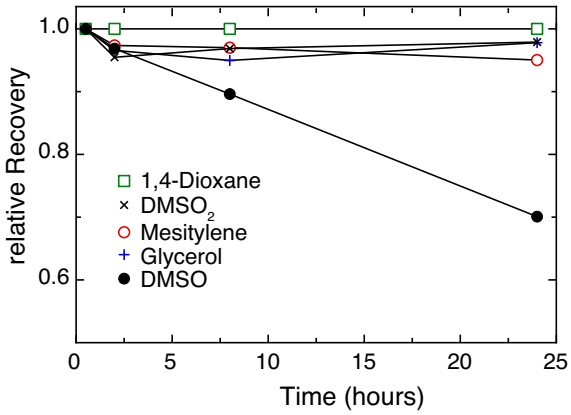

Figure 6.2: Stability of internal standards over time for the reaction of xylose by Sn-Beta in methanol at 160 °C. The recovery of NMR signal for five standards is displayed after 0.5, 2, 8, and 24 hours.[89]

6.2 Quantitative 2D-NMR

Quantitative ^{13}C NMR provides highly resolved spectra for detailed quantification of complex mixtures. However, ^{13}C qNMR is prone to long experiment times, as a result of the low natural abundance (1.1%) of ^{13}C, its long T_1 relaxation time and its low gyromagentic ratio (67.3 10^6 rad $s^{-1}T^{-1}$).[90] In comparison, ^{1}H has a high natural abundance (∼100%) and gyromagnetic ratio (267.5 10^6 rad $s^{-1}T^{-1}$),[90] but ^{1}H-NMR spectra have a 20-fold smaller chemical shift range and give splitted multiplet signals, often leading to spectral congestion and signal overlap.

By application of two dimensional ^{1}H-^{13}C HSQC NMR, it is possible to overcome these issues and obtain spectra with higher resolution and sensitivity at vastly reduced experiment times, as compared to ^{13}C qNMR. To this end, response factors were determined for ^{1}H-^{13}C HSQC spectra relative to quantitative ^{13}C spectra, normalised to an internal standard (Figure 6.3). By this method, the analysis may be performed directly on complex mixtures.

In the ^{13}C qNMR, the correlation between the concentration (c) of an internal standard (IS) and an analyte (i) in the sample, may be expressed by equation 6.1, where N is the number of identical carbons producing the signal and $Area$ refers to the peak area. Equation 6.2 then describes the response factor of an analyte in ^{1}H-^{13}C HSQC (RF_i^{HSQC}) relative to the ^{13}C signal, normalised to the internal standard.

$$\frac{c_i}{c_{IS}} = \frac{Area_i^{^{13}CqNMR}/N_i^{Carbon}}{Area_{IS}^{^{13}CqNMR}/N_{IS}^{Carbon}} \tag{6.1}$$

$$RF_i^{HSQC} = \frac{Volume_i^{HSQC}}{Volume_{IS}^{HSQC}} / \left[\frac{Area_i^{^{13}qNMR}}{Area_{IS}^{^{13}qNMR}}\right] \tag{6.2}$$

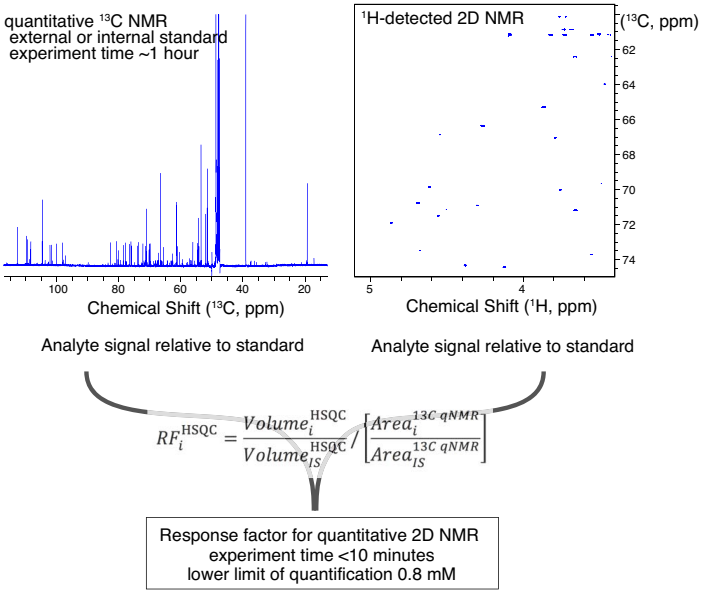

Figure 6.3: Strategy for the rapid and accurate quantitative analysis of reaction mixtures using response factors in 2D NMR.[89]

Upon combination of these two equations, a general expression is formed for the determination of the concentration of an analyte by ^{1}H-^{13}C HSQC based on a predetermined response factor and the concentration of an internal standard (equation 6.3). The concentration of the internal standard will be known from the sample preparation, making determination of the response factor the most laborious part of the method.

$$c_i = \frac{Volume_i^{HSQC}}{Volume_{IS}^{HSQC}} \times c_{IS} \times \frac{N_i^{Carbon}}{N_{IS}^{Carbon}} / RF_i^{HSQC} \tag{6.3}$$

6.2.1 Determining Response Factors

For demonstration and testing of this method, four of the most abundant α-hydroxy ester products were selected (DPM, MMHB, MVG and ML), and the CH group of the secondary alcohol in the α position was used for the analysis. To form the product mixtures, D-xylose was reacted with Sn-Beta in methanol, and the reactions were stopped at different degrees of conversion. The calibration curves produced from the signal volume/area ratios of ^{1}H-^{13}C HSQC to ^{13}C NMR all displayed linear trends (Figure 6.4), allowing for extrapolation to lower concentration ranges than accessible by ^{13}C NMR.

To validate the demonstrated method, a single reference sample of methyl lactate (9.2 mg of 98% purity, 0.087 mmol) in methanol was prepared in the presence of DMSO as internal standard. A quantitative ^{13}C NMR spectrum and a ^{1}H–^{13}C HSQC NMR spectrum were recorded to determine the response factor of methyl lactate. Subsequently, four samples were prepared of varying amounts of methyl lactate dissolved in methanol with

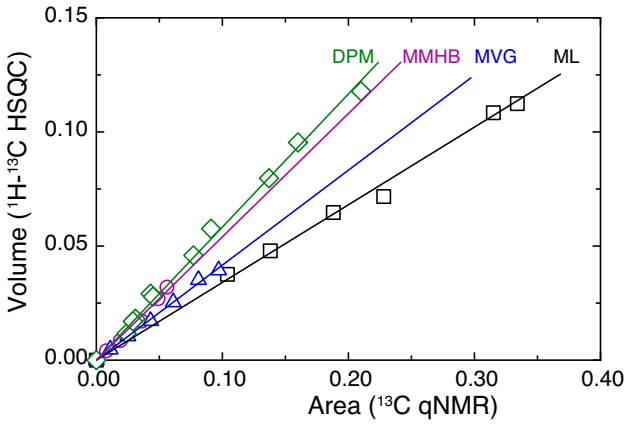

Figure 6.4: Correlations between integrals from ^{1}H–^{13}C HSQC normalised to the internal standard (DMSO) integral and quantitative ^{13}C NMR integrals normalised to internal standard. Correlations and linear regressions are shown for four selected products of the Sn-Beta catalysed xylose conversion in methanol. [89]

DMSO as the internal standard. The amounts of methyl lactate were determined gravimetrically. Quantification with ^{1}H–^{13}C HSQC NMR was performed using the response factor calculated with a single independent calibration sample and was compared to gravimetric determinations (Figure 6.5A) and to quantification by more time consuming ^{13}C qNMR (Figure 6.5B).

Linear regression between ^{1}H–^{13}C HSQC and gravimetric determinations yielded a Pearson correlation coefficient of 0.9995 and a slope of 0.998. Linear regression between ^{1}H–^{13}C HSQC and quantitative ^{13}C NMR determinations yielded a Pearson correlation coefficient of 0.9997 and a slope of 1.016. Overall, comparison of the ^{1}H–^{13}C HSQC determinations using response factors with gravimetric and quantitative NMR determination show excellent consistency.

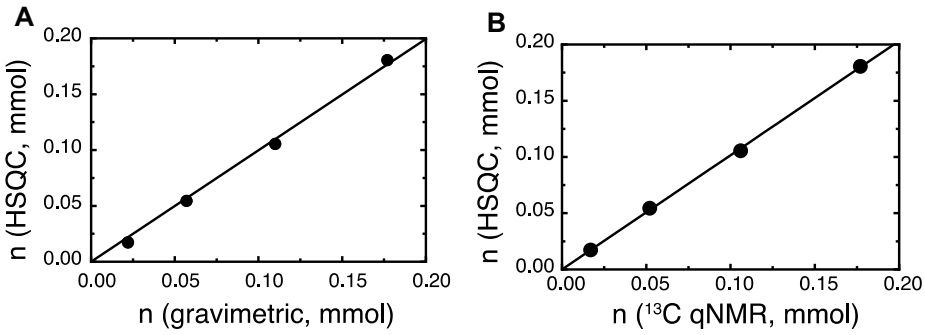

Figure 6.5: Comparison of methyl lactate amounts determined by ^{1}H-^{13}C HSQC with gravimetric analysis (A) and with quantitative ^{13}C NMR analysis (B). [89]

6.2.2 Rationalisation of Response Factors

Due to the chemical similarity of the compounds tested and the signals employed for quantification (all signals are secondary alcohols in α-hydroxy esters), the difference in the resulting response factors cannot be rationalised by variations in structural parameters, such as scalar couplings. Measurement of ^{1}H-^{13}C scalar couplings were performed to confirm their similarity (Figure 6.6). The couplings were all measured to be between 146 and 147 Hz, too similar in size to have any significant influence on the determined response factors.

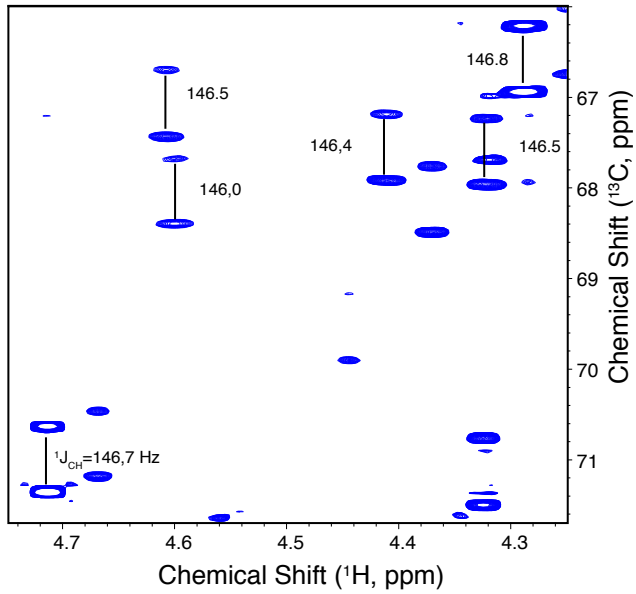

Figure 6.6: Contour plot of a ^{1}H–^{13}C HSQC spectrum recorded without ^{1}H decoupling during the ^{13}C evolution time. Only small variation (and highly similar ^{1}H–^{13}C magnetization transfer efficiency) exists for different α-hydroxy esters.[89]

On the other hand, comparison of the response factors to molecular mass displayed a linear correlation (Figure 6.7). This correlation indicates that the difference in response factor may be due to the smaller molecules having longer T_1 relaxation times, and that the inter-scan delays of one second, used to reduce analysis time, were insufficient to allow full relaxation of the smaller molecules. When a new analysis was subsequently performed with a longer T_1 relaxation time (15 seconds), the response factors normalised towards a value of approximately 0.33 (Figure 6.8). This change confirmed that an insufficiently long relaxation delay was the source of variations in response factors. A response factor of 0.33 is expected, as the analytes have a CH group while the internal standard has a CH_3 group leading to three times the number of C-H pairs and thereby three times the signal contribution.

The effect of molecular weight on response factors opens new analytical opportunities. In a case, where an unknown compound is analysed, it would be possible to predict the

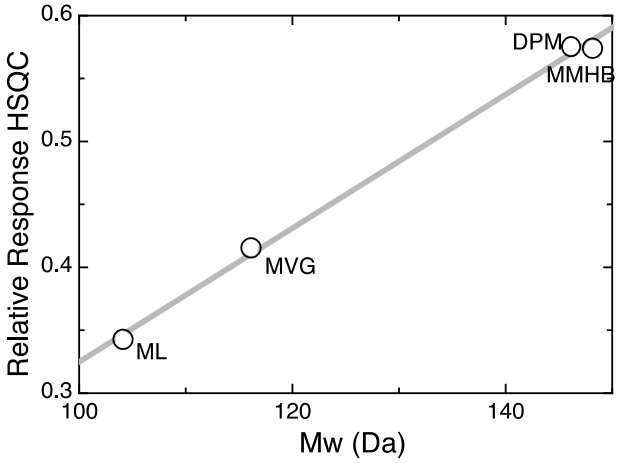

Figure 6.7: Response factors as a function of molecular weight when using inter-scan recycle delays of 1 sec.[89]

molecular weight, based on the compounds response factor. There are of course certain conditions: The compound must possess a CH pair to be detectable by ^{1}H–^{13}C HSQC. The scalar CH coupling of the unknown substrate must be similar to the reference compounds, which will typically require that they possess similar functionality. As NMR is typically good at structure determination, by which the molecular mass may also be determined, this may initially seem like an unnecessary method. However, if the molecule in question is very small and/or possesses a high number of heteroatoms, the determination of molecular mass may be very useful for structure determination. Reversely, response factors may be predicted from molecular weight according to the correlation shown in Figure 6.7).

6.2.3 Accelerated Data Acquisition

The acquisition time of the 2D NMR spectra were optimised by two methods. The first was to reduce the spectral width, resulting in a "magnification" of a spectral range (Figure 6.9A). As the spectrum is smaller it required less time to produce at high resolution. The second method demonstrated was non-uniform sampling. Here, a reduced number of data-points were acquired in the ^{13}C dimension and a mathematical model was then employed to compute the Fourier Transformation in the second dimension. The amount of data acquired was reduced by simulating some of the data-points computationally and thereby reducing analysis time with little loss in spectral resolution (Figure 6.9B) Both these methods are highly efficient for 2D NMR, because the vast majority of a 2D spectrum does not contain any signals.

The spectra of Figure 6.9 show that high resolution spectra can be acquired within 5 minutes by employing these techniques. The lower limit of detection obtained in the experiment was 0.3 mM corresponding to 0.07 mol%. Hence, the qNMR approach proposed here emerges as a rapid, accurate means of quantifying complex reaction mixtures.

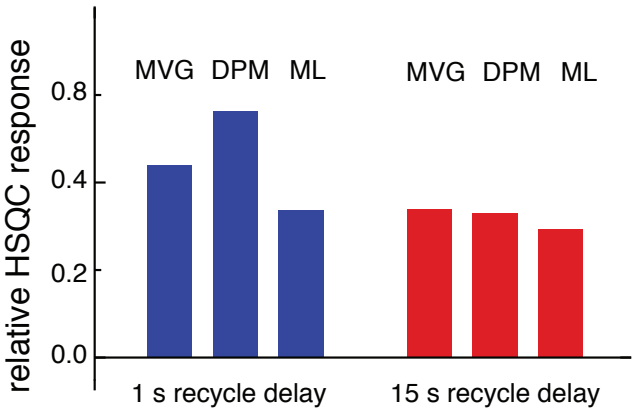

Figure 6.8: ^{1}H–^{13}C HSQC response factors for the indicated α-hydroxy esters when using inter-scan recycle delays of 1 s and 15 s, respectively. Complete ^{1}H relaxation leads to more homogeneous response factors near 0.33 relative to DMSO.[89]

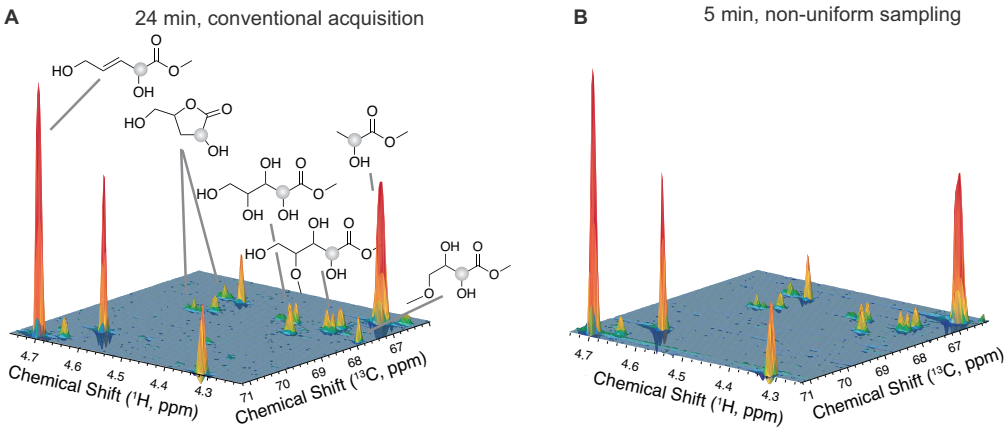

Figure 6.9: ^{1}H–^{13}C HSQC spectra obtained by a conventional (A) method employing 24 min acquisition time, and a non-uniform sampling method (B) using 5 min acquisition time. Reaction conditions: 360 mg D-xylose (8.3 wt%), 90 mg Sn-Beta (2.1 wt%), 5 mL methanol and 50 mg DMSO as internal standard, for 2 h at 160 °C and with 600 rpm stirring

7 | Optimising Operational Conditions

Upon identification of new compounds with potential for commercial applications it is essential to optimise reaction selectivity and yields to create the strongest business case possible. With the aim of improving control of reaction selectivity between the three major product pathways, acetalisation, retro-aldol and dehydration, the effect of different reaction parameters on product selectivity was assessed. Additionally, these results could lead to improved insight into the reaction system and mechanisms taking place. In the following sections the effects of temperature, catalyst framework and metal species, reactant and solvent were studied.

7.1 Optimisation in Methanol

7.1.1 Optimisation of THM Formation from Hexoses[†]

The identification of new reaction products from hexoses lead to attempted re-optimisation of the Lewis acid catalysed conversion of hexoses, with focus on formation of the double dehydration product THM rather than methyl lactate (Table 7.1). These optimisations encompassed four reaction parameters: the substrate, the catalyst framework, the catalyst metal species and the reaction temperature. Of these parameters, the substrate was observed to have the least effect on the reaction selectivity (Table 7.1, entries 5-10). The reaction was robust towards changes in substrate stereo chemistry, as well as changes between ketose and aldose substrates, demonstrating the strong isomerisation capacity of the catalyst. A slight benefit was observed with the use of fructose, obtaining up to 18% of the new THM product. Fructose likely benefits from formation of fewer stable methyl glycopyranosides, due to a larger natural occurrence of furanosides in when fructose is in solution.

Temperature experiments showed that higher temperatures favoured retro-aldol cleavage while lower temperatures benefited glycoside formation (Table 7.1, entries 1-4). Meanwhile, double dehydration and triple dehydration products showed a discrete optimum at 160 °C and 140 °C, respectively. From these results it appears that dehydration benefits from higher temperatures, but is out-competed by reto-aldol cleavage, which also benefits from the temperature elevation.

Variation of the catalyst metal species to other Lewis acidic metals clearly displayed tin's superior properties for the dehydration reactions. Use of a Brønsted acidic aluminium zeolite resulted in high formation of the triple dehydrated furanic species, a possible indicator that both a Brønsted acidic and a Lewis acidic pathway to these products may exist. Meanwhile, control reactions with dealuminated Al-Beta and Si-Beta showed the expected lack of activity, as did SnO_2-Beta. The more defect free, hydrothermally synthesised Sn-Beta showed a similar but slightly higher selectivity for THM than the

[†]This section is adapted from Tolborg *et al.*, *Green Chem.*, 2016, **18**, 3360–3369.

Table 7.1: Conversion of hexoses using a selection of Beta-framework and/or tin containing catalysts at 120-180 °C

Entry	Catalyst	Substrate	Temperature	Glycosides	Retro-aldol	Dehydration	
						Double	Triple
			°C	%	%	%	
1	Sn-Beta (PT)	Glucose	120	44	4	8	10
2	Sn-Beta (PT)	Glucose	140	21	10	12	16
3	Sn-Beta (PT)	Glucose	160	13	17	14	13
4	Sn-Beta (PT)	Glucose	180	5	26	8	10
5	Sn-Beta (PT)	Fructose	160	9	19	18	14
6	Sn-Beta (PT)	Mannose	160	12	20	15	12
7	Sn-Beta (PT)	Sorbose	160	13	15	17	14
8	Sn-Beta (PT)	Galactose	160	26	10	12	13
9	Sn-Beta (PT)	Tagatose	160	11	11	9	18
10	Sn-Beta (PT)	Sucrose	160	10	22	15	13
11	Sn-Beta (HF)	Glucose	160	8	24	16	9
12	Zr-Beta (HF)	Glucose	160	27	25	2	2
13	Ti-Beta (HF)	Glucose	160	14	28	3	3
14	Hf-Beta (HF)	Glucose	160	35	18	4	8
15	Al-Beta	Glucose	160	32	<1	<1	14
16	deAl-Beta	Glucose	160	86	<1	<1	<1
17	Si-Beta (HF)	Glucose	160	46	3	<1	3
18	Sn-MCM-41	Glucose	160	16	26	18	13
19	Sn-MFI	Glucose	160	40	8	<1	<1
20	SnO2-Beta (HF)[a]	Glucose	160	37	1	<1	2

The standard reaction conditions employed were 360 mg substrate (8.3 wt%), 4 g methanol, 180 mg catalyst, for 6 h at 160 °C and with 600 rpm stirring. Yields (carbon%) of methyl glycosides, combined yields of ML, MVG, MMHB and GA-DMA (retro-aldol), yields of THM (double dehydration) and combined yields of HMF, MMF and F-DMA (triple dehydration products) from the conversion of hexose sugars, using a variety of temperatures (1-4), sugars (5-10) and catalysts (11-20). a) Dispersed SnO_2 nanoparticles on Si-Beta.

post-treatment synthesised catalyst. Two alternative frameworks were tested, Sn-MCM-41 with larger pores (45 Å) and Sn-MFI with smaller pores (5.6 Å) than Sn-Beta (6.7 Å). Sn-MCM-41 showed activity similar to Sn-Beta, pointing to limited shape selectivity effects. However, the Sn-MFI showed almost no activity, indicating that the pores were too small for the substrate diffusion. A glucopyranose molecule (the most abundant form of glucose in solution) has an estimated diameter of 5.5-6.2 Å (simulated in Chem3D, PerkinElmer), which is slightly larger than the the pores of a MFI zeolite, consistent with the observed results.

In summary, the optimal conditions for double dehydration (formation of THM) of fructose or glucose were found at 160 °C using a Sn-Beta or Sn-MCM-41 zeolite catalyst in order to avoid substrate diffusion limitations.

7.1.2 Optimisation of DPM Formation from Pentoses[†]

This process of optimisation was repeated for the conversion of pentoses to DPM, with the further addition of yields of single dehydration C5 products, DPL and TPM (Table 7.2). The trends observed for formation of DPM from pentoses coincided with those observed for THM formation from hexoses with regards to temperature, substrates, catalyst structure and metal species. Likewise, single dehydration yields followed similar patterns for pentoses and hexoses. The strong correlation between pentose and hexose selectivity supports that the same reaction pathways are present for both systems.

In addition to the previous studies, here it is demonstrated that the reaction system, comprising of xylose and Sn-Beta (HT) in methanol, is very robust towards increases in concentration. The reaction showed no significant change in product distributions upon increasing the concentration from 8.3 wt% to 23 wt% xylose. The possibility for high concentration reactions can greatly reduce purification costs and increase reactor productivity. The concentration increases were performed while keeping the substrate to catalyst ratio constant and subsequently the effect of the the catalyst/substrate ratio was assessed. Catalyst to substrate ratios of 0.5 wt/wt and higher yielded comparable reaction selectivity, and were optimal for single and double dehydration product yields. Meanwhile, lower ratios showed an increase in the yield of retro-aldol products. Formation of both glycosides and triple dehydration products showed no significant change upon variation of the catalyst to substrate ratio or variation of substrate concentrations.

7.1.3 Conclusion

Overall, it can be concluded that Sn-Beta is one of the best catalysts for both retro-aldol and dehydration reactions, and to control selectivity between retro-aldol and dehydration pathways, changes to temperature and catalyst loading have the greatest effect. Retro-aldol products are favoured by high temperatures and low catalyst loadings, while, single and double dehydration reactions are favoured by temperatures near 160-170 °C and high catalyst loadings.

[†]This section is adapted from Elliot *et al.*, *RSC Adv.*, 2017, **7**, 985–996.

Table 7.2: Conversion of pentoses using a selection of Beta-framework and/or tin containing catalysts, at varying temperature, concentration and loading.

Entry	Catalyst	Substrate	Temp.	Conc.	Loading	Glycosides	Retro-Aldol	Dehydration		
								Single	Double	Triple
			°C	wt%	wt/wt	%	%	%		
1	Sn-Beta (HT)	Xylose	140	8.3	0.5	4.4	16	23.3	31	17
2	Sn-Beta (HT)	Xylose	150	8.3	0.5	3.3	19	22	32	13.4
3	Sn-Beta (HT)	Xylose	160	8.3	0.5	4	19	23	33	11
4	Sn-Beta (HT)	Xylose	170	8.3	0.5	3	25	19.7	34	9
5	Sn-Beta (HT)	Xylose	180	8.3	0.5	3.4	24	19	32	7.7
6	Sn-Beta (HT)	Ribose	160	8.3	0.5	3	17	20.5	30	0
7	Sn-Beta (HT)	Lyxose	160	8.3	0.5	2.6	20	24.2	31	11
8	Sn-Beta (PT)	Xylose	160	8.3	0.5	23	15	15	23	17
9	Sn-MFI	Xylose	160	8.3	0.5	30	24	6	11	10
10	Sn-MCM-41	Xylose	160	8.3	0.5	23	18	20	16	20
11	Sn-SBA-15	Xylose	160	8.3	0.5	32	18	13	12	18
12	SnO2-Beta[(a)]	Xylose	160	8.3	0.5	42	3	3	<1	1
13	Ti-Beta	Xylose	160	8.3	0.5	48	22	11	<1	5
14	Zr-Beta	Xylose	160	8.3	0.5	39	25	4	<1	4
15	Al-Beta	Xylose	160	8.3	0.5	82	0	n.d.	n.d.	1
16	Si-Beta	Xylose	160	8.3	0.5	42	8	5	<1	3
17	Blank	Xylose	160	8.3	0.5	6	1	n.d.	n.d.	<1
18	Sn-Beta (HT)	Xylose	160	8.3	0.5	4	19	23.3	33	11
19	Sn-Beta (HT)	Xylose	160	15	0.5	6	17	24.37	34	8.7
20	Sn-Beta (HT)	Xylose	160	23	0.5	6	17	24.1	32	11
21	Sn-Beta (HT)	Xylose	160	8.3	0.125	3.8	32	20.19	19	14.3
22	Sn-Beta (HT)	Xylose	160	8.3	0.25	3.7	28	21.8	28	11
23	Sn-Beta (HT)	Xylose	160	8.3	0.5	4	19	23.3	33	11
24	Sn-Beta (HT)	Xylose	160	8.3	0.75	3.02	17	21.9	34	9.9
25	Sn-Beta (HT)	Xylose	160	8.3	1	3.5	15	25.1	34	10

The standard reaction conditions employed were 360 mg substrate (8.3 wt%), 4 g methanol, 180 mg catalyst, for 2 h at 160 °C and with 600 rpm stirring. Yields (carbon%) of methyl glycosides, combined yields of ML, MVG, MMHB, GA-DMA (retro-aldol), combined yields of DPL, TPM and DMPM (single dehydration), yield of DPM (double dehydration) and combined yields of furfural and furfural-DMA (triple dehydration products) from the conversion of pentose sugars, using a variety of temperatures (1-5), sugars (3,6-7), catalysts (3,8-17), concentrations (18-20) and loadings (21-25). n.d. = not detected. Refer to Chapter 5 for product abbreviations. a) Dispersed SnO_2 nanoparticles on Si-Beta.

7.2 The Effect of Solvent on Reaction Selectivity[†]

Variation of the reaction solvent is common practice in the exploration of chemical reactions, the changes to compound solubility and solvent-substrate interactions can greatly affect the selectivity of reactions. In the conversion of carbohydrates by Sn-Beta, the solvent is expected to play a particularly strong role, due to its participation as nucleophiles in the formation of esters, acetals and hemiacetals in the reaction. Previous studies have primarily employed water to form acids and methanol to form methyl esters, in this work other simple alcohols with longer and/or larger aliphatic chains are also explored.

Employing xylose as the starting substrate, reactions were conducted with water, methanol, ethanol, n-propanol, n-butanol and iso-propanol. As the solvent is participating in the reaction, different esters/acids are formed in each mixture. Despite this chemical diversity, little change is observed for the ^{13}C NMR signals of products, allowing ^{13}C NMR to identify and quantify compounds in all of the solvents employed (Figure 7.1).

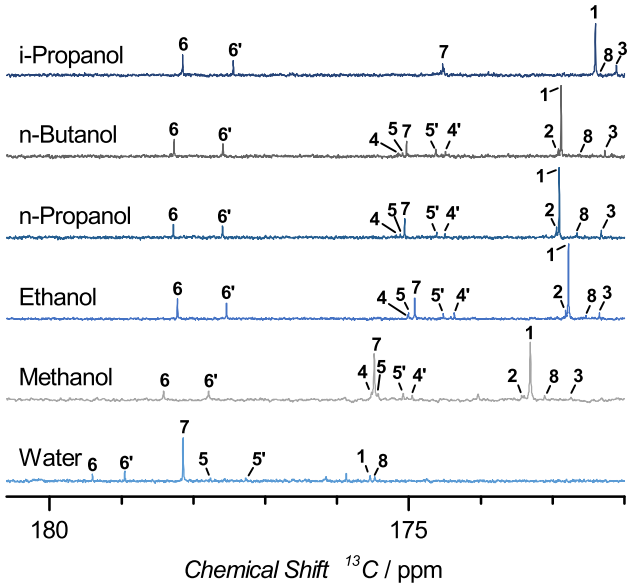

Figure 7.1: ^{13}C NMR spectra after converting 360 mg D-xylose with 180 mg Sn-Beta in 5 mL solvent. The carbonyl spectral region is shown and signals are assigned to the respective solvent equivalents of 1. trans-DPM, 2. cis-DPM, 3. cyclo-DPM, 4. DMPM, 5. TPM, 6. DPL, 7. ML, 8. MVG; an apostrophe denotes the diastereomer of a compound. Chemical shifts are relative to deuterated methanol (added to 10% v/v) set to 47.85 ppm for all solvents.

The resulting product distributions are displayed in Figure 7.2. Here, it is observed that the yield of retro-aldol products is diminished by increasing the size of the solvent alkyl group, starting as the major product in water (20%) and becoming a minor product in almost all other solvents. The opposite effect is observed for yields of the 3,4-dideoxy esters, which benefit from larger solvent groups, progressing from the minor product in

[†]This section is adapted from Elliot *et al.*, *ChemSusChem*, 2017, **10**, 2990–2996.

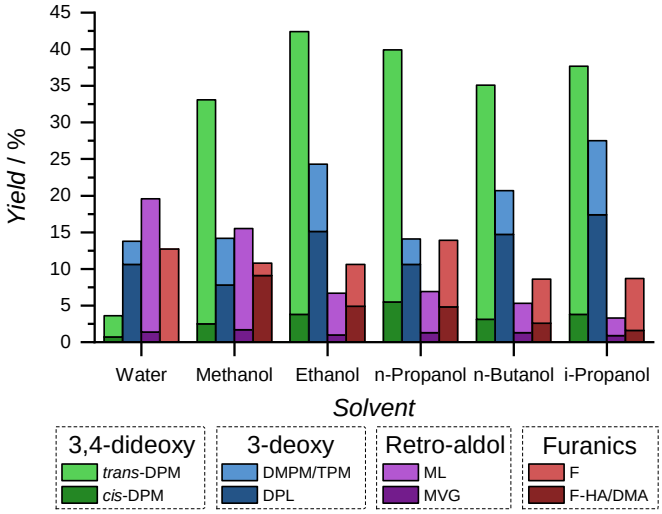

Figure 7.2: Product distribution of reactions in alcohols or water. The reactions were conducted with 180 mg Sn-Beta, 360 mg D-xylose, 5 mL solvent and 50 mg DMSO as internal standard, and run for 2 hours at 160 °C with 600 rpm stirring. An experimental uncertainty within ±1% was achieved in all cases. Legend abbreviations for the methyl products are used, although the corresponding solvent alkyl or acid equivalents are formed.

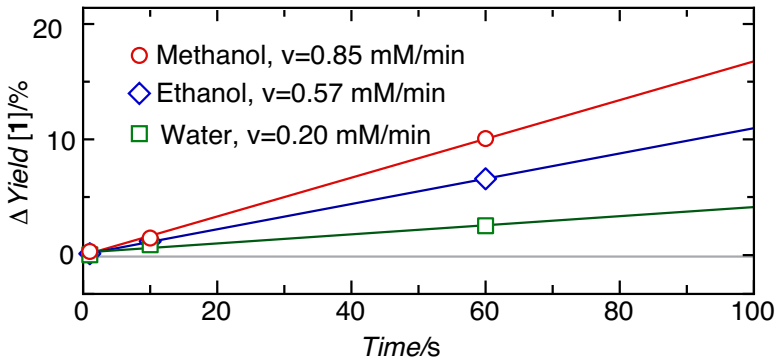

Figure 7.3: Initial rate of formation for 3,4-dideoxy esters/acids in methanol, ethanol and water.

water (4%) to the major product in all alcohols with the highest recorded yield in ethanol (42%). Although the trends from water to methanol to ethanol appear clear, selectivity in larger alcohols appears more unpredictable, showing yields generally distributed between those observed in methanol and ethanol, which can be indicative of multiple effects simultaneously influencing reaction selectivity.

Further insight was sought into the change in selectivity between methanol, ethanol and water, by measuring initial rates of formation for 3,4-dideoxy ester formation (Figure 7.3). Water showed the lowest rate of formation, which could be expected as it also has the lowest 3,4-dideoxy acid selectivity. Ethanol, which produced the highest 3,4-dideoxy ester yields, had only the second fastest rate of formation, which was 33% lower than that of methanol. These results may be interpreted to suggest that ethanol is suppressing side reactions rather than enhancing the formation of 3,4-dideoxy esters.

7.2.1 Temperature Variations

Variation of reaction temperature in ethanol was performed in an attempt to further improve the maximum obtainable yield of DPE. Further beneficial effects on the yield of DPE were not obtained by temperature variation (Figure 7.4), which displayed a broad optimum in the range of 140 °C and 160 °C, values slightly lower than the methanol optimum from 160 °C to 180 °C (Table 7.2 on page 48). Overall product distributions showed little change in the tested range, with the greatest change observed for the DPE, which varied from 36-42% yield.

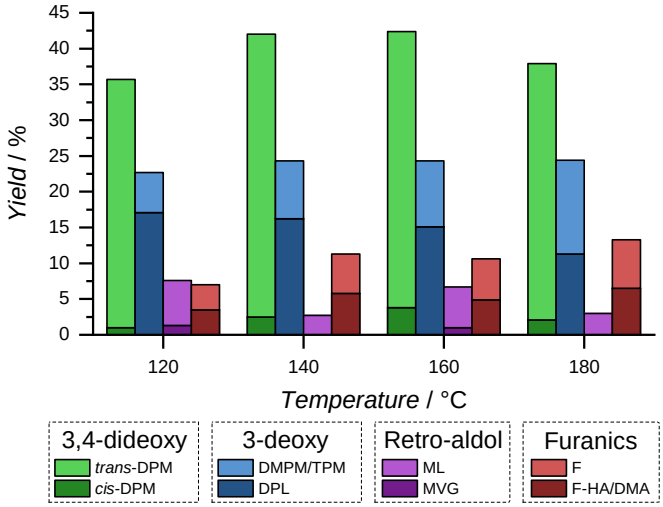

Figure 7.4: Product distribution upon temperature variation of reactions conducted in ethanol. Reaction conditions: 360 mg D-xylose, 180 mg Sn-Beta and 5 mL ethanol with 50 mg DMSO as internal standard, reactions were run for 2 h at the selected temperature. Legend abbreviations for the methyl products are used, although the ethyl equivalents are formed.

7.2.2 The Effect of Ethanol on THE Formation from Glucose

The beneficial effect of ethanol over methanol in the formation of *trans*-DPE was also tested for the formation of *trans*-THM/THE from glucose. Experiments showed a similar beneficial effect of ethanol in the formation of *trans*-THE. NMR analysis of the olefinic region of *trans*-THM/THE (Figure 7.5) showed 25% higher formation of *trans*-THE in ethanol than *trans*-THM in methanol, which is roughly equivalent to the increase observed from DPM to DPE (Figure 7.2). In contrast, a significant drop in alkyl lactate (major retro-aldol product) is observed, declining from 31.5% in methanol to 12.6% in ethanol.

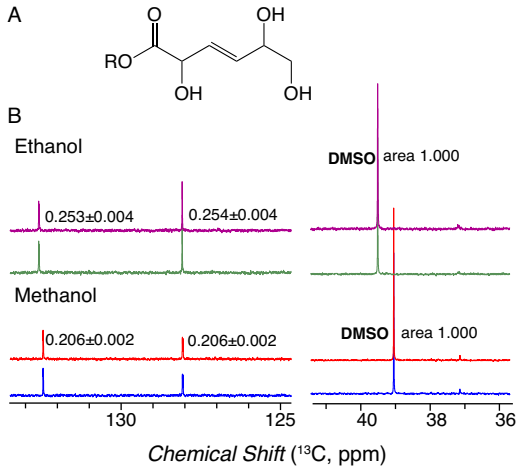

Figure 7.5: (A) Structure of the C6 analogue of *trans*-DPM, trans-2,5,6-trihydroxy-3-hexenoic acid methyl ester (*trans*-THM). (B) Spectral comparison of the areas of the olefinic carbon shifts of *trans*-THM/THE in ethanol and methanol reaction solvents. Duplicate samples are shown, including errors of determination of signal areas relative to DMSO as an internal quantification standard. Reaction conditions: 360 mg D-glucose, 180 mg Sn-Beta, 5 mL ethanol or methanol and 50 mg DMSO as internal standard, reactions were run for 2 hours at 160 °C with 600 rpm stirring.

8 | Alkali Effect

The addition of alkali has previously been shown to greatly affect reaction selectivity in the conversion of hexoses by stannosilicates.[54,60,68,91] Here, the aim was to improve the understanding of the alkali effect, and in doing so obtain the capability to further control reaction selectivity, thereby creating an optimised and reproducible process. This process involves expansion of the number of products monitored, comparison of both yields and reaction rates, distinction of anion and cation effects, and comparing reaction effects with measured changes in the catalyst.

8.1 Alkali Concentration vs Product Yields[†]

The effect of alkali salts on the product distributions of both hexoses and pentoses follows the same general trend (Figure 8.1). It can be seen that dehydration products, be that single, double or triple dehydration, are reduced in yield by the addition of alkali salts. In contrast, retro-aldol products, products involving the breaking of a carbon-carbon bond, benefit from the addition of alkaline salts up to a specific optimum. Above this optimum concentration of alkali salt, the yields of retro-aldol products also drop significantly.

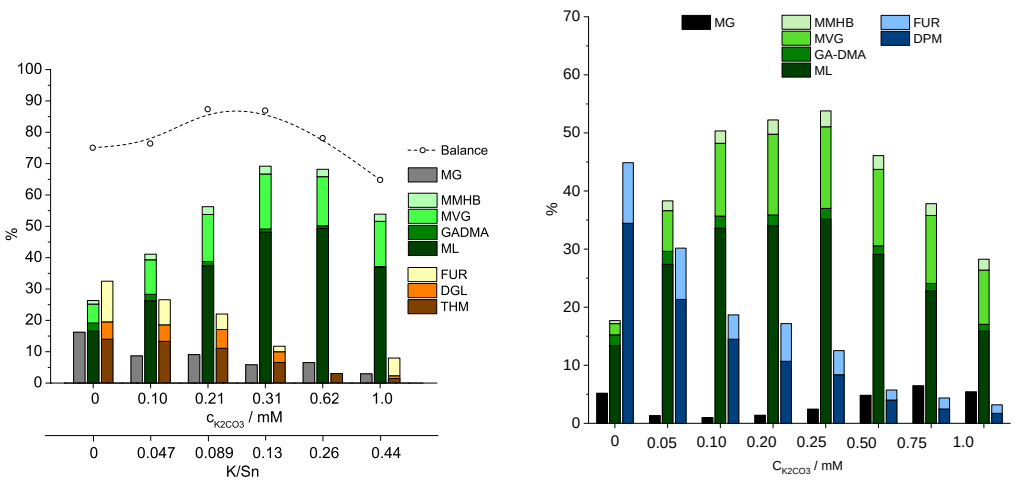

Figure 8.1: The effect of alkali on the product distributions from hexoses using a Sn-Beta (PT) catalyst (left, this figure was made by Dr Søren Tolborg) and pentoses using a Sn-Beta (HT) catalyst. Reaction conditions: 360 mg substrate, 180 mg Sn-Beta (PT, Si/Sn = 125 or HT, Si/Sn = 150), 5 mL of a solution with 0 – 1.0 mM K_2CO_3 in methanol, 160 °C.

[†]This section is adapted from Elliot *et al.*, *RSC Adv.*, 2017, **7**, 985–996., Tolborg *et al.*, *Green Chem.*, 2016, **18**, 3360–3369. and Elliot *et al.*, *ChemSusChem*, 2018, **11**, 1198-1203.

The optimum appears to shift to slightly lower concentrations in the pentose system, where a Sn-Beta (PT) catalyst is used. However, any decisive conclusions remain elusive as the HT and PT catalysts also have slightly different tin loadings. In the hexose system, methyl glycosides contribute significantly to the product yields, and the addition of alkali is seen to be very beneficial in suppressing their formation.

Initial rates are also affected by changes in the alkali salt concentration (Figure 8.2). Stepwise concentration change in basic alkali salts (Figure 8.2), exhibit trends closely resembling the trends observed for product yields (Figure 8.1), consistent with kinetic reaction control. All quantified products show decreasing initial rates of formation with increasing salt concentrations, with the exception of methyl lactate, which has an optimum concentration at approximately 0.3 mM potassium carbonate. Changes to the reaction rate and the reaction selectivity can be interpreted as alkali modifying the catalytic properties of the catalyst active site to favour methyl lactate formation.

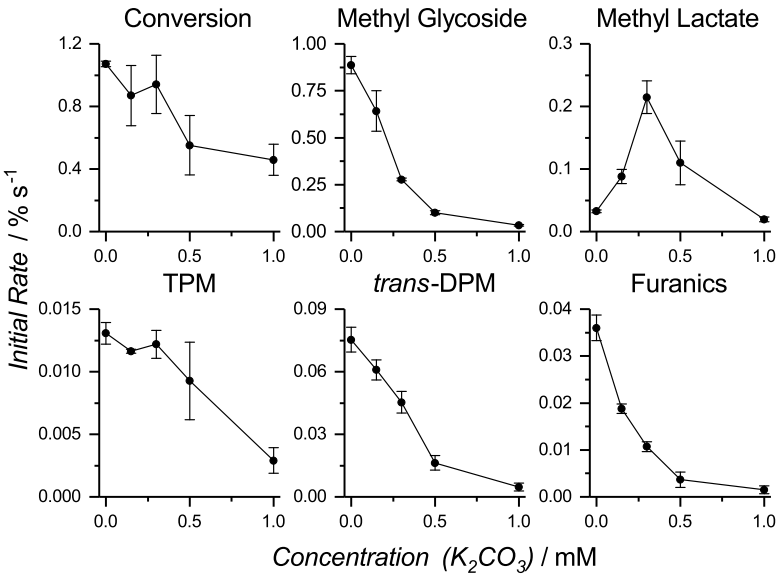

Figure 8.2: Initial rates of conversion and of formation for different compound classes as a function of K_2CO_3 concentration. Reaction conditions: 360 mg D-xylose, 90 mg Sn-Beta (PT), 5 mL methanol, and 50 mg DMSO at 160 °C.

8.2 Alkali Counter-ion†

The anion of the alkali salt has a very profound effect on the optimum concentration for methyl lactate formation. The anions form two groups following one of two trends (Figure 8.3), one with a sharp optimum characterized by a basic anion, and the other a exponential trend with a flat optimum at high concentrations, characterized by a neutral

†This section is adapted from Elliot *et al.*, *ChemSusChem*, 2018, **11**, 1198-1203.

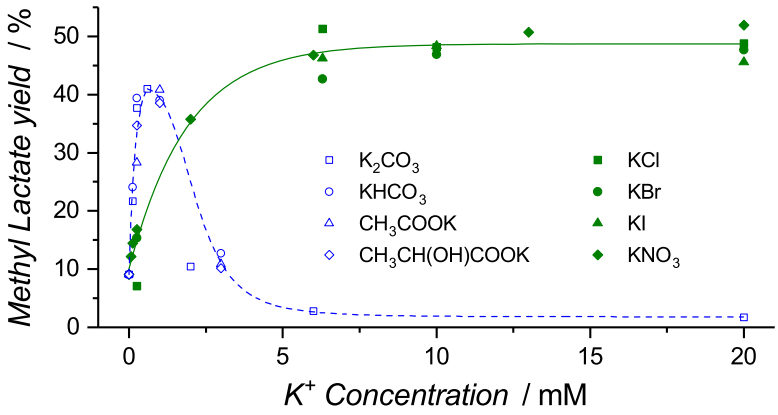

Figure 8.3: Methyl lactate yield as a function of potassium concentration for various salts of strong acids (filled green symbols) and salts of weak acids (open blue symbols). Reaction conditions: 250 mg glucose, 100 mg Sn-Beta (HT), 5 mL methanol (5 mL), 120 °C, 19 h. The experimental work and figure were produced by Dr. Søren Tolborg.[92,93]

anion. This finding indicates that part of the alkali salt effect observed in Figure 8.1 may also be an acid-base effect, due to the use of potassium carbonate.

8.2.1 The Effect of Anions on Initial Rates

The effect of the alkali ion and counter anions is also prevalent in the initial rates of formation of the reaction products (Figure 8.4). Reaction rates were determined at reaction times below 30 sec where the reaction is not limited by the substrate concentration, and thereby a pseudo-first order reaction, depending only on the catalyst concentration, was obtained.

The formation of methyl glycosides is largely unaffected by neutral salts, but greatly affected by basic salts. The apparent mechanism of methyl glycoside formation is acetalisation, a reaction commonly considered to be Brønsted acid catalysed. Addition of a basic salt may reduce the amount of free acid and thus result in a drop in reaction rate (and also yield when there are unaffected competing reactions), as is observed. Meanwhile the lack of effect of neutral salts indicates that alkali ions and Lewis acid sites do not play a great role in the formation of glycosides.

The same pattern is observed for the formation of furanic compounds (triple dehydration products); Basic salts greatly inhibit formation of furanics, while the neutral salts only show a slight inhibitory effect. Once again reduction of Brønsted acidity may be the explanation. It has previously been demonstrated that furfural (or HMF) may be formed by Brønsted acid catalysed dehydration of ketoses i.e. xylulose and fructose.[94–97] This is an important observation in relation to the development of a reaction mechanism. Despite our studies indicating that HMF may readily be formed from commercial 3DG, these results indicate that in a reaction mixture the primary source of furanics is most likely Brønsted acid catalyst dehydration of ketoses not proceeding *via* an intermediate resembling 3DG.

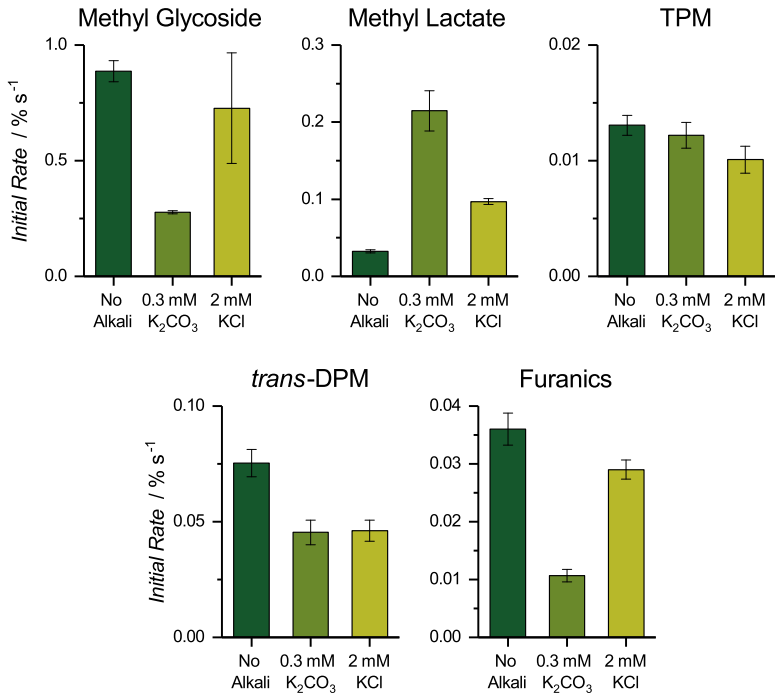

Figure 8.4: Overview of the effects of KCl and K_2CO_3 on the formation rates for the designated products. Errors are calculated based on a linear fit of experimental data points. Reaction conditions: D-xylose (360 mg), Sn-Beta (PT) (90 mg), methanol (5 mL), and DMSO (50 mg) at 160 °C. The designated amounts of K_2CO_3 and KCl were dissolved in the methanol solvent prior to reaction.

The formation of TPM and *trans*-DPM (single and double dehydration products) show no significant difference between the effect of a neutral and a basic alkali salt (Figure 8.4), but a detrimental effect of both. Based on this observation, the formation of TPM and DPM must largely follow the same Lewis acid catalysed pathway, one distinctly different to that towards furfural. In contrast, the rate of methyl lactate formation follows the inverse trend of glycoside and furanic formation rates, benefitting from both low Brønsted acidity and potassium ion exchange.

8.3 Catalyst Titration with Alkali Salts[†]

Previously, the effect of alkali salts has been shown by systematic variation of the alkali additive.[60] In this study, in addition to varying the amount of alkali salt, the tin content in the Sn-Beta catalyst was also varied (Figure 8.5). The catalysts were all synthesized from the same batch of dealuminated Al-Beta by the same post-treatment method.[‡] The only change in the procedure was the amount of tin(IV)chloride that was used for impregnation, which was adjusted to obtain nominal Si/Sn ratios of 25, 50, 100, 150, 200 and 400. The catalysts were tested in a reaction containing 360 mg D-glucose, 90 mg Sn-Beta, 55 mg DMSO (internal standard) and 5 mL methanol with pre-dissolved potassium carbonate, and using a separate experiment for each data-point (Figure 8.5). Reactions were conducted in a microwave reactor at 160 °C for 4 hours to ensure full conversion even with low tin-content catalysts. The reaction performance was evaluated primarily based on methyl lactate yields, as methyl lactate has previously shown the most interesting and significant effects (Figure 8.5).

Each catalyst yield showed a distinct optimum potassium concentration for formation of methyl lactate. Increasing tin content results in the optimum shifting towards higher potassium concentrations. This trend points to a correlation between the amount potassium and the amount of tin. To enable quantitative evaluation of this correlation, the optimum potassium concentration for methyl lactate formation was determined relative to the Si/Sn ratio (Figure 8.6). A close linear correlation was observed for catalysts with nominal Si/Sn ratios between 50 and 400, while high tin content (Si/Sn 25) lead to deviation from linearity.

XRD indicated that the high tin loading (Si/Sn 25) catalyst contains large amounts of extra-framework tin oxide, in contrast to the other catalysts. Tin oxide is known to be catalytically inactive, but will contribute to catalyst tin and may be the cause of this deviation. NH_3-TPD was employed to obtain a quantitative assessment of catalytically active tin sites (Figure 8.7).

The catalysts in the range of 50-200 Si/Sn had comparable desorption of ammonia per tin. Meanwhile, the Si/Sn 25 exhibited a 35% drop in the ammonia per tin, consistent with increased presence of catalytically inactive tin sites as expected from the presence of extra-framework tin oxide. The Si/Sn 400 catalyst exhibited a large increase in ammonia desorption per tin, however, due to the very weak TPD signal at such low tin contents the value may be unreliable. As such, the Si/Sn 400 catalyst was omitted from further

[†]This section is adapted from Elliot *et al.*, Alkali Ion Titrations of Sn-Beta Active Sites Provide Insight into Structure-Activity Relations

[‡]The catalysts were synthesised by PhD student Irene Tosi, Department of Chemistry, DTU.

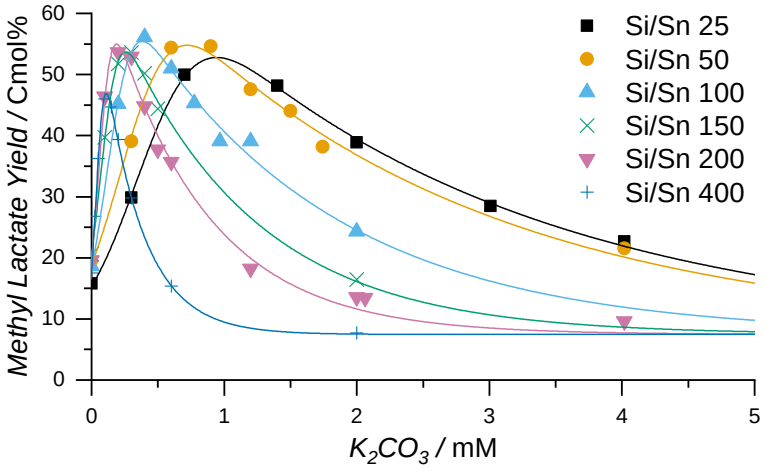

Figure 8.5: Methyl lactate yield from glucose at varying concentrations of potassium carbonate using Sn-Beta (PT) catalysts with different tin contents. The curves are a guide to the eye. Reaction conditions: 360 mg D-Glucose, 90 mg Sn-Beta, 55 mg DMSO (internal standard) and 5 mL methanol with potassium carbonate, reacted for 4 hours at 160 °C.

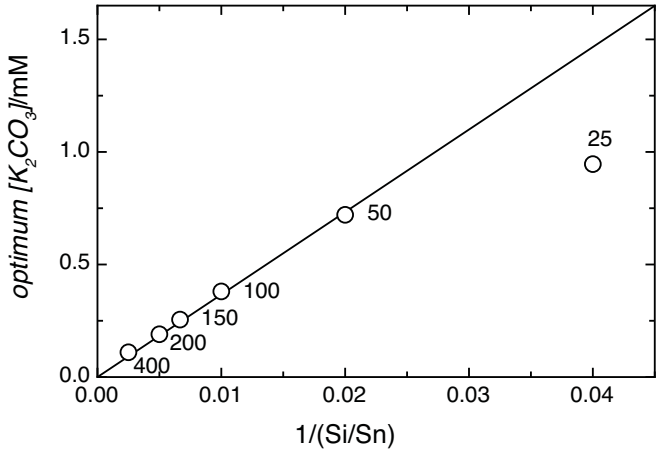

Figure 8.6: Optimum potassium carbonate concentration for methyl lactate formation as a function of tin content determined by elemental analysis, indicating a linear correlation between framework tin and alkali. Reaction conditions: 360 mg D-Glucose, 90 mg Sn-Beta, 55 mg DMSO (internal standard) and 5 mL potassium carbonate in methanol, reacted for 4 hours at 160 °C.

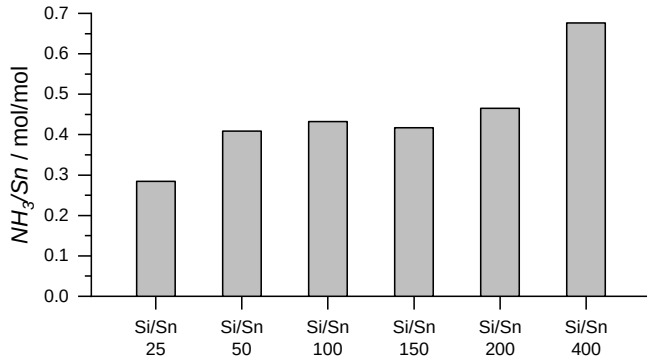

Figure 8.7: Ammonia desorption per tin (mol/mol) of Sn-Beta catalysts with tin loadings from 25 to 400 Si/Sn. Values were determined by integration of the NH_3-TPD absorption/desorption peak at 255 °C.

interpretations.

The results of Figure 8.5 were normalised to the measured ammonia absorption, leading to alignment of the methyl lactate yields for the different catalysts (Figure 8.8). The catalysts in the range of Si/Sn 25-200 now show a single optimum at approximately K/NH_3 = 0.6 mol/mol. Most importantly, it may be concluded that optimal alkali concentrations for a Sn-Beta catalyst with a Si/Sn ratio of 25-200 (synthesized by the post-treatment method) may be predicted from catalyst characterization by NH_3-TPD, omitting the need for empirical optimisation of each new catalyst.

8.3.1 A Two-Step Titration Model.

Observed product selectivities upon alkali addition show three selectivity regimes. The first regime shows a high propensity for dehydration and is predominant when no alkali is present. The second regime is responsible for formation of retro-aldol products and is most strongly expressed at the optimum alkali concentration for methyl lactate formation. The last regime is inactive for formation of both dehydration and of retro-aldol products and predominates at high alkali concentrations.

As the transition between these regimes is induced by addition of alkali, the transition may be described as a two-step titration (equation 8.1), where $X(OH)_2$, X(OH)OK and $X(OK)_2$, are the protonated, single alkali exchanged and double alkali exchanged states, respectively, and k1 and k2 are dissociation constants.

$$X(OK)_2 \overset{k_1}{\rightleftarrows} X(OH)OK \overset{k_2}{\rightleftarrows} X(OH)_2 \tag{8.1}$$

The titration of two sites of different acidity was modelled by fitting all data points (from Figure 8.8) to a $[K^+]$-dependent double dissociation model (Figure 8.9, blue). The model shows good consistency with the experimental data and the residual error of the model can be attributed to the simplicity of the model, as the model does not account for possible structural inhomogeneities, alkali exchange positions or catalyst pore confinement effects.

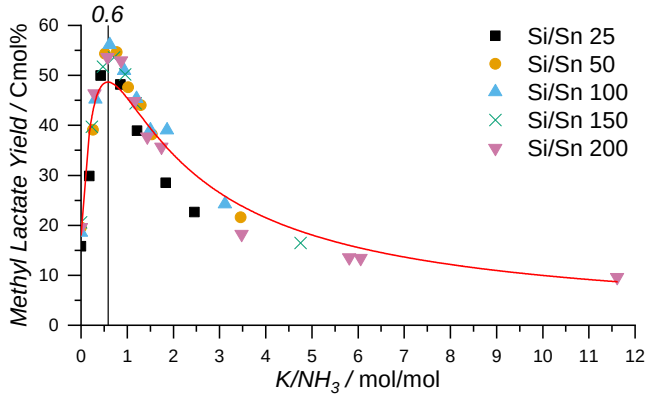

Figure 8.8: Effect of addition of potassium carbonate on methyl lactate yield in the catalytic conversion of glucose by Sn-Beta containing different amounts of Sn. The yields are displayed relative to the K/NH_3 ratio determined by NH_3-TPD, thus excluding inactive/inaccessible tin. The line shows a double dissociation model fitted to the data from the Si/Sn 25 to 200 catalysts.

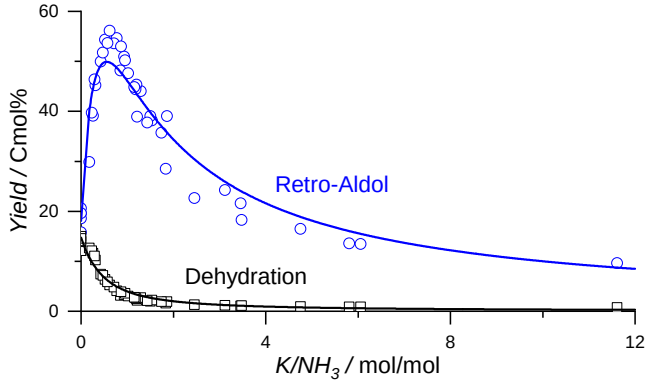

Figure 8.9: Fitting of methyl lactate yields to a $[K^+]$-dependent double dissociation model (blue), demonstrating the optimal regimes for retro-aldol product formation, and fitting of THM yields to a corresponding double dissociation model (black), to show the dehydration regime. Data points from catalysts with Si/Sn 25 to 200 were employed, normalized to the number of Sn-active sites using NH_3-TPD. The fit of THM yields only varies the selectivity of the three different sites, but employs dissociation constants obtained from the alkali-dependence of methyl lactate yields.

From this model the first dissociation constant is determined to 1.11 (normalized to ammonia) almost three fold higher that the second dissociation constant which is 0.44 (normalized to ammonia). These values were then used to fit the same model to data from the dehydration product THM (Figure 8.9, black), which also showed excellent agreement between model and data. The model predicts 0% selectivity for the double alkali exchanged site to both products. More interesting is the single alkali exchanged site, which the model predicts to have >70% selectivity towards methyl lactate. This is of course providing that the single alkali exchanged site may be completely isolated. Nonetheless, the results are reasonably consistent with literature where optimised Sn-Beta systems have achieved up to 72% methyl lactate from sucrose.[60]

8.3.2 Catalyst Structure Elucidation by FT-IR†

The linear correlation between alkali and tin content points to a stoichiometric effect on the tin active site. To substantiate this stoichiometric effect, the catalyst was characterised by FT-IR and using CD_3CN as probe molecule both in the presence and the absence of alkali. Samples of the Si/Sn 100 catalyst were impregnated with solutions of 0.4 and 3.0 mM potassium carbonate, filtered and dried at 120 °C, to simulate the ion exchange occurring in the reaction solution at and above optimum alkali content, respectively. A unmodified catalyst sample (K/NH_3 at 0) was characterised along with the impregnated samples (K/NH_3 at 0.59 and 4.43).

FT-IR of these samples showed distinct changes to the O-H region of the spectrum (Figure 8.10). The O-H stretch of terminal silanols at 3735 cm^{-1} and the O-H stretch of hydrogen-bonded silanols with weak Brønsted acidic character at 3696 cm^{-1} were both significantly decreased by addition of alkali, with the latter completely eliminated at high concentration.[49] These observations corroborate our previous assertion of the exchange of protons with potassium.

Absorption of CD_3CN probe molecules shows a change in the binding affinity of the three catalysts (Figure 8.11A-C). Based on the ratio between the peaks at 2310 cm^{-1} (CD_3CN adsorbed on tin) and at 2275 cm^{-1} (CD_3CN adsorbed on silanol groups), the unmodified catalyst first absorbs CD_3CN to the tin site, which has the strongest binding affinity, and thereafter to the silanol groups (Figure 8.11A). As alkali is added, the binding affinity of the tin sites is decreased and at high alkali content is exceeded by the silanol binding affinity (Figure 8.11C).

Likewise, after desorption under vacuum at room temperature for one hour, the tin to silanol ratio increases, also showing that tin has a stronger binding affinity for CD_3CN than silanols (Figure 8.11D). When comparing the samples with and without alkali it is also clear that the binding affinity of tin is decreased by alkali, a clear indicator that the tin active site is being modified.

8.3.3 Three Catalyst States

From combined structural and activity data, we propose a correlation between the active site and product yields as depicted in Figure 8.12. Here, the initial protonated site

†The experimental data in section 8.3.2 were provided by PhD Student Irene Tosi, Department of Chemistry, DTU

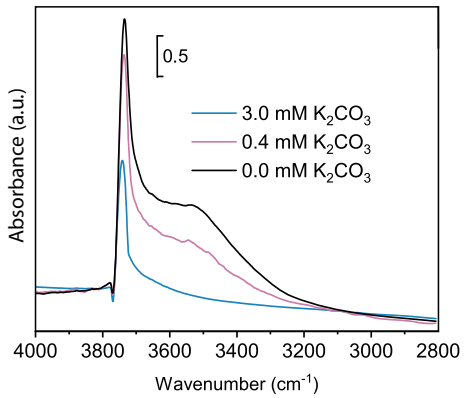

Figure 8.10: The OH stretching region of the FT-IR spectra of post-treated Sn-Beta zeolite (100) without alkali (black) and after impregnation in 0.4 mM (pink) and 3 mM (blue) aqueous potassium carbonate solution, corresponding to the optimum concentration for the production of methyl lactate and a 7.5-fold excess. FT-IR spectra were compared after normalization to the framework bands at 1875 cm-1 and 1988 cm-1. The experimental work and figure were produced by PhD Student Irene Tosi.

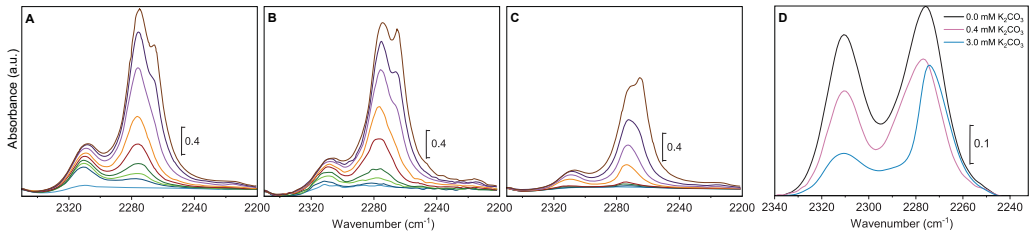

Figure 8.11: In-situ FT-IR measurements of CD_3CN adsorption on Sn-Beta zeolites increasing the pressure from 1.5 x 10^{-2} mbar to 5 mbar (A-C). Post-treated Sn-Beta without impregnation (a), after treatment in 0.4 mM (b) and after treatment in 3 mM (c) aqueous solution of potassium carbonate. FT-IR signals of CD_3CN bands of Sn-Beta zeolites with and without alkali after desorption of CD_3CN at room temperature for one hour under vacuum (D). A higher amount of probe molecule remains adsorbed in the absence of alkali. FT-IR spectra were compared after normalization to the framework bands at 1875 cm^{-1} and 1988 cm^{-1}. The experimental work and figure were produced by PhD Student Irene Tosi.

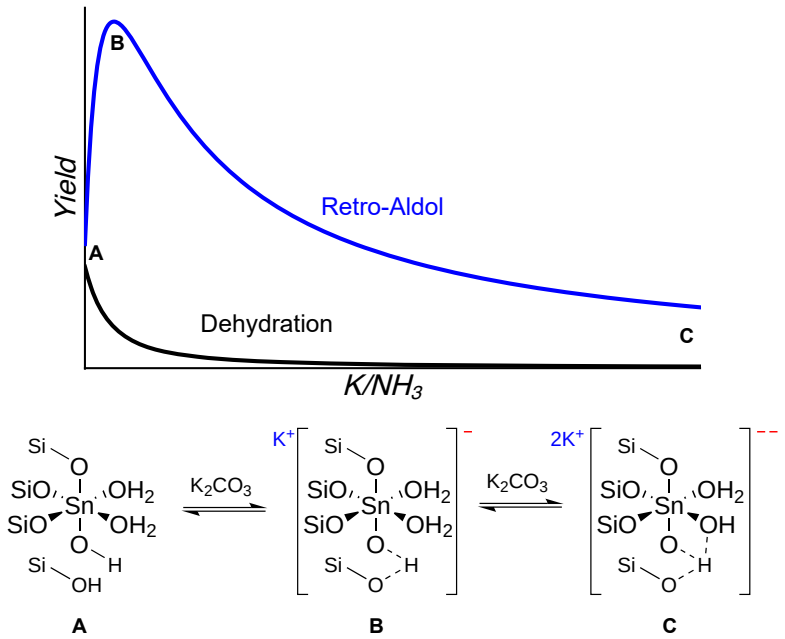

Figure 8.12: Identical titration behaviour of the active site lead to an optimum of yields for retro-aldol products and to decreasing THM yields (top). A plausible model for stochiometric alkali exchange at the active side is shown on the bottom.

A is active for both dehydration and retro-aldol reactions. The single deprotonated B site is highly selective for retro-aldol cleavage and as the fraction of states transition toward predominance of the B site, retro-aldol products increase. However, once the double deprotonated C site is formed, no significant formation of retro-aldol or dehydration products is observed. Although the C site is inactive for these types of reactions, other degradation reactions are clearly taking place, as may be observed by low substrate recovery (Figure 8.1 on page 53) and strong dark discolouration of the reaction mixture. The lack of meaningful signals in NMR could point towards formation of oligomers.

9 | Mechanistic Elucidation Through Isotopic Labelling†

The use of isotopically labelled substrates for mechanistic elucidation is well parred with high resolution NMR spectroscopy. When combined, it is possible to track the progression of singular atoms from the reactant to the substrates formed. From these observations it is possible to glean important information about the reaction mechanisms taking place. In the following chapter, multiple studies are covered, where substrates with ^{13}C or ^{2}H isotopic labelling have been used to obtain important mechanistic information about the Sn-Beta catalysed conversion of carbohydrates.

9.1 Alkali Salts Facilitate a C1-C2 Shift in Carbohydrates

From the formation of 2-^{13}C mannose from 1-^{13}C glucose it is known that epimerisation by a 1-2 carbon exchange is catalysed by Sn-Beta.[54] It has previously been proposed that a 1-2 carbon shift may occur by either a retro-aldol-aldol or Bilik type mechanism (Figure 9.1). Although it has been demonstrated that the epimerisation is occurring primarily by the Bilik type mechanism,[67,99] there may be a great resemblance between epimerisation and retro-aldol cleavage. It is hypothesised that after an initial retro-aldol cleavage the subsequent dehydration out-competes aldol condensation. It was previously demonstrated

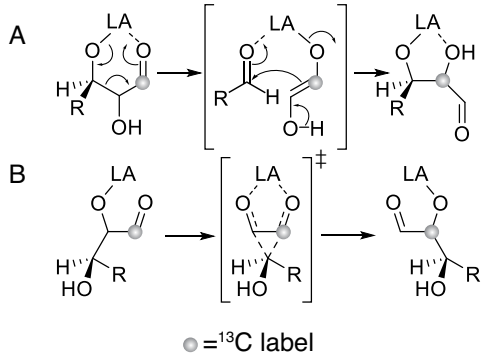

Figure 9.1: Comparison of 1,2-carbon shift by a retro-aldol (A) and a Biliktype (B) cleavage mechanism.[67] The conversion of a ^{13}C-labelled C1 position to a ^{13}C-labelled C2 position is indicated for both cases.

†This chapter is adapted from Elliot *et al.*, *ChemCatChem*, 2018, **10**, 1414-1419. and Elliot *et al.*, *ChemSusChem*, 2018, **11**, 1198-1203.

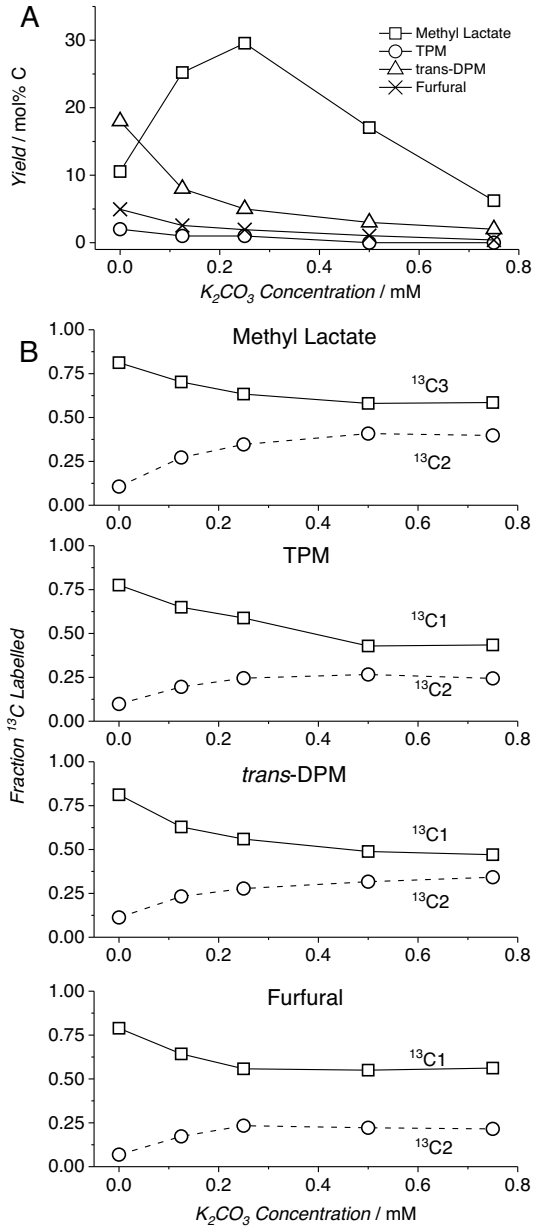

Figure 9.2: A) Yields of methyl lactate, TPM, trans-DPM, and furfural (analysed in its dimethyl acetal form) at varying potassium carbonate concentrations. B) Corresponding ^{13}C distribution at the C1 and C2 positions of methyl lactate, TPM, trans-DPM, and furfural (dimethyl acetal form). For ML, the C3 position derived from pentose C1 is shown instead of C1. Reactions were conducted with D-[1-^{13}C]-xylose (36 mg), Sn-Beta (HT) (18 mg), methanol (500 μL), and DMSO (5 mg), which were reacted at 160 °C for 5 min. K_2CO_3 was dissolved in the solvent methanol prior to reaction.

that alkali salts greatly affect retro-aldol cleavage (Chapter 8). Therefore, a series of tests were performed on isotopically labelled 1-^{13}C xylose with increasing concentrations of potassium carbonate. The degree of carbon exchange from the C1 to the C2 position was compared with corresponding product yields (Figure 9.2).

It is seen that epimerisation is increased upon addition of alkali following an exponentially increasing trend. However, the degree of epimerisation does not display an optimum, like methyl lactate, instead the curve levels out, closely resembling the inverse of dehydration product trends. In the Sn-Beta/carbohydrate system this is a significant case of a reaction not being inhibited by high concentrations of a basic alkali salt.

9.2 Solvent Incorporation

The incorporation of solvent protons into a uniformly labelled $^{2}H_6$-pentose was aided by ^{1}H-^{13}C HSQC NMR and has provided several insights to the reaction system. As seen in Figure 9.3, the number of deuterium may be determined based on the number of peaks produced in a ^{1}H-^{13}C HSQC spectrum. Each addition of deuterium produces two extra peaks until there are no more hydrogen atoms left, in which case no signal is observed in ^{1}H-^{13}C HSQC.

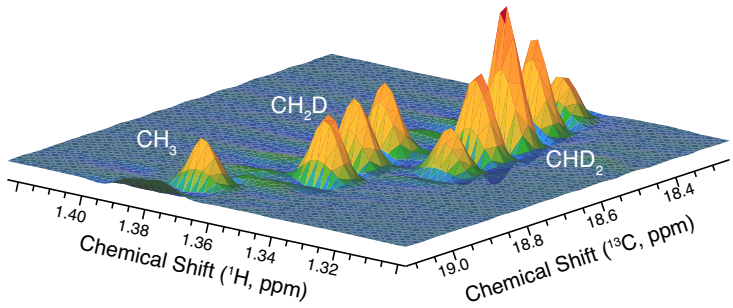

Figure 9.3: Multiplet pattern of the C3-position of ML that results from the incorporation of three, two, and one ^{1}H atoms (from left to right).

9.2.1 Solvent Proton Incorporation into Methyl Lactate

The methyl lactate produced in the reaction shows no incorporation of solvent hydrogen at the C2 position (Figure 9.4). On the other hand the C3 position shows multiple degrees of incorporation, for which the spectra are displayed in Figure 9.4. The predominant form involves the incorporation of a single solvent hydrogen. For that to be the case the C3 position of methyl lactate must originate from a carbohydrate carbon atom possessing two deuterium before retro-aldol cleavage. This is only the case for the C5 position of the aldose, or after isomerisation, the C1 and C5 positions of a ketose.

The incorporation of two and even three solvent hydrogens is observed in up to 14 mol%. Based on the observed incorporation and the reaction scheme for methyl lactate formation (Figure 2.4) it may be deduced that tautomerisaiton to methylglyoxal is

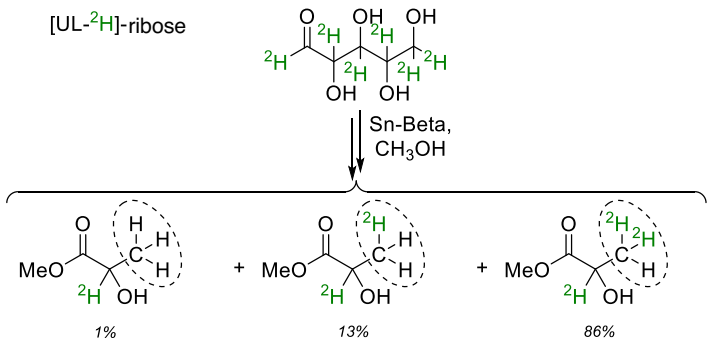

Figure 9.4: Fraction of methyl lactate isotopologues produced upon reaction of D-[UL-$^2H_6$]-ribose. Reactions consisted of D-[UL-$^2H_6$]-ribose (36 mg), Sn-Beta (HT) (18 mg), methanol (500 μL), and dimethylsulphoxide (5 mg) (internal standard) heated to 160 °C for 2 h.

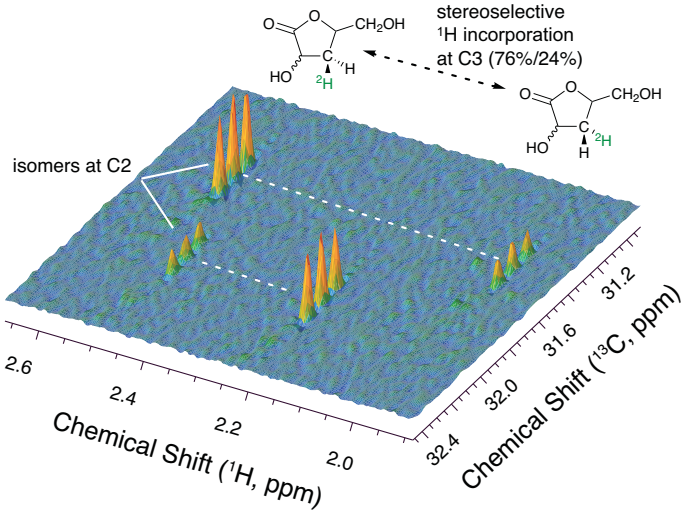

Figure 9.5: ^{1}H-^{13}C HSQC signals for the C3 position of DPL. The four potential diastereomer products (isomerism at C2 and C3) produced by reaction of enantiomerically pure D-[UL-$^2H_6$]-ribose yield four triplets, one for each CH group at C3, as the ^{2}H nuclei was not decoupled.

reversible and that the rate of the subsequent hydride shift is faster than reverse tautomerisaiton, but not incomparably faster.

9.2.2 Stereoselective Incorporation of Hydrogen in DPL

Solvent incorporation into single-dehydration products was expected at the C3 position, and with the two diastereoisomers of DPL, containing the C2 and C4 sterocenters either in co-planar or anti-planar configuration. The isomers produce a signal for each C-H pair, leading to two signals per carbon which each split into three peaks as the result of a deuterium and hydrogen on the same carbon (Figure 9.5). From this spectrum it is seen that the co- and anti-planar configurations are equally distributed (the sum of signal volumes at 31.8 ppm versus those at 31.4 ppm). However, the incorporation of a solvent proton occurs highly stereo-selectively, with 52% ee (the peaks at 2.2 ppm versus 2.5 ppm and the peaks at 2.55 ppm versus those at 2.0 ppm).

Although this has no effect on the DPL formed in a normal reaction, it does tell us that the incorporation of a solvent proton is controlled by the catalyst and that the catalyst is able to impose stereoselective control on the substrate. This observation is also intriguing in relation to *trans*-DPM, where high selectivity for the *trans* isomer may be found (Section 5.2 on page 32). Coupling these observations strengthens the image of Sn-Beta as a stereoselective catalyst.

9.2.3 DPM Shows No Incorporation of Solvent Protons

The degree of incorporation of solvent protons into *trans*-DPM, formed from a uniformly labelled $^2H_6$-pentose, is an important indicator for reversibility of the initial dehydration step of the reaction. If there is a high degree of reversibility, a solvent proton will incorporate into the C2 position of the sugar, isomerise with the C1 position and ultimately end up in the C2 position of DPM through a hydride shift in the final catalytic step.

As may be seen from the reaction results in Figure 9.6, no solvent protons are observed

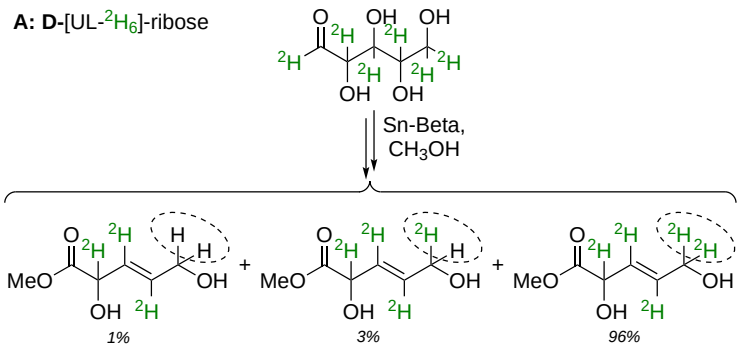

Figure 9.6: Isotopologues of *trans*-DPM fromed from D-[UL-$^2H_6$]-ribose, therby showing solvent ^1H incorporation. Reaction Conditions: D-[UL-$^2H_6$]-ribose (36 mg), Sn-Beta (HT) (18 mg), methanol (500 μL), and DMSO (5 mg) (internal standard) heated to 160 °C for 2 h.

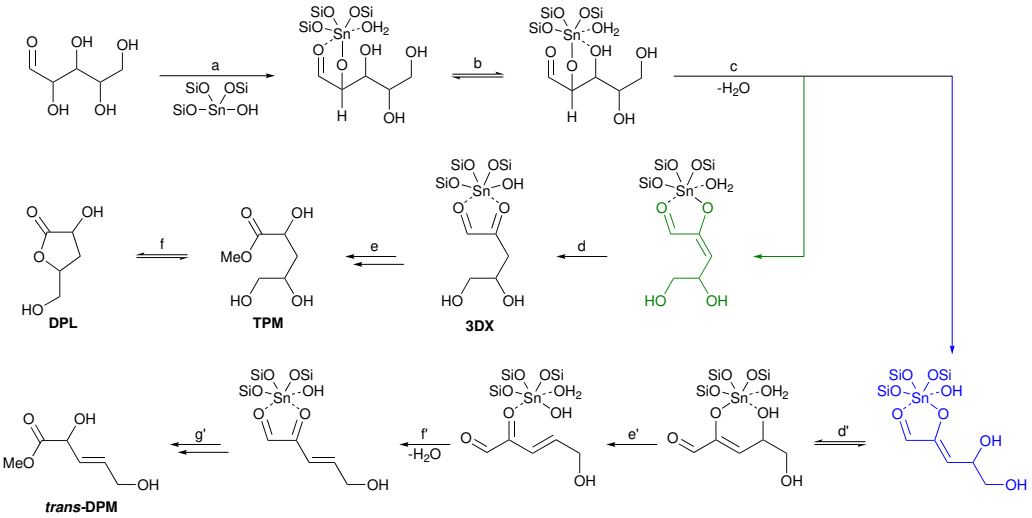

Figure 9.7: Proposed mechanism for the formation of *trans*-DPM via a pathway not including 3DX and formation of TPM/DPL via 3DX. The mechanism proposes that the enol *cis/trans* stereochemistry plays an important role in determining product selectivity.

at the C2 position of DPM, leading to the conclusion that the first dehydration step is not reversible to any significant degree. Furthermore, there is also no observed solvent incorporation at the C3 position of DPM. The lack of incorporation of solvent protons in the C3 position tells us that tautomerisation to 3DX does not occur in the pathway to DPM. When coupled with the results for DPL (Section 9.2.2), which shows that only one solvent proton is incorporated in the structure, it is also possible to deduce that the tautomerisation of 3DX must be irreversible.

From these conclusions it is possible to propose a mechanism for the formation of single dehydration products (DPL) and double dehydration products (DPM) and how they differ (Figure 9.7). Here, the stereochemical configuration of the first dehydration step is presented as the determining step for selectivity between single and double dehydration, reasoning that the *trans* configuration of the first dehydration product will be sterically hindered in coordinating the C4 hydroxy group to the catalyst and will therefore favour tautomerisation. Meanwhile, the *cis* configuration will allow for coordination of the C4 hydroxyl group facilitating further dehydration. In short, the selectivity can be said to be a competition between tautomerisation and C4-dehydration, where the energy barrier for dehydration is determined by coordination to the catalyst, which is controlled by the *cis/trans*-stereochemistry.

9.3 No 1-^{13}C Scrambling in Methyl Lactate

1-^{13}C labelled aldo-pentose was use as a method to track the C1 carbon to the methyl lactate product. Depending on whether methyl lactate originates primarily from the starting aldose or from the corresponding ketose, the resulting methyl lactate is expected

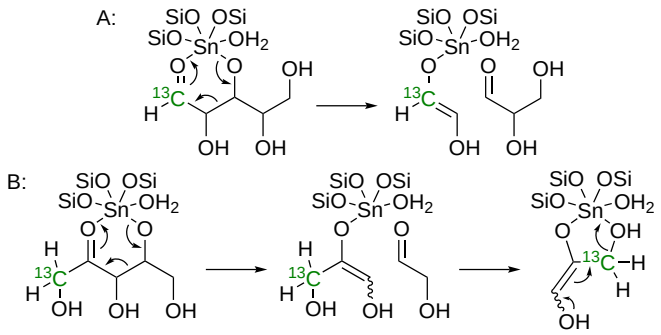

Figure 9.8: Retro-aldol cleavage mechanism for a 1-^{13}C labelled aldose (A) and ketose (B) substrate yielding different methyl lactate and glycolaldehyde isotopolouges.

to be either unlabelled (Figure 9.8A) and showing a uniform ^{13}C distribution, or labelled (Figure 9.8B) showing up to 100 fold higher ^{13}C contribution from one position.

The experimental results (Figure 9.9) showed that the ^{13}C distribution is non-uniform, and that there is an increased prevalence of ^{13}C at the C3 position of methyl lactate. This distribution is surprising considering the expected formation of a symmetrical dihydroxy acetone intermediate. From this result it may be deduced that methyl lactate is primarily formed from the ketose form in accordance with the mechanism of Figure 9.9B. In addition, the C3 position of methyl lactate must be originating from the C1 position of the ketose, consistent with the observations from solvent incorporation experiments (section 9.2.1 on page 67), and resembling biocatalysis. [100]

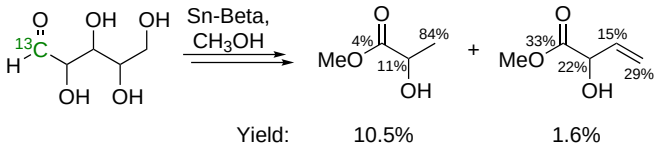

Figure 9.9: Relative distributions of ^{13}C in methyl lactate and MVG upon conversion of D-[1-^{13}C-xylose. Reaction conditions: 36 mg D-[1-^{13}C]-xylose, 18 mg Sn-Beta (HT), 500 μL methanol, and 5 mg DMSO (internal standard) heated to 160 °C for 5 min. Yields were determined by using ^{1}H NMR spectroscopy (mol% carbon).

Finally, the high selectivity of labelling on the C3 over the C1 position of methyl lactate is indicative of the substrate remaining bound to the catalyst throughout the reaction cascade. That is to say that no free trioses are formed in the reaction after retro-aldol cleavage, as it would lead to rapid isomerisation resulting in scrambling of the C1/C3 labelling through formation of symmetric dihydroxy acetone.

9.4 Observation of a 5,1-Hydride Shift

Non-cleavage products were observed in the conversion of 1-^{13}C labelled aldo-pentose to detect the breakage and reforming of carbon-carbon bonds and detect the corresponding position of the carbohydrate aldehyde carbon in the end products. For the major dehydration product DPM, the results confirmed that the C1 of the reactant xylose was also the C1 position of the product (Figure 9.10). The results also showed a small exchange of labelled carbon to the C2 and C5 positions of the molecule.

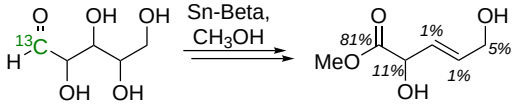

Figure 9.10: Relative distributions of ^{13}C in *trans*-DPM upon conversion of D-[1-^{13}C]-xylose. Reaction conditions: 36 mg D-[1-^{13}C]-xylose, 18 mg Sn-Beta (HT), 500 μL methanol, and 5 mg DMSO (internal standard) heated to 160 °C for 5 min. Yields were determined by using ^{1}H NMR spectroscopy (mol% carbon).

Epimerisation of carbohydrates through a 1,2-carbon shift is known from literature, consistent with the observed exchange of the ^{13}C labelling from the C1 to the C2 position.[53,54,101] Exchange between the C1 and C5 positions have not been reported for Sn-Beta. However, Ti-Beta, another lewis acidic zeolite, has been reported to perform a 5,1-hydride shift of carbohydrates in their cyclic pyranose form.[102] To discern if a similar reaction is taking place with Sn-Beta, reactions were performed with 5,5-$^{2}H_2$-arabinose (Figure 9.11). In DPM formed from the reaction, 20% of the deuterium labelling had migrated from the C5 position to C2, confirming that a 5,1-hydride shift had taken place. In addition, methyl lactate showed that 78% of the C3 position (corresponding to the carbohydrate C1 position) contained no deuterium and 22% contained a single deuterium, confirming the conclusions obtained from DPM isotopomers and isotopologues.

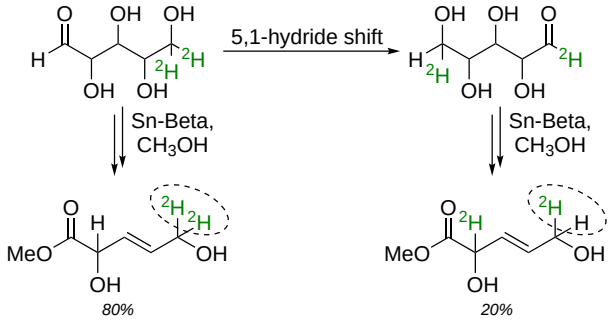

Figure 9.11: Yields of *trans*-DPM isotopomers produced upon conversion of [5,5'-$^{2}H_2$]-arabinose, providing evidence of a 5,1-hydride shift. Reactions conditions: 36 mg [5,5'-$^{2}H_2$]-arabinose, 18 mg Sn-Beta (HT), 500 μL methanol, and 5 mg DMSO heated to 160 °C for 5 min.

10 | Application

In the commercialisation of new chemicals the assessment of applications and related properties is just as essential as optimising reaction and purification processes. The following chapter covers preliminary testing of *trans*-DPM and MVG as monomers for us in polymer blends.

10.1 Polymerisation of *trans*-DPM[†]

In order to evaluate DPM as a monomer building block, DPM was tested in polymerization reactions. The process involved development of a scaled-up synthesis and purification procedure, consisting of a 1 L auto-clave setup and subsequent vacuum dry column chromatography for purification. Although, these methods are feasible on lab scale, it should be noted that a flow set-up and distillation would be more suited for further scale-up.

The poly esterification of lactate to poly-lactic acid (PLA) is a known commercial process, and co-polymerisation of MVG and ML has been shown by Sels and coworkers.[36,69,103] In the latter process, it was also shown that the vinyl groups of MVG could be modified post-polymerisation. Similar capabilities are envisioned for DPM: Polyesterification employing the ester and primary alcohol group, then the possibility of post-modification of the double bond, and in addition the possibility of post-modifying the secondary alcohol group.

The work was conducted in collaboration with master's student Christian Andersen (under supervision of Assoc. Prof. Anders Daugaard) from DTU Polymer, who performed the co-polymerisation of DPM with ethyl-6-hydroxy-hexanoate (E6-HH). An enzymatic catalyst (Candida Antarctica lipase B) selective for primary alcohols was used and the resulting co-polymer could be positively identified by NMR (Figure 10.1).

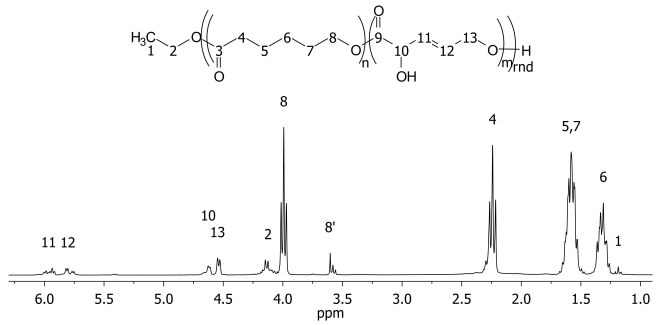

Figure 10.1: ^{1}H NMR assignment of the co-polymer product of ethyl-6-hydroxy-hexanoate (E6-HH) and DPM, poly(E6-HH-co-DPM) (Figure 10.2, Polymer I).

[†]This sections is adapted from Elliot *et al.*, *RSC Adv.*, 2017, **7**, 985–996.

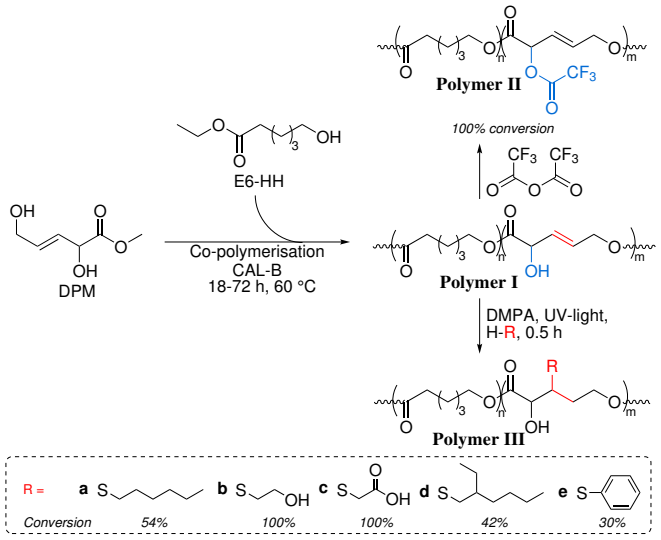

Figure 10.2: Enzymatic co-polymerisation of DPM and ethyl 6-hydroxy-hexanoate (E6-HH) using Candida Antarctica lipase B (CAL-B) and subsequent functionalisation. The reaction of the thiols can supposedly occur on either carbon of the olefinic moieties, but only one form is represented in the figure for clarity.

The polymer (NMR spectrum in Figure 10.1) had a 0.17 molar ratio of DPM having incorporated 77% of the added DPM and had a molecular weight of 12 350 g/mol. Higher amounts of DPM were also tested (0.44 and 0.66 molar ratio), which resulted in 100% incorporation, but the resultant polymers showed significantly lower molecular weights (4500 and 3700 g/mol, respectively). These preliminary tests showed that DPM may be successfully polymerised in a poly-esterification reaction.

To explore the versatility of poly(E6-HH-co-DPM), post-modification reactions were performed on the α-hydroxyl and olefinic groups (Figure 10.2). For testing post-functionalisation of the α-hydroxyl group, modification by triflouroacetic anhydride (TFAA) was employed. This method is widely used for hydroxyl labelling of polymers and the high reactivity of TFAA provides the best possible conditions for the hydroxyl group to react.[104,105] ^{1}H-NMR analysis showed that full TFAA functionalisation of the hydroxyl groups in poly(E6-HH-co-DPM) was obtained (Figure 10.2, Polymer II).

Simultaneously, thiol-ene chemistry was employed to assess the reactivity of the intra-chain alkene, a well-established method for post-modification of alkenes by formation of alkyl sulfides.[69,106,107] Thiol-ene reactions were performed with five different substrates, which achieved 30-100% incorporation (Figure 10.2, Polymer III a-e), generally showing higher incorporation for smaller substrates. Based on these results, the olefinic group in DPM is available for post-polymerisation modifications.

The results obtained from these initial co-polymerisation and post-modification tests of DPM, show great promise for DPM as a highly versatile tunable monomer in polymer applications.

10.2 MVG as a New Commercial Chemical

As previously discussed, MVG has shown interesting capabilities for application as a polymer building block (Section 2.5 on page 14), and can be produced in high yields from glycolaldehyde (Section 5.4 on page 35). To pursue the use of MVG along the track to commercialisation, the following studies have focussed on the evaluation of MVG stability under typical storage conditions, and the evaluation of MVG and MVG analogues in polymer blends for making polymer films.

10.2.1 Long-term Stability Tests

Assessing the long term stability of MVG under typical chemical storage conditions is necessary, both in the long term sales perspective, but also for guaranteeing substrate quality and composition during downstream upgrading and application development. Three storage locations were selected, a fridge (5 °C), a dark storage cupboard and a light storage cupboard with a glass front (Figure 10.3). The locations were selected due to their common availability in a laboratory and in order to vary storage temperature and UV exposure to the sample. The samples stored in the fridge and dark cupboard were stored in brown flasks to further prevent any possibility of UV exposure, a sample with atmospheric air and one with nitrogen atmosphere were prepared for each of the two locations. The sample stored in the light cupboard was prepared in a colourless glass flask with atmospheric air, providing the worst storage conditions. The samples were analysed after 59 and 150 days in storage (Figure 10.3), with a separate vial prepared for each time interval.

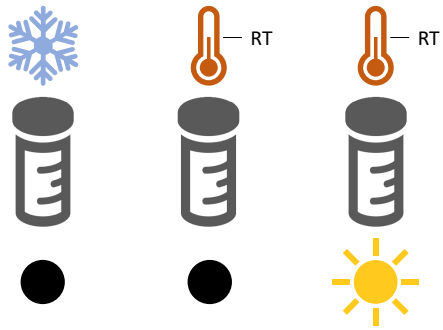

	Air	N_2	Air	N_2	Air
59 days	98.1	97.8	97.9	97.6	97.6
150 days	97.3	97.4	97.6	96.9	97.0

Figure 10.3: Long term storage conditions for MVG stability testing and measured purities of MVG in mol% carbon (Initial purity was 98.7%).

After 59 days, the samples all showed between 0.6 and 1.1 mol% decrease in MVG purity by carbon and after a total of 150 days the decrease was between 1.1 mol% and 1.8 mol%. Examination of the ^{13}C NMR spectra shows two areas of particular interest (Figure 10.4). Most significant is the observation of three new peaks at 162.2, 159.5 and 158.9 ppm, characteristic of highly oxidized carbon such as anhydrides, formates and carbonates.[108] $^{1}H^{13}C$ HSQC-TOCSY NMR experiments revealed no additional structural

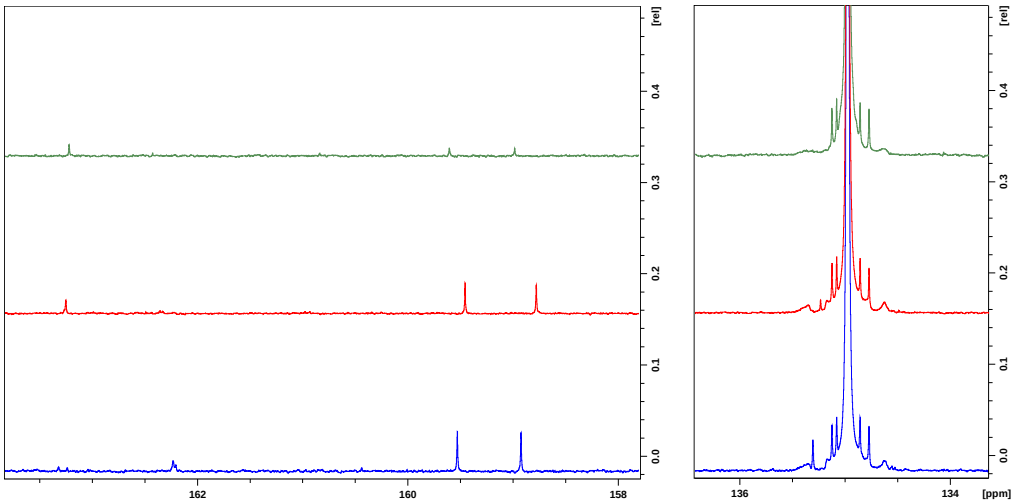

Figure 10.4: NMR spectra of long term storage experiments stored in a light cupboard after 0 (top), 59 (middle) and 150 (bottom) days.

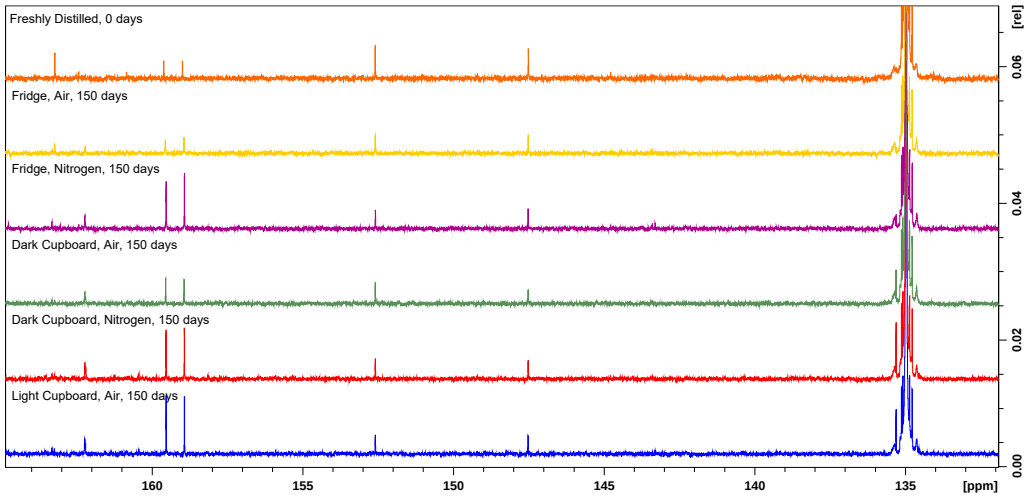

Figure 10.5: NMR spectra of long term storage experiments stored in a light cupboard after 0 (top), 59 (middle) and 150 (bottom) days.

information on these peaks consistent with isolated carbon atoms with a high amount of oxygen, leading to the conclusion that oxidation reactions are taking place. It is also possible to observe the formation of VGA through its C3 peak at 135.3 ppm, and an increase in the amount of methanol in the reaction corroborates this observation. In addition, on either side of the MVG C3 peak (134.9 ppm) two low broad peaks are visible. The broad peaks could come from formation of oligomers of MVG, but other than an increase in methanol exceeding the formation of VGA, our results have been unable to confirm this proposition.

Generally there is little difference between the degradation observed in the storage conditions tested. All samples show the same impurities, but in slightly varying amounts (Figure 10.5), and besides the peaks shown here, no additional impurities were observed that were not also present in the initial mixture. Based on the products formed, the primary degradation routes under storage are oxidation, hydrolysis and potentially oligomerisation.

10.2.2 MVG in coatings

To illuminate possible future applications of MVG, MVG and MVG analogues were tested in three different types of coatings: acrylate, epoxide and alkyd coatings. The acrylate coating is cured by UV radiation curing, where a small UV active acrylate initiates a cascade polymerisation forming linkages between double bonds. Epoxide coatings use UV cationic curing to form strong acids that initiate polymerisation (primarily) between the epoxide groups. Lastly, the alkyd coating follows a thermally activated polycondensation reaction, leading to the release of water which is removed from the system.

Reactive Diluent in Alkyd Paints

The alkyds used, for instance in alkyd paints, are very viscous making them difficult to apply as a thin, even film. Therefore, along with a drying agent a diluent is often added. It is preferable for this diluent to be a reactive diluent, rather than to evaporate as a solvent would. The diluent should react with the alkyd becoming part of the final film and potentially modifying properties of the film. MVG was tested as a reactive diluent for this application and compared to Lacknafta. The reference formulation consisted of 70 wt% alkyd, 30 wt% Lacknafta, <1 wt% BOCH OXY T616 (drying agent), <1 wt% BYK 346 (surface smoothener), and a test sample consisted of 30 wt% MVG instead of Lacknafta, 100 μm films were made of each blend on aluminium plates and dried overnight at ambient conditions. Weighting of the plate containing the MVG blend revealed that 30 wt% of the blend had been lost. From that it may be concluded that the MVG evaporated rather than reacted as was desired and is therefore not suitable as a reactive diluent for alkyd paints.

Radiation Curing

MVG was modified to HDO-VG[†] (Figure 10.6) and tested as an monomer in a radiation curing formulation. The formulation was done both with and without a reactive diluent

[†]Synthesised by Senior Laboratory Engineer Pia Wennerberg, Perstorp AB

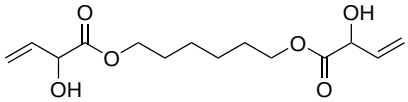

HDO-VG
1,6-hexandiol di(2-vinyl-glycolate)

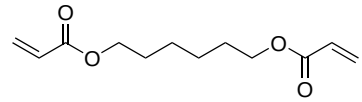

HDDA
1,6-hexandiol diacrylate

Figure 10.6: Chemical structure a polyacrylate monomer (HDDA) and the MVG derived substitute monomer (HDO-VG).

Table 10.1: Acrylate blends for testing of HDO-VGs properties in radiation curing films

Blend	HDO-VG	HDDA	TP30[a]	Irg500[b]	Film Thickness	Curing[c]	König Hardness	Ericson Hardness[d]	Chemical Resistance[e]
	g	*g*	*g*	*g*	μm	*runs*	*k/s*	*mm*	*swipes*
1	9.59			0.39	6	41	32	4.8	6
2	4.81		4.78	0.39	6	45	76	4.4	142
3		9.58		0.39	12	3	n.a.	1.9	200
4		4.78	4.80	0.39	12	1	200	2.3	200

[a]Bisphenol A epoxy diacrylate in 30% tripropylene glycol diacrylate. [b]IRGACURE 500 photoinitiator. [c]Number of runs under a UV lap at 100% power with a 5 m/min belt transport rate. [d]Performed to films on a glass plate. [e]Number of swipes back and forth with a cotton bud soaked in methyl ethyl ketone and 0.5 kg of pressure.

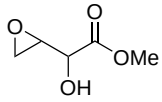

epoxy-MVG
methyl 2-hydroxy-3,4-epoxy-butanoate

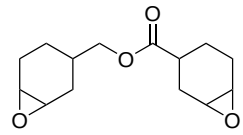

ECC
3,4-epoxycyclohexylmethyl
3',4'-epoxycyclohexanecarboxylate

Figure 10.7: Chemical structure the reference epoxide monomer (ECC)and the MVG derived substitute monomer (*epoxy*-MVG).

Table 10.2: Epoxide blends for testing of *epoxy*-MVGs properties in cationic curing films.

Blend	ECC	*epoxy* -MVG	TMPO[a]	Irg250[b]	Film Thickness	Curing[c]	König Hardness	Ericson Hardness[d]	Chemical Resistance[e]
	g	*g*	*g*	*g*	μm	*runs*	*k/s*	*mm*	*swipes*
1	9.68			0.53	12	3	233	2.8	200
2	8.68	1.05		0.48	12	1	233	3.5	200
3	7.7	1.16	1.02	0.53	12	2	233	3.8	200

[a]Trimethylolpropane oxetane. [b]IRGACURE 250 photoinitiator.[c]Number of runs under a UV lap at 100% power with a 5 m/min belt transport rate. [d]Performed to films on a glass plate. [e]Number of swipes back and forth with a cotton bud soaked in methyl ethyl ketone and 0.5 kg of pressure.

(TP30) and compared to a reference sample containing HDDA (Table 10.1). Films were formed on aluminium plates and cured under a UV lamp. The most notable distinction between HDDA and HDO-VG samples was a drastic increase in the amount of UV exposure need to cure the film. The HDO-VG films were generally softer (König hardness), less resistant to chemicals and had a higher flexibility (Ericson hardness), although these effects were slightly reduced by addition of the reactive diluent (TP30). Also, the HDO-VG films showed a lower propensity to coalesce when applied to glass plates.

These results indicate that HDO-VG may be a viable additive when forming acylate polymer films, which require higher flexibility. However, the very slow curing needs to be addressed to improve the usability and ease of application.

Cationic Curing

MVG was modified to *epoxy*-MVG[†] and tested as an additive in an epoxide cationic curing blend in comparison to ECC (Figure 10.7). Addition of *epoxy*-MVG improved the curing rate of the film and the flexibility of the film (Ericson hardness) was also greatly improved (Table 10.2). Meanwhile the König hardness and the chemical resistance of the films were retained. In addition, the films formed on glass showed a reduced propensity to coalesce.

The effects of addition of *epoxy*-MVG are highly interesting. The ability to tune the flexibility of a film without modifying other film properties makes the *epoxy*-MVG very useful as an additive. In addition, the reduced propensity of the films to coalesce is an overall improvement to the application of the film.

[†]Synthesised by PhD student Bo Jessen, Department of Chemistry, Technical University of Denmark

11 | Conclusion

This conclusion compiles results from six chapters, which can be grouped into reaction analysis (Chapter 5 and 6), optimisation (Chapter 7), understanding (Chapter 8 and 9) and application development of reaction products (Chapter 10). The main findings are as follows:

Reaction Analysis The most significant products identified were the α-hydroxy esters DPM and THM, new five and six carbon analogues of MVG, respectively. The identification of additional reaction products lead to significant improvements in carbon balances in reactions from pentoses, hexose and glycolaldehyde. Dimethylsulphone was found to be a highly suitable internal standard for NMR analyses of the reaction mixture, with good stability under the employed reaction conditions. A quantitative 2D NMR method was developed, which employed calibration of response factors from ^{13}C NMR, thereby avoiding the need for isolated referencing standards.

Reaction Optimisation Towards Formation of DPM and THM Optimisation showed that the most favourable conditions for formation of double dehydration products (DPM and THM) were at 160 °C with a 1 to 2 ratio (wt/wt) of Sn-Beta catalyst to carbohydrate. The reaction selectivity showed high stability to changes in substrate stereochemistry and concentration (from 8.3-23 wt%). Changing from methanol to more bulky solvents lead to a large increase in single and double dehydration products with up to 42% yield of DPE and 19.4% THE obtainable in ethanol, corresponding to a 1.25 fold increase. In contrast, the presence of an alkali salt additive was detrimental for the formation of dehydration products.

Understanding the Alkali Effect The effect of increasing alkali concentrations has been seen to suppress dehydration and solvolysis in favour of formation of retro-aldol products. The initial rates of formation are observed to follow the same trends, but are also dependent on whether a neutral or basic salt is employed. A basic salt has a more beneficial effect on retro-aldol formation rates, and reduces rates of glycoside and furanic product formation, more than neutral salts. It was shown that the optimum concentration for methyl lactate formation is directly dependent on accessible tin sites. Furthermore, the peak follows a double dissociation trend, which is dependent on the alkali to active site ratio. From this trend, it may be deduced that the tin active site is in an active equalibrium between three states, with either no, one or two alkali substituted, with the latter being inactive for the observed reaction pathways. Alkali is observed to have equivalent effects on epimerisation by 1,2-carbon shift and retro-aldol cleavage, supporting that the presence of alkali salts reduces the energy barrier for carbon-carbon bond cleavage.

Mechanistic Understanding Experiments with isotopically labelled substrates showed that in addition to high trans selectivity, tautomerisation also occurs stereo-selectively. Meanwhile, the second dehydration step towards the formation of *trans*-DPM, and in extension *trans*-THM, competes with tautomeristion towards formation of DPL/TPM via 3DX, which is formed irreversibly. It is proposed that the stereochemistry of the enol formed after the first dehydration is important in determining the continued pathway, as the stereo-chemistry may limit coordination of the C4 hydroxyl group to the active site. Furthermore, reto-aldol cleavage initiates a reaction cascade to form methyl lactate, without releasing the substrate before methyl lactate is formed. Sn-Beta also was also shown to catalyse a 5,1-hydride shift in pentoses.

Applications MVG and DPM were tested for further applications in polymers. DPM was successfully co-polymerised with E6-HH by the enzyme CAL-B to form a co-polyester. Modification was successfully carried out of the resulting polymer at both the alcohol and the alkene functionality. Modified MVG was tested in polymer blends and found suitable for applications in radiation curing as HDO-VG and cationic curing as epoxidised MVG. The storage stability of MVG was tested and MVG was found to decompose slowly over time by oxidation.

Bibliography

[1] E. Dlugokencky and P. Tans, *Trends in Atmospheric Carbon Dioxide*, `www.esrl.noaa.gov/gmd/ccgg/trends`, accessed March 2019.

[2] P. D. Jones, D. E. Parker, T. J. Osborn and K. R. Briffa, *Global and Hemispheric Temperature Anomalies - Land and Marine Instrumental Records*, CDIAC Oak Ridge National Laboratory technical report, 2016.

[3] D. J. Griggs and M. Noguer, *Weather*, 2002, **57**, 267–269.

[4] G.-R. Walther, E. Post, P. Convey, A. Menzel, C. Parmesan, T. J. C. Beebee, J.-M. Fromentin, O. Hoegh-Guldberg and F. Bairlein, *Nature*, 2002, **416**, 389.

[5] J. G. Haubrich and B. Meyer, *Econ. Comment.*, 2007, 1–4.

[6] J. Tennant, *World Oil*, 2013, **234**, 121–123.

[7] T. Mitchell, *J. Cult. Econ.*, 2010, **3**, 189–204.

[8] P. N. R. Vennestrøm, C. M. Osmundsen, C. H. Christensen and E. Taarning, *Angew. Chemie Int. Ed.*, 2011, **50**, 10502–10509.

[9] C. H. Christensen, J. Rass-Hansen, C. C. Marsden, E. Taarning and K. Egeblad, *ChemSusChem*, 2008, **1**, 283–289.

[10] D. R. Dodds and R. A. Gross, *Science*, 2007, **318**, 1250–1251.

[11] W. Keim, *Pet. Chem.*, 2010, **50**, 298–304.

[12] R. Rinaldi and F. Schüth, *Energy Environ. Sci.*, 2009, **2**, 610–626.

[13] A. Corma, S. Iborra and A. Velty, *Chem. Rev.*, 2007, **107**, 2411–2502.

[14] F. W. Lichtenthaler and S. Mondel, *Pure Appl. Chem.*, 1997, **69**, 1853–1866.

[15] F. Leonard, A. J. Szlachtun and I. Cort, *J. Polym. Sci.*, 1953, **11**, 539–544.

[16] P. M. Lorz, F. K. Towae, W. Enke, R. Jäckh, N. Bhargava and W. Hillesheim, *Phthalic Acid and Derivatives*, in *Ullmann's Encyclopedia of Industrial Chemistry*, Wiley, 2007.

[17] Acetic Acid, *Eur. Chem. News*, 2003, **78**, 15.

[18] Acetic Acid, *Chem. Week*, 2004, **166**, 40.

[19] A. Castellan, J. C. J. Bart and S. Cavallaro, *Catal. Today*, 1991, **9**, 237–254.

[20] E. J. North and R. U. Halden, *Rev. Environ. Health*, 2013, **28**, 1–8.

[21] J. Hopewell, R. Dvorak and E. Kosior, *Philos. Trans. R. Soc. B Biol. Sci.*, 2009, **364**, 2115–2126.

[22] Y. Zhu, C. Romain and C. K. Williams, *Nature*, 2016, **540**, 354–362.

[23] J. R. Jambeck, R. Geyer, C. Wilcox, T. R. Siegler, M. Perryman, A. Andrady, R. Narayan and K. L. Law, *Science*, 2015, **347**, 768–771.

[24] A. L. Andrady, *J. Macromol. Sci. Part C*, 1994, **34**, 25–76.

[25] PlasticsEurope and EPRO, *Plastics – the Facts 2018*, PlasticsEurope technical report, 2018.

[26] A. L. Andrady, *Persistence of Plastic Litter in the Oceans*, in *Marine Anthropogenic Litter*, Springer, 2015, pp. 29–56.

[27] R. C. Thompson, Y. Olsen, R. P. Mitchell, A. Davis, S. J. Rowland, A. W. G. John, D. McGonigle and A. E. Russell, *Science*, 2004, **304**, 838–838.

[28] C. B. Crawford and B. Quinn, *The Biological Impacts and Effects of Contaminated Microplastics*, in *Microplastic Pollutants*, Elsevier, 2017, ch. 7, pp. 159–178.

[29] F. Aeschelmann and M. Carus, *Bio-based Building Blocks and Polymers - Global Capacities and Trends*, Nova-Institute technical report, 2016.

[30] L. Shen, E. Worrell and M. Patel, *Biofuels, Bioprod. Bioref.*, 2009, **4**, 25–40.

[31] F. A. C. Martinez, E. M. Balciunas, J. M. Salgado, J. M. D. González, A. Converti and R. P. D. S. Oliveira, *Trends Food Sci. Technol.*, 2013, **30**, 70–83.

[32] J. F. Garrett, *Ind. Eng. Chem.*, 1930, **22**, 1153–1154.

[33] R. Datta and M. Henry, *J. Chem. Technol. Biotechnol.*, 2006, **81**, 1119–1129.

[34] S. M. Ameen and G. Caruso, *Chemistry of Lactic Acid*, in *Lactic Acid in the Food Industry*, Springer, 2017, pp. 7–17.

[35] M. A. Abdel-Rahman, Y. Tashiro and K. Sonomoto, *J. Biotechnol.*, 2011, **156**, 286–301.

[36] E. Castro-Aguirre, F. Iñiguez-Franco, H. Samsudin, X. Fang and R. Auras, *Adv. Drug Deliv. Rev.*, 2016, **107**, 333–366.

[37] M. San-Martín, C. Pazos and J. Coca, *J. Chem. Technol. Biotechnol.*, 1992, **54**, 1–6.

[38] A. Corma and M. Renz, *Angew. Chem. Int. Ed.*, 2007, **46**, 298–300.

[39] A. C. Albertsson, U. Edlund and K. Stridsberg, *Macromol. Symp.*, 2000, **157**, 39–46.

[40] K. Matsumoto and S. Taguchi, *Appl. Microbiol. Biotechnol.*, 2010, **85**, 921–932.

[41] W. Groot, J. van Krieken, O. Sliekersl and S. de Vos, in *Poly(Lactic Acid)*, Wiley, 2010, ch. 1.

[42] E. M. Filachione and C. H. Fisher, *Ind. Eng. Chem.*, 1946, **38**, 228–232.

[43] M. S. Holm, S. Saravanamurugan and E. Taarning, *Science*, 2010, **328**, 602–605.

[44] R. De Clercq, M. Dusselier and B. F. Sels, *Green Chem.*, 2017, **19**, 5012–5040.

[45] A. Corma, *J. Catal.*, 2003, **216**, 298–312.

[46] Y. G. Kolyagin, A. V. Yakimov, S. Tolborg, P. N. R. Vennestrøm and I. I. Ivanova, *J. Phys. Chem. Lett.*, 2016, **7**, 1249–1253.

[47] P. Wolf, M. Valla, A. J. Rossini, A. Comas-Vives, F. Núñez-Zarur, B. Malaman, A. Lesage, L. Emsley, C. Copéret and I. Hermans, *Angew. Chem. Int. Ed.*, 2014,

53, 10179–10183.

[48] M. Boronat, P. Concepción, A. Corma, M. Renz and S. Valencia, *J. Catal.*, 2005, **234**, 111–118.

[49] R. Otomo, R. Kosugi, Y. Kamiya, T. Tatsumi and T. Yokoi, *Catal. Sci. Technol.*, 2016, **6**, 2787–2795.

[50] P. Wolf, W.-C. Liao, T.-C. Ong, M. Valla, J. W. Harris, R. Gounder, W. N. P. van der Graaff, E. A. Pidko, E. J. M. Hensen, P. Ferrini, J. Dijkmans, B. Sels, I. Hermans and C. Copèret, *Helv. Chim. Acta*, 2016, **99**, 916–927.

[51] C. M. Osmundsen, M. S. Holm, S. Dahl and E. Taarning, *Proc. R. Soc. A*, 2012, **468**, 2000–2016.

[52] A. V. Yakimov, Y. G. Kolyagin, S. Tolborg, P. N. Vennestrøm and I. I. Ivanova, *J. Phys. Chem. C*, 2016, **120**, 28083–28092.

[53] R. Bermejo-Deval, R. Gounder and M. E. Davis, *ACS Catal.*, 2012, **2**, 2705–2713.

[54] R. Bermejo-Deval, M. Orazov, R. Gounder, S.-J. J. Hwang and M. E. Davis, *ACS Catal.*, 2014, **4**, 2288–2297.

[55] M. Boronat, A. Corma and M. Renz, *J. Phys. Chem. B*, 2006, **110**, 21168–21174.

[56] Y. Hayashi and Y. Sasaki, *Chem. Commun.*, 2005, **7**, 2716–2718.

[57] E. Taarning, S. Saravanamurugan, M. S. Holm, J. Xiong, R. M. West and C. H. Christensen, *ChemSusChem*, 2009, **2**, 625–627.

[58] M. S. Holm, Y. J. Pagán-Torres, S. Saravanamurugan, A. Riisager, J. A. Dumesic and E. Taarning, *Green Chem.*, 2012, **14**, 702–706.

[59] C. Hammond, S. Conrad and I. Hermans, *Angew. Chemie Int. Ed.*, 2012, **51**, 11736–11739.

[60] S. Tolborg, I. Sadaba, C. M. Osmundsen, P. Fristrup, M. S. Holm, E. Taarning, I. Sádaba, C. M. Osmundsen, P. Fristrup, M. S. Holm and E. Taarning, *ChemSusChem*, 2015, **8**, 613–617.

[61] I. A. Rose and J. S. Nowick, *J. Am. Chem. Soc.*, 2002, **124**, 13047–13052.

[62] K. P. Janssen, J. S. Paul, B. F. Sels and P. A. Jacobs, *Stud. Surf. Sci. Catal.*, 2007, **170**, 1222–1227.

[63] P. P. Pescarmona, K. P. F. Janssen, C. Delaet, C. Stroobants, K. Houthoofd, A. Philippaerts, C. De Jonghe, J. S. Paul, P. a. Jacobs and B. F. Sels, *Green Chem.*, 2010, **12**, 1083–1089.

[64] G. Zhong, D. Shabat, B. List, J. Anderson, S. C. Sinha, R. A. Lerner and C. F. Barbas, *Angew. Chemie Int. Ed.*, 1998, **37**, 2481–2484.

[65] A. H. Romano and T. Conway, *Res. Microbiol.*, 1996, **147**, 448–455.

[66] Y. Román-Leshkov, M. Moliner, J. a. Labinger, M. E. Davis, Y. Román-Leshkov, M. Moliner, J. a. Labinger and M. E. Davis, *Angew. Chemie Int. Ed.*, 2010, **49**, 8954–8957.

[67] W. R. Gunther, *Ph.D. thesis*, Massachusetts Institute of Technology, 2015.

[68] N. Rai, S. Caratzoulas and D. G. Vlachos, *ACS Catal.*, 2013, **3**, 2294–2298.

[69] M. Dusselier, P. Van Wouwe, S. De Smet, R. De Clercq, L. Verbelen, P. Van Puyvelde, F. E. Du Prez and B. F. Sels, *ACS Catal.*, 2013, **3**, 1786–1800.

[70] M. Dusselier, P. VanWouwe, F. DeClippel, J. Dijkmans, D. W. Gammon and B. F. Sels, *ChemCatChem*, 2013, **5**, 569–575.

[71] S. Tolborg, S. Meier, S. Saravanamurugan, P. Fristrup, E. Taarning and I. Sádaba, *ChemSusChem*, 2016, **9**, 3054–3061.

[72] R. R. Forseth and F. C. Schroeder, *Curr. Opin. Chem. Biol.*, 2011, **15**, 38–47.

[73] J. L. Markley, R. Brüschweiler, A. S. Edison, H. R. Eghbalnia, R. Powers, D. Raftery and D. S. Wishart, *Curr. Opin. Biotechnol.*, 2017, **43**, 34–40.

[74] S. Valencia and A. Corma, *US Patent 6306364 B1*, 1999.

[75] A. Corma, L. Nemeth, M. Renz and S. Valencia, *Nature*, 2001, **412**, 423–425.

[76] S. Tolborg, A. Katerinopoulou, D. D. Falcone, I. Sádaba, C. M. Osmundsen, R. J. Davis, E. Taarning, P. Fristrup and M. S. Holm, *J. Mater. Chem. A*, 2014, **2**, 20252–20262.

[77] N. N. K. Mal, V. Ramaswamy, P. R. P. Rajamohanan and A. V. a.V. Ramaswamy, *Microporous Mater.*, 1997, **12**, 331–340.

[78] L. Li, C. Stroobants, K. Lin, P. a. Jacobs, B. F. Sels and P. P. Pescarmona, *Green Chem.*, 2011, **13**, 1175–1181.

[79] V. Ramaswamy, P. Shah, K. Lazar and A. V. Ramaswamy, *Catal. Surv. Asia*, 2008, **12**, 283–309.

[80] S. Tolborg, S. Meier, I. Sádaba, S. G. Elliot, S. K. Kristensen, S. Saravanamurugan, A. Riisager, P. Fristrup, T. Skrydstrup and E. Taarning, *Green Chem.*, 2016, **18**, 3360–3369.

[81] S. G. Elliot, C. Andersen, S. Tolborg, S. Meier, I. Sadaba, A. E. Daugaard and E. Taarning, *RSC Adv.*, 2017, **7**, 985–996.

[82] S. G. Elliot, S. Tolborg, I. Sádaba, E. Taarning and S. Meier, *ChemSusChem*, 2017, **10**, 2990–2996.

[83] Y. Román-Leshkov, J. N. Chheda and J. A. Dumesic, *Science*, 2006, **312**, 1933.

[84] H. Chen, A. Wang, H. Sorek, J. D. Lewis, Y. Román-Leshkov and A. Bell, *ChemistrySelect*, 2016, **1**, 4167–4172.

[85] S. Czernik and A. V. Bridgwater, *Energy and Fuels*, 2004, **18**, 590–598.

[86] M. Sasaki, K. Goto, K. Tajima, T. Adschiri and K. Arai, *Green Chem.*, 2002, **4**, 285–287.

[87] P. A. Majerski, J. K. Piskorz and D. S. A. G. Radlein, *US Patent 7094932 B2*, 2006.

[88] V. P. McCaffrey, N. E. Zellner, C. M. Waun, E. R. Bennett and E. K. Earl, *Orig. Life Evol. Biosph.*, 2014, **44**, 29–42.

[89] S. G. Elliot, I. Tosi, A. Riisager, E. Taarning and S. Meier, *Top. Catal.*, 2019, DOI: 10.1007/s11244–019–01131–y.

[90] M. H. Levitt, *Spin Dynamics: Basics of Nuclear Magnetic Resonance*, John Wiley & Sons, 2nd edn., 2001.

[91] J. R. Christianson, S. Caratzoulas and D. G. Vlachos, *ACS Catal.*, 2015, **5**, 5256–5263.

[92] S. G. Elliot, S. Tolborg, R. Madsen, E. Taarning and S. Meier, *ChemSusChem*, 2018, **11**, 1198–1203.

[93] S. Tolborg, *Ph.D. thesis*, Technical University of Denmark, 2016.

[94] V. Choudhary, A. B. Pinar, S. I. Sandler, D. G. Vlachos and R. F. Lobo, *ACS Catal.*, 2011, **1**, 1724–1728.

[95] X. Hu, R. J. M. Westerhof, D. Dong, L. Wu and C.-Z. Li, *ACS Sustain. Chem. Eng.*, 2014, **2**, 2562–2575.

[96] V. Choudhary, S. H. Mushrif, C. Ho, A. Anderko, V. Nikolakis, N. S. Marinkovic, A. I. Frenkel, S. I. Sandler and D. G. Vlachos, *J. Am. Chem. Soc.*, 2013, **135**, 3997–4006.

[97] E. Nikolla, Y. Román-Leshkov, M. Moliner and M. E. Davis, *ACS Catal.*, 2011, **1**, 408–410.

[98] S. G. Elliot, E. Taarning, R. Madsen and S. Meier, *ChemCatChem*, 2018, **10**, 1414–1419.

[99] S. Li, T. Josephson, D. G. Vlachos and S. Caratzoulas, *J. Catal.*, 2017, **355**, 11–16.

[100] A. Bar-Even, A. Flamholz, E. Noor and R. Milo, *Nat. Chem. Biol.*, 2012, **8**, 509–517.

[101] W. R. Gunther, Y. Wang, Y. Ji, V. K. Michaelis, S. T. Hunt, R. G. Griffin and Y. Román-Leshkov, *Nat. Commun.*, 2012, **3**, 1109–1116.

[102] R. Gounder and M. E. Davis, *ACS Catal.*, 2013, **3**, 1469–1476.

[103] R. De Clercq, M. Dusselier, C. Christiaens, J. Dijkmans, R. I. Iacobescu, Y. Pontikes and B. F. Sels, *ACS Catal.*, 2015, **5**, 5803–5811.

[104] C. Hoffmann, M. C. Stuparu, A. Daugaard and A. Khan, *J. Polym. Sci. Part A Polym. Chem.*, 2015, **53**, 745–749.

[105] A. Holländer, S. Kröpke and F. Pippig, *Surf. Interface Anal.*, 2008, **40**, 379–385.

[106] C. E. Hoyle and C. N. Bowman, *Angew. Chemie Int. Ed.*, 2010, **49**, 1540–1573.

[107] M. J. Kade, D. J. Burke and C. J. Hawker, *J. Polym. Sci. A Polym. Chem.*, 2010, **48**, 743–750.

[108] E. Pretsch, P. Buehlmann and C. Affolter, *Structure Determination of Organic Compounds*, Springer, 4th edn., 2009.

Appendix

A | Published Work

The following appendix displays full reproductions of the published articles and corresponding supporting material listed bellow. The articles are displayed in chronological order by publication date.

S. Tolborg, S. Meier, I. Sádaba, **S. G. Elliot**, S. K. Kristensen, S. Saravanamurugan, A. Riisager, P. Fristrup, T. Skrydstrup, E. Taarning, Tin-Containing Silicates: Identification of a Glycolytic Pathway via 3-Deoxyglucosone, *Green Chem.*, 2016, **18**, 3360–3369.

S. G. Elliot, C. Andersen, S. Tolborg, S. Meier, I. Sadaba, A. E. Daugaard, E. Taarning, Synthesis of a Novel Polyester Building Block from Pentoses by Tin-Containing Silicates, *RSC Adv.*, 2017, **7**, 985–996.

S. G. Elliot, S. Tolborg, I. Sadaba, E. Taarning, S. Meier, Quantitative NMR Approach to Optimize the Formation of Chemical Building Blocks from Abundant Carbohydrates, *ChemSusChem*, 2017, **10**, 2990–2996.

S. G. Elliot, E. Taarning, R. Madsen, S. Meier, NMR Spectroscopic Isotope Tracking Reveals Cascade Steps in Carbohydrate Conversion by Tin-Beta, *ChemCatChem*, 2018, **10**, 1414-1419.

S. G. Elliot, S. Tolborg, R. Madsen, E. Taarning, S. Meier, Effects of Alkali-Metal Ions and Counter Ions in Sn-Beta-Catalyzed Carbohydrate Conversion, *ChemSusChem*, 2018, **11**, 1198-1203.

S. G. Elliot, I. Tosi, A. Riisager, E. Taarning, S. Meier, Response Factors Enable Rapid Quantitative 2D NMR Analysis in Catalytic Biomass Conversion to Renewable Chemicals, *Top. Catal.*, 2019, doi:10.1007/s11244-019-01131-y.

I. Tosi, **S. G. Elliot**, B. M. Jessen, A. Riisager, E. Taarning, S. Meier, Uncharted Pathways for $CrCl_3$ Catalyzed Glucose Conversion in Aqueous Solution, *Top. Catal.*, 2019, doi:10.1007/s11244-019-01144-7.

S. G. Elliot, I. Tosi, S. Meier, J. S. Martinez-Espin, S. Tolborg, E. Taarning, Alkali Ion Titrations of Sn-Beta Active Sites Provide Insight into Structure-Activity Relations, *Submitted*, 2019.

Green Chemistry

PAPER

View Article Online
View Journal | View Issue

Cite this: Green Chem., 2016, 18, 3360

Tin-containing silicates: identification of a glycolytic pathway *via* 3-deoxyglucosone†

S. Tolborg,[a,b] S. Meier,[a] I. Sádaba,[b] S. G. Elliot,[a,b] S. K. Kristensen,[c] S. Saravanamurugan,[a] A. Riisager,[a] P. Fristrup,[a] T. Skrydstrup[c] and E. Taarning*[b]

Received 27th November 2015,
Accepted 24th February 2016

DOI: 10.1039/c5gc02840j

www.rsc.org/greenchem

Inorganic glycolytic systems, capable of transforming glucose through a cascade of catalytic steps, can lead to efficient chemical processes utilising carbohydrates as feedstock. Tin-containing silicates, such as Sn-Beta, are showing potential for the production of lactates from sugars through a cascade of four to five sequential steps. Currently, there is a limited understanding of the competing glycolytic pathways within these systems. Here we identify dehydration of glucose to 3-deoxyglucosone as an important pathway that occurs in addition to retro-aldol reaction of hexoses when using tin-containing silicates. It is possible to influence the relative carbon flux through these pathways by controlling the amount of alkali metal salts present in the reaction mixture. In the absence of added potassium carbonate, at least 15–30% carbon flux *via* 3-deoxyglucosone is observed. Addition of just a few ppm of potassium carbonate makes retro-aldol pathways dominant and responsible for about 60–70% of the overall carbon flux. The 3-deoxyglucosone pathway results in new types of chemical products accessible directly from glucose. Furthermore, it is argued that 3-deoxyglucosone is a contributing source of some of the methyl lactate formed from hexoses using tin-containing silicates in the presence of alkali metal salts. Further catalyst design and system tuning will permit even better control between these two different glycolytic pathways and will enable highly selective catalytic transformations of glucose to a variety of chemical products using tin-containing silicates.

Introduction

Processes, in which glucose is directly converted to useful chemical products, have a high potential for industrial implementation.[1] Inorganic catalytic systems, although with limited examples of industrial implementation, have potential advantages over enzymatic and fermentative systems in terms of scalability, tolerance to a broad range of harsh reaction conditions and tolerance to cytotoxic intermediates or products.[2] So far, direct industrial conversion of glucose with inorganic catalytic systems has been limited to the production of sorbitol and gluconic acid, but several other chemicals have been reported as being accessible directly from glucose in high yields. These include fructose, ethylene glycol, propylene glycol, levulinic acid, 5-(hydroxymethyl)furfural (HMF) and lactic acid derivatives.[3–9]

The use of tin-containing silicates for the conversion of sugars to lactates has received considerable attention. The first report from 2009 described the isomerisation of triose sugars to lactic acid and methyl lactate (ML) in near quantitative yields using Sn-Beta at low temperatures.[10] The scope was expanded the following year with a report that also hexoses can be converted to ML at higher temperatures (160 °C) in 68% yield, with formation of small amounts of methyl vinyl glycolate (MVG).[4] At the same time, Sn-Beta was reported to be an active catalyst for the isomerisation of glucose to fructose and mannose in water at moderate temperatures (100 °C).[3]

This dependence on temperature enables some degree of versatility in the use of Sn-Beta as a catalyst. At moderate temperatures the Lewis acidic tin sites primarily catalyse a 1,2-hydride shift leading to isomerisation. At higher temperatures a C–C bond cleaving retro-aldol reaction is catalysed resulting in the fragmentation of monosaccharides to either the aforementioned triose sugars, which subsequently lead to ML (in methanol) or to C_2- and C_4-sugar fragments (glycolaldehyde and tetrose sugars) that form MVG (and glycolaldehyde dimethyl acetal, GA-DMA).[11,12] Additionally, Sn-based catalysts have also been used to catalyse the C–C bond formation to

[a]Technical University of Denmark, Department of Chemistry, Kemitorvet, 2800-Kgs. Lyngby, Denmark
[b]Haldor Topsøe A/S, Haldor Topsøes Allé 1, 2800-Kgs. Lyngby, Denmark. E-mail: esta@topsoe.dk
[c]Aarhus University, Carbon Dioxide Activation Center, Interdisciplinary Nanoscience Center, Department of Chemistry, Gustav Wieds Vej 14, 8000-Aarhus C, Denmark
†Electronic supplementary information (ESI) available. See DOI: 10.1039/c5gc02840j

form similar products (*e.g.* MVG, α-hydroxy-γ-butyrolactone) starting from small sugar-like fragments, such as formaldehyde, glycolaldehyde and the triose sugars.[11,13–15]

In addition to the reaction temperature, the presence of co-solutes is known to affect tin-catalysed reactions dramatically. Especially the presence of alkali metal salts has been reported to influence the catalytic properties of stannosilicate materials in a variety of reactions involving monosaccharides.[16–19]

It was reported in 2012 by Gunther *et al.* that addition of sodium tetraborate to aqueous glucose solutions, using Sn-Beta as catalyst at 80 °C, promotes an intramolecular 1,2-carbon shift over a 1,2-hydride shift. This leads to the epimerisation of glucose into mannose, rather than the isomerisation to fructose. In 2014 it was reported by Bermejo-Deval *et al.* that addition of sodium chloride and sodium exchanged Sn-Beta displays a similar catalytic performance as the one described by Gunther *et al.*, suggesting that the observed change in reaction pathway is attributable to the sodium ions and not to the tetraborate anion as first reported.[16,17] The epimerisation reaction has been hypothesised to occur as an intramolecular 1,2-carbon shift.[17,20] An alternative interpretation of the observed results could be that the 1,2-carbon shift occurs *via* a retro-aldol reaction of glucose to erythrose and glycolaldehyde, followed by an aldol reaction of the same species to form either glucose or mannose, effectively leading to the observed epimerisation.

An effect of alkali salts on the conversion of sugars into methyl lactate in reactions using stannosilicates was first reported in 2013.[18] It was found that addition of alkali metal salts to the reaction medium increases the yield of methyl lactate obtained from sugars in methanol using Sn-Beta at 170 °C from 30 to 75%.[19] The pronounced effect of alkali ions at trace amounts has led us to identify alkali metal contaminants, originating from the templating agent used in the synthesis of the Sn-Beta zeolite.

While Sn-Beta is not a commercial catalyst, recent developments have facilitated the production of the catalyst and thus increased its availability and attractiveness. Two approaches are currently employed to obtain active stannosilicate catalysts: (i) a direct synthesis route in which tin atoms are incorporated in the zeolite framework during hydrothermal synthesis, and (ii) a post-synthetic procedure, where vacancies are created within a crystalline Beta zeolite, in which tin is subsequently introduced. For Sn-Beta, approach (i) involves reacting a silicate- and a tin source at hydrothermal conditions (140 °C) in the presence of an organic structure directing agent, in an autoclave. This results in aluminium-free, highly hydrophobic and defect-free crystals.[21,22] Though currently only possible on laboratory scale, optimisations have been implemented to make the preparation industrially feasible.[23–25] Several stannosilicate materials are obtainable by direct synthesis including the zeotype Sn-MFI and the amorphous ordered mesoporous stannosilicates Sn-SBA-15 and Sn-MCM-41.[26–28]

Using the post-synthetic technique (ii), active Sn-Beta catalyst can be obtained for instance through dealumination of a commercial Beta zeolite, followed by incorporation of tin within the vacancies formed in the lattice.[29,30] This approach, which can also include deboronation or desilication, has expanded the accessible framework types, in which tin can successfully and with relative ease be incorporated (Sn-MWW, Sn-USY, *etc.*).[31–34] Changes in pore dimensions of various silicates can result in a complete change in product selectivity as recently shown by De Clercq *et al.*[35]

Despite of the great interest in catalytic glucose conversion to produce lactates, mechanistic details of the conversion and its modulation by co-solutes have remained sparse. The catalytic cascade involved in the conversion of sugars using Sn-Beta can be compared to its biological counterpart, the Embden–Meyerhof–Parnas glycolysis. Several main features are present in both cases: the isomerisation of glucose to fructose, the retro-aldol reaction to form two trioses and the isomerisation of the two trioses to the thermodynamic sink, lactic acid.[4] An additional glycolytic pathway, the Entner–Doudoroff glycolysis (ED), is also found in some bacteria and archaea. This biological pathway involves oxidation of phosphorylated glucose to gluconic acid followed by dehydration to produce 3-deoxyglucosonic acid. This intermediate then undergoes a retro-aldol reaction to produce a triose and glycerate, which are subsequently transformed to lactate.[36]

We report here, that stannosilicates in the absence of alkali metal salts catalyse reactions which bear resemblance to the first part of the ED glycolysis. The central intermediate in the inorganic glycolysis is 3-deoxyglucosone (3-deoxy-D-*erythro*-hexosulose, 3DG) instead of 3-deoxyglucosonic acid in the ED glycolysis. Further conversion of 3DG can lead to several products, most notably unbranched and deoxygenated C_6-esters and -lactones. They comprise multi-functionalised molecules, which could find applications within the specialty polymer segment. Finally, we argue that in the presence of alkali metal salts, some of the 3DG formed also undergoes a retro aldol reaction, forming pyruvaldehyde and glyceraldehyde which contributes to the overall yield of ML. This final pathway is an inorganic analogue to the ED pathway.

Results and discussion

Identification of the reaction products

The pronounced effect of alkali metal salts on the selectivity towards methyl lactate demands a further understanding of all the other products formed, especially in the absence of alkali metal salts. Therefore, the first step towards the unveiling of the reaction mechanism was the identification of all the by-products formed (Scheme 1). These were identified by means of NMR spectroscopy (assignment spectra recorded of the reaction mixtures) and GC-MS. Apart from the known retro-aldol reaction products methyl vinyl glycolate (MVG), glycolaldehyde dimethyl acetal (GA-DMA) and methyl 4-methoxy-2-hydroxybutyrate (MMHB) and unconverted sugars, the presence of several other major end-products was observed.

Among the most abundant species many were anticipated: methyl glycosides ('MG'), *i.e.* acetals of hexoses consisting

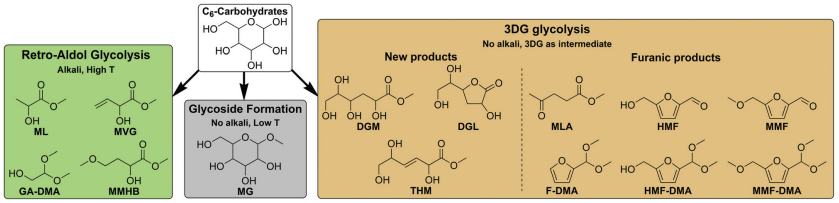

Scheme 1 Identified products from the conversion of glucose with Sn-Beta in methanol.

primarily of methyl glucopyranoside and methyl mannopyranoside were formed. Furanic end-products represented as 'FUR' including 5-(hydroxymethyl)furfural (HMF) and 5-(methoxymethyl)furfural (MMF), and the corresponding dimethyl acetals (HMF-DMA and MMF-DMA). Furfural dimethyl acetal (F-DMA) and methyl levulinate (MLA), although found in very small amounts, are also considered as furanic end-products. We speculate that F-DMA is formed by aldol reaction of C_2- and C_3-sugars to form small amounts of C_5-sugars, some of which are transformed to furfural by dehydration. We confirmed that F-DMA is not formed from HMF under the reaction conditions, ruling out this alternative explanation. Small amounts of formaldehyde dimethyl acetal were also observed.

In addition to the expected products, three interesting compounds were identified in the reaction mixture. They are partially dehydrated C_6-sugar acid derivatives, both in acyclic methyl ester form and cyclic lactone forms. These new compounds were identified by multidimensional NMR spectroscopy (Fig. 1) as *trans*-2,5,6-trihydroxy-3-hexenoic acid methyl ester (THM), 3-deoxy-γ-lactones (DGL) consisting of 3-deoxy-γ-gluconolactone and 3-deoxy-γ-mannonolactone and 3-deoxy-gluconic acid methyl ester (DGM). Identification of the products is provided in ESI (Fig. S1–S5†). A pure sample of THM was isolated from a scaled-up experiment (18 g of glucose, see ESI† for more information), and NMR spectroscopy was used to confirm the structure on this pure sample.

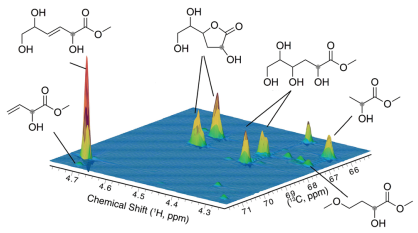

Fig. 1 $^{1}H–^{13}C$ spectral region of secondary alcohol CH-groups (indicated by small spheres) adjacent to carboxylic groups in the displayed compounds of a reaction mixture produced by the catalytic conversion of glucose in methanol at 140 °C. Compounds were identified by homo- and heteronuclear NMR assignment spectra recorded on the mixture.

These new findings enable the catalytic production of new molecules from sugars. THM in particular possesses a very interesting structure, where multiple functionalities are found. Promising applications, for instance, as a monomer or additive to synthesise materials with improved properties, can be foreseen. Earlier studies related to the degradation of sugars under alkaline conditions had reported the presence of *trans*-2,5,6-trihydroxy-3-hexenoic acid in very small amounts (<0.5%).[37,38] However, much higher THM yields are reported here (up to 18%).

Effect of the addition of alkali

In order to study the effect of alkali metal salts, 9 wt% solutions of glucose in methanol were reacted at 160 °C with Sn-Beta catalyst (alkali free) in the presence and in the absence of potassium carbonate in methanol (0–1.0 mM solutions) in high pressure glass reaction vessels. The yields of different components were calculated from GC, HPLC and multidimensional NMR spectroscopy and are shown in Fig. 2 and are grouped into three main classes, as shown in Scheme 1, based on the type of glycolytic reaction pathway they are formed in: (1) methyl glycosides (MG); (2) retro-aldol reaction products comprising ML, MVG, MMHB and GA-DMA; (3) glycolytic reaction involving dehydration to 3DG and further reaction products comprising furanics ('FUR'), such as HMF, MMF and F-DMA; methyl levulinate (MLA); 3-deoxy-γ-lactones (DGL) as well as THM, which is the main product in this category. These three product categories are respectively termed 'Methyl Glycosides' (MG), 'RA products' and '3DG products' throughout this paper.

It can be observed that the addition of alkali changes the distribution of the products drastically. While the '3DG products' represent almost 35% of the yield in the absence of alkali, 'RA products' become dominant for K_2CO_3 concentrations above 0.1 mM. In the presence of alkali metal salts, the retro-aldol reaction pathway is responsible for about 70% of the overall glucose conversion.

Here, the main products are the C_2–C_4 products methyl lactate (ML, ~50%), methyl vinyl glycolate (MVG, ~18%), glyco-

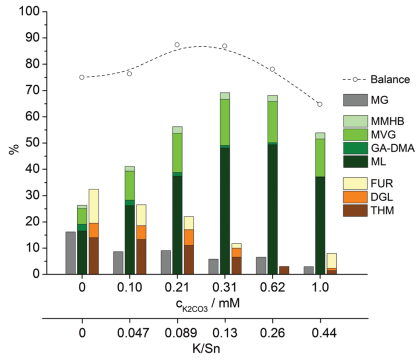

Fig. 2 Effect of alkali concentration on glucose conversion by Sn-Beta. Nuances of green and brown are retro-aldol and 3DG products, respectively. Reaction conditions: 0.180 g Sn-Beta (PT, Si/Sn = 125), 0.360 g glucose, 4.0 g of a solution with 0–1.0 mM K_2CO_3 in methanol, 160 °C, 6 h. The data is reported in ESI Table S1.†

laldehyde dimethyl acetal (GA-DMA) and methyl 4-methoxy-2-hydroxybutyrate (MMHB). THM is formed in yields of 6% in the presence of 0.31 mM K_2CO_3, illustrating that carbon flux *via* the 3DG pathway is still occurring even under these conditions.

Standard deviation was calculated for triplicates of selected alkali concentrations and the results are shown in Table S2.† It can be observed that the deviation is below 3% in all the cases, indicating that the results obtained are reliable.

From the results depicted in Fig. 2, it is clear that the 3DG reaction pathway is dominant in the absence of added alkali metal salts. In this case, THM is formed in a yield of 14%, together with 6% lactones (DGL) and 13% furanics. The effect of alkali metal salts results primarily from favouring the RA reaction pathway over the 3DG reaction pathway. This might suggest that the glycolytic pathways are affected by the acidic environment in the stannosilicate material. Hydroxyl groups in the near vicinity of the tin-sites, as well as partially-hydrolysed tin-sites have been proposed to constitute the active site in Sn-Beta.[20,39,40] The observed effect of alkali metals is thus likely related to an ion-exchange of these Brønsted acidic sites, as has been hypothesised for comparable materials (TS-1 and Ti-Beta) in various reports.[41–43] Homogeneous systems involving tin are also affected by the presence of alkali salts, which could indicate a degree of simultaneous homogeneous catalytic activity of the alkali metal salts.[44,45]

For Sn-Beta, the mass balance in the absence of added alkali metal salts is 75% and has an optimum at almost 90% for alkali concentrations between 0.21 and 0.31 mM (Fig. 2). For higher amounts of alkali a decrease in the carbon balance to 65% occurs, which is accompanied by a darkening of the product mixture after reaction, as shown in Fig. S6.† Blank experiments without Sn-Beta both with and without addition of alkali metal salts lead to formation of methyl glycosides (see Table S4,† entries 4 and 5). Again, the addition of alkali decreased the mass balance considerably, showing that the stability of the sugar is low under alkaline conditions.

ICP analyses of the liquid after reaction in the absence of added alkali indicated the presence of very low amounts of sodium (Na^+, 4 wt ppm). This minor contamination was constant in all of the reactions, without any correlation to the addition of K_2CO_3 and is probably due to small amounts of sodium remaining in the catalyst or the borosilicate glassware used for the reactions. This alkali should therefore be considered as 'background' alkali and it is likely that higher selectivity *via* the 3DG pathway than reported here could be reached.

A series of kinetic experiments were conducted in order to better evaluate the effect of the presence of alkali. It is clear from Fig. 3 that the addition of alkali ions to the reaction medium modifies the progress of the reaction. The conversion of glucose to methyl glycosides is lowered in the presence of alkali. While almost 50% MG are produced after ten minutes in the absence of added alkali, this amount decreases to 15% when the experiment was performed in the presence of 0.6 mM K_2CO_3. When attempting to convert the commercially available methyl glucosides (methyl α-D-glucopyranoside, methyl β-D-glucopyranoside and methyl α-D-mannopyranoside) almost no conversion was achieved after 6 h at 160 °C in the absence of added alkali (3–15%, see Table S4,† entries 1–3). The formation of MG as pyranosides essentially limits the further reaction towards the desired products. No methyl furanosides were observed, which is in good agreement with previous studies showing that furanosides have an increased reactivity.[46] Moreover, the rate of formation of ML and the other 'RA products' is substantially increased upon addition of small amounts of alkali. The ML yield increased from 4 to

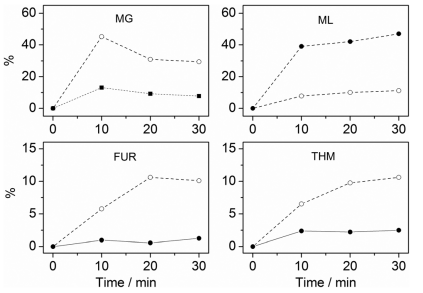

Fig. 3 Kinetic experiments on product formation at low conversion with (open circle) and without (solid circle) addition of alkali metal salts. Reaction conditions: 0.180 g Sn-Beta (PT, Si/Sn = 125), 0.360 g glucose, 4.0 g of a solution with either 0 or 0.62 mM K_2CO_3 in methanol, 160 °C. The data are reported in ESI Table S3.†

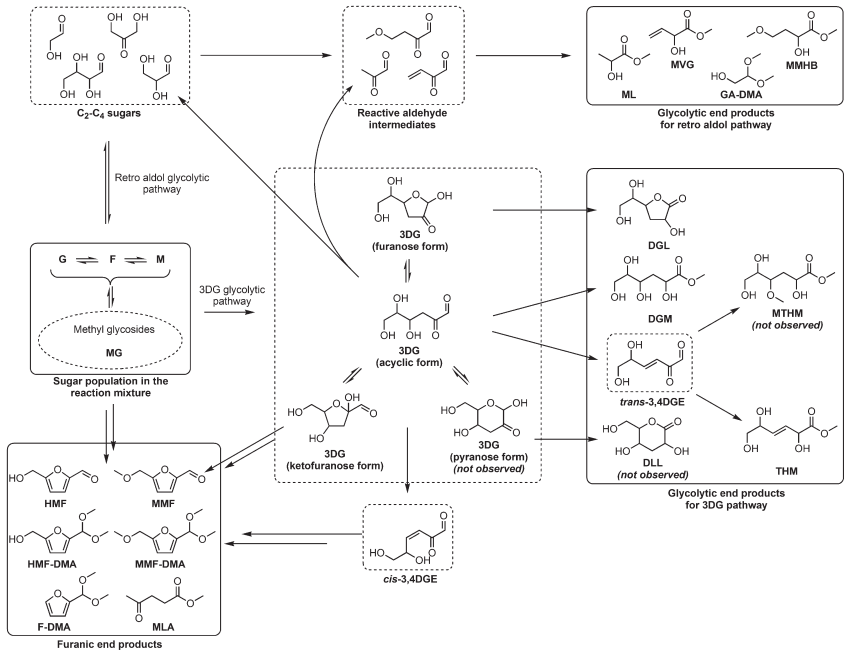

Scheme 2 Different glycolytic pathways in the conversion of glucose by Sn-Beta in methanol.

20% after ten minutes in the presence of 0.6 mM K_2CO_3. Finally, the formation of furanics ('FUR') and THM was also minimised in the presence of added alkali. The addition of alkali diminishes both THM and furanics in a comparable manner, indicating that they are indeed formed along similar reaction pathways. These kinetic experiments further illustrate the pronounced effect of alkali metal salts and the delicate balance of Brønsted acidity in the Sn-Beta catalyst when using sugars. Selectivity to different products is clearly affected by small changes in acidity of the system.

Elucidation of the reaction mechanism

Based on these results, a comprehensive reaction scheme (Scheme 2) can be proposed, in which 3-deoxyglucosone (3DG) is the central intermediate. The presence of 3DG in the reaction solutions was confirmed by direct observation of the methyl acetal of 3DG at incomplete conversion (Fig. 4). At full conversion, the presence of 3DG isomers is greatly diminished, confirming its role as a reaction intermediate.

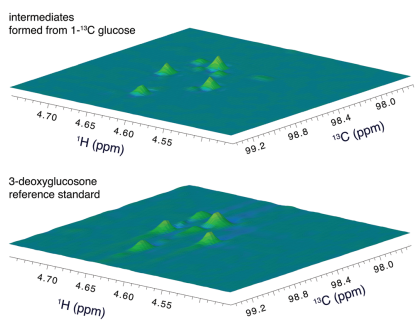

Fig. 4 Identification of 3DG as a reaction intermediate by comparison of the acetal region between a reaction mixture and an authentic standard by 2D ^1H–^{13}C HSQC.

The formation of 3DG from glucose is effectively a β-dehydration reaction that is likely to proceed *via* a retro-Michael addition of water from the 1,2-enol form of the sugar (Scheme 2). Hence, it is not a dehydration that is likely to be catalysed by conventional Brønsted acid catalysis. This reaction pathway has been suggested by Sels and co-workers for the analogous formation of C_4-compounds from tetroses.[12] The outcome is that glucose is transformed into the enol form of 3DG, which upon tautomerisation is fully converted into 3DG. This dehydration reaction is likely irreversible under the applied reaction conditions in analogy to pyruvaldehyde, which is known not to undergo rehydration to form trioses. In addition, fructose should follow the same reaction pathway once it has enolised on an active tin-site, since the 1,2-enol form of fructose is identical to the enol form of glucose (and of mannose). Hence, the same distribution of end-products for 3DG should be expected from glucose, fructose and mannose.

The further conversion of 3DG can occur *via* several routes. The most important ones involve further dehydration of 3DG *via* a subsequent β-elimination of water (Scheme 2) to form 3,4DGE. We have not observed 3,4DGE directly in our reaction mixture, and its presence is hypothesised from the formation of THM and HMF.[47] We speculate that *trans*-3,4DGE is converted into THM in an analogous fashion as vinyl glyoxal is transformed into MVG, *i.e.* by addition of methanol to the aldehyde moiety, followed by a 1,2-hydride shift resulting in the formation of the resulting α-hydroxy ester.[12] Interestingly, the THM identified in the reaction product is entirely the *trans*-isomer and no traces of the *cis*-isomer are seen in the reaction mixtures. We speculate that the *cis*-3,4DGE is also formed on the active sites of Sn-Beta, but that it is readily converted into HMF *via* an intramolecular cyclisation and dehydration reaction, and this is the major source of HMF and other derivatives formed from hexoses (in the absence of strong Brønsted acids).[47] It is likely that different *cis*/*trans* ratios are in part defined by the stereochemistry of the C_4 (or more precisely on the relative stereochemistry of the C_4- and C_5-positions). However, when comparing glucose–fructose–mannose and galactose–tagatose (Table 1), we did not observe any major differences in the ratios of HMF and THM, suggesting that this effect is not significant, if present at all.

A minor part of the 3DG does not undergo β-elimination of water, and is instead converted to end-products *via* 1,2-hydride shift reactions. In methanol, at $T > 140$ °C, 3-deoxy γ-gluconoand γ-mannonolactones (DGL) are the main end-products from 3DG in combined yields of about 8%. These are either formed by direct lactonisation of the 3DG furanoside or from methyl 3-deoxygluconolactone, which undergoes lactonisation and elimination of methanol. Addition of methanol to

Table 1 Conversion of monosaccharides in the absence of alkali using a selection of Beta-framework and/or tin containing catalysts

						3DG products	
				MG	Retro-aldol products[a]	FUR[a]	THM
Entry	Catalyst	Substrate	Temperature °C	%	%	%	
1	Sn-Beta (PT)	Glucose	120	44	4	10	8
2	Sn-Beta (PT)	Glucose	140	21	10	16	12
3	Sn-Beta (PT)	Glucose	160	13	17	13	14
4	Sn-Beta (PT)	Glucose	180	5	26	10	8
5	Sn-Beta (PT)	Fructose	160	9	19	14	18
6	Sn-Beta (PT)	Mannose	160	12	20	12	15
7	Sn-Beta (PT)	Sorbose	160	13	15	14	17
8	Sn-Beta (PT)	Galactose	160	26	10	13	12
9	Sn-Beta (PT)	Tagatose	160	11	11	18	9
10	Sn-Beta (PT)	Sucrose	160	10	22	13	15
11	Sn-Beta (HF)	Glucose	160	8	24	9	16
12	Zr-Beta (HF)	Glucose	160	27	25	2	2
13	Ti-Beta (HF)	Glucose	160	14	28	3	3
14	Hf-Beta (HF)	Glucose	160	35	18	8	4
15	Al-Beta	Glucose	160	32	<1	14	<1
16	deAl-Beta	Glucose	160	86	<1	<1	<1
17	deAl-Beta	Fructose	160	51	2	14	<1
18	Sn-MCM-41	Glucose	160	16	26	13	18
19	Sn-MFI	Glucose	160	40	8	<1	<1
20	SnO_2-Beta (HF)	Glucose	160	37	1	2	<1
21	Si-Beta (HF)	Glucose	160	46	3	3	<1

Yields (carbon%) of methyl glycosides (MG), methyl lactate (ML), methyl vinylglycolate (MVG), glycolaldehyde dimethylacetal (GA-DMA), methyl 4-methoxy-2-hydroxybutanoate (MMHB), combined yield of 5-(hydroxymethyl)furfural (HMF), 5-(methoxymethyl)furfural (MMF) and furfural dimethylacetal (F-DMA) denoted FUR and *trans*-2,5,6-trihydroxy-3-hexenoic acid methyl ester (THM) from the conversion of various sugars using a variety of catalysts, different sugars and at different temperatures. Reaction conditions: 160 °C, 360 mg substrate, 4 g methanol, 180 mg catalyst, 6 h, 600 rpm stirring. [a] Combined yield of quantified retro-aldol products (ML, GA-DMA, MVG and MMHB) and furanics (HMF, MMF, MLA and F-DMA). For yields of the individual products see Table S5.

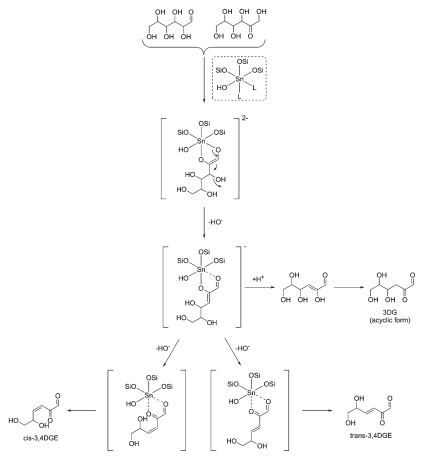

Scheme 3 Proposed mechanism for the dehydration of sugars to 3DG.

3,4DGE (Scheme 3) would lead to the formation of 4-methoxy-2,5,6-trihydroxyhexanoic acid methyl ester (MTHM), but this compound is below the detection limit in our reaction mixture.

When using commercial 3DG as substrate, the main products from the glycolytic 3DG pathway (DGL, THM and furanics) are observed as end-products (Fig. S7†). In contrast to experiments using monosaccharides as substrates, the major products formed from commercial 3DG are a complicated mixture with the two 3-deoxy-γ-lactones being predominant. Small amounts of THM and HMF derivatives are seen from 3DG, suggesting that a commercial sample of 3DG does not fully represent the reactive 3DG formed from monosaccharides in the pores of Sn-Beta. It has been reported previously that 3DG consists of a complex mixture of aldo-furanosides, keto-furanosides and pyranosides in methanol, with very little acyclic 3DG.[48] It is therefore likely that the product composition of commercial 3DG reflects preformed conformational distributions rather than the inherent reactivity of 3DG formed as a pathway intermediate. Interestingly, the ratio of THM to furanics obtained from 3DG seems to be lower than in the case of glucose. This means that more furanics are produced from 3DG. This fact supports the hypothesis that most of the furanics produced in the reaction from sugars are indeed formed *via* 3DG as intermediate, and not directly from sugars. This has previously been confirmed for the formation of furanics *via* 3DG by Bols and coworkers.[49]

It has been reported that 3DG can undergo a retro-aldol reaction and form glyceraldehyde and pyruvaldehyde (enol form) which are both readily transformed into methyl lactate.[50–52] If 3DG is indeed a major source for methyl lactate, then the reaction cascade would greatly resemble the ED glycolysis. From the commercial 3DG sample there were also observed trace amounts of methyl lactate in the product mixture (1–2%). Again, the absence of acyclic 3DG in the commercial reference might explain the low amount of methyl lactate obtained. However, due to the complexity of the commercial 3DG used in this experiment, it is not possible to use this direct experiment to determine the extent of retro-aldol reaction products formed *via* 3DG *versus* direct reaction from sugars. An indirect indication of the contribution of the 3DG pathway to the production of methyl lactate can be obtained from the effect of alkali addition (Fig. 2, data of Table S1†). The ratio of methyl lactate to the total amount of 'RA products' has been calculated (ML/'RA products'). The retro-aldol reaction from 3DG will only lead to ML. The only route for the formation of C_2 and C_4 products is *via* a 'conventional' retro-aldol reaction of the aldohexoses. An increase in the percentage of methyl lactate will thus indicate the contribution of the 3DG route to ML formation. From the results in Table S1,† it is clear that there is an increase in the proportion of methyl lactate (from 63% to 72% of the total 'RA products') when increasing the concentration of alkali (Table S1,† entries 1–5). This observed deviation is corroborated by the kinetic experiments shown in Fig. 3 (data shown in Table S3†), where the percentage of methyl lactate follows the same trend with the addition of alkali (from 59% to 69%). The percentage seems to be independent of the conversion level and it is only related to the amount of alkali added to the reaction medium. Bearing this in mind, we propose that 3DG can be a source of methyl lactate, despite the very low amounts we observed in our experiment using authentic 3DG as a substrate. Further studies are needed to determine the extent of retro-aldol reaction of 3DG and evaluate whether ED glycolysis mechanism has a significant contribution to the formation of methyl lactate using stannosilicates.

Other important parameters affecting the reaction

Different reaction parameters and catalysts were investigated in the absence of added alkali and the reaction mixtures were analysed thoroughly by HPLC and GC. As can be seen in Table 1 (entries 1–4), the temperature plays an important role. When the reactions were carried out at 120 °C, 40% of methyl glycosides (MG) were obtained as the main product formed at low temperatures. As the temperature increases, 'RA glycolysis' products become dominant. The production of THM reached a maximum at 160 °C (14%, Table 1, entry 3), while the furanics (FUR) were formed in similar amounts over the temperature range tested.

The effect of the preparation method of the Sn-Beta and the metal incorporated in the framework of the zeolite Beta were also investigated. Characterisation of the catalysts can be found in ESI Fig. S8, S9 and Table S6.† A slightly higher yield of 16% THM was observed when using a Sn-Beta catalyst crystallised in a fluoride medium (entry 10) compared to a catalyst

prepared by post-treatment of a commercial Beta, which gave 14% THM (entry 3).

Other metals (Zr, Ti and Hf) showed a considerably lower yield of '3DG glycolysis' products (entries 12–14). Only small amounts of THM were observed, suggesting that these catalysts are not highly active catalysts for β-elimination of water. It is interesting to note that only minor changes in product distribution were observed with increase in alkali content with Zr-Beta (see Table S7†), indicating that the alkali effect is directly related to the nature of the active site.

Different Sn-based catalysts were also tested. It was found that Sn-MCM-41 (entry 18) displays a similar reaction profile as Sn-Beta and a substantial yield of THM (18%) was observed for this catalyst. Sn-MCM-41 has also been reported previously to be capable of forming high amounts (~60%) of methyl lactate from sucrose in the presence of alkali metal salts,[19] suggesting that it has a similar catalytic behaviour as Sn-Beta both in the presence and in the absence of alkali. The other stannosilicate material, Sn-MFI, was not very active in the formation of products from hexoses, as has been reported previously and related to its smaller pores limiting its usefulness as a catalyst for the conversion of hexoses.[35] As expected, SnO_2 on Si-Beta and pure Si-Beta (entries 20 and 21) were inactive for the formation of both RA products and 3DG products. Using these catalysts, most of the glucose was transformed into methyl glycosides (MG). No THM was observed using Al-containing zeolites as catalysts. Commercial zeolite Beta (Si/Al = 12.5) yielded some FUR (14%) from glucose but the mass balance was low (<50%), illustrating that high concentration of Brønsted acidity catalyses degradation reactions under the applied reaction conditions. At lower temperature it is, however, possible to suppress such degradation reactions and obtain a high carbon balance along with a high yield of fructose.[46] Using the de-aluminated Beta zeolite, which has been used as the precursor in the preparation of the post-treated Sn-Beta zeotype, resulted in the formation of large amounts of MG and neither 3DG nor RA products were observed. From fructose, some furanics (FUR, 14%) and small amounts of RA products (~2%) were formed as expected, but no THM was observed. It can therefore not be ruled out that residual Brønsted acidity in the finished Sn-Beta zeolite could contribute to the formation of furanics during conversion of the aldohexoses. On the other hand, THM is formed by catalysis involving the Sn-site, clearly demonstrating the unique catalytic properties of tin-containing silicates.

Conclusions

We report a detailed investigation of the glycolytic reaction pathways that are catalysed by stannosilicates. A new glycolytic reaction pathway involving 3DG as the central intermediate was discovered. This reaction pathway could lead to new ways of converting abundant and cheap glucose into new and interesting chemicals such as THM and 3-deoxy-γ-lactones. In the absence of alkali metal salts, stannosilicates catalyse the β-elimination of water converting glucose–fructose–mannose into 3DG. Under the reaction conditions studied here, most of the 3DG underwent a further β-elimination of water leading to 3,4DGE which was converted into THM (*trans*-3,4DGE) and HMF (*cis*-3,4DGE) and related derivatives. In the presence of alkali metal salts the rate of formation of retro aldol products is increased, making the retro aldol pathway dominant. Further, alkali metal salts reduce the rate of formation of methyl glycosides, thereby effectively leading to more free monosaccharides in solution than in the absence of alkali. It is remarkable that the presence or the absence of ppm levels of alkali metal salts can influence the catalytic properties of stannosilicates so dramatically. From the increase of methyl lactate with respect to the total 'RA products', indirect evidence for a ED type glycolysis pathway has been found. The presence of this alternative pathway may be responsible for the improvement of the yield of ML. We envisage that further control of the active sites of stannosilicate materials such as Sn-Beta will enable a much higher degree of control between these two glycolytic pathways, and thereby enable the low cost transformation of glucose into a variety of chemicals using inorganic catalytic systems.

Experimental

Catalytic tests

Catalytic conversion of sugars was performed in a 5 mL glass microwave reaction vial (Biotage). Typically, 120 mg (0.67 mmol) of glucose (Sigma-Aldrich, >99.0%), 60 mg of catalyst (prepared as described in the ESI†), and 4.0 g of methanol (Sigma-Aldrich, >99.8%) were added to the reaction vial. The reactor was sealed and heated to 160 °C under stirring (600 rpm) in a microwave synthesiser (either a Biotage Initiator or a Biotage Initiator+). After 6 h, the reaction was cooled and aliquots were retrieved from the reactor vessel and filtered using a 0.22 μm syringe filter. In reactions involving alkali-containing solutions, the alkali metal source (K_2CO_3, Sigma-Aldrich, ≥99.0%) was dissolved directly in methanol before use in the desired concentration.

Analysis

Reaction solutions were analysed thoroughly using NMR spectroscopy and the reaction components were identified. Quantification was performed using NMR spectroscopy, GC-FID/MS and HPLC-RI/DAD. The reported yields of the individual components are carbon yields based on glucose (further information in ESI†).

The yields of methyl lactate (ML), methyl vinyl glycolate (MVG), glycolaldehyde dimethylacetal (GA-DMA) and methyl 4-methoxy-2-hydroxybutanoate (MMHB) were quantified using a 7890A Series GC system (Agilent Technologies) with a SolGel-WAX column (Phenomenex). No commercial source of MMHB was available and the response factor of MVG was used to approximate the amount of the compound.

trans-2,5,6-Trihydroxy-3-hexenoic acid methyl ester (THM) was identified and quantified by GC-MS on an Agilent 6890 with a Phenomenex Zebron ZB-5 column equipped with an Agilent 5973 mass selective detector. Since no commercial source was available for THM, this compound was purified and used for calibration, see ESI† for purification method. Methyl levulinate (MLA) was likewise analysed and quantified from GC-MS spectra of the reaction liquids.

For the quantification of furanics an Agilent 1200 series HPLC equipped with an Aminex HPX-87H (BioRad) column (0.004 M H_2SO_4, 0.6 mL min^{-1}, 65 °C) using a refractive index and diode array detector was used. During the reaction, any furanics formed will undergo acetalisation with the methanol solvent. These acetals hydrolyse under the acidic conditions during the HPLC analysis and are therefore quantified as 5-(hydroxymethyl)furfural (Aldrich, ≥99%), 5-(methoxymethyl) furfural (Manchester Organics) and furfural (Sigma-Aldrich, 99%) using the appropriate standards.

Sugar conversion as well as an estimation of the remaining methyl sugars were quantified on an Agilent 1200 series HPLC equipped with a Carbohydrate (Zorbax) column (60 wt% acetonitrile/water, 0.5 mL min^{-1}, 30 °C). The response factor used for the combined methylated sugar yield was based on an average of the three commercially available methyl sugars; methyl α-D-glucopyranoside (Sigma, ≥99%), methyl β-D-glucopyranoside (Sigma, ≥99%) and methyl α-D-mannopyranoside (Sigma, ≥99%), see ESI Fig. S10.† The estimate was additionally verified by NMR of the reaction liquids.

For the discovery of chemicals formed in the stannosilicate-catalysed conversion of glucose, high-field NMR spectroscopy was employed on a Bruker Avance II 800 MHz spectrometer equipped with a TCI Z-gradient CryoProbe and an 18.7 T magnet (Oxford Magnet Technology, Oxford, U.K.). To this end, 10% (w/v) natural abundance glucose in methanol was reacted at 140 °C in the absence of added alkali ions for 6 h in methanol. Subsequently 1 mL of the sample was condensed and re-dissolved in d_4-methanol (99.96 atom%, Sigma-Aldrich, St. Louis, MO). Standard homonuclear 1D, 2D COSY and 2D TOCSY were carried out on the non-enriched sample in addition to heteronuclear ^1H–^{13}C HMBC and highly ^{13}C resolved ^1H–^{13}C HSQC and ^1H–^{13}C HSQC-TOCSY spectra. All spectra were recorded at 30 °C. Identification of compounds in the reaction mixture was aided by the use of pure reference standards (including 3DG, monosaccharides, methyl-glycosides, furanics and methyl lactate).

The NMR quantification of identified compounds in reaction mixtures was performed by addition of 10% d_4-methanol to 500 μl of reaction mixture and subsequent ^{13}C 1D NMR spectroscopy sampling 16 384 complex data points during an acquisition time of 1.6 seconds and using a recycle delay of 58.4 seconds between 400 scans. This method was used for verification of other analysis procedures and quantification of 3-deoxy-γ-lactones (DGL).

The metallosilicate materials used were synthesised according to previously published procedures.[21,22,26,27] More details on each individual synthesis and characterisation are included in the ESI.†

Acknowledgements

The work of ST, SGE and SKK is funded by the Bio-Value platform (http://biovalue.dk) under the SPIR initiative by The Danish Council for Strategic Research and The Danish Council for Technology and Innovation, case number 0603-00522B. SM gratefully acknowledges funding by Grant 2013_01_0709 of the Carlsberg Foundation. 800 MHz NMR spectra were recorded on the spectrometer of the Danish National Instrument Center for NMR Spectroscopy of Biological Macromolecules at the Technical University of Denmark.

References

1 P. N. R. Vennestrøm, C. M. Osmundsen, C. H. Christensen and E. Taarning, *Angew. Chem., Int. Ed.*, 2011, **50**, 10502–10509.
2 R. Datta and M. Henry, *J. Chem. Technol. Biotechnol.*, 2006, **81**, 1119–1129.
3 M. Moliner, Y. Román-Leshkov and M. E. Davis, *Proc. Natl. Acad. Sci. U. S. A.*, 2010, **107**, 6164–6168.
4 M. S. Holm, S. Saravanamurugan and E. Taarning, *Science*, 2010, **328**, 602–605.
5 N. Ji, T. Zhang, M. Zheng, A. Wang, H. Wang, X. Wang and J. G. Chen, *Angew. Chem., Int. Ed.*, 2008, **120**, 8638–8641.
6 Y. Román-Leshkov, J. N. Chheda and J. A. Dumesic, *Science*, 2006, **312**, 1933–1937.
7 Y. Liu, C. Luo and H. Liu, *Angew. Chem., Int. Ed.*, 2012, **124**, 3303–3307.
8 E. Nikolla, Y. Román-Leshkov, M. Moliner and M. E. Davis, *ACS Catal.*, 2011, **1**, 408–410.
9 S. Saravanamurugan and A. Riisager, *ChemCatChem*, 2013, **5**, 1754–1757.
10 E. Taarning, S. Saravanamurugan, H. M. Spangsberg, J. Xiong, R. M. West and C. H. Christensen, *ChemSusChem*, 2009, **2**, 625–627.
11 M. S. Holm, Y. J. Pagán-Torres, S. Saravanamurugan, A. Riisager, J. A. Dumesic and E. Taarning, *Green Chem.*, 2012, **14**, 702–706.
12 M. Dusselier, P. Van Wouwe, F. de Clippel, J. Dijkmans, D. W. Gammon and B. F. Sels, *ChemCatChem*, 2013, **5**, 569–575.
13 S. Van de Vyver, C. Odermatt, K. Romero, T. Prasomsri and Y. Román-Leshkov, *ACS Catal.*, 2015, **5**, 972–977.
14 M. Dusselier, P. Van Wouwe, S. De Smet, R. De Clercq, L. Verbelen, P. Van Puyvelde, F. E. Du Prez and B. F. Sels, *ACS Catal.*, 2013, **3**, 1786–1800.
15 S. Yamaguchi, T. Matsuo, K. Motokura, Y. Sakamoto, A. Miyaji and T. Baba, *ChemSusChem*, 2015, **8**, 853–860.
16 W. R. Gunther, Y. Wang, Y. Ji, V. K. Michaelis, S. T. Hunt, R. G. Griffin and Y. Román-Leshkov, *Nat. Commun.*, 2012, **3**, 1109.
17 R. Bermejo-Deval, M. Orazov, R. Gounder, S.-J. Hwang and M. E. Davis, *ACS Catal.*, 2014, **4**, 2288–2297.

18 M. S. Holm, I. Sábaba, S. Tolborg, C. M. Osmundsen and E. Taarning, *WO* 2015024875A1, 2015.
19 S. Tolborg, I. Sádaba, C. M. Osmundsen, P. Fristrup, M. S. Holm and E. Taarning, *ChemSusChem*, 2015, **8**, 613–617.
20 N. Rai, S. Caratzoulas and D. G. Vlachos, *ACS Catal.*, 2013, **3**, 2294–2298.
21 A. Corma, L. T. Nemeth, M. Renz and S. Valencia, *Nature*, 2001, **412**, 423–425.
22 S. Tolborg, A. Katerinopoulou, D. D. Falcone, I. Sádaba, C. M. Osmundsen, R. J. Davis, E. Taarning, P. Fristrup and M. S. Holm, *J. Mater. Chem. A*, 2014, **2**, 20252–20262.
23 C.-C. Chang, Z. Wang, P. Dornath, H. J. Cho and W. Fan, *RSC Adv.*, 2012, **2**, 10475–10477.
24 Z. Kang, X. Zhang, H. Liu, J. Qiu and K. L. Yeung, *Chem. Eng. J.*, 2013, **218**, 425–432.
25 C.-C. Chang, H. J. Cho, Z. Wang, X. Wang and W. Fan, *Green Chem.*, 2015, **17**, 2943–2951.
26 C. M. Osmundsen, M. S. Holm, S. Dahl and E. Taarning, *Proc. R. Soc. London, Ser. A*, 2012, **468**, 2000–2016.
27 L. Li, C. Stroobants, K. Lin, P. A. Jacobs, B. F. Sels and P. P. Pescarmona, *Green Chem.*, 2011, **13**, 1175–1181.
28 N. K. Mal and A. V. Ramaswamy, *Appl. Catal., A*, 1996, **143**, 75–85.
29 C. Hammond, S. Conrad and I. Hermans, *Angew. Chem., Int. Ed.*, 2012, **51**, 11736–11739.
30 P. Li, G. Liu, H. Wu, Y. Liu, J.-G. Jiang and P. Wu, *J. Phys. Chem. C*, 2011, **115**, 3663–3670.
31 P. Y. Dapsens, C. Mondelli and J. Pérez-Ramírez, *ChemSusChem*, 2013, **6**, 831–839.
32 X. Yang, L. Wu, Z. Wang, J. Bian, T. Lu, L. Zhou, C. Chen and J. Xu, *Catal. Sci. Technol.*, 2016, DOI: 10.1039/C5CY01037C.
33 Q. Guo, F. Fan, E. A. Pidko, W. N. P. van der Graaff, Z. Feng, C. Li and E. J. M. Hensen, *ChemSusChem*, 2013, **6**, 1352–1356.
34 J. Dijkmans, J. Demol, K. Houthoofd, S. Huang, Y. Pontikes and B. Sels, *J. Catal.*, 2015, **330**, 545–557.
35 R. De Clercq, M. Dusselier, C. Christiaens, J. Dijkmans, R. I. Iacobescu, Y. Pontikes and B. F. Sels, *ACS Catal.*, 2015, **5**, 5803–5811.
36 A. H. Romano and T. Conway, *Res. Microbiol.*, 1996, **147**, 448–455.
37 L. Löwendahl and O. Samuelson, *Sven. Papperstidn.*, 1974, **77**, 593–602.
38 K. Niemela and E. Sjostrom, *Holzforschung*, 1986, **40**, 9–14.
39 M. Boronat, P. Concepcion, A. Corma, M. Renz and S. Valencia, *J. Catal.*, 2005, **234**, 111–118.
40 G. Li, E. A. Pidko and E. J. M. Hensen, *Catal. Sci. Technol.*, 2014, **4**, 2241–2250.
41 B. Notari, *Stud. Surf. Sci. Catal.*, 1991, **67**, 243–256.
42 T. Tatsumi, K. A. Koyano and Y. Shimizu, *Appl. Catal., A*, 2000, **200**, 125–134.
43 M. Ogura, S. I. Nakata, E. Kikuchi and M. Matsukata, *J. Catal.*, 2001, **199**, 41–47.
44 L. Zhou, L. Wu, H. Li, X. Yang, Y. Su, T. Lu and J. Xu, *J. Mol. Catal. A: Chem.*, 2014, **388–389**, 74–80.
45 K. Nemoto, Y. Hirano, K.-I. Hirata, T. Takahashi, H. Tsuneki, K.-I. Tominaga and K. Sato, *Appl. Catal., B*, 2016, **183**, 8–17.
46 S. Saravanamurugan, M. Paniagua, J. A. Melero and A. Riisager, *J. Am. Chem. Soc.*, 2013, **135**, 5246–5249.
47 M. Hellwig, J. Degen and T. Henle, *J. Agric. Food Chem.*, 2010, **58**, 10752–10760.
48 H. Weenen and S. B. Tjan, in *Flavor Precursors*, American Chemical Society, 1992, vol. 490, ch. 17, pp. 217–231.
49 H. Jadhav, C. M. Pedersen, T. Solling and M. Bols, *ChemSusChem*, 2011, **4**, 1049–1051.
50 Y. V. Pfeifer, P. T. Haase and L. W. Kroh, *J. Agric. Food Chem.*, 2013, **61**, 3090–3096.
51 T. Fiedler, T. Moritz and L. Kroh, *Eur. Food Res. Technol.*, 2006, **223**, 837–842.
52 P. J. Thornalley, A. Langborg and H. S. Minhas, *Biochem. J.*, 1999, **344**, 109–116.

Supporting Information

Tin-Containing Silicates: Identification of a Glycolytic Pathway via 3-Deoxyglucosone

S. Tolborg,[a,b] S. Meier[a], I. Sádaba,[b] S. G. Elliot,[a,b] S. K. Kristensen,[c] S. Saravanamurugan,[a]
A. Riisager,[a] P. Fristrup,[a] T. Skrydstrup,[c] and E. Taarning[*,b]

a. Technical University of Denmark, Department of Chemistry, Kemitorvet, 2800-Kgs. Lyngby, Denmark
*b. Haldor Topsøe A/S, Haldor Topsøes Allé 1, 2800-Kgs. Lyngby, Denmark *e-mail: esta@topsoe.dk*
c. Aarhus University, Carbon Dioxide Activation Center, Interdisciplinary Nanoscience Center, Department of Chemistry, Gustav Wieds Vej 14, 8000-Aarhus C, Denmark

Contents

Catalyst Preparation

Sn-, Zr-, Ti and Hf-Beta zeolites via hydrothermal synthesis procedure

Sn-Beta zeolites (Si/Sn = 125) were synthesized by modifying the route described by Valencia *et al.*[1] In a typical synthesis procedure, 30.6 g of tetraethyl orthosilicate (TEOS, Aldrich, 98%) was added to 33.1 g of tetraethylammonium hydroxide (TEAOH, Sigma-Aldrich, 35% in water) under careful stirring, forming a two-phase solution. After stirring (~60 min) one phase is obtained and tin(IV) chloride pentahydrate ($SnCl4{\cdot}5H_2O$, Aldrich, 98%) dissolved in 2.0 mL of demineralized water was added drop wise. Stirring was maintained for several hours to allow ethanol formed from the hydrolysis of TEOS to evaporate. Finally, 3.1 g hydrofluoric acid (HF, Fluka, 47-51%) in 1.6 g of demineralized water was added to the gel, yielding a solid with the molar composition; $1.0Si{:}0.005Sn{:}0.02Cl^{-}{:}0.55TEA^{+}{:}0.55F^{-}{:}7.5H_2O$. All samples were then homogenized and transferred to a Teflon-container placed in a stainless steel autoclave. This was then placed at 140°C for 14 days. The solid was recovered by filtration and washed with demineralized water, followed by drying overnight at 80°C in air. The organic template contained within the material was removed by heating the sample at 2°C/min to 550 °C in static air and maintaining this temperature for 6 h.

Zr-Beta (Si/Zr = 150) and Hf-Beta (Si/Hf = 200) zeolites were prepared by the aforementioned procedure, exchanging the tin source with $ZrOCl_2{\cdot}8H_2O$ (Sigma-Aldrich, 98 %) or $HfCl_4$ (Aldrich, 98 %), respectively. For Ti-Beta (Si/Ti = 150), tetraethyl orthosilicate (Aldrich) was first dissolved in a mixture of H_2O_2 and water and then used in a similar fashion as the metal source.

Purely siliceous Beta (Si-Beta) was prepared by omitting the addition of tin source and SnO_2-Beta was synthesized using tin oxide (SnO_2, Aldrich, <100 nm) as the tin source.[2]

Sn-Beta (Si/Sn = 125) via post-treatment procedure

Sn-Beta (Si/Sn = 125) was prepared according to a modification of the procedure described by Hammond *et al*.[3] Commercial zeolite Beta (Zeolyst, Si/Al = 12.5, NH_4^{+}-form) was calcined (550 °C for 6 h) to obtain the H-form and treated with 10 g of concentrated nitric acid (HNO_3, Sigma-Aldrich, ≥65 %) per gram of zeolite Beta powder for 12 h at 80 °C. The resulting solid was filtered, washed with ample water and calcined (550°C for 6 h using a ramp of 2°C/min) to obtain the dealuminated Beta (deAl-Beta). This solid was then impregnated by incipient wetness methodology with a Si/Sn ratio of 125. For this purpose, tin(II) chloride (0.128 g, Sigma-Aldrich, 98 %) was dissolved in water (5.75 mL) and added to the dealuminated Beta (5 g). After the impregnation process, the samples were dried 12 h at 110°C and calcined again (550°C for 6 h).

Sn-MFI (Si/Sn = 400)

Sn-MFI was prepared following a procedure described by Mal *et al*.[4] In a typical synthesis, 5.35 g of ammonium fluoride (Sigma-Aldrich, ≥98 %) was dissolved in 25 g of demineralized water under stirring. A solution of $SnCl_4{\cdot}5H_2O$ in 10 g of water was then added under rapid stirring, followed by slow addition of a solution of 9.8 g of tetrapropylammonium bromide (Aldrich, 98 %) in 56 g of demineralized water. Finally, 8.6 g of fumed silica (Aldrich) was dissolved. The mixture was then stirred for approx. 3 hours and transferred to a Teflon-lined autoclave and crystallized at 200°C for 6 days. The solid was then recovered by filtration, washed with ample water and dried overnight at 80°C followed by calcination (2°C/min, 550°C, 6 hours dwell time) to obtain the finished material.

Sn-MCM-41 (Si/Sn = 200)

The ordered mesoporous stannosilicate, Sn-MCM-41, was prepared according to the route described by Li *et al*.[5] In a typical synthesis, 26.4 g of tetraethylammonium silicate (TMAS, Aldrich, 15-20 wt% in water, ≥99.99%) was added slowly to a solution of 13.0 g of hexadecyltrimethylammonium bromide (CTABr, Sigma, ≥99.0%) dissolved in 38.0 g of water, and the mixture was allowed to stir for approx. 1 hour. At this point, $SnCl_4{\cdot}5H_2O$ and hydrochloric acid (HCl, Sigma-Aldrich, min. 37%) in 2.1 g of water was added drop wise to the solution and allowed to stir for 1.5 h. To this solution 12.2 g of TEOS was added and stirred for 3 h, giving a gel composition of; $1.0Si{:}0.005Sn{:}0.44CTABr{:}0.27TMA{:}0.08Cl^{-}{:}46H_2O$. The samples were then transferred to a Teflon-lined container placed in a stainless steel autoclave and placed in a pre-heated oven at 140°C for 15 h. The solid was recovered by filtration and washed with ample water and dried overnight at 80°C. The material was finalized by calcination, heating the sample to 550°C at 2°C/min in static air and maintaining this temperature for 6 h.

Catalyst Characterization

Powder X-ray diffraction (XRD) patterns of the calcined samples were measured on an X'Pert diffractometer (Philips) using Cu-Kα radiation. Surface area and pore volume measurements were performed using multipoint N_2 adsorption/desorption on an Autosorb automatic surface area and pore size analyzer (Quantachrome Instruments). The total surface area of the samples was obtained using the BET method and the micropore volume was calculated by the *t*-plot method using the Autosorb3 software. UV-Vis measurements were done using a DH-2000-BAL balanced deuterium, halogen light source (Ocean Optics). Mesoporous materials were characterized using low angle x-ray diffraction to verify the ordered nature of these materials.

Supplementary Information (SI) for Green Chemistry

Production of 2,5,6-trihydroxy-3-hexenoic acid methyl ester (THM)

Synthesis and Purification

Post-treated Sn-Beta (3 g), Glucose (12 g, Sigma-Aldrich, >99.0%) and methanol (200 g, Sigma-Aldrich, >99.8%) were added to the Teflon liner of a 1 L autoclave reactor (Autoclave Engineers). The reactor was sealed and heated to 160°C under stirring (450 rpm) for 16 hours. The reaction mixture was then cooled and filtered resulting in the crude reaction mixture. The crude reaction mixture was concentrated under reduced pressure at 40°C. 2.1 g of the concentrate was dissolved in methanol, evaporated onto Celite and purified by flash column chromatography (silica gel 15-40 Mesh, CH_2Cl_2, 20:1 CH_2Cl_2:MeOH) affording 0.30 g of pure THM.

Analysis and Identification

NMR experiments were recorded on a Bruker Ascend 400 spectrometer, ^{1}H -NMR was recorded at 400 MHz and ^{13}C-NMR was recorded at 100 MHz. The chemical shifts are given in ppm relative to the residual solvent signals and the chemical shifts are reported downfield to TMS. HRMS was recorded on an LC-TOF (ES).

^{1}H-NMR (400 MHz, CD_3OD): δ (ppm) 5.93 (dd, J = 15.3, 4.3 Hz, 1H), 5.88 (dd, J = 15.3, 4.1 Hz, 1H), 4.69 (d, J = 4.1 Hz, 1H), 4.14 (ddd, J = 6.7, 4.7, 4.1 Hz, 1H), 3.73 (s, 3H), 3.51 (dd, J = 10.9, 4.7 Hz, 1H) 3.45 (dd, J = 10.9, 6,7 Hz, 1H). ^{13}C-NMR (100 MHz, CD_3OD) : δ (ppm) 174.6, 133.8, 129.4, 73.4, 72.2, 67.0, 52.6. HRMS (ESI+) *m/z* calculated for $C_7H_{12}O_5$ [M + **Na**]$^+$: 199.0577; found: 199.0572.

Figures

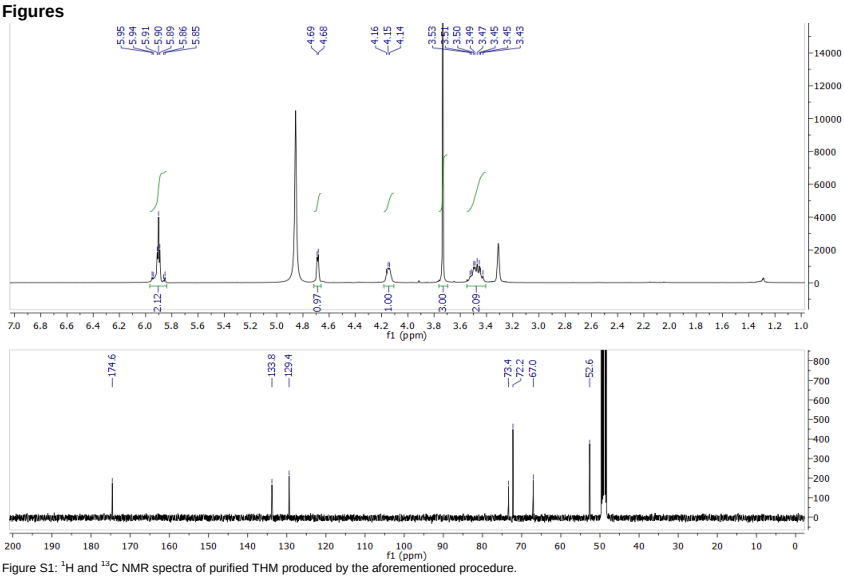

Figure S1: ^{1}H and ^{13}C NMR spectra of purified THM produced by the aforementioned procedure.

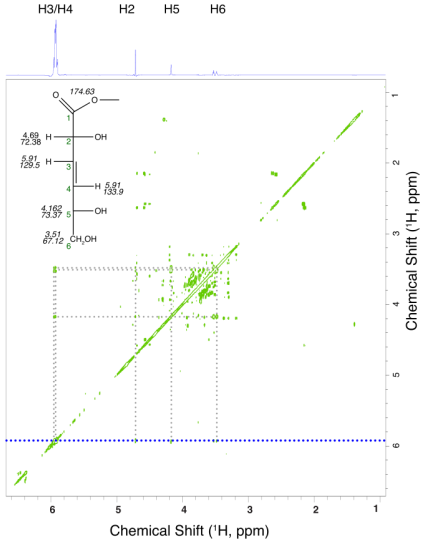

Figure S2: ^{1}H-^{1}H TOCSY correlations between protons of the THM spin system in a reaction mixture produced by Sn-Beta catalyzed glucose conversion in methanol.

Supplementary Information (SI) for Green Chemistry
This journal is © The Royal Society of Chemistry 20XX

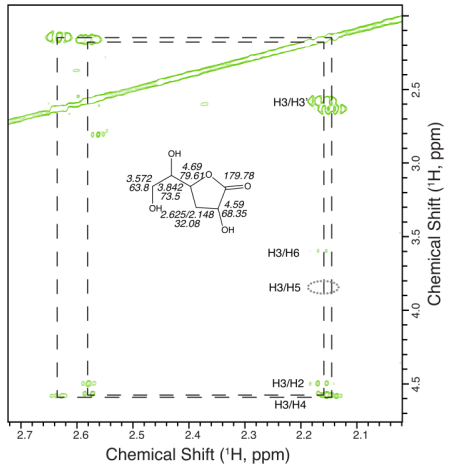

Figure S3: ^{1}H-^{1}H TOCSY correlations from the methylene protons to other protons in the spin systems of 3-deoxy-γ–lactones present in a glucose-derived reaction mixture.

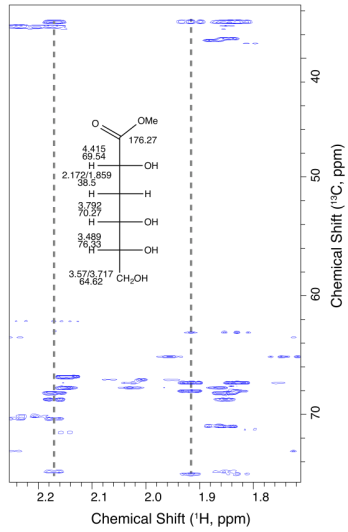

Figure S4: ^{1}H-^{13}C HSQC-TOSCY correlations between the protons and carbons of the DGM spin system in a reaction mixture produced by Sn-Beta catalyzed glucose conversion in methanol,

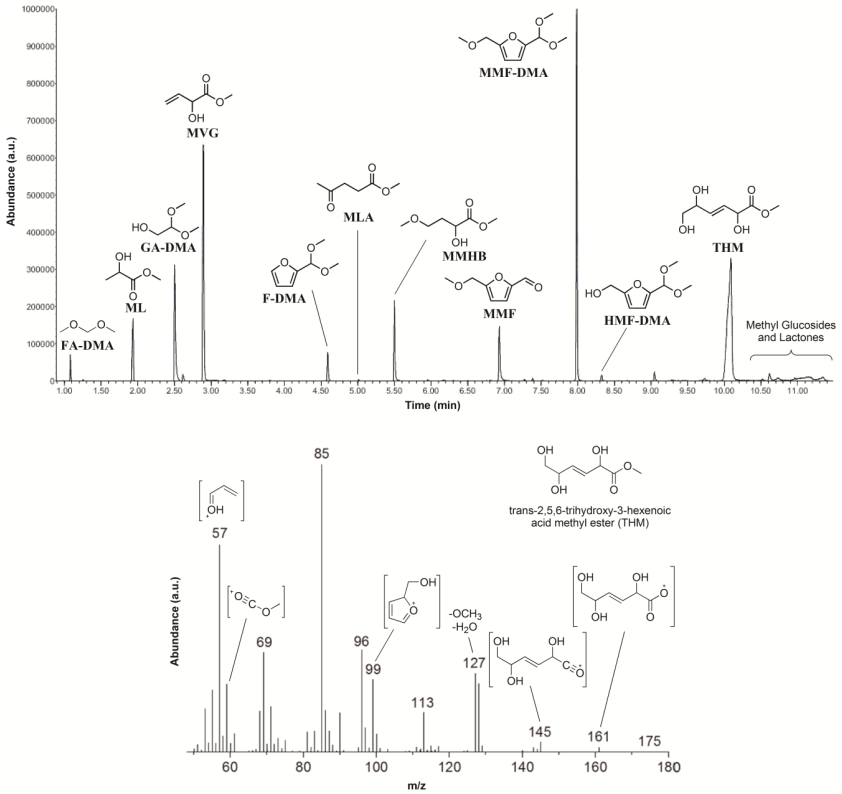

Figure S5: GC-MS analysis of the reaction liquid obtained from the reaction between glucose and alkali-free Sn-Beta at 140°C in methanol showing a) chromatogram and b) the specific fragmentation pattern of trans-2,5,6-trihydroxy-3-hexenoic acid methyl ester taken at 10.062 min.

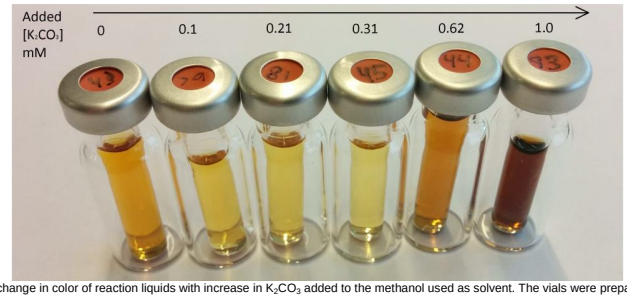

Figure S6: Visual change in color of reaction liquids with increase in K_2CO_3 added to the methanol used as solvent. The vials were prepared using 180 mg Sn-Beta (PT), 360 mg glucose, 4 g of solvent, reacted for 6 hours at 160°C.

Supplementary Information (SI) for Green Chemistry

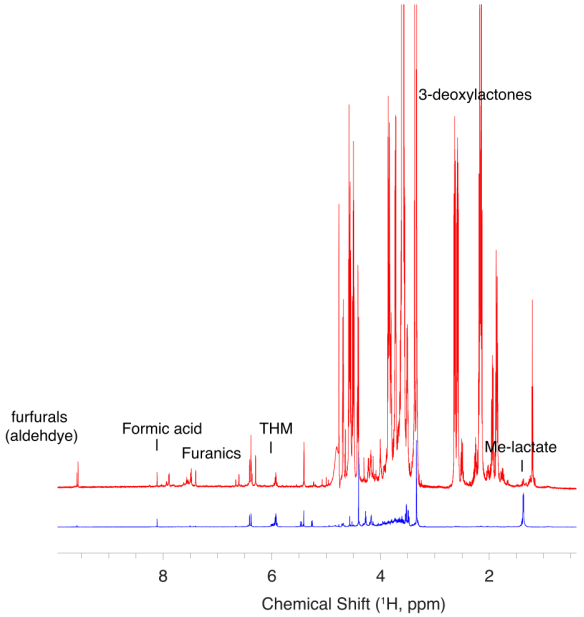

Figure S7: ^{1}H-NMR spectrum of the product mixture formed by reaction of a commercial 3-deoxyglucosone (red) and glucose (blue) substrate with a Sn-Beta catalysis in methanol at 160°C. Spectra are renormalized to identical THM signal amplitude to highlight the higher ratio of furanics/THM using 3-deoxyglucosone as the substrate.

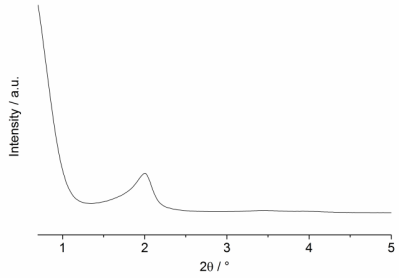

Figure S8: Low angle XRD diffractogram of Sn-MCM-41 (Si/Sn = 200).

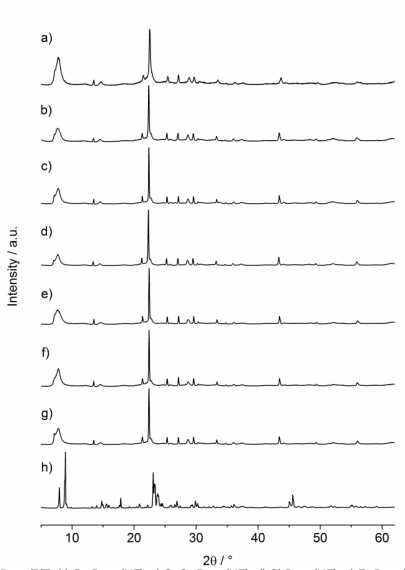

Figure S9: XRD diffractograms of a) Sn-Beta (PT), b) Sn-Beta (HF), c) SnO_2-Beta (HF), d) Si-Beta (HF), e) Zr-Beta (HF), f) Ti-Beta (HF), g) Hf-Beta (HF) and h) Sn-MFI.

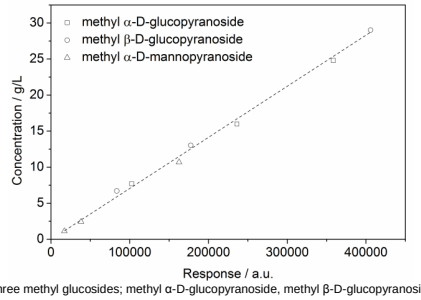

Figure S10: Calibration curve for the three methyl glucosides; methyl α-D-glucopyranoside, methyl β-D-glucopyranoside and methyl α-D-mannopyranoside measured on an an Agilent 1200 series HPLC equipped with a Carbohydrate (Zorbax) column (60 wt% acetonitrile/water, 0.5 mL/min, 30°C).

Supplementary Information (SI) for Green Chemistry

Tables

Table S1: Conversion of glucose in the presence and absence of alkali using Sn-Beta prepared by the post-treatment method (PT Sn-Beta).

			Retro-aldol pathway					3DG pathway					
Entry	c_{K2CO3} (in methanol)	MG	ML	GA-DMA	MVG	MMHB	ML/'RA products'	HMF	MMF	MLA	F-DMA	DGL	THM
	mM	%	%				%	%					
1	0	16	17	3	6	1	63	0	10	2	<1	6	14
2	0.10	9	26	2	11	2	64	0	7	<1	<1	5	13
3	0.21	9	37	1	15	3	66	0	4	<1	<1	6	11
4	0.31	6	48	1	18	3	70	0	2	<1	<1	3	6
5	0.62	7	49	<1	16	2	72	<1	0	<1	<1	0	3
6	1.03	3	37	<1	14	2	69	2	4	<1	<1	<1	1

Yields (carbon%) of methoxylated sugars (MG), methyl lactate (ML), glycolaldehyde dimethylacetal (GA-DMA), methyl vinylglycolate (MVG), methyl 4-methoxy-2-hydroxybutanoate (MMHB), 5-(hydroxymethyl)furfural (HMF), 5-(methoxymethyl)furfural (MMF), methyl levulinate (MLA), furfural dimethylacetal (F-DMA), 3-deoxy γ-lactones (DGL), and trans-2,5,6-trihydroxy-3-hexenoic acid methyl ester (THM).
Reaction conditions: 160°C, 360 mg glucose, 4 g solvent, 180 mg Sn-Beta (PT) (Si/Sn = 125), 6 hours, 600 rpm stirring.

Table S2: Standard deviations given in parenthesis at alkali concentrations of 0 and 0.31 mM K_2CO_3/methanol for the conversion of glucose using PT Sn-Beta.

Entry	c_{K2CO3} (in methanol)	MG	ML	GA-DMA	MVG	MMHB	MMF	MLA	THM
	mM	%							
1	0	16(3)	17(1)	2(0.2)	7(1)	1(0.1)	10(1)	2(0.3)	14(1)
2	0.31	6(0.4)	49(2)	1(0.3)	18(1)	3(0.1)	2(1)	<1	6(0.9)

Yields (carbon%) of methoxylated sugars (MG), methyl lactate (ML), glycolaldehyde dimethylacetal (GA-DMA), methyl vinylglycolate (MVG), methyl 4-methoxy-2-hydroxybutanoate (MMHB), 5-(hydroxymethyl)furfural (HMF), 5-(methoxymethyl)furfural (MMF), methyl levulinate (MLA), and trans-2,5,6-trihydroxy-3-hexenoic acid methyl ester (THM).
Reaction conditions: 160°C, 360 mg glucose, 4 g solvent, 180 mg Sn-Beta (PT) (Si/Sn = 125), 6 hours, 600 rpm stirring.

Table S3. Conversion of glucose in the presence and absence of alkali using Sn-Beta prepared by the post-treatment method (PT Sn-Beta) for 10-30 mins.

			Retro-aldol pathway						3DG pathway					
Entry	Time	Solvent	MG	ML	GA-DMA	MVG	MMHB	ML/'RA products'	HMF	MMF	MLA	F-DMA	FUR	THM
	min		%	%				%	%					
1	10	Methanol	45	8	2	3	<1	59	2	4	<1	<1	6	7
2	20	Methanol	31	10	3	4	<1	59	1	8	<1	<1	11	10
3	30	Methanol	29	11	3	4	<1	59	1	8	<1	<1	10	11
4	10	0.62 mM K_2CO_3 /methanol	13	39	<1	15	2	69	<1	<1	<1	<1	1	2
5	20	0.62 mM K_2CO_3 /methanol	9	42	<1	16	2	69	<1	<1	<1	<1	1	2
6	30	0.62 mM K_2CO_3 /methanol	8	47	<1	17	2	69	1	<1	<1	<1	1	2

Yields (carbon%) of methoxylated sugars (MG), methyl lactate (ML), glycolaldehyde dimethylacetal (GA-DMA), methyl vinylglycolate (MVG), methyl 4-methoxy-2-hydroxybutanoate (MMHB), 5-(hydroxymethyl)furfural (HMF), 5-(methoxymethyl)furfural (MMF) and furfural dimethylacetal (F-DMA) and the combined furan yield of HMF, MMF, F-DMA and MLA denoted FUR as well as *trans*-2,5,6-trihydroxy-3-hexenoic acid methyl ester (THM).
Reaction conditions: 160°C, 360 mg substrate, 4 g methanol, 180 mg catalyst, 600 rpm stirring.

Table S4: Conversion of various methyl glucosides using Sn-Beta (PT) and blank experiments both in the presence of and in the absence of alkali, reacted at 160 °C.

						Retro-aldol pathway				3DG pathway	
Entry	Catalyst	Substrate	Solvent	Unconverted sugars	MG	ML	GA-DMA	MVG	MMHB	FUR	THM
				%		%				%	
1	Sn-Beta (PT)	Methyl *α*-D-glucopyranoside	Methanol	-	85	1	<1	1	<1	<1	<1
2	Sn-Beta (PT)	Methyl *β*-D-glucopyranoside	Methanol	-	82	1	<1	1	<1	<1	<1
3	Sn-Beta (PT)	Methyl *α*-D-mannopyranoside	Methanol	-	97	2	<1	<1	<1	<1	<1
4	-	Glucose	Methanol	78	18	<1	<1	<1	<1	1	<1
5	-	Glucose	0.62 mM K_2CO_3/ methanol	39	34	<1	<1	<1	<1	2	<1

Yields (carbon%) of unconverted sugars, methoxylated sugars (MG), methyl lactate (ML), methyl vinylglycolate (MVG), glycolaldehyde dimethylacetal (GA-DMA), methyl 4-methoxy-2-hydroxybutanoate (MMHB), combined yield of 5-(hydroxymethyl)furfural (HMF), 5-(methoxymethyl)furfural (MMF) and furfural dimethylacetal (F-DMA) denoted FUR and *trans*-2,5,6-trihydroxy-3-hexenoic acid methyl ester (THM).
Reaction conditions: 160°C, 360 mg substrate, 4 g methanol, 180 mg catalyst, 6 hours, 600 rpm stirring.

Supplementary Information (SI) for Green Chemistry

Table S5: Conversion of monosaccharides in the absence of alkali using a selection of Beta-framework and/or tin containing catalysts.

					Retro-aldol pathway				3DG pathway				
Entry	Catalyst	Substrate	Temperature	MG	ML	GA-DMA	MVG	MMHB	HMF	MMF	MLA	F-DMA	THM
			°C	%	%				%				
1	Sn-Beta (PT)	Glucose	120	44	4	1	1	<1	1	9	<1	<1	8
2	Sn-Beta (PT)	Glucose	140	21	10	2	3	1	2	12	<1	<1	12
3	Sn-Beta (PT)	Glucose	160	13	17	3	6	1	<1	10	2	1	14
4	Sn-Beta (PT)	Glucose	180	5	26	2	11	1	<1	7	2	1	8
5	Sn-Beta (PT)	Fructose	160	9	19	2	7	1	<1	11	2	1	18
6	Sn-Beta (PT)	Mannose	160	12	20	2	8	1	<1	10	1	1	15
7	Sn-Beta (PT)	Sorbose	160	13	15	3	9	2	<1	11	2	1	17
8	Sn-Beta (PT)	Galactose	160	26	10	2	6	1	<1	11	2	1	12
9	Sn-Beta (PT)	Tagatose	160	11	11	<1	6	1	<1	14	2	2	9
10	Sn-Beta (PT)	Sucrose	160	10	22	2	8	2	<1	11	1	<1	15
11	Sn-Beta (HF)	Glucose	160	8	24	1	8	1	4	5	<1	<1	16
12	Zr-Beta (HF)	Glucose	160	27	25	5	7	<1	<1	1	<1	<1	2
13	Ti-Beta (HF)	Glucose	160	14	28	3	6	1	2	1	<1	<1	3
14	Hf-Beta (HF)	Glucose	160	35	18	3	5	<1	<1	7	<1	<1	4
15	Al-Beta	Glucose	160	32	<1	<1	<1	<1	<1	2	12	<1	<1
16	deAl-Beta	Glucose	160	86	<1	<1	<1	<1	<1	<1	<1	<1	<1
17	deAl-Beta	Fructose	160	51	<1	<1	<1	<1	<1	12	<1	<1	<1
18	Sn-MCM-41	Glucose	160	16	26	3	5	3	4	7	<1	<1	18
19	Sn-MFI	Glucose	160	40	8	8	4	<1	<1	<1	<1	<1	<1
20	SnO_2-Beta (HF)	Glucose	160	37	1	<1	<1	<1	2	<1	<1	<1	<1
21	Si-Beta (HF)	Glucose	160	46	3	2	1	<1	3	<1	<1	<1	<1

Yields (carbon%) of methoxylated sugars (MG), methyl lactate (ML), methyl vinylglycolate (MVG), glycolaldehyde dimethylacetal (GA-DMA), methyl 4-methoxy-2-hydroxybutanoate (MMHB), combined yield of 5-(hydroxymethyl)furfural (HMF), 5-(methoxymethyl)furfural (MMF) and furfural dimethylacetal (F-DMA) and *trans*-2,5,6-trihydroxy-3-hexenoic acid methyl ester (THM) from the conversion of various sugars using a variety of catalysts, different sugars and at different temperatures.
Reaction conditions: 360 mg substrate, 4 g methanol, 180 mg catalyst, 6 hours, 600 rpm stirring.

Table S6. Physical properties of the various catalysts used in the study measured using N_2-adsorption/desorption and from XRD diffraction.

Entry	Catalyst	X-ray diffraction	N_2-adsorption/desorption			
		Primary phase	S_{BET}	$S_{micropore}$[a]	V_{total}	$V_{micropore}$[a]
			m^2/g		mL/g	
1	Sn-Beta (PT)	*BEA	557	373	0.37	0.19
2	Sn-Beta (HF)	*BEA	486	362	0.33	0.19
3	SnO_2-Beta	*BEA	457	365	0.27	0.19
4	Si-Beta	*BEA	465	378	0.27	0.20
5	Zr-Beta (HF)	*BEA	490	391	0.27	0.20
6	Ti-Beta (HF)	*BEA	481	392	0.27	0.20
7	Hf-Beta (HF)	*BEA	541	376	0.32	0.20
8	Sn-MFI	MFI	377	191	0.20	0.09
9	Sn-MCM-41	Mesoporous silica, a = 45 Å[b]	962	-	1.00	-

a. Determined using the *t*-plot method.

b. Determined using low angle x-ray diffraction (0.5-5° 2θ)

Table S7: Conversion of glucose using Zr-Beta (HF) in different concentration of K_2CO_3 in methanol.

Entry	Catalyst	Substrate	Solvent	Retro-aldol pathway					3DG pathway	
				MG	ML	GA-DMA	MVG	MMHB	FUR	THM
				%	%				%	
1	Zr-Beta (HF)	Glucose	Methanol	27	25	5	7	<1	2	2
2	Zr-Beta (HF)	Glucose	0.31 mM K_2CO_3/methanol	15	27	2	10	2	2	1
3	Zr-Beta (HF)	Glucose	0.62 mM K_2CO_3/methanol	12	25	1	10	3	1	1

Yields (carbon%) of unconverted sugars, methoxylated sugars (MG), methyl lactate (ML), glycolaldehyde dimethylacetal (GA-DMA), methyl vinylglycolate (MVG), methyl 4-methoxy-2-hydroxybutanoate (MMHB), combined yield of 5-(hydroxymethyl)furfural (HMF), 5-(methoxymethyl)furfural (MMF) and furfural dimethylacetal (F-DMA) denoted FUR and *trans*-2,5,6-trihydroxy-3-hexenoic acid methyl ester (THM).
Reaction conditions: 160°C, 360 mg substrate, 4 g methanol, 180 mg catalyst, 6 hours, 600 rpm stirring.

References

1. US6306364 B1, 1999.
2. S. Tolborg, A. Katerinopoulou, D. D. Falcone, I. Sádaba, C. M. Osmundsen, R. J. Davis, E. Taarning, P. Fristrup and M. S. Holm, *J. Mater. Chem. A*, 2014, **2**, 20252-20262.
3. C. Hammond, S. Conrad and I. Hermans, *Angew. Chem., Int. Ed.*, 2012, **51**, 11736-11739.
4. N. K. Mal, V. Ramaswamy, P. R. Rajamohanan and A. V. Ramaswamy, *Microporous Materials*, 1997, **12**, 331-340.
5. L. Li, C. Stroobants, K. Lin, P. A. Jacobs, B. F. Sels and P. P. Pescarmona, *Green Chem.*, 2011, **13**, 1175-1181.

RSC Advances

PAPER

View Article Online
View Journal | View Issue

Cite this: RSC Adv., 2017, 7, 985

Synthesis of a novel polyester building block from pentoses by tin-containing silicates†

S. G. Elliot,[ac] C. Andersen,[b] S. Tolborg,[ac] S. Meier,[c] I. Sádaba,[a] A. E. Daugaard[b] and E. Taarning*[a]

Received 12th November 2016
Accepted 28th November 2016

DOI: 10.1039/c6ra26708d

www.rsc.org/advances

We report here the direct formation of the new chemical product *trans*-2,5-dihydroxy-3-pentenoic acid methyl ester from pentoses using tin-containing silicates as catalysts. The product is formed under alkali-free conditions in methanol at temperatures in the range 140–180 °C. The highest yields are found using Sn-Beta as the catalyst. Under optimised conditions, a yield of 33% is achieved. Purified *trans*-2,5-dihydroxy-3-pentenoic acid methyl ester was used for co-polymerisation studies with ethyl 6-hydroxyhexanoate using *Candida antarctica* lipase B as the catalyst. The co-polymerisation yields a product containing functional groups originating from *trans*-2,5-dihydroxy-3-pentenoic acid methyl ester in the polyester backbone. The reactivity of the incorporated olefin and hydroxyl moieties was investigated using trifluoroacetic anhydride and thiol–ene chemistry, thus illustrating the potential for functionalising the new co-polymers.

Introduction

The emergence of bio-based chemical products from sugars has been particularly successful in the area of polyester materials. Simple polyester building blocks include hydroxy acids, diacids and dialcohols, such as lactic acid, succinic acid and 1,3-propylene glycol. These building blocks can be produced from sugars by fermentation or chemocatalysis.[1–3] While fermentation has been the preferred method, research aimed at transforming sugars into polyester building blocks using chemocatalytic processing has proliferated during the last decade.[4–9] These activities are driven partly by the prospect of chemocatalysis offering cost advantages over fermentation, but also by the prospect of gaining access to chemical products that are inaccessible by fermentation. Polyester building blocks that are accessible in few steps from sugars using chemo-catalysis include 2,5-furandicarboxylic acid, ethylene glycol, adipic acid, isosorbide, lactic acid and 2-hydroxy-3-butenoic acid.

2,5-Furandicarboxylic acid is accessible *via* acid catalysed dehydration of fructose, followed by oxidation.[10–12] When 2,5-furandicarboxylic acid is polymerised with ethylene glycol, polyethylene furanoate is formed.[13] This polyester has been shown to have favourable barrier properties compared to PET plastics, indicating that it may be developed as a useful material in the packaging materials segment.[6] Ethylene glycol itself can be produced in various ways for instance by catalytic hydrogenation of sorbitol in yields of up to 37% [14] or directly from glucose in combination with retro-aldol co-catalysts such as tungsten salts in yields of 35–75%.[15,16] In a different catalytic approach using acid catalysis, sorbitol can be dehydrated to give isosorbide. This diol has been successfully polymerised with different dicarboxylic acids resulting in new types of polyester materials, some of which have already become commercial products.[6,7] Adipic acid is accessible from glucose in two steps by catalytic hydrogenation of glucaric acid.[17] Racemic methyl lactate can be made directly from C_6 sugars in yields up to 75% using tin-containing silicates as catalysts.[18] Lactic acid is an established polyester building block used in the production of poly(lactic acid) which has become widely used as a bio-based polyester material within the packaging materials segment.[19] The newest and least known member of this group is methyl vinyl glycolate (MVG), which can be made directly from C_6 sugars in yields up to 20% as a co-product to methyl lactate and from C_4 sugars in yields up to 60%.[8,20–22] Due to its chemical similarity to lactic acid, MVG can be co-polymerised with lactic acid to produce a co-polyester having pendant vinyl groups that allow for post functionalisation.[23] Here, we report that pentose sugars can be converted into a new activated polyester building block, *trans*-2,5-dihydroxy-3-pentenoic acid methyl ester (DPM), in one step using tin-containing silicates as catalysts. We have furthermore isolated gram quantities of DPM and we show the successful co-polymerisation of DPM and ethyl 6-hydroxyhexanoate (E6-HH) using enzymatic polymerisation. The co-polymers can be functionalised by thiolation or acetylation of the olefin and hydroxyl moiety, respectively.

[a]Haldor Topsøe A/S, Haldor Topsøes Allé 1, 2800-Kgs. Lyngby, Denmark. E-mail: esta@topsoe.dk
[b]Danish Polymer Centre, Department of Chemical and Biochemical Engineering Technical University of Denmark, Sølvtoftsplads, 2800-Kgs Lyngby, Denmark
[c]Department of Chemistry, Technical University of Denmark, Kemitorvet, 2800-Kgs. Lyngby, Denmark

† Electronic supplementary information (ESI) available. See DOI: 10.1039/c6ra26708d

The catalytic conversion of sugars to lactic acid derivatives using tin-containing silicates has been reported for all simple monosaccharides.[20,21,24,25] The first report was related to triose sugars in water and methanol and later reports described similar chemistry occurring for hexoses, tetroses and pentoses. The product selectivity varies, depending on the length of the sugar molecule. Trioses form exclusively lactates while tetroses lead to high yields of MVG. Pentoses and hexoses form multiple products, depending amongst other factors on the presence of co-solutes in the reaction medium. Recently we have shown that *trans*-2,5,6-trihydroxy-3-hexenoic acid methyl ester (THM) is formed in yields of 15–18% from hexoses using tin-containing silicates as catalysts and in the absence of added co-solutes. The reaction pathway was elucidated and 3-deoxyglucosone was identified as the intermediate responsible for the formation of this product and of related lactones and 5-hydroxymethyl furfural derivatives.[26]

We here continue our exploration of chemo-catalytic sugar processing, taking these reports into consideration. A product pattern emerges based on the prior reports consisting of the homologous series of α-hydroxy esters: THM from hexoses, MVG from tetroses and methyl lactate from trioses. From this trend, a similar C_5 product can be predicted for pentoses (Scheme 1). This product, DPM, is the activated and biocompatible ester version of *trans*-2,5-dihydroxy-3-pentenoic acid recently identified among trihydroxypentanoic acid derivatives formed from xylose in water.[29] Here, we verify that this product, DPM, is indeed formed in yields of up to 33% from the pentoses xylose, lyxose and ribose. This finding shows that tin-containing silicates display a remarkable ability to catalyse consecutive dehydrations of sugars to afford intermediary β,γ-unsaturated α-keto-aldehydes which are converted into the β,γ-unsaturated α-hydroxy ester end products (Scheme 1).

Tin-containing silicates are solid Lewis acid materials that are capable of activating carbonyl groups in small molecules and catalyse simple transformations. Examples include Baeyer–Villiger oxidation, Meerwein–Ponndorf–Verley–Oppenauer redox reactions, monosaccharide isomerisation, aldol- and retro-aldol reactions and certain dehydration reactions.[30–36] The most studied tin-containing silicate is Sn-Beta, in which tin is incorporated into a framework of silica having the *BEA topology. Sn-Beta is often reported as being a superior catalyst compared to other tin-containing silicates for these reactions.[18,30,31,37,38] Currently, this supposed superiority of Sn-Beta is not well understood, especially under *operando* conditions. Recent work aimed at elucidating the catalytic functioning of Sn-Beta includes DFT calculations, FT-IR, TPR and ^{119}Sn-NMR spectroscopy.[39–44] Despite it being a crystalline material, the preparation method often greatly influences the catalytic performance. Two principally different preparation methods are normally used, direct synthesis under hydrothermal conditions using hydrofluoric acid as mineralising agent [Sn-Beta (HT)] and synthesis by post treatment of a dealuminated Beta zeolite with a tin source [Sn-Beta (PT)]. The Sn-Beta (HT) typically consists of large hydrophobic crystals of 3–5 μm with few defects. Tin loadings up to 2% are typically employed, as it is difficult to incorporate higher loadings of tin.[45] Sn-Beta (PT) is made from a parent Al-Beta zeolite which has been dealuminated. The Sn-Beta (PT) crystal size is inherited from the parent material and is often in the range of 0.2–1 μm in diameter. The material contains many defects, causing it to be more hydrophilic than the Sn-Beta (HT). Several different methods of incorporating tin into the dealuminated zeolite are being employed such as vapour-phase deposition,[46] solid state ion exchange[47] and reflux in isopropyl alcohol with a tin salt.[48]

We synthesised Sn-Beta (HT) and Sn-Beta (PT) with a tin content of 1.25–1.5% alongside other tin-containing silicates and other Lewis acidic Beta zeolites. These materials were tested in the production of DPM from xylose in methanol with the aim of identifying activity patterns and optimising the DPM yield.

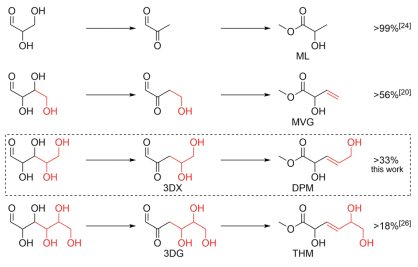

Scheme 1 Formation of homologous α-hydroxy ester products from C_3–C_6 sugars catalysed by tin-containing silicates. The reaction is applicable both to aldoses and ketoses.

Experimental

Catalyst synthesis

Sn-, Zr-, Ti- and Al-Beta (Si/M = 150) *via* hydrothermal synthesis were prepared by modifying the route described by Valencia *et al.*[45,49] In a typical Sn-Beta (Si/Sn = 150) synthesis procedure, 30.6 g of tetraethyl orthosilicate (Aldrich, 98%) was added to 33.1 g of tetraethylammonium hydroxide (Sigma-Aldrich, 35% in water) under careful stirring (~60 min), and tin(IV) chloride pentahydrate (Aldrich, 98%) dissolved in 2.0 mL of demineralised water was added drop wise. The mixture was then left to stir for several hours. Finally, 3.1 g hydrofluoric acid (Fluka, 47–51%) in 1.6 g of demineralised water was added. All samples were then homogenised and transferred to a Teflon®-container placed in a stainless steel autoclave. The samples were then incubated at 140 °C for 14 days. The solid was recovered by filtration and washed with demineralised water, followed by drying overnight at 80 °C in air. The organic template contained within the material was removed by heating the sample at 2 °C min^{-1} to 550 °C in static air and maintaining this temperature for 6 h.

Zr-Beta (Si/Zr = 150) and Al-Beta (Si/Al = 150) zeolites were prepared by the aforementioned procedure, exchanging the tin source with zirconyl chloride octahydrate (Sigma-Aldrich, 98%)

or aluminium chloride hexahydrate (Fluka, ≥99%), respectively. Furthermore, Al-Beta was incubated for only 5 days at 140 °C. For Ti-Beta (Si/Ti = 150), tetraethyl orthotitanate (Aldrich) was first dissolved in a mixture of hydrogen peroxide and water and then used in a similar fashion as the metal source. SnO_2-Beta (Si/Sn = 200) was synthesised using tin oxide (Aldrich, <100 nm) as the tin source. Purely siliceous Beta (Si-Beta) was prepared by omitting the addition of a metal source.

Sn-Beta (Si/Sn = 125) *via* post-treatment was prepared according to a modification of the procedure described by Hammond *et al.*[47] Commercial zeolite Beta (Zeolyst, Si/Al = 12.5, NH_4^+-form) was calcined at 550 °C for 6 h and dealuminated by treatment with 10 g of concentrated nitric acid (Sigma-Aldrich, ≥65%) per gram of zeolite Beta powder for 12 h at 80 °C. The solid was recovered by filtration, washed and calcined (550 °C for 6 h). The dealuminated zeolite was then impregnated by incipient wetness methodology with a Si/Sn ratio of 125. For this purpose, tin(II) chloride (0.128 g, Sigma-Aldrich, 98%) was dissolved in water (5.75 mL) and added to 5 g of the solid. After the impregnation process, the sample was dried at 110 °C for 12 h and calcined again.

Sn-MFI (Si/Sn = 100) was prepared following a procedure described by Mal *et al.*[50] In a typical synthesis, tin(IV) chloride pentahydrate (Aldrich, 98%) was dissolved in 5 g of demineralised water and added to 15.6 g of tetraethyl orthosilicate (98%, Aldrich). This mixture was then stirred for 30 min. Afterwards, 13.4 g of tetrapropylammonium hydroxide (40%, AppliChem) in 13.4 g of demineralised water was added and stirred for 1 h, and subsequently an additional 60 g of demineralised water was added. The solution was then left stirring for 20 h. The gel was transferred to a Teflon®-lined autoclave and synthesised at 160 °C for 2 days under static conditions. The solid was recovered by filtration, washed with ample water and dried overnight at 80 °C followed by calcination (2 °C min^{-1}, 550 °C, 6 h dwell time) to obtain the finished material.

Sn-MCM-41 (Si/Sn = 200) was prepared according to the method described by Li *et al.*[51] In a typical synthesis, 26.4 g of tetraethylammonium silicate (Aldrich, 15–20 wt% in water, ≥99.99%) was slowly added to a solution of 13.0 g of hexadecyltrimethylammonium bromide (Sigma, ≥99.0%) dissolved in 38.0 g of water and allowed to stir for 1 h. At this point, tin(IV) chloride pentahydrate (Aldrich, 98%) and hydrochloric acid (Sigma-Aldrich, min. 37%) in 2.1 g of water was added drop wise to the solution and allowed to stir for 1.5 h. To this solution, 12.2 g of tetraethylorthosilicate (98%, Aldrich) was added and stirred for 3 h. The sample was then transferred to a Teflon®-lined container in a stainless steel autoclave and placed in a pre-heated oven at 140 °C for 15 h. The solid was recovered by filtration, washed with ample water and dried overnight at 80 °C. The material was finalised by calcination, heating the sample to 550 °C at 2 °C min^{-1} in static air and maintaining this temperature for 6 h.

Sn-SBA-15 (Si/Sn = 200) was prepared following the synthesis route described by Ramaswamy *et al.*[52] In a typical synthesis, 1.0 g of hydrochloric acid (37 wt%, Fluka) in 140 g of demineralised water was added to a solution of 8.0 g of Pluronic® P-123 (PEG–PPG–PEG polymer, Aldrich, M_w = ~5800 g mol^{-1}) in 60 g of demineralised water. The solution was then stirred for 2 h. To the synthesis mixture 18.0 g of tetraethyl orthosilicate (98%, Aldrich) was added followed by tin(IV) chloride pentahydrate (Aldrich, 98%) dissolved in 2.0 g of demineralised water. The mixture was then stirred for 24 h at 40 °C and then transferred to a Teflon®-lined autoclave and heated to 100 °C for 24 h. The solid was recovered by filtration, washed with ample water and then calcined at 550 °C for 6 hours.

Catalyst characterisation

Catalyst characterisation was performed by XRD, BET, N_2-sorption and ICP-OES. Powder X-ray diffraction (XRD) patterns of the prepared and calcined samples were measured on an X'Pert diffractometer (Philips) using Cu-Kα radiation. Surface area and pore volume measurements were performed using multipoint N_2 adsorption/desorption on an Autosorb automatic surface area and pore size analyser (Quantachrome Instruments). The total surface area (S_{BET}) of the samples was obtained using the BET method and the micropore volume (V_{micro}) was calculated by the *t*-plot method using the Autosorb3 software. The characterisation results are shown in the ESI, Fig. S2, S3 and Table S1.† The elemental composition of the prepared materials was measured using inductively coupled plasma-atomic emission spectroscopy (ICP-OES) on a PerkinElmer model Optima 3000 (Varian Vista).

Catalytic tests

In a typical experiment, 4.0 g methanol (Sigma-Aldrich, >99.8%), 360 mg (2.4 mmol) xylose (Sigma-Aldrich, >99%) and 180 mg of catalyst were added to a 5 mL glass microwave vial (Biotage). No special precautions were taken to avoid moisture or oxygen. The reaction vessel was heated under stirring (600 rpm) for 2 h in a Biotage Initiator+ microwave synthesiser. After cooling, samples were retrieved and analysed. In some experiments, an alkali salt co-solute was added by replacing the appropriate portion of the methanol solvent with a 1.0 mM standard solution of potassium carbonate (Sigma-Aldrich, ≥99.0%) in methanol to obtain the desired concentration.

Product analysis for catalyst testing

Analysis of the reaction mixtures was performed using a combination of GC-FID, HPLC and 1D and 2D NMR. A Bruker (Fällanden, Switzerland) Avance II 800 MHz spectrometer equipped with a TCI Z-gradient CryoProbe and an 18.7 T magnet (Oxford Magnet Technology, Oxford, U.K.) was used for the identification of unknown products. A 7890A Series GC system (Agilent Technologies) with a Phenomenex Zebron ZB-5 column and a FID detector was used for the quantification of glycolaldehyde dimethylacetal (GA-DMA), methyl lactate (ML), methyl vinyl glycolate (MVG), methyl 4-methoxy-2-hydroxybutanoate (MMHB) and 2,5-dihydroxy-3-pentenoic acid methyl ester (DPM). With the exception of DPM, commercial standards were used for the calibration. DPM was synthesised and purified as described under "Isolation of *trans*-2,5-dihydroxy-3-pentenoic acid methyl ester (DPM)" and the pure material was used in calibration standards.

An Agilent 1200 series HPLC equipped with an Aminex HPX-87H (BioRad) column (0.004 M H_2SO_4, 0.6 mL min^{-1}, 65 °C) using a refractive index and diode array detector was used for detection and quantification of furfural, furfural dimethylacetal and other analogues. The aqueous acidic eluent hydrolyses all furfural analogues back to furfural, resulting in a collective quantification of all furanics (FUR).

One-dimensional ^{1}H NMR spectra were used to quantify 3-deoxy-γ-pentonolactones (DPL), 2,4,5-trihydroxy-3-pentanoic acid methyl ester (TPM) and 2,5-dihydroxy-4-methoxy-pentanoic acid methyl ester (DMPM) using the CH_3 signal at 1.39 ppm from ML as a reference. Spectra were recorded directly on reaction mixtures in methanol after removal of catalyst and upon addition of 10% (v/v) D_4-methanol (Cambridge Isotopes). Spectra were recorded on a Bruker Avance III spectrometer equipped with a 9.4 T magnet and a BBO probe. Methanol proton resonances were suppressed by presaturation at frequencies of 3.36 ppm, 4.786 ppm using the two logical channels of the spectrometer. Spectra were recorded at 30 °C by sampling 8096 complex data points during an acquisition time of 1.02 seconds, employing an inter-scan delay of 10 seconds and accumulating 16 scans.

Two-dimensional ^{1}H–^{13}C HSQC spectra were used to quantify methyl glycosides (MG) and residual substrate relative to DPM at natural ^{13}C isotopic abundance. The ^{1}H–^{13}C HSQC spectra had a ^{13}C carrier offset of 101 ppm and employed a spectral width of 22 ppm to sample the anomeric region of xylose and its methyl glycosides at high resolution and sensitivity. Samples were prepared by condensing 1 mL of the filtered reaction mixture using a SpeedVac vacuum concentrator and redissolving the resultant residue in D_4-methanol. These spectra were recorded on a Bruker Avance III HD spectrometer equipped with a 9.4 T magnet and a Bruker CryoProbe Prodigy, sampling 1024 and 128 complex data points in the ^{1}H and ^{13}C spectral dimensions for acquisition times of 292 and 58 milliseconds, respectively. Spectra were processed with extensive zero filling in all dimensions and integrated in Topspin 3.5.

In samples where DPM or ML were present in less than 10%, estimations of DPL, TPM, DMPM, MG and residual substrate were quantified by a combination of an Agilent 1200 series HPLC equipped with a Carbohydrate (Zorbax) column (60 wt% acetonitrile/water, 0.5 mL min^{-1}, 30 °C) and two-dimensional ^{1}H–^{13}C HSQC employing standard addition of xylose. 50 μL of a 100 mM stock solution in D_4-methanol was added to the sample and spectra were re-recorded by the aforementioned two-dimensional ^{1}H–^{13}C HSQC procedure.

Isolation of *trans*-2,5-dihydroxy-3-pentenoic acid methyl ester

Up-scaled reactions were performed in a 1 liter autoclave (Autoclave Engineers) with mechanical stirring. The autoclave was loaded with 300 g of methanol, 18 g of xylose and 4.5 g of Sn-Beta (PT) and heated under stirring to 160 °C for 16 h. The autoclave was allowed to cool, the catalyst was then removed by filtration and the reaction mixture was dried overnight with 50 g molecular sieves. The molecular sieves were filtered from the product mixture and methanol was removed *in vacuo* affording a crude brown residue. *trans*-2,5-Dihydroxy-3-pentenoic acid methyl ester was isolated from the crude by dry column vacuum chromatography using ethyl acetate/heptane as the eluent, typically yielding 2.6 g *trans*-2,5-dihydroxy-3-pentenoic acid methyl ester of >94% purity (GC-MS, Fig. S4,† ^{1}H-NMR, Fig. S5†).

***trans*-2,5-Dihydroxy-3-pentenoic acid methyl ester.** ^{1}H NMR (400 MHz, CD_3OD) δ 5.89 (dtd, J = 15.5, 5.0, 1.4 Hz, 1H), 5.72 (ddt, J = 15.5, 5.7, 1.7 Hz, 1H), 4.76 (s, 4H), 4.58 (ddt, J = 5.7, 1.4, 1.4 Hz, 1H), 3.99 (ddd, J = 5.0, 1.6, 1.4 Hz, 2H), 3.63 (s, 3H), 3.21 (p, J = 3.3, 1.6 Hz, 1H). ^{13}C NMR (101 MHz, CD_3OD) δ 173.2, 132.2, 126.8, 70.9, 61.3, 51.2.

Enzymatic polymerisation of ethyl 6-hydroxyhexanoate and *trans*-2,5-dihydroxy-3-pentenoic acid methyl ester to poly(E6-HH-*co*-DPM)

For the co-polymerisation, 0.40 g (3 mmol) of *trans*-2,5-dihydroxy-3-pentenoic acid methyl ester, 2.0 g (13 mmol) of ethyl 6-hydroxyhexanoate (Sigma-Aldrich, 97%) and 0.24 g of N435 (Novozymes) was added to a Schlenk tube. The mixture was placed in an oil bath under magnetic stirring at 60 °C and 200 mbar pressure for 2 h, before being reduced to 5 mbar for another 70 h. The product was dissolved in tetrahydrofuran (Sigma-Aldrich, ≥99.9%) and immediately filtered by suction. The filtrate was evaporated *in vacuo*, re-dissolved in tetrahydrofuran and precipitated in cold methanol (Sigma-Aldrich, ≥99%). Refrigeration at 5 °C for 30 min followed by filtration, yielded poly(E6-HH-*co*-DPM) as an orange sticky solid (1.088 g, 62% yield).

Polymer I – poly(E6-HH-*co*-DPM). FT-IR (cm^{-1}) 3496, 2943, 2865, 1721. ^{1}H-NMR (300 MHz, $CDCl_3$) δ 5.97 (dt, J = 15.49, 5.68 Hz, 0.16H), 5.79 (dd, J = 15.48, 4.58 Hz, 0.17H), 4.62 (d, J = 4.37 Hz, 0.18H), 4.54 (d, J = 5.59 Hz, 0.26H), 4.17 (m, 0.37H), 3.99 (t, J = 6.64 Hz, 1.64H), 3.58 (t, J = 8.23 Hz, 0.18H), 2.24 (t, J = 7.47 Hz, 2.00H), 1.58 (m, 4.13H), 1.31 (m, 2.11H), 1.19 (t, J = 7.19 Hz, 0.06H). ^{13}C-NMR (75 MHz, $CDCl_3$) δ 173.5, 172.8, 130.0, 126.7, 70.4, 67.9, 65.9, 64.1, 34.0, 28.3, 25.4, 24.5.

Trifluoroacetic anhydride esterification of poly(E6-HH-*co*-DPM)

In a typical esterification, 63 mg poly(E6-HH-*co*-DPM) was dissolved in 0.7 mL D-chloroform (Sigma-Aldrich, 99.8%) and transferred to a NMR tube and 4 drops of trifluoroacetic anhydride (Sigma-Aldrich, >99%) were added. The mixture was precipitated in cold methanol (Sigma-Aldrich, ≥99%) and refrigerated at 5 °C for 30 min. The mixture was transferred to a syringe and filtered using a Teflon® syringe filter. The filter was washed with chloroform and the liquid was collected. The solvent was evaporated under ambient conditions and the product was dried overnight in a vacuum oven at 30 mbar at room temperature, yielding the functionalised polyester (polymer II). Coupling yield was determined by ^{1}H-NMR, based on the change in chemical shift of the protons vicinal to the alcohol group of DPM.

Polymer II. FT-IR (cm^{-1}) 3500, 2960, 2864, 1723. ^{1}H-NMR (300 MHz, $CDCl_3$) δ 6.11 (dt, J = 15.68, 5.39 Hz, 0.19H), 5.92

(dd, $J = 15.61, 6.39$ Hz, 0.18H), 5.63 (d, $J = 6.37$ Hz, 0.16H), 4.67 (d, $J = 5.23$ Hz, 0.28H), 4.21 (m, 0.38H), 4.10 (t, $J = 6.56$, 1.70H), 3.91 (t, $J = 6.63$, 0.11H), 2.37 (t, $J = 7.49$, 2.00H), 1.66 (m, 4.21H), 1.39 (m, 2.32H), 1.26 (m, 0.14H). ^{13}C-NMR (75 MHz, $CDCl_3$) δ 175.8, 175.7, 166.6, 158.9, 149.7 (q), 131.5, 123.2, 113.7 (q), 74.8, 68.01, 67.9, 66.6, 65.1, 34.3, 28.2, 25.5, 24.6.

Thiol–ene functionalisation of poly(E6-HH-*co*-DPM)

For the thiol–ene functionalisation, 15 mg poly(E6-HH-*co*-DPM), 4 drops of mercaptoacetic acid (Sigma-Aldrich, ≥98%) and 2.9 mg (0.02 mmol) 2,2-dimethoxy-2-phenylacetophenone (Sigma-Aldrich, 99%) was dissolved in 0.6 mL D-chloroform (Sigma-Aldrich, 99.8%). The mixture was transferred to a NMR tube and irradiated with UV light (λ = 365 nm) for 30 min, yielding the thiol functionalised polyester (polymer IIIc). The conversion of the double bond was determined by ^{1}H-NMR from the signals at 5.97 and 5.79 ppm corresponding to the substitution of the double bond in poly(E6-HH-*co*-DPM). This functionalisation was further confirmed by detection of increased presence of carboxylic acid functionality in FT-IR at 3461 cm^{-1}. Polymers IIIa, b, d and e were prepared by the aforementioned procedure, exchanging the derivatising agent with 1-mercaptohexane, mercaptoethanol, 2-ethylhexanethiol or thiophenol respectively, and coupling yields are given in Scheme 3.

Polymer characterisation

NMR characterisation of polymers was performed on a 7 Tesla Spectrospin-Bruker AC 300 MHz spectrometer at room temperature using $CDCl_3$ as solvent. Assignments of NMR spectra were based on homonuclear and heteronuclear correlation spectroscopy (^{1}H–^{1}H COSY and ^{1}H–^{13}C HSQC spectra). Glass transition temperatures (T_g) and melting temperatures (T_m) were obtained using a Discovery DSC from TA Instruments. Thermal analyses were performed at a heating and cooling rate of 10 °C min^{-1} from −100 to 150 °C. T_g and T_m were measured at the inflection point and at the peak temperature, respectively. Fourier transform infrared (FT-IR) spectroscopy was conducted on an attenuated total reflection (ATR)-FT-IR (Thermo iS50 with a built-in diamond ATR with a resolution of 4 cm^{-1}) in order to confirm the presence of functional groups. Molecular weight and polydispersities were determined using Size Exclusion Chromatography (SEC). SEC was performed in THF on a Viscotek GPCmax autosampler equipped with a Viscotek TriSEC model 302 triple detector array (RI detector, viscometer detector and light scattering detectors measuring at 90° and 7°) and a Knauer K-2501 UV detector on two Polymer Laboratories PLgel MIXED-D columns. The samples were run at a flow rate of 1 mL min^{-1} at 35 °C and molecular weights were determined from a PS calibration.

Film casting

In a typical procedure 0.27 g of ε-polycaprolactone (Perstop, M_n = 50 000 g mol^{-1}) and 0.030 g of poly(E6-HH-*co*-DPM) was dissolved in 6 mL of tetrahydrofuran. The mixture was transferred to a Teflon® mold and the solvent was allowed to evaporate in a closed vessel at room temperature to ensure a slow evaporation of the solvent. The resulting film was hot-pressed at 70 °C for 10 min to ensure a uniform, flat film.

Water contact angle measurements

A water droplet of 15 μL was placed on the surface with the needle inside the drop, and the drop was expanded and contracted on the surface of the polymer film at a rate of 2.0 μL s^{-1}. All water contact angle measurements were determined as an average of three measurements of three different drops at different positions on the polymer surface.

Results and discussion

Identification of *trans*-2,5-dihydroxy-3-pentenoic acid methyl ester and co-products

Thorough analyses of product mixtures from reactions using xylose as the substrate and Sn-Beta (HT) as the catalyst were initially performed by GC-MS. Here it was found that in addition to the previously reported retro-aldol and dehydration products, additional products were present.[9,25,26] Analysis of the product mixtures using 2D heteronuclear (^{1}H–^{13}C) spectroscopy, confirmed the presence of DPM alongside 3-deoxy-γ-pentonolactones (DPL), 2,4,5-trihydroxypentanoic acid methyl ester (TPM) and 2,5-dihydroxy-4-methoxy-pentanoic acid methyl ester (DMPM). These products are thus homologues of those reported for the conversion of hexoses to THM and 3-deoxygluconolactones. Following this initial work, a comprehensive analysis procedure was established, combining GC, HPLC and NMR spectroscopy to quantify the different reaction products for the conversion of pentoses (Scheme 2). This analysis procedure was used for comparing different catalysts, conditions and co-solutes and for optimising the yield of DPM.

Reaction pathways for pentoses

In the presence of Lewis acidic silicates, pentose sugars react along three primary reaction pathways leading to a variety of products (Scheme 2). These are grouped accordingly: (1) formation of methyl glycosides (MG) catalysed by Brønsted acids in the absence of alkali co-solutes; (2) retro-aldol reactions leading to C_3–C_4 α-hydroxy esters and glycolaldehyde dimethylacetal which are catalysed by Lewis acidic silicates in the presence of alkali co-solutes; (3) dehydration *via* 3-deoxyxylosone (3-DX) to give DPM, DPL, TPM, DMPM and furfural derivatives (F and F-DMA), catalysed by tin-containing silicates in the absence of alkali co-solutes.

The central intermediate 3-DX can be transformed into DPL *via* a 1,2-hydride shift of its intramolecular hemiacetal. Xylose give rise to two different DPL diastereomers that can be discerned by NMR spectroscopy. We speculate these to be 3-deoxy-γ-D-xylonolactone and 3-deoxy-γ-D-lyxonolactone, formed by racemisation on C_2 in the 1,2-hydride shift step. In an analogous open chain form, 3-DX can react with methanol to form a hemiacetal which can undergo a 1,2-hydride shift leading to TPM. From 3-DX a subsequent dehydration can also occur, leading to *cis*/*trans*-3,4-dideoxyxylos-3-enone (*cis*/*trans*-3,4-DXE).

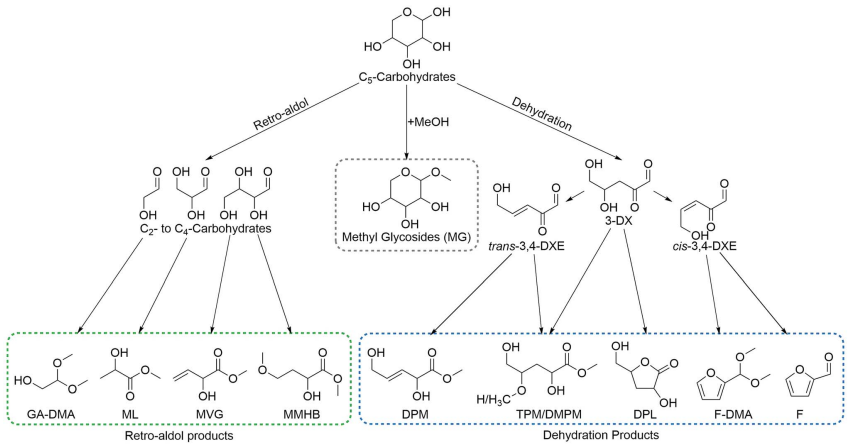

Scheme 2 Major pathways, intermediates and products in the conversion of pentoses by Sn-Beta. Compound abbreviations: 3-deoxyxylosone (3-DX), *cis*-3,4-dideoxyxylos-3-enone (*cis*-3,4-DXE), *trans*-3,4-dideoxyxylos-3-enone (*trans*-3,4-DXE), 2,5-dihydroxy-4-methoxy-pentanoic acid methyl ester (DMPM), 3-deoxypentonolactone (DPL), *trans*-2,5-dihydroxy-3-pentenoic acid methyl ester (DPM), furfural (F), furfural dimethylacetal (F-DMA), glycolaldehyde dimethyl acetal (GA-DMA), methyl glycosides (MG), methyl lactate (ML), methyl 4-methoxy-2-hydroxybutanoate (MMHB), methyl vinyl glycolate, (MVG) and 2,4,5-trihydroxy-3-pentanoic acid methyl ester (TPM).

The *trans*-3,4-DXE isomer can undergo reactive esterification leading to DPM while *cis*-3,4-DXE is a likely precursor for furfural *via* a third dehydration step. Interestingly, 3-deoxy xylosone has previously been reported as an intermediate in the formation of furfural from pentoses.[27,28] In the current study, we often find that the yields of furfural derivatives and DPM are correlated, supporting that this is indeed an important intermediate in the formation of furfural species using Lewis acidic catalysts. This interpretation is furthermore supported by the use of the Brønsted acidic Al-Beta as the catalyst, resulting in the formation of only trace amounts of furfural products (1%) and no detectable DPM. In contrast, Sn-Beta forms 11–17% furfural products and 23–33% DPM under comparable conditions. A small amount of DMPM was also observed as a product. This is likely formed *via* Michael addition of methanol to 3,4-DXE, prior to a 1,2-hydride shift, thereby being analogous to the formation of MMHB from tetroses.[20,21]

Testing of different catalysts

Significant yields of DPM (10–33%) were obtained only for catalysts containing tin incorporated into a siliceous matrix (Table 1, entries 1–5). A comparison of the yields of products obtained from xylose using the different tin-containing silicates is shown in Fig. 1. The products are grouped into the three categories mentioned above, according to the primary reaction pathways responsible for their formation. The highest DPM yield of 33% was obtained using Sn-Beta (HT) (Table 1, entry 1) which also resulted in the highest ratio of DPM to total dehydration products (3 : 5), while Sn-Beta (PT) resulted in a lower DPM yield of 23% (Table 1, entry 2) and showed a lower ratio (1 : 2). This difference is likely attributable to the balance of Brønsted and Lewis acidity in the two materials. Sn-Beta (PT) contains more defects due to being synthesised by a post treatment method, likely resulting in a more Brønsted acidic character.[39,53] Additionally, the different preparation methods may lead to a different incorporation of tin into the *BEA siliceous matrix.[39,53,54] An indication of the different acidity balance for Sn-Beta (HT) and Sn-Beta (PT) is seen when comparing their yields of MG being 6% and 23%, respectively. Of all the tin-containing silicates tested, the small pore Sn-MFI material displays the lowest selectivity towards DPM and dehydration products. The main products formed after two hours are methyl glycosides, indicating that the pentoses are not converted preferentially *via* Lewis acid catalysed pathways but instead have time to undergo acetalisation reactions which are typically catalysed by Brønsted acids.[55] Other tin-containing silicates such as the ordered mesoporous materials Sn-SBA-15 and Sn-MCM-41 were also active for the formation of DPM, resulting in yields of 12% and 16% yield, respectively. These catalysts all belong to the group of tin-containing silicates and are all able to form DPM in significant yields. In contrast, materials having tin outside of the siliceous matrix, such as dispersed SnO_2 nanoparticles on Si-Beta, did not catalyse the formation of DPM under these reaction conditions (Table 1, entry 6). This finding highlights the importance of successfully incorporating tin in the silicate matrix to obtain catalytically active heterogeneous catalysts.

Table 1 Conversion of xylose using a variety of catalysts[a]

				Retro-aldol					Dehydration					
Entry	Catalyst	XYL, %	MG, %	GA-DMA, %	ML, %	MVG, %	MMHB, %	Total, %	DPL, %	TPM/DMPM[b], %	FUR[c], %	DPM, %	Total, %	Carbon balance, %
1	Sn-Beta (HT)	n.d.	4	2	14	2	<1	19	10	13	11	33 (3)	68	90 (4)
2	Sn-Beta (PT)	n.d.	23	3	11	<1	<1	15	6	9	17	23 (1)	55	93 (3)
3	Sn-MFI	<1	30	6	17	1	<1	24	3	3	10	11 (1)	27	82 (5)
4	Sn-MCM-41	n.d.	23	4	12	<1	<1	18	6	14	20	16 (1)	57	98 (5)
5	Sn-SBA-15	<1	32	6	11	<1	<1	18	3	10	18	12 (1)	42	92 (6)
6	SnO_2-Beta[d]	53	42	2	<1	<1	<1	3	1	2	1	<1	6	104 (7)
7	Ti-Beta	<1	48	7	11	3	<1	22	4	7	5	<1	16	86
8	Zr-Beta	<1	39	12	10	2	<1	25	2	2	4	<1	9	73
9	Al-Beta	6	82	n.d.	n.d.	n.d.	n.d.	0	n.d.	n.d.	1	n.d.	1	89 (1)
10	Si-Beta	13	42	5	2	<1	<1	8	2	3	3	<1	8	71
11	Blank	88	6	<1	<1	<1	<1	1	n.d.	n.d.	<1	n.d.	1	96 (1)

[a] All reactions employed the standard reaction conditions: 360 mg xylose (8.3 wt%), 4 g methanol, 180 mg catalyst, 2 h, 160 °C and 600 rpm stirring. Reactions were performed in triplicates and standard deviations of the last digit are given in parenthesis for DPM; full values and deviations for all products are provided in Table S2. n.d. = not detected. Refer to Scheme 2 for product abbreviations. [b] Combined yields (carbon%) of 2,4,5-trihydroxy-3-pentanoic acid methyl ester and 2,5-dihydroxy-4-methoxy-pentanoic acid methyl ester. [c] Combined yields (carbon%) of furfural and furfural dimethyl acetal. [d] Dispersed SnO_2 nanoparticles on Si-Beta.

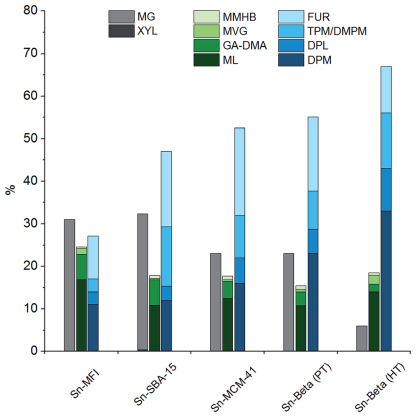

Fig. 1 Product distribution of tin-containing silicates based on data from Table 1. Reaction conditions: 0.360 g xylose, 0.180 g catalyst, 4.0 g methanol, 160 °C, 2 hours.

The purely siliceous material Si-Beta did not catalyse the formation of significant amounts of DPM, and the main product observed was MG (Table 1, entry 10). Catalysts having other metals than tin incorporated into the framework such as titanium, zirconium and aluminium did not form significant yields of DPM from xylose either (Table 1, entry 7–9). However, both Ti-Beta and Zr-Beta gave appreciable yields of retro-aldol products (22–25%), which is in accordance with previous reports of these materials being active for the formation of lactates.[20] The formation of DPM, in contrast, occurs *via* a different reaction pathway that is seemingly only catalysed by the tin-containing silicates. The same trend was reported for the formation of THM from hexoses using the same types of materials.[26] The highly Brønsted acidic Al-Beta was found to convert xylose into methyl glycosides with a high selectivity, which is in accordance with previous findings.[56] No formation of DPM was observed, while small amounts of furfural were detected (*ca.* 1%).

We would like to draw attention to the yields of furanic products and DPM in the comparison of Zr-Beta and Ti-Beta with all the tin-containing silicates. Low yields of furanic products (4–5%) are observed for the zirconium and titanium materials while all tin-containing silicates form substantially higher yields (10–20%). This observation supports the aforementioned hypothesis, that the majority of the furanic products is formed *via* a 3-DX route for the tin-containing silicates. The inability of the titanium and zirconium materials to catalyse the formation of 3-DX from xylose thus also prevents a substantial co-production of furanic compounds.

Effect of reaction parameters and co-solutes for DPM formation using Sn-Beta

The catalyst screening clarified that Sn-Beta gives higher DPM yields than other tin-containing silicates. We therefore assessed the reaction parameters in detail using Sn-Beta (HT) as the catalyst. To this end, we varied the reaction temperature (140–180 °C), the catalyst to substrate ratio (0.125–1.0), the concentration of xylose in the reaction solution (8.3–23 wt%) and examined the effect of adding alkali co-solutes in the form of potassium carbonate. Furthermore, we tested if other pentoses could be used for DPM formation. From these studies, it was deduced that high catalyst to substrate ratios and the absence of alkali co-solutes are important parameters to obtain high yields of DPM.

The effect of reaction temperature on the yield of DPM was insignificant and similar yields (31–34%) were obtained in the temperature range of 140–180 °C (Table S4†). The reaction temperature effect appeared to be more pronounced for yields of other reaction products, with higher temperatures favouring retro-aldol products (9% difference) and lower temperatures favouring furanics (8% difference).

It had previously been shown for hexoses that alkali co-solutes significantly diminish the yield of THM and furanic products, leading to increased yields of retro-aldol products, from 30% in the absence of alkali to 75% in the presence of 0.065 mM of added potassium carbonate.[18] We find that an analogous effect exists for the conversion of pentoses (Fig. 2), illustrating that optimal yields of DPM require a strict control of alkali contaminants. We found by ICP measurements that a background alkali level of 1.3 wt ppm was present even under "alkali free" conditions, possibly originating from the borosilicate glassware.

The catalyst to substrate ratio was varied from 0.125 to 1.0 on weight basis, while keeping the substrate concentration constant at 8.3 wt% xylose. Interestingly, a strong dependence on catalyst loading was found, as selectivity towards DPM increased significantly from a catalyst to substrate ratio of 0.125 (19% DPM) up to 0.5 (34% DPM) (Table S4†). The formation of retro-aldol products followed the opposite trend, decreasing with increased catalyst to substrate ratios from a combined yield of 32% at a catalyst to substrate ratio of 0.125 to just 15% at a ratio of 1.0.

The effect of the xylose concentration in the reaction mixture was tested, keeping the catalyst to substrate ratio constant at 0.5. Surprisingly, increasing the concentration did not lower the yield of DPM and using a 23 wt% solution of xylose in methanol gave a similar yield of 32% as an 8.3 wt% solution (Table S3†).

Finally, two other pentoses (ribose and lyxose) were tested as substrates and found to give DPM yields of 30% and 31%, respectively (Table S3†).

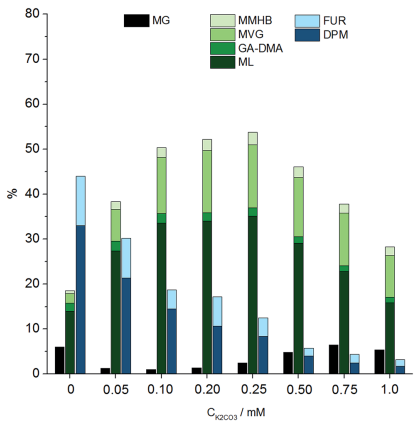

Fig. 2 Product distribution at different alkali concentrations using Sn-Beta, based on data from Table S5.† Reaction conditions: 0.360 g xylose, 0.180 g Sn-Beta (HT, Si/Sn = 150), 4.0 g methanol, 160 °C, 2 hours. Yields of TPM and DMPM and DPL are not included in this graph. Refer to Scheme 2 for abbreviations.

Polymerisation potential

In order to evaluate the usefulness of DPM as a novel polyester monomer, and having shown that DPM can be formed in acceptable yields (above 30%), the synthesis and purification of DPM was performed at larger scale (1 L). Due to the simpler synthesis route of Sn-Beta (PT), this catalyst was used at the expense of a lower overall DPM yield. From these large-scale experiments, 2.6 g of ≥94% pure (as estimated by ^{1}H-NMR) DPM was synthesised. Having shown that DPM can be prepared in acceptable amounts, we became interested in its use as a polymer building block. It has previously been shown by Sels and co-workers that MVG can be co-polymerised with lactic acid with a 1,2-linkage to afford a polyester material having pendant vinyl groups available for post functionalisation.[23] Additionally, it has recently been reported that MVG can be converted into dimethyl (*E*)-2,5-dihydroxyhex-3-enedioate, *via* a metathesis reaction.[57,58] This new product has also been successfully co-polymerised with lactic acid.[57] In contrast to MVG, DPM contains both a secondary and a primary alcohol, which prevents the use of classical polymerisation catalysts due to poor selectivity control. However, enzymatic polymerisation methods permit polymerisation of such highly functional monomers.[59,60] Especially the enzyme selectivity between primary and secondary alcohols enables the specific synthesis of functional linear polymers that cannot be prepared using chemo-catalysis.[61,62] Unfortunately, homo-polymerisation of DPM was unsuccessful and resulted only in the formation of oligomers. As an alternative to homo-polymerisation, co-polymerisations were conducted using the commercially available monomer ethyl 6-hydroxyhexanoate (E6-HH) as shown in Scheme 3. Polymerisation of pure E6-HH affords polycaprolactone (PCL) which is a linear and biodegradable polyester produced on industrial scale. Co-polymerisation with DPM could be envisaged to be a useful way to modify the properties of PCL. This approach incorporates DPM into linear polymers with a linear 1,5-linkage, leaving the secondary alcohol and olefin moieties available for post-functionalisation (Scheme 3, polymer I).

The enzymatic co-polymerisations between DPM and E6-HH were performed at 60 °C in bulk monomer in accordance with the general procedure described in the Experimental section. The NMR spectrum of the resulting polymer (Fig. 3) shows that that the vinylic hydrogen atoms from DPM are present, while the alcohol, alkene and ester functional groups were confirmed by FT-IR spectroscopy (Fig. S6†).

The polymer synthesis procedure was varied to study the effects of feed ratio and polymerisation time on the resulting polymers. Polymerisation time was studied by conducting co-polymerisation experiments using a DPM to E6-HH molar

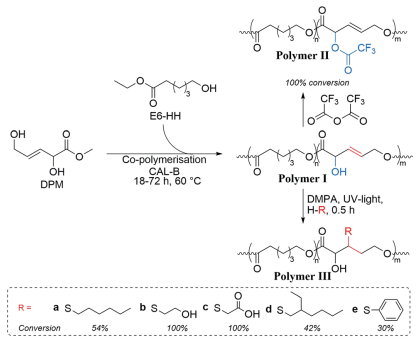

Scheme 3 Enzymatic co-polymerisation of DPM and ethyl 6-hydroxyhexanoate (E6-HH) using *Candida antarctica* lipase B (CAL-B) and subsequent functionalisation. The reaction of the thiols can supposedly occur on either carbon of the olefinic moieties, but only one form is represented in the scheme for clarity.

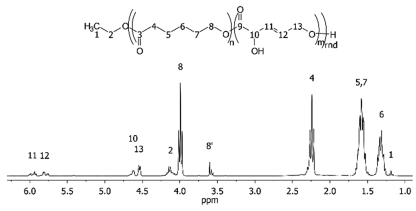

Fig. 3 ^{1}H NMR assignment of the co-polymer product, poly(E6-HH-*co*-DPM), from Table 2 entry 4.

ratio of 0.22 and varying the reaction times (Table 2, entries 2–4). The shortest polymerisation time of 18 h resulted in the incorporation of approximately 55% (0.12 molar ratio) of the DPM from the feed into the co-polymer. By increasing the polymerisation time to first 42 h and subsequently to 72 h, incorporation was increased to 77% (0.17 molar ratio). At all tested reaction times reasonable degrees of polymerisation (M_w = 10 000–12 350 g mol^{-1}) and polydispersity indices (PDI = 2.1–2.5) were obtained, comparable to typical results from enzymatic polymerisation of monomers containing both secondary and primary alcohols.[61,62]

These findings clearly showed that DPM was more challenging to polymerise than E6-HH, which was also evident by DPM being unable to homo-polymerise. Nevertheless, DPM should become incorporated at longer polymerisation times and higher DPM fractions in the feed (Table 2).

A study of varying the feed ratio of E6-HH to DPM from a molar ratio of 0.22 to 0.66 showed that the content of DPM in the co-polymer increased with increased ratio. This lead to full incorporation of DPM into the co-polymers at polymerisation times of 72 h and molecular ratios above 0.44. Despite full incorporation of DPM, these polymerisations resulted in molecular weights of only 4500 and 3700 g mol^{-1} for 0.44 and 0.66 molar ratio, respectively. Molecular weights above 10 000 g mol^{-1} as observed with 0.22 molar ratio DPM could not be obtained for these co-polymerisations.

The thermal properties of all the co-polymers were investigated by DSC and showed glass transition temperatures (T_g) between −49 °C to −56 °C, which is typical for aliphatic polyesters and confirms the flexible nature of the polymer chain. The melting temperature (T_m) at 0.12 molar ratio of DPM was determined to be 42.8 °C and T_m decreased with increasing content of DPM to 7.5 °C at 0.66 molar ratio DPM. The incorporation of DPM clearly prevents the regularity and close chain-to-chain packing required for the polymer to crystallise, thereby reducing the melting temperature.

These initial studies clearly show that DPM can be successfully polymerised with other similar monomers thereby providing access to functional polymers. Furthermore, the degree of incorporation may be used to manipulate the physical properties of the co-polymer.

Post-functionalisation

Post-functionalisation of polymers offers the possibility to tailor their properties. The DPM containing co-polymers were tested for their ability to undergo functionalisation of the α-hydroxyl and olefinic groups (Scheme 3). Functionalisation of the α-hydroxyl groups of DPM was performed using trifluoroacetic anhydride (TFA), a highly reactive reagent widely used in

Table 2 Enzymatic co-polymerisation of E6-HH and DPM[a]

Entry	Time h	Feed MR[b]	Prod. MR[b,c]	T_g[d], °C	T_m[d], °C	M_n[e], g mol^{-1}	M_w[e], g mol^{-1}	PDI[e]
1[f]	18	0	0	−60.2	48.9	3600	4700	1.3
2	18	0.22	0.12	−49.3	42.8	5150	10 050	2.1
3	42	0.22	0.14	−49.3	42.5	4490	10 750	2.4
4	72	0.22	0.17	−50.0	34.2	5000	12 350	2.5
5	72	0.44	0.44	−55.5	15.1	1900	4500	2.4
6	72	0.66	0.66	−52.3	7.5	1760	3700	2.1

[a] All reactions were performed at 60 °C and the pressure was held at 200 mbar for 2 h whereafter it was reduced to 5 mbar in accordance with optimisations performed with E6-HH (see ESI). [b] Molar ratio (MR) listed as DPM/E6-HH [mol mol^{-1}]. [c] Determined by ^{1}H NMR. [d] Determined by DSC. [e] Determined by SEC in THF using PS standards. [f] Using only E6-HH as monomer.

hydroxyl labelling of polymers, allowing for clear detection of functionality by NMR analysis.[63,64] The structure of the TFA modified co-polymer (Scheme 3, polymer II) was verified by ^{1}H NMR (see experimental section "Thiol–ene functionalisation of poly(E6-HH-*co*-DPM)"), showing that full functionalisation was achieved.

Additionally, thiol–ene chemistry was used to demonstrate the reactivity of the intra-chain alkene.[23] Thiol–ene chemistry is a well-established protocol for functionalisation of polymers by formation of alkyl sulphides *via* reaction of a thiol and an alkene using radical chemistry.[65,66] Here, a photo initiator (2,2-dimethoxy-2-phenylacetophenone, DMPA) was used together with a selection of thiol compounds (Scheme 3) to illustrate the potential for post-polymerisation functionalisation.

The functionalisation of DPM sub-units in the thiol–ene experiments was determined using ^{1}H and ^{1}H–^{13}C NMR following diminished double bond proton intensities within the polymer upon functionalisation. Thiol–ene reactions varied between 30 and 100% conversion, with the least sterically hindered substituents yielding the highest conversion (Scheme 3, polymers IIIa–e). Poor solubility of the functionalised co-polymer materials in DMSO and chloroform prevented conclusive studies of the regioselectivity in the thiol–ene reactions. We found that in particular mercaptoacetic acid and mercaptoethanol (Scheme 3, polymer IIIb–c) were effective grafting reagents, making it possible to fully convert the in-chain double bond, clearly demonstrating the polymers high potential for functionalisation. In-chain alkenes are estimated to have an approximately 10-fold lower reactivity compared to corresponding pendent alkenes.[67] The high extent of functionalisation in the polymer observed herein is thus extraordinary and underlines the potential of in-chain alkenes for preparation of functional polymers.

Co-polymer blends with polycaprolactone in thin films

The prepared co-polymers have a high structural similarity to PCL and therefore blends between some of the co-polymers and PCL were investigated. PCL often finds uses in biomedical devices, where control of surface properties and functionality are highly desired properties and therefore simple blending could be an interesting application of the new co-polymers.

Three different films consisting of pure PCL, a PCL blend with 10 wt% poly(E6-HH-*co*-DPM) (PECD–PCL) and a PCL blend with 10 wt% trifluroacetic acid functionalised poly(E6-HH-*co*-DPM) (PECD(TFA)–PCL) were prepared by solvent casting and hot-pressing. The prepared films were investigated by water contact angle (WCA) measurements to determine the impact on surface properties of the blend (Table 3).

The pure PCL film had an advancing WCA of 85°, which was reduced to 75° by blending with the DPM co-polymer. This shows the impact of the free hydroxyl groups from the co-polymer, and could be exploited to increase the hydrophilicity of the thin film. This was corroborated with the receding WCA, which is reduced by almost 10° for the blend, indicating the presence of more polar groups in the system. Conversely, blending PCL with the trifluroacetic acid functionalised poly(E6-HH-*co*-DPM) resulted in an increase in the advancing WCA up to 93°, which is expected from increasing the hydrophobicity of the film due to the fluorine in the co-polymer. The receding WCA was not affected from blending in the fluorinated co-polymer, which showed that the system is still amphiphilic. Both results show that the co-polymer is able to modify the surface properties of the thin film blend, and that post-modification of the co-polymer permits exploitation of the functional groups for further modification of the surface of thin film blends.

Table 3 Advancing and receding water contact angle measurements for PCL, PECD–PCL and PECD(TFA)–PCL films[a]

Film	Advancing WCA deg	Receding WCA deg
PCL[b]	90 (1)	46 (1)
PCL	85 (2)	46 (2)
PECD–PCL[c]	75 (1)	38 (2)
PECD(TFA)–PCL[d]	93 (2)	36 (2)

[a] All water contact angles (WCA) were determined as averages of three measurements of three different drops at different positions on the polymer surface and standard deviations of the last digit are given in parenthesis. [b] WCA value for PCL from literature.[68] [c] The film contained 10 wt% poly(E6-HH-*co*-DPM). [d] The film contained 10 wt% TFA functionalised poly(E6-HH-*co*-DPM).

Conclusion

In the current study, we have shown that the novel polyester building block DPM can be synthesised from pentoses using tin-containing silicates as catalysts in yields up to 32% with xylose concentrations of 23 wt%. This approach provides a simple and low cost route from a plentiful and sustainable feedstock to an intriguing chemical product. Future improvements to the DPM synthesis may encompass ways to suppress the formation of furanics or of retro-aldol products, or to better control the formation of ester products from 3-DX. DPM has been shown to be an interesting monomer for the preparation of functional polyesters in co-polymerisation with E6-HH. Enzymatic polymerisations were effective for the synthesis of the highly functional polyesters with 0.17 to 0.66 molar ratio content of DPM. The co-polymers could easily be post-functionalised using either TFA or thiol–ene chemistry to extend the potential applications of these co-polymers. As an example, simple blends with PCL were investigated and it was shown how the co-polymer could be used to affect the surface properties of the polymer film.

The chemoenzymatic approach described herein thus enables future bio-refineries to better utilise pentoses from hemicellulose-containing biomass, providing the chemical industry with new types of interesting polymer building blocks.

Acknowledgements

We gratefully acknowledge funding by the Bio-Value platform (biovalue.dk) under the SPIR initiative by The Danish Council

for Strategic Research and The Danish Council for Technology and Innovation (case number 0603-00522B), as well as the Innovation Fund Denmark (case number 5150-00023B). SM gratefully acknowledges funding by Grant 2013_01_0709 of the Carlsberg Foundation. Novozymes A/S is gratefully acknowledged for supplying enzymes for polymerisation. 800 MHz NMR spectra were recorded on the spectrometer of the DTU NMR center.

References

1 E. Castro-Aguirrea, F. Iñiguez-Francoa, H. Samsudinb, X. Fangc and R. Auras, *Adv. Drug Delivery Rev.*, 2016, **107**, 333–366.
2 A. Carlson, B. Coggio, K. Lau, C. Mercogliano and J. Millis, in *Chemicals and Fuels from Bio-Based Building Blocks*, Wiley-VCH, 2016, ch. 7, pp. 173–190.
3 H. Liu, Y. Xu, Z. Zheng and D. Liu, *Biotechnol. J.*, 2010, **5**, 1137–1148.
4 M. Sara, S. K. Brar and J. F. Blais, in *Platform Chemical Biorefinery*, Elsevier Inc., 1st edn, 2016, ch. 14, pp. 249–283.
5 M. Dusselier, P. Van Wouwe, A. Dewaele, P. A. Jacobs and B. F. Sels, *Science*, 2015, **349**, 78–80.
6 E4tech, *Re-CORD and WUR, From the Sugar Platform to biofuels and biochemicals, Report ENER/C2/423–2012/SI2.673791*, European Commission Directorate-General Energy, 2015.
7 F. Fenouillot, A. Rousseau, G. Colomines, R. Saint-Loup and J.-P. Pascault, *Prog. Polym. Sci.*, 2010, **35**, 578–622.
8 R. De Clercq, M. Dusselier, C. Christiaens, J. Dijkmans, R. I. Iacobescu, Y. Pontikes and B. F. Sels, *ACS Catal.*, 2015, **5**, 5803–5811.
9 Y. Wang, J. D. Lewis and Y. Román-Leshkov, *ACS Catal.*, 2016, **6**, 2739–2744.
10 P. Verdeguer, N. Merat and A. Gaset, *J. Mol. Catal.*, 1993, **85**, 327–344.
11 X. Tong, Y. Ma and Y. Li, *Appl. Catal., A*, 2010, **385**, 1–13.
12 Y. Y. Gorbanev, S. K. Klitgaard, J. M. Woodley, C. H. Christensen and A. Riisager, *ChemSusChem*, 2009, **2**, 672–675.
13 J. Ma, Y. Pang, M. Wang, J. Xu, H. Ma and X. Nie, *J. Mater. Chem.*, 2012, **22**, 3457–3461.
14 S. P. Chopade, D. J. Miller, J. E. Jackson, T. A. Werpy, J. G. Frye Jr and A. H. Zacher, Board of Trustees operating Michigan State University, US 6291725 B1, Battelle Memorial Institute, Pacific Northwest Laboratory, 2001.
15 M.-Y. Zheng, A.-Q. Wang, N. Ji, J.-F. Pang, X.-D. Wang and T. Zhang, *ChemSusChem*, 2010, **3**, 63–66.
16 R. Ooms, M. Dusselier, J. A. Geboers, B. O. de Beeck, R. Verhaeven, E. Gobechiya, J. A. Martens, A. Redl and B. F. Sels, *Green Chem.*, 2014, **16**, 695–707.
17 T. R. Boussie, E. L. Dias, Z. M. Fresco and V. J. Murphy, US 8501989 B2, Rennovia Inc., 2013.
18 S. Tolborg, I. Sádaba, C. M. Osmundsen, P. Fristrup, M. S. Holm and E. Taarning, *ChemSusChem*, 2015, **8**, 613–617.
19 M. Dusselier, P. Van Wouwe, A. Dewaele, E. Makshina and B. F. Sels, *Energy Environ. Sci.*, 2013, **6**, 1415–1442.
20 M. S. Holm, S. Saravanamurugan and E. Taarning, *Science*, 2010, **328**, 602–605.
21 M. Dusselier, P. Van Wouwe, F. de Clippel, J. Dijkmans, D. W. Gammon and B. F. Sels, *ChemCatChem*, 2013, **5**, 569–575.
22 I. Z. Sádaba and E. Taarning, Haldor Topsøe A/S, WO 2016083137 A1, 2016.
23 M. Dusselier, P. Van Wouwe, S. De Smet, R. De Clercq, L. Verbelen, P. Van Puyvelde, F. E. Du Prez and B. F. Sels, *ACS Catal.*, 2013, **3**, 1786–1800.
24 E. Taarning, S. Saravanamurugan, M. S. Holm, J. Xiong, R. M. West and C. H. Christensen, *ChemSusChem*, 2009, **2**, 625–627.
25 M. S. Holm, Y. J. Pagán-Torres, S. Saravanamurugan, A. Riisager, J. A. Dumesic and E. Taarning, *Green Chem.*, 2012, **14**, 702–706.
26 S. Tolborg, S. Meier, I. Sádaba, S. G. Elliot, S. K. Kristensen, S. Saravanamurugan, A. Riisager, P. Fristrup, T. Skrydstrup and E. Taarning, *Green Chem.*, 2016, **18**, 3360–3369.
27 T. Usui, S. Yanagisawa, M. Ohguchi, M. Yoshino, R. Kawabata, J. Kishimoto, Y. Arai, K. Aida, H. Watanabe and F. Hayase, *Biosci., Biotechnol., Biochem.*, 2007, **71**, 2465–2472.
28 M. Hellwig, J. Degen and T. Henle, *J. Agric. Food Chem.*, 2010, **58**, 10752–10760.
29 H. S. Chen, A. Wang, H. Sorek, J. D. Lewis, Y. Román-Leshkov and A. Bell, *ChemistrySelect*, 2016, **1**, 4167–4172.
30 A. Corma, L. T. Nemeth, M. Renz and S. Valencia, *Nature*, 2001, **412**, 423–425.
31 A. Corma, M. E. Domine, L. Nemeth and S. Valencia, *J. Am. Chem. Soc.*, 2002, **124**, 3194–3195.
32 C.-C. Chang, Z. Wang, P. Dornath, H. J. Cho and W. Fan, *RSC Adv.*, 2012, **2**, 10475–10477.
33 R. Bermejo-Deval, R. S. Assary, E. Nikolla, M. Moliner, Y. Román-Leshkov, S.-J. Hwang, A. Palsdottira, D. Silverman, R. F. Lobo, L. A. Curtiss and M. E. Davis, *Proc. Natl. Acad. Sci. U. S. A.*, 2012, **109**, 9727–9732.
34 Q. Guo, F. Fan, E. A. Pidko, W. N. P. van der Graaff, Z. Feng, C. Li and E. J. M. Hensen, *ChemSusChem*, 2013, **6**, 1352–1356.
35 P. Y. Dapsens, C. Mondelli, J. Jagielski, R. Hauert and J. Perez-Ramirez, *Catal. Sci. Technol.*, 2014, **4**, 2302–2311.
36 M. Orazov and M. E. Davis, *Proc. Natl. Acad. Sci. U. S. A.*, 2015, **112**, 11777–11782.
37 M. Sasidharan, Y. Kiyozumi, N. K. Mal, M. Paul, P. R. Rajamohanan and A. Bhaumik, *Microporous Mesoporous Mater.*, 2009, **126**, 234–244.
38 M. Moliner, Y. Román-Leshkov and M. E. Davis, *Proc. Natl. Acad. Sci. U. S. A.*, 2010, **107**, 6164–6168.
39 P. Wolf, M. Valla, F. Núñez-Zarur, A. Comas-Vives, A. J. Rossini, C. Firth, H. Kallas, A. Lesage, L. Emsley and C. Copéret, *ACS Catal.*, 2016, **6**, 4047–4063.
40 G. Yang, X. Li and L. Zhou, *RSC Adv.*, 2016, **6**, 8838–8847.
41 B. D. Montejo-Valencia, J. L. Salcedo-Pérez and M. C. Curet-Arana, *J. Phys. Chem. C*, 2016, **120**, 2176–2186.

42 Y. G. Kolyagin, A. V. Yakimov, S. Tolborg, P. N. Vennestrøm and I. I. Ivanova, *J. Phys. Chem. Lett.*, 2016, **7**, 1249–1253.
43 J. W. Harris, M. J. Cordon, J. R. Di Iorio, J. C. Vega-Vila, F. H. Ribeiro and R. Gounder, *J. Catal.*, 2016, **335**, 141–154.
44 R. Otomo, R. Kosugi, Y. Kamiya, T. Tatsumi and T. Yokoi, *Catal. Sci. Technol.*, 2016, **6**, 2787–2795.
45 S. Tolborg, A. Katerinopoulou, D. D. Falcone, I. Sádaba, C. M. Osmundsen, R. J. Davis, E. Taarning, P. Fristrup and M. S. Holm, *J. Mater. Chem. A*, 2014, **2**, 20252–20262.
46 P. Li, G. Liu, H. Wu, Y. Liu, J.-g. Jiang and P. Wu, *J. Phys. Chem. C*, 2011, **115**, 3663–3670.
47 C. Hammond, S. Conrad and I. Hermans, *Angew. Chem., Int. Ed.*, 2012, **51**, 11736–11739.
48 J. Dijkmans, D. Gabriels, M. Dusselier, F. de Clippel, P. Vanelderen, K. Houthoofd, A. Malfliet, Y. Pontikes and B. F. Sels, *Green Chem.*, 2013, **15**, 2777–2785.
49 S. Valencia and A. Corma, UOP LLC, US 6306364 B1, 1999.
50 N. K. Mal, V. Ramaswamy, P. R. Rajamohanan and A. V. Ramaswamy, *Microporous Mater.*, 1997, **12**, 331–340.
51 L. Li, C. Stroobants, K. Lin, P. A. Jacobs, B. F. Sels and P. P. Pescarmona, *Green Chem.*, 2011, **13**, 1175–1181.
52 V. Ramaswamy, P. Shah, K. Lazar and A. V. Ramaswamy, *Catal. Surv. Asia*, 2008, **12**, 283–309.
53 J. Dijkmans, M. Dusselier, W. Janssens, M. Trekels, A. Vantomme, E. Breynaert, C. Kirschhock and B. F. Sels, *ACS Catal.*, 2015, **6**, 31–46.
54 P. Wolf, W.-C. Liao, T.-C. Ong, M. Valla, J. W. Harris, R. Gounder, W. N. P. van der Graaff, E. A. Pidko, E. J. M. Hensen, P. Ferrini, J. Dijkmans, B. Sels, I. Hermans and C. Copèret, *Helv. Chim. Acta*, 2016, **99**, 916–927.
55 S. Saravanamurugan, A. Riisager, E. Taarning and S. Meier, *ChemCatChem*, 2016, **8**, 3107–3111.
56 M. Paniagua, S. Saravanamurugan, M. Melian-Rodriguez, J. A. Melero and A. Riisager, *ChemSusChem*, 2015, **8**, 1088–1094.
57 A. Dewaele, L. Meerten, L. Verbelen, S. Eyley, W. Thielemans, P. Van Puyvelde, M. Dusselier and B. Sels, *ACS Sustainable Chem. Eng.*, 2016, **4**, 5943–5952.
58 A. Sølvhøj, E. Taarning and R. Madsen, *Green Chem.*, 2016, **18**, 5448–5455.
59 S. Kobayashi and A. Makino, *Chem. Rev.*, 2009, **109**, 5288–5353.
60 N. Miletić, K. Loos and R. A. Gross, in *Biocatalysis in Polymer Chemistry*, Wiley-VCH, 2010, ch. 4, pp. 83–129.
61 B. J. Kline, E. J. Beckman and A. J. Russell, *J. Am. Chem. Soc.*, 1998, **120**, 9475–9480.
62 A. S. Kulshrestha, W. Gao and R. A. Gross, *Macromolecules*, 2005, **38**, 3193–3204.
63 A. Holländer, S. Kröpke and F. Pippig, *Surf. Interface Anal.*, 2008, **40**, 379–385.
64 C. Hoffmann, M. C. Stuparu, A. Daugaard and A. Khan, *J. Polym. Sci., Part A: Polym. Chem.*, 2015, **53**, 745–749.
65 C. E. Hoyle and C. N. Bowman, *Angew. Chem., Int. Ed.*, 2010, **49**, 1540–1573.
66 M. J. Kade, D. J. Burke and C. J. Hawker, *J. Polym. Sci., Part A: Polym. Chem.*, 2010, **48**, 743–750.
67 N. Ten Brummelhuis, C. Diehl and H. Schlaad, *Macromolecules*, 2008, **41**, 9946–9947.
68 D. S. Jones, J. Djokic, C. P. McCoy and S. P. Gorman, *Biomaterials*, 2002, **23**, 4449–4458.

Electronic Supplementary Material (ESI) for RSC Advances.

Supporting Information

Synthesis of a novel polyester building block from pentoses by tin-containing silicates

S. G. Elliot, C. Andersen, S. Tolborg, S. Meier, I. Sádaba, A. E. Daugaard, E. Taarning

Table of Contents

Polymerization of Ethyl 6-Hydroxyhexanoate (E6-HH)

Ethyl 6-hydroxyhexanoate (E6-HH) (2.0 g, 12 mmol) and CAL-B (NZ435, 0.20 g) was transferred to a Schlenk tube. The suspension was then immersed in an oil bath at 80 °C under stirring and va cuum (200 mbar) for 18 h and terminated by cooling in a dry i ce bath. The product was dissol ved in THF and enzyme particles were filtered off by suction filtra tion (particle retention 5-13 µm). The residue was washed with THF several times. The fil trate was evapora ted *in vacuo*, re-dissol ved in THF and precipitated in cold methanol. The precipitate was fil tered and the residue were dried under va cuum at room temperature overnight yielding 0.40 g polyester as a white solid. The procedure was repeated for 50, 60 and 70 °C respecti vel y (results in Table S6) showinga linear increase in molecular weight as seen in the figure below. The yield of the polymerization was 20% after precipitation.

SEC: M_n = 5421 g mol^{-1}, M_w = 6878 g mol^{-1}, PDI = 1.27. DSC: T_m = 51.82°C. IR: $\tilde{\nu}$ / cm^{-1} = 3425, 2944, 2864, 1721, 1167, 1043. ^{1}H NMR (300 MHz, $CDCl_3$) δ 4.09 (m, 0.02H), 4.03 (t, J = 6.7 Hz, 1H), 3.61 (t, J = 6.4 Hz, 0.09H), 2.27 (t, J = 7.5 Hz 1H), 1.61 (m, 2H), 1.35 (qv, J = 8.3 Hz, 1H), 1.22 (t, J = 7.1 Hz, 0.08H). ^{13}C NMR (75 MHz, $CDCl_3$) δ 173.5, 64.0, 62.5, 60.2, 34.0, 28.3, 25.4, 24.5, 14.2.

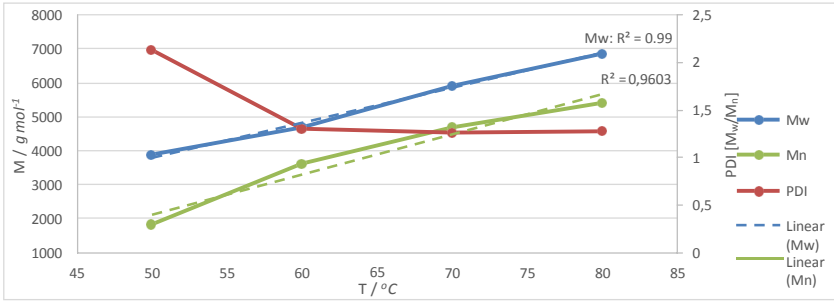

Figure S1. Polymerization Results. Influence of temperature on Mn, Mw and PDI for enzymatic polymerization of E6 -HH.

Figures

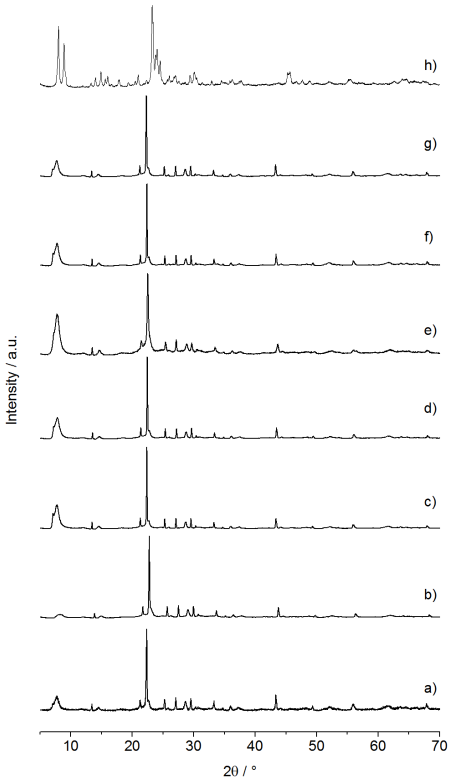

Figure S2. XRD Diff racto grams. XRD diffractograms of a) Sn-Beta (HT, Si/Sn = 150), b) Zr-Beta (HT, Si/Zr = 150), c) Ti-Beta (HT, Si/Ti = 150), d) Al-Beta (HT, Si/Al =150), e) Sn-B eta (PT, Si/Sn = 125), f) SnO_2-Beta (HT, Si/Sn = 200), g) Si-Beta (HT), and h) Sn-MFI (OH^-, Si/Sn = 100)

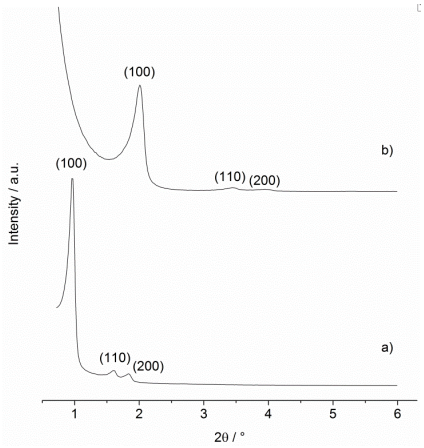

Figure S3. Low Angle XRD Diffractograms . Low angle XRD diffractograms of a) Sn-MCM-41 (Si/Sn = 200) and b) Sn-SBA-15 (Si/Sn = 200).

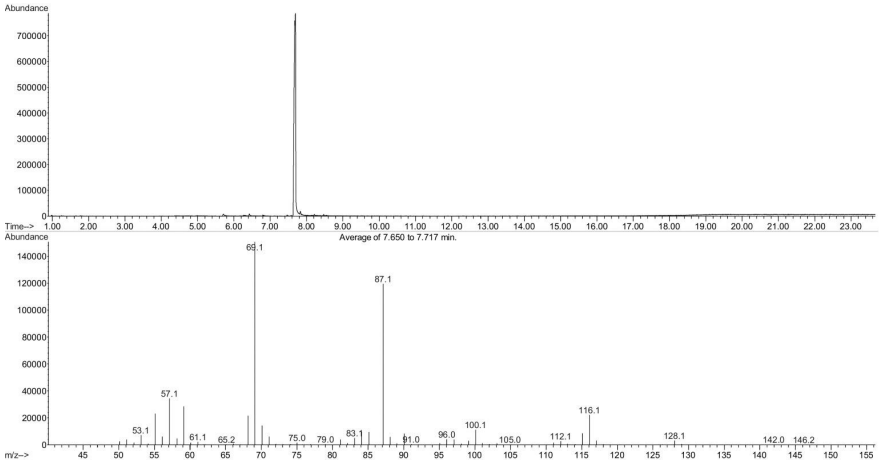

Figure S4. DPM GC-MS Spectru m. GC-MS spectrum of purified trans-2,5-dihydroxy-3-pentenoic ac id methyl ester (DPM), an alysed on an Agilent 6890 with a Phonomenex Zebron ZB-5 column.

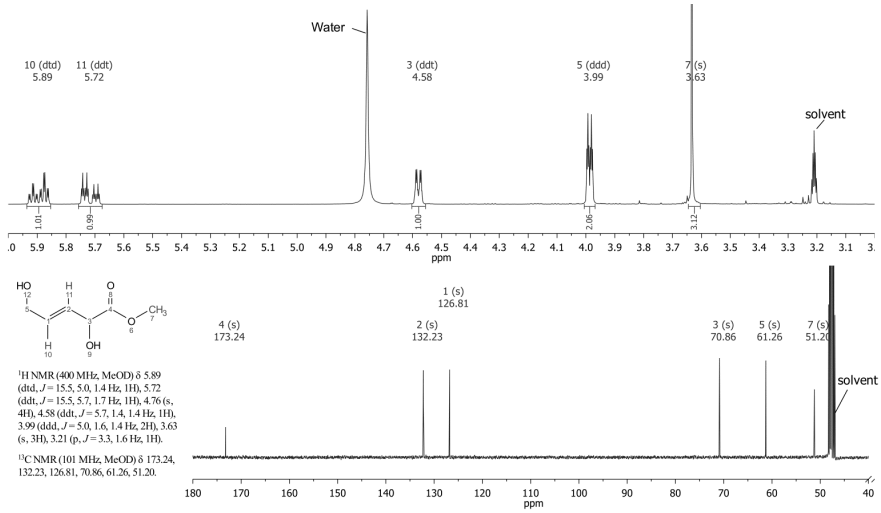

Figure S5. DPM NMR Spectra. Spectra and assign ment of ^{1}H NMR (400 MHz) and ^{13}C NMR (100 MHz) signals in trans-2,5-dihydroxy-3-pentenoic acid methyl ester (DPM). NMR spectra were record ed on a Bruker Ascend 400 spectrometer, ^{1}H NMR was recorded at 400 MHz and ^{13}C NMR was record ed at 100 MHz. The chemical shifts are given in ppm relative to the residual solvent signals and the chemical shifts are reported downfield to TMS.

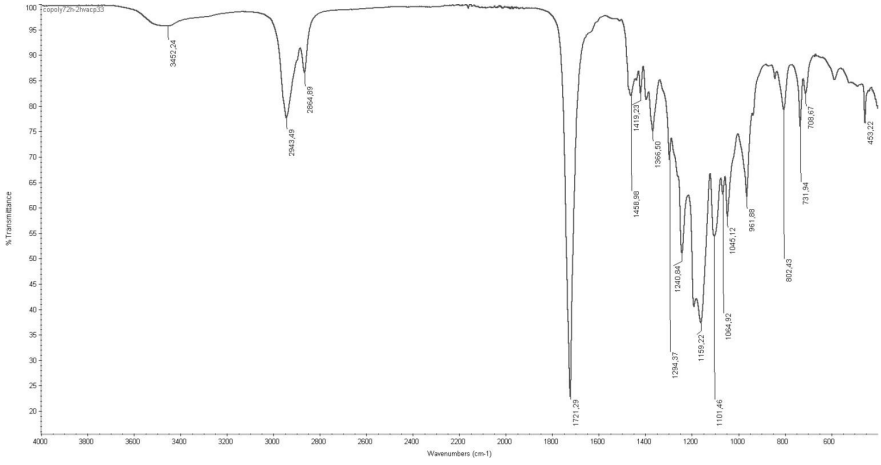

Figure S6. FT- IR of poly(E6-HH-co-DPM). FT-IR spectru m of poly(E6-HH-co-DPM) showing a bro ad signal at 3496 cm^{-1} arising f rom th e O-H stretch as well as a ch aracteristic C =O stretch at 1721 cm^{-1} and C-O stretch at 1159 cm^{-1} and 1045 cm^{-1} from the ester functionality. A weak signal from th e C=C stretch is visible on the shoulder of the C=O stretch and a strong C=C out-of-plane bend signal is visible at 961 cm^{-1}.

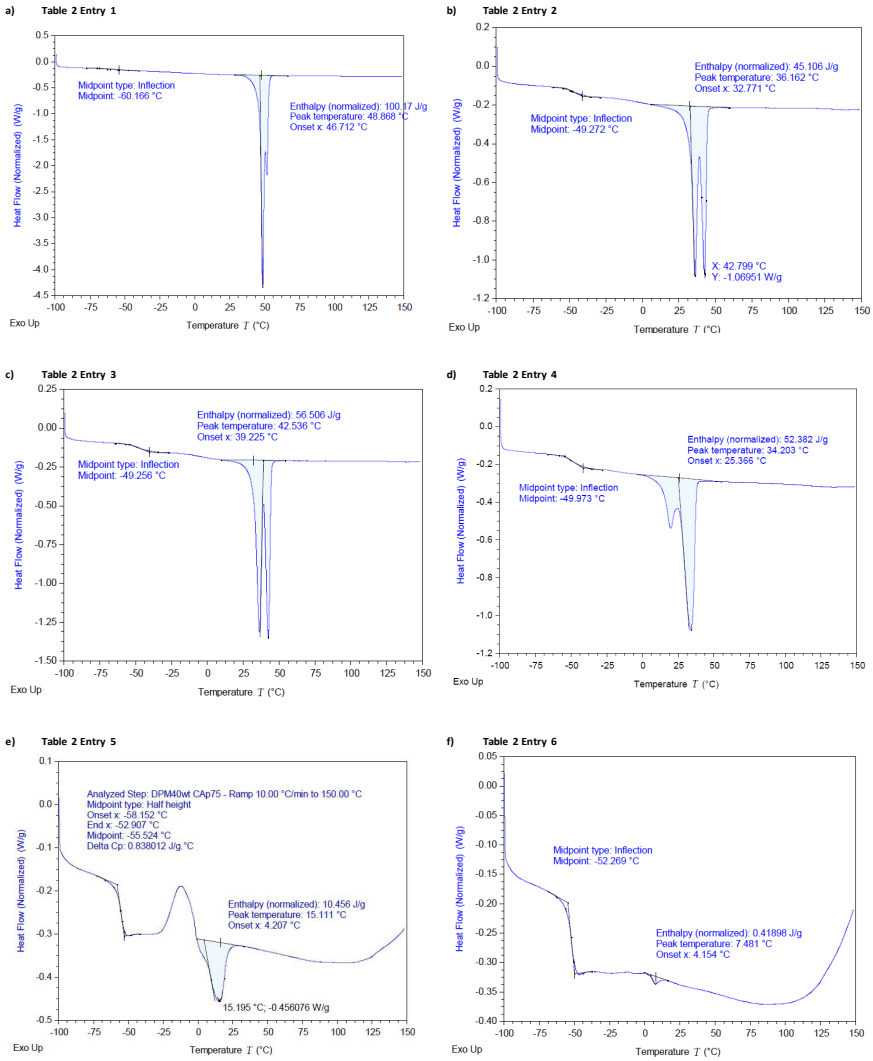

Figure S7. DSC of poly(E6-HH-co-DPM). DSC spectra of different poly(E6-HH-co-DPM) synthesis. a) table 2 entry 1, 18 hours reaction time, 100% E6 -HH. b) table 2 entry 2, 18 hours reaction time, 0.22 DPM/E6-HH. c) table 2 entry 3, 42 hours reaction time, 0.22 DPM/E6 -HH. d) table 2 entry 4, 72 hours reaction time, 0.22 DPM/E6-HH. e) table 2 entry 5, 72 hours reaction time, 0.44 DPM/E6-HH. f) table 2 entry 6, 72 hours reaction time, 0.66 DPM/E6 -HH.

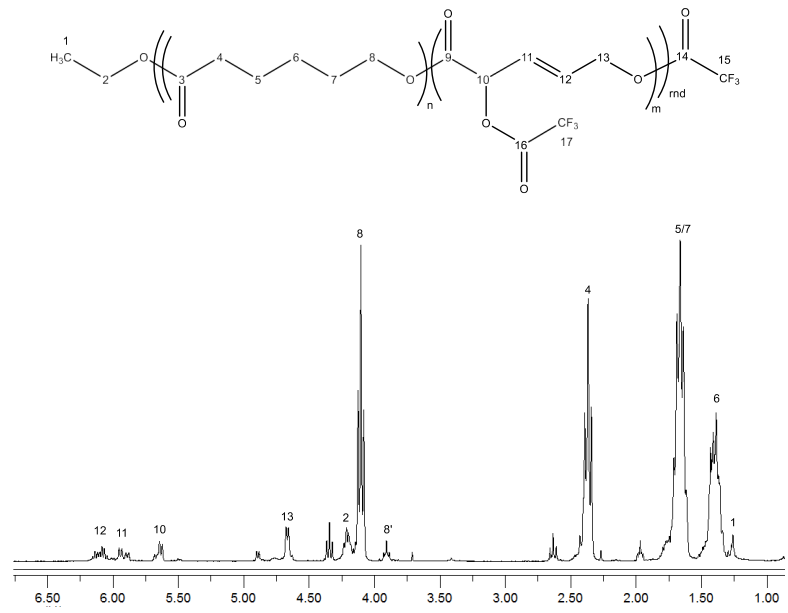

Figure S8. ^{1}H-NMR of Polymer II. ^{1}H NMR assignment of TFA modified poly(E6-HH-co-DPM).

7

Tables

Table S1. Physical properties of the various catalysts used in the study measured using N 2-adsorption/desorption and from XRD diffraction.

Entry	Catalyst	Elemental Analysis	X-ray diffraction	N2-adsorption			
				S_{BET}	$S_{micropore}$[a]	V_{total}	$V_{micropore}$[a]
		Si / Metal	Primary Phase	m^2/g		mL/g	
1	Sn-Beta (HT, 150)	186	*BEA	486	362	0.33	0.19
2	Sn-Beta (PT, 125)	113	*BEA	557	373	0.37	0.19
3	Sn-MFI (100)	82	MFI	404	273	0.25	0.14
4	Sn-MCM-41 (200)	252	-	962	-	1.00	-
5	Sn-SBA-15 (200)	271	-	918	111	1.09	0.06
6	SnO_2-Beta (200)	303	*BEA	457	365	0.27	0.19
7	Ti-Beta (HT, 150)	245	*BEA	460	372	0.27	0.19
8	Zr-Beta (HT, 150)	167	*BEA	470	374	0.27	0.19
9	Al-Beta (HT, 150)	142	*BEA	472	366	0.27	0.19
10	Si-Beta	-	*BEA	465	378	0.27	0.20

n.a. = not available

[a] Determined using the t-plot method.

Table S2. Conversion of xylose using a variety of catalysts.

Entry	Catalyst	XYL	MG	Retro-Aldol					Dehydration				
				GA-DMA	ML	MVG	MMHB	**Total**	DPL	TPM/DMPM[a]	FUR[b]	DPM	**Total**
		%		%					%				
1	Sn-Beta (HT)	n.d.	4 (1)	1.81 (7)	14 (1)	2.1 (6)	0.6 (3)	**19**	10.3 (5)	13 (1)	11 (1)	33 (3)	**68**
2	Sn-Beta (PT)	n.d.	23 (1)	3.18 (2)	10.8 (3)	0.63 (4)	0.8 (8)	**15**	5.7 (9)	9 (1)	17.4 (6)	23 (1)	**55**
3	Sn-MFI	0.9 (9)	30 (4)	6.0 (2)	16.9 (4)	1.29 (6)	0.36 (3)	**24**	3.0 (2)	3.0 (2)	10.1 (5)	11 (1)	**27**
4	Sn-MCM-41	n.d.	23 (5)	4.0 (8)	12.5 (7)	0.40 (6)	0.8 (2)	**18**	6 (1)	14 (1)	20.5 (7)	16 (1)	**57**
5	Sn-SBA-15	0.3 (2)	32 (6)	6.0 (1)	10.9 (3)	0.30 (2)	0.6 (3)	**18**	3.3 (1)	9.5 (3)	17.7 (8)	12 (1)	**42**
6	SnO_2-Beta[c]	53 (5)	42 (5)	2.3 (2)	0.45 (4)	0.39 (4)	0.1 (1)	**3**	1.281 (3)	2.3 (6)	1.4 (2)	0.42 (2)	**6**
7	Ti-Beta	0.46 (4)	48	7.4 (1)	11.2 (8)	2.81 (5)	0.34 (1)	**22**	3.8 (2)	6.7 (2)	4.8 (3)	0.83 (2)	**16**
8	Zr-Beta	0.3 (2)	39	12.0 (2)	10.3 (1)	2.0 (1)	0.54 (2)	**25**	2.5 (3)	2.1 (1)	3.9 (3)	0.65 (7)	**9**
9	Al-Beta	6 (1)	81.9 (5)	n.d.	n.d.	n.d.	n.d.	**0**	n.d.	n.d.	1.2 (2)	n.d.	**1**
10	Si-Beta	13	42	5.1 (2)	2.01 (6)	0.37 (6)	0.321 (4)	**8**	1.61 (5)	3.1 (3)	3.4 (6)	0.2 (2)	**8**
11	Blank	87.7 (6)	6.2 (3)	0.28 (7)	0.2 (3)	0.6 (1)	0.1 (1)	**1**	n.d.	n.d.	0.3 (2)	n.d.	**1**

Reactions were performed in triplicate and employed the standard reaction conditions: 360 mg xylose (8.3 wt%), 4 g methanol, 180 mg catalyst, 2 h, 160 °C, 600 rpm stirring. Standard deviations of the last digit are given in parenthesis. Compound abbreviations: 2,5-dihydroxy-4-methoxy-pentanoic acid methyl ester (DMPM), 3-deoxypentonolactone (DPL), *trans*-2,5-dihydroxy-3-pentenoic acid methyl ester (DPM), furanics (FUR), glycolaldehyde dimethyl acetal (GA-DMA), methyl glycosides (MG), methyl lactate (ML), methyl 4-methoxy-2-hydroxybutanoate (MMHB), methyl vinyl glycolate (MVG), 2,4,5-trihydroxy-3-pentanoic acid methyl ester (TPM) and xylose (XYL). n.d. = not detected.

[a] Combined yields (carbon%) of 2,4,5-trihydroxy-3-pentanoic acid methyl ester and 2,5-dihydroxy-4-methoxy-pentanoic acid methyl ester.

[b] Combined yields (carbon%) of furfural and furfural dimethyl acetal.

[c] Dispersed SnO_2 nanoparticles on Si-Beta.

Table S3. Reaction yields from the conversion of pentoses with varying substrates and concentrations.

Entry	Substrate	Substrate	PENT	MG	Retro-Aldol					Dehydration				
					GA-DMA	ML	MVG	MMHB	**Total**	DPL	TPM/DMPM[a]	FUR[b]	DPM	**Total**
			%		%					%				
1	Ribose	8.3	n.d.	3 (2)	2.0 (1)	12 (2)	2.0 (7)	0.5 (2)	**17**	10.37 (3)	10.1 (3)	12 (2)	30 (2)	**63**
2	Lyxose	8.3	n.d.	2.6 (6)	2.1 (1)	15 (3)	2 (1)	0.5 (3)	**20**	11.6 (2)	12.6 (1)	11 (3)	31 (2)	**66**
3	Xylose	8.3	n.d.	4 (1)	1.81 (7)	14 (1)	2.1 (6)	0.6 (3)	**19**	10.3 (5)	13 (1)	11 (1)	33 (3)	**68**
4	Xylose	15	0.06 (9)	6 (1)	0.3 (1)	14 (1)	1.9 (4)	0.3 (1)	**17**	11.37 (4)	13 (1)	8.7 (9)	34 (4)	**68**
5	Xylose	23	n.d.	6 (1)	2 (2)	13 (1)	1.7 (4)	0.3 (2)	**17**	11.1 (5)	13 (2)	11 (2)	32 (2)	**67**

Reactions were performed in triplicate and employed the reaction conditions: 180 -1200 mg pentose (4.3-23 wt%), 4 g methanol, 180 mg Sn- Beta (HT, 150), 2 h, 160 °C, 600 rpm stirring. Standard deviations of the last digit are given in parenthesis. Compound abbreviations: 2,5-dihydroxy-4-methoxy-pentanoic acid methyl ester (DMPM), 3-deoxypentonolactone (DPL), *trans*-2,5-dihydroxy-3-pentenoic acid methyl ester (DPM), furanics (FUR), glycolaldehyde dimethyl acetal (GA-DMA), methyl glycosides (MG), methyl lacta te (ML), methyl 4-methoxy-2-hydroxybutanoate (MMHB), methyl vinyl glycolate (MVG), reactant pentose (PENT) and 2,4,5-trihydroxy-3-pentanoic acid methyl ester (TPM). n.d. = not detected.

[a] Combined yields (carbon%) of 2,4,5-trihydroxy-3-pentanoic acid methyl ester and 2,5-dihydroxy-4-methoxy-pentanoic acid methyl ester.

[b] Combined yields (carbon%) of furfural and furfural dimethyl acetal.

Table S4. Reaction yields from the conversion of xylose, varying catalyst to substrate ratio and temperature.

Entry	Catalyst/ Substrate	Temp.	XYL	MG	Retro-Aldol					Dehydration				
					GA-DMA	ML	MVG	MMHB	**Total**	DPL	TPM/DMPM[a]	FUR[b]	DPM	**Total**
		°C	%		%					%				
1	0.00[c]	160	87.7 (6)	6.2 (3)	0.28 (7)	0.2 (3)	0.6 (1)	0.1 (1)	**1**	n.d.	n.d.	0.3 (2)	n.d.	**1**
2	0.125	160	n.d.	3.8 (3)	3 (2)	23 (1)	4.3 (2)	1.0 (6)	**32**	9.0 (5)	11.19 (6)	14.3 (4)	19 (3)	**53**
3	0.25	160	n.d.	3.7 (1)	2.5 (9)	21 (2)	3 (1)	0.8 (5)	**28**	8.8 (5)	13 (1)	11 (1)	28 (3)	**60**
4	0.50	160	n.d.	4 (1)	1.81 (7)	14 (1)	2.1 (6)	0.6 (3)	**19**	10.3 (5)	13 (1)	11 (1)	33 (3)	**68**
5	0.75	160	n.d.	3.02 (7)	1.00 (7)	13.2 (9)	1.9 (2)	0.5 (1)	**17**	10.1 (2)	11.8 (2)	9.9 (4)	34 (3)	**67**
6	1.00	160	n.d.	3.5 (4)	0.61 (7)	11 (2)	1.2 (5)	1.5 (7)	**15**	12.4 (6)	12.7 (5)	10 (2)	34 (3)	**70**
7	0.5	140	n.d.	4.4 (4)	2.5 (1)	11 (3)	1.0 (7)	0.5 (1)	**16**	9.7 (1)	13.6 (9)	17 (2)	31 (3)	**72**
8	0.5	150	n.d.	3.3 (6)	2.1 (4)	15 (4)	2 (1)	0.5 (3)	**19**	10 (1)	12 (2)	13.4 (7)	32 (3)	**68**
9	0.5	170	n.d.	3.0 (3)	1.31 (4)	18 (4)	4 (1)	1.3 (5)	**25**	10 (1)	9.7 (3)	9 (1)	34 (3)	**63**
10	0.5	180	n.d.	3.4 (7)	0.8 (4)	18 (3)	3.9 (9)	1.2 (3)	**24**	10 (1)	9 (0)	7.7 (4)	32 (3)	**59**

Reactions were performed in triplicate and employed the reaction conditions: 360 mg xylose (8.3 wt%), 4 g methanol, 0 -360 mg Sn- Beta (HT, 150), 2 h, 600 rpm stirring. Standard deviations of the last digit are given in parenthesis. Compound abbreviations: 2,5-dihydroxy-4-methoxy-pentanoic acid methyl ester (DMPM), 3-deoxypentonolactone (DPL), *trans*-2,5-dihydroxy-3-pentenoic acid methyl ester (DPM), furanics (FUR), glycolaldehyde dimethyl acetal (GA-DMA), methyl glycosides (MG), methyl lactate (ML), methyl 4-methoxy-2-hydroxybutanoate (MMHB), methyl vinyl glycolate (MVG), 2,4,5-trihydroxy-3-pentanoic acid methyl ester (TPM) and xylose (XYL). n.d. = not detected.

[a] Combined yields (carbon%) of 2,4,5-trihydroxy-3-pentanoic acid methyl ester and 2,5-dihydroxy-4-methoxy-pentanoic acid methyl ester.

[b] Combined yields (carbon%) of furfural and furfural dimethyl acetal.

[c] Blank sample; contains no catalyst.

Table S5. Reaction yields from the conversion of xylose using Sn-Beta with addition of K_2CO_3.

Entry	K_2CO_3	XYL	MG	Retro-Aldol					Dehydration		
				GA-DMA	ML	MVG	MMHB	**Total**	FUR[a]	DPM	**Total**
	mM	%		%					%		
1	0.00	n.d.	6	2	14	2	<1	**19**	11	33	**54**
2	0.05	n.d.	1	2	27	7	2	**38**	9	21	**30**
3	0.10	n.d.	1	2	34	13	2	**51**	4	14	**28**
4	0.15	n.d.	1	2	34	14	2	**52**	6	11	**17**
5	0.25	n.d.	2	2	35	14	3	**54**	4	8	**12**
6	0.50	n.d.	5	1	29	13	2	**45**	2	4	**6**
7	0.75	n.d.	6	1	23	12	2	**38**	2	2	**4**
8	1.00	n.d.	5	1	16	9	2	**28**	1	2	**3**

All reactions employed the reaction conditions: 360 mg xylose (8.3 wt%), 4 g methanol, 180 mg Sn-Beta (HT, 150), 2 h, 160 °C, 600 rpm stirring. Compound abbreviations: *trans*-2,5-dihydroxy-3-pentenoic acid methyl ester (DPM), furanics (FUR), glycolaldehyde dimethyl acetal (GA-DMA), methyl glycosides (MG), methyl lactate (ML), methyl 4-methoxy-2-hydroxybutanoate (MMHB), methyl vinyl glycolate (MVG) and xylose (XYL). n.d. = not detected, n.a. = not available.

[a] Combined yields (carbon%) of furfural and furfural dimethyl acetal.

Table S6. Enzymatic polymerization of E6-HH

Polymer[a]	Temperature	M_n[b]	M_w[b]	PDI[b]
	°C	g mol^{-1}	g mol^{-1}	
I-1	50	1816	3874	2.1
I-2	60	3616	4701	1.3
I-3	70	4688	5905	1.3
I-4	80	5421	6878	1.3

[a] All reactions were conducted at 200 mbar for 18 h.

[b] Determined by SEC in THF.

ChemPubSoc Europe

DOI: 10.1002/cssc.201700587

CHEMSUSCHEM Full Papers

Quantitative NMR Approach to Optimize the Formation of Chemical Building Blocks from Abundant Carbohydrates

Samuel G. Elliot,[a] Søren Tolborg,[b] Irantzu Sádaba,[b] Esben Taarning,[b] and Sebastian Meier*[a]

The future role of biomass-derived chemicals relies on the formation of diverse functional monomers in high yields from carbohydrates. Recently, it has become clear that a series of α-hydroxy acids, esters, and lactones can be formed from carbohydrates in alcohol and water solvents using tin-containing catalysts such as Sn-Beta. These compounds are potential building blocks for polyesters bearing additional olefin and alcohol functionalities. An NMR approach was used to identify, quantify, and optimize the formation of these building blocks in the Sn-Beta-catalyzed transformation of abundant carbohydrates. Record yields of the target molecules can be achieved by obstructing competing reactions through solvent selection.

The need to establish more sustainable methods of obtaining the chemicals needed by society for the production of food, materials, fuels, and energy is widely recognized. The current chemical industry is based on the availability of a small number of petroleum-derived building blocks. Biomass can be utilized to provide access to both existing and new types of building blocks, and research into this area has steeply increased during the last decade. It is important for these chemicals to be accessible at low cost and at the same time to have useful properties to be commercially utilized. Direct conversion of sugars to a target chemical by heterogeneous catalysis offers the best chance of lowering the process costs.[1–4] A plethora of reaction products have been identified in the acid-catalyzed conversion of C5 and C6 carbohydrates.[5] Amidst them acyclic α-hydroxy esters and acids have recently emerged as an attractive group of biomonomers (Scheme 1).

For potential use in biopolymer applications, the production, polymerization, and upgrading of the C3 building block lactate (**7**) and the C4 building block vinyl glycolate (**8**) has previously been demonstrated.[3,6–11] Recently, the production and polymerization of the C5 building block 2,5-dihydroxy-3-pentenoic acid methyl ester (Me-**1**) as well as the formation of the C6 building block *trans*-2,5,6-trihydroxy-3-hexenoic acid methyl ester (Me-**12**) have been described (Table 1).[12–14]

Conversions of C5 and C6 carbohydrates into the acyclic unsaturated α-hydroxy compounds **1** and **12** have been achieved using Sn-Beta in methanol[13,14] or in water[12] at temperatures

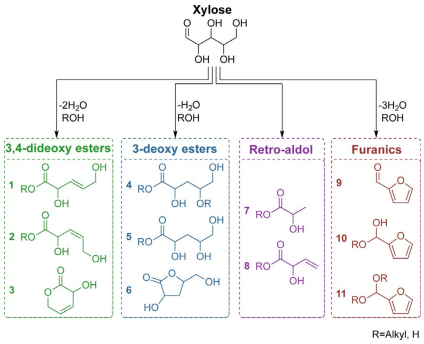

Scheme 1. Overview of major pathways in the catalytic conversion of xylose by Sn-Beta and the major products identified in the reaction mixtures at high temperatures (> 100 °C). The products are shown for reactions in alcohol (R = alkyl) or water (R = H) and are grouped (from left to right) as 3,4-dideoxy esters, 3-deoxy esters, retro-aldol products, and furanics.

Table 1. Conversion of C4, C5, and C6 carbohydrates by Sn-Beta to homologous 3,4-dideoxy esters with declining yield.

Carbon Backbone	Substrate	Compound	Structure	Yield [%]
C4	Erythrulose	Me-**8**		56[7]
C5	Xylose	Me-**1**		33[13]
C6	Glucose	Me-**12**		16[14]

[a] *S. G. Elliot, Dr. S. Meier*
Department of Chemistry
Technical University of Denmark
Kemitorvet, Bygning 207, 2800 Kgs. Lyngby (Denmark)
E-mail: semei@kemi.dtu.dk

[b] *Dr. S. Tolborg, Dr. I. Sádaba, Dr. E. Taarning*
Haldor Topsøe A/S
Haldor Topsøes Allé 1, 2800 Kgs. Lyngby (Denmark)

Supporting Information and the ORCID identification number(s) for the author(s) of this article can be found under https://doi.org/10.1002/cssc.201700587.

ChemPubSoc Europe

CHEMSUSCHEM Full Papers

above 100 °C in the absence of further additives. A Sn-Beta–zeolite synthesized under hydrothermal conditions using hydrofluoric acid as the mineralizing agent was the most efficient catalyst for this reaction.[12–14] C5 and C6 carbohydrates yield around 30% for C5-carbohydrate substrate Me-**1** and around 15% for C6-carbohydrate substrate Me-**12**, respectively. The yields for the formation of the C4 analogue vinyl glycolate methyl ester (Me-**8**) can exceed 50% (Table 1).[7,13,14] Alkali-salt additives were shown to reduce product yields and to strongly enhance the formation of smaller compounds such as methyl lactate.[8]

Optimizing carbohydrate conversion into new chemicals and detection of the products requires consideration of the analytical approaches employed. Methods that rely on the use of reference standards for identification and quantification, including liquid and gas chromatography, may be challenging to implement in work streams targeting new chemicals. In cases where commercial standards are unavailable, either production of standards or calculations to estimate response factors are necessary.[10] In contrast, methodologies that combine detailed structural information and the possibility of quantitatively detecting an accurate signal would be more valuable in the push toward bio-based economies.

Herein, we combine in situ NMR spectroscopy for the identification of reaction products with an accurate quantitative NMR (qNMR) methodology to assess solvent effects in the Sn-Beta-catalyzed conversion of abundant carbohydrates. The methodology operates on a timescale comparable to commonly used chromatography methods but avoids empirical instrument- and analyte-dependent response factors altogether. Instead, qNMR signals are simply proportional to the number of contributing atoms. Moreover, identifying new chemicals in situ makes intensive purification and characterization steps obsolete. Water and a series of short-chain alcohols are used as solvents that provide sufficient substrate solubility for the carbohydrates. The motivation for testing longer-chain alcohols as reaction solvents as opposed to methanol and water is to compare the physicochemical properties of the solvents and to investigate the stoichiometric participation of the solvent as a nucleophile in the reaction. Thus, the choice of solvent will affect the formation of alkyl-glycoside and acetal-type intermediates during the reaction, modulate the microenvironment and Lewis-acid properties of tin active sites in the stannosilicates, and alter molecular dynamics and energetics within the reaction pathway.[9,10] Hence, solvent variation is a means of optimizing operational conditions toward increased profitability of bioprocesses.

For the analysis of solvent effects, optimized spectra of complex reaction mixtures without prior purification or sample pre-treatment in protic, non-deuterated solvents were obtained. An advantage of this approach is that it does not rely on the availability of purified reference compounds. Changes in the product structures upon reaction with the solvent do not critically complicate product identification or quantification for the eleven main reaction products (Scheme 1).

Results and Discussion

Detection of products in reaction mixtures without relying on reference compounds

NMR spectroscopy is widely used for chemical structure elucidation and mixture analysis. The use of NMR spectroscopy for component identification and quantification is particularly well-developed for biological samples, including biofluids, extracts, and foods, but has also gained popularity within biomass conversion, for instance in the study of carbohydrate isomerization reactions[15–17] or for lignin structure and depolymerization reactions.[18] Herein, we use a suite of homo- and heteronuclear NMR experiments for the detection and identification of carbohydrate degradation products in situ. Specifically, DQF-COSY, TOCSY, ^{1}H-^{13}C HMBC, conventional and edited ^{1}H-^{13}C HSQC, as well as ^{1}H-^{13}C HSQC-TOCSY spectra were employed for compound identification. Band-selective ^{13}C excitation[19] and optimized decoupling sequences[20,21] were used to suppress non-informative signals and artefacts and to obtain higher quality ^{1}H-^{13}C 2D NMR spectra. NMR spectroscopy has notorious shortcomings in the detection of heteroatoms, but this problem was negligible for reactions involving carbohydrate fragmentation or dehydration, as oxygen positions could be inferred from ^{13}C chemical shifts. At the same time, the detection of discrete signals for individual atomic positions by NMR spectroscopy allows for the distinction of isomers. Such distinction of isomers is crucial, as several potential products in carbohydrate dehydration cannot be distinguished based on their mass alone.

Major products that were identified in reaction mixtures produced from xylose at 160 °C using a Sn-Beta–zeolite catalyst are shown in Scheme 1. These compounds were identified through de novo structure determination and ^{1}H/^{13}C chemical shift assignments in unpurified reaction mixtures in six different protic solvents (water, methanol, ethanol, *n*-propanol, *iso*-propanol and *n*-butanol). This approach was aided by the use of high-field NMR instrumentation (18.7 Tesla magnets) equipped with cryogenically cooled detection electronics to reduce electronic noise approximately threefold. The identified reaction products are derived from pathways including C–C bond breakage in retro-aldol reactions to yield C2, C3, and C4 fragments, which may subsequently undergo dehydration to various α-hydroxy esters (**7**–**8**). Alternatively, direct dehydration of the C5 compound to α-hydroxy-, 3-deoxy-, or 3,4-dideoxy esters (**1**–**6**) or triple dehydration to furanics (**9**–**11**) can occur. The most interesting of these products may be the *trans*-2,5-dihydroxy-3-pentenoic acid alkyl ester (**1**). We recently showed that this prospective chemical building block could be co-polymerized enzymatically in a selective 1,5-polymerization reaction with ethyl 6-hydroxy-hexanoate, yielding polymers that could be specifically functionalized at the secondary alcohol group or at the olefinic bond of the monomer.[13] Thus, 2,5-dihydroxy-3-pentenoic acid alkyl esters could provide a platform for a vast variety of functional materials derived from C5 carbohydrates.

Standard reaction conditions were defined based on optimizations of *trans*-2,5-dihydroxy-3-pentenoic acid methyl ester (Me-**1**) formation in methanol.[13] In these studies, a Sn-Beta catalyst was found to be most effective for the formation of Me-**1**, and therefore Sn-Beta was also employed herein to probe the effects of different solvents.

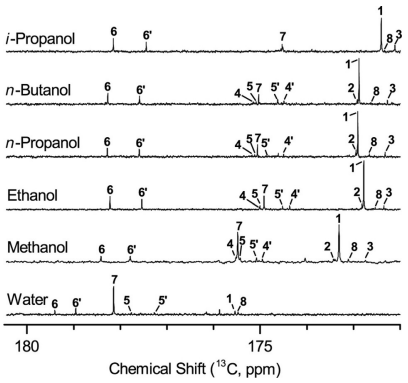

Figure 1. ^{13}C NMR spectra from a reaction mixture containing D-xylose (360 mg) and Sn-Beta (180 mg) in the appropriate solvent (5 mL). The carboxyl spectral region is shown and signals are assigned to the molecules found in Scheme 1; an apostrophe denotes the diastereomer of a compound. Chemical shifts are relative to MeOH-d_4 (10% *v*/*v*) set at 47.85 ppm for all solvents.

1D ^{13}C NMR spectra of reaction mixtures in various solvents were obtained and the carbonyl regions are shown in Figure 1. The spectral signals corresponding to compounds in Scheme 1 were assigned. In these reaction mixtures, careful inspection allowed for the identification of the minor *cis*-2,5-dihydroxy-3-pentenoic acid alkyl ester (**2**) as well as the dominant *trans*-form (**1**). The ^{1}H-^{13}C HSQC spectral region showing chemical-shift assignments of **1** and **2** in methanol is displayed in Figure 2. Long-range correlations through $^{2}J_{CH}$ couplings across the double bond are indicated by white lines and serve to identify the signals connected within the same NMR spin system. The *cis*- and *trans*-configurations were identified by characteristic $^{3}J_{HH}$ scalar couplings across the olefinic bond and by the characteristic signal shifts to lower frequencies for carbon atoms adjacent to the *cis*-double bond. This *cis*-isomer was identified as the minor product in all solvents. Together with these products, six additional 3-deoxy ester/acid compounds were identified within the carbonyl region shown in Figure 1. These signals cluster within different spectral regions in accordance with their functionality: olefinic esters (**1**–**3**, **8**) at 172–174 ppm, alkyl esters (**4**, **5**, **7**) at 174–176 ppm, and lactones (**6**) downfield of 177 ppm. Further inspection of the ^{13}C NMR spectra of Figure 1 indicates that rather dramatic compositional changes result upon changing the solvent from water to an alcohol. Furthermore, it was possible to distinguish the diastereomers of compounds **4**–**6** as signified by an apostrophe associated with the compound number in Figure 1.

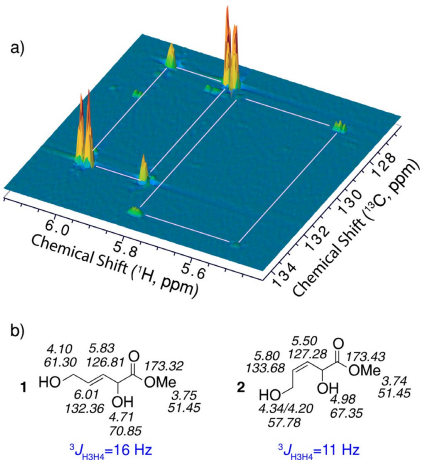

Figure 2. a) ^{1}H-^{13}C HSQC spectral region displaying the olefinic signals of compound **1** (*trans*-isomer) and compound **2** (*cis*-isomer) in a reaction mixture. $^{2}J_{CH}$ correlations across the double bond are indicated by thin white lines. b) Chemical shift assignments of compound **1** (*trans*-isomer) and compound **2** (*cis*-isomer).

Quantification of bio-based chemicals in reaction mixtures

Reliable quantification of the compound series shown in Scheme 1 was subsequently pursued by quantitative NMR (qNMR) spectroscopy. As qNMR can operate at the highest level of quantitative measurement[22,23] the method is free of empirical factors in the uncertainty analysis of the experiment, and signal areas are directly proportional to the concentration of atoms contributing to the signal.

Cryogenically cooled detection electronics and high-field instrumentation enabled absolute quantification of reaction mixtures by quantitative 1D ^{13}C NMR spectroscopy at natural ^{13}C isotope abundance (1.11%). Inverse gated decoupling experiments were used exclusively to avoid enhancement of the ^{13}C signals by the nuclear Overhauser effect.[24] Crude reaction mixtures analyzed by ^{13}C qNMR spectroscopy contained dimethyl sulfoxide as an internal standard for absolute quantification. Dilute dimethyl sulfoxide showed good recovery after reactions without detectable degradation, was miscible with the solvents tested in this study, and did not result in ^{1}H or ^{13}C NMR signal overlap with analyte signals. Dimethyl sulfoxide was thus deemed preferable to compounds such as mesitylene, dioxane, glycerol, or other alditols screened as standards

ChemPubSoc Europe

CHEMSUSCHEM Full Papers

for the spectroscopic characterization of reaction mixtures formed through catalytic carbohydrate conversion.

Quantitative 1D ^{13}C NMR rather than the more commonly used ^{1}H NMR spectroscopy was employed for quantification, as ^{13}C NMR experiments provide excellent signal resolution and sharp, non-split signals. Protonated carbon positions were generally used for quantification owing to their shorter T_1-NMR relaxation times, yielding quantitative measurements for sub-minute-timescale inter-scan relaxation delays. Alternatively, improved ^{13}C NMR spectra could be obtained by adding 1 mM of the relaxation agent $GdCl_3$ to the NMR sample, shortening the ^{13}C-carbonyl T_1 relaxation time to about 1 s at room temperature and 18.7 T magnetic field. The reduced ^{13}C T_1 relaxation time also permits accurate measurement of ^{13}C NMR signal areas for quaternary carbons without the need for long inter-scan recycle delays. The signal-to-noise ratio obtained within 1 h of experiment time per sample translated into an estimated error of determination of 0.2–1.0% for product yields. This small experimental uncertainty was validated by performing the analyses for reaction mixtures in all six different solvents in duplicate, yielding near-identical ^{13}C NMR spectra for repetitions in each solvent (Figure S1, see the Supporting Information).

Solvent effects on the Sn-Beta-catalyzed reaction

Quantified yields of the eight major compounds in non-purified reaction mixtures in different solvents are displayed in Figure 3. Various trends become evident upon variation of the solvent. Increasing the length of the alkyl chain of alcohol solvents decreases the amount of retro-aldol products (**7**–**8**) formed, consistent with previously reported observations.[7] Simultaneously, an increased yield of 3,4-dideoxy esters (**1**–**3**) and related 3-deoxy esters (**4**–**6**) is observed. Notably, all of the longer-chain alcohols tested gave higher yields of 3,4-dideoxy esters than for methanol, even under conditions that were specifically optimized for reactions in methanol. The formation of 3,4-dideoxy esters was most pronounced in ethanol with yields of around 42% (38% of the *trans* compound (**1**) and 4% of the *cis* (**2**–**3**) forms), which were 1.2-fold higher than in methanol. Consistently increased yields were also found for the lactone (**6**), formed in 15% yield in ethanol as compared to 8% in methanol. Overall, the 3-deoxy and 3,4-dideoxy esters (**1**–**6**) account for 66% of the carbon balance in ethanol and in *iso*-propanol. Quantifications of these related compounds are summarized in Table 2. Furfural derivatization to alkyl acetals predominates for methanol and is less pronounced in larger alcohols and especially in *iso*-propanol. In all solvents, 3,4-dideoxy esters are primarily formed as the *trans* compound (**1**), with yields that are also higher than a combination of the *cis*-3,4-dideoxy forms (**2**–**3**) and the potentially related furfural forms (**9**–**11**).

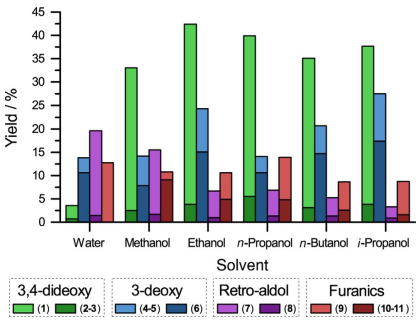

Figure 3. Product distribution of reactions in alcohols or water. The reactions were conducted with D-xylose (360 mg) and Sn-Beta (180 mg) in the appropriate solvent (5 mL) with dimethyl sulfoxide (50 mg) as an internal standard, and run for 2 h at 160 °C with 600 rpm stirring. An experimental uncertainty within ±1% was achieved in all cases. Legend numbers reference to the compounds in Scheme 1.

Table 2. Yield of 3,4-dideoxy compounds (**1**–**3**) and 3-deoxy compounds (**4**–**6**) from xylose in various solvents.

Product mixture	Water [%]	Methanol [%]	Ethanol [%]	*n*-Propanol [%]	*n*-Butanol [%]	*iso*-Propanol [%]
1–**3**	4	33	42	40	35	38
4–**6**	14	14	24	14	21	28
Sum	17	47	66	54	56	66

Reactions conducted in water exhibited a significantly altered composition compared to reactions conducted in alcohols, which also exhibited a greater tendency toward humin formation and catalyst discoloration. Thus, 3,4-dideoxy compounds are formed at lower levels than for retro-aldol products, furanics, and 3-deoxy compounds in water. A principal difference in the use of water and alcohol is brought about by the formation of free Brønsted acids as products in reactions conducted in water. Brønsted acids are known to catalyze a multitude of reactions including dehydration and acetalization.[3] The continuous formation of Brønsted acids during the reactions will have an impact on the catalytic system and alter the product distribution, thus rationalizing the principally different compositions of products in water and alcohol solvents. Especially in cases where the 3,4-dideoxy compounds are targeted, water is generally less useful as a solvent compared to the alcohols.

We finally note that reaction selectivity has been partially attributed to steric hindrance at the Sn active site in zeolite pores.[17] In the current analysis of solvent effects, the use of less nucleophilic and more bulky solvents increases the selectivity toward the formation of C5 lactones (compound **6**). This change in selectivity suggests that bulkier alcohols promote an intramolecular reaction rather than a reaction with the solvent inside the Sn-Beta–zeolite pores.

Temperature effects in ethanol

As improved yields of 3,4-dideoxy esters were achieved in alcohols other than methanol (even under conditions that had been optimized for methanol) we evaluated the prospect for further improvements of the reaction system using ethanol as the solvent. In the range of 140–160 °C, the product selectivity was reasonably consistent, giving similar yields of 3,4-dideoxy esters (42%, see Table S2 in the Supporting Information). Overall, we find the formation of the 3-deoxy and 3,4-dideoxy dehydration products (**1**–**6**) to be only weakly sensitive toward temperature variation between 120 and 180 °C. Nevertheless, exploring solvent and temperature effects resulted in a combined yield above 40% for 3,4-dideoxy esters; an almost 10% increase relative to previously achieved yields in methanol (33%, Table 1).[13]

The product ratios of cyclic γ-lactone compound **6** and open-chain 3-deoxy compounds **4** and **5** are temperature-dependent (Figure 4). Lower temperatures favor the formation of compound **6** relative to the open-chain compounds **4** and **5**. This observation correlates with an increasing fraction of acyclic products following endothermic γ-lactone solvolysis forming compound **5**.[25] Tabulated yields of the variable-temperature experiments are collected in the Supporting Information (Table S2).

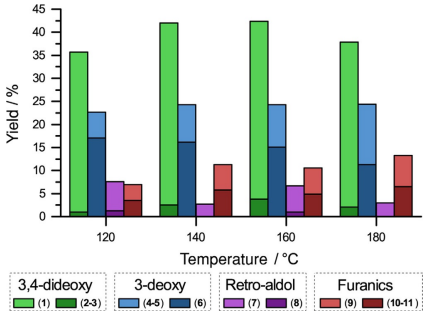

Figure 4. Product distribution of reactions run between 120 and 180 °C using ethanol as the solvent. The reactions were conducted with D-xylose (360 mg) and Sn-Beta (180 mg) in ethanol solvent (5 mL) with dimethyl sulfoxide (50 mg) as an internal standard, and run for 2 h at the selected temperature. An uncertainty within ±1% was achieved in all cases. Legend numbers reference to the compounds in Scheme 1.

Time-resolved reaction analysis

Additional insight into solvent effects on the acyclic reaction of xylose to potential polyester building blocks was sought by tracking the reaction progress in water, methanol, and ethanol over time. Reactions were conducted under microwave heating for varying lengths of time and were subsequently analyzed by quantitative ^{13}C NMR spectroscopy (full datasets are provided in Table S3 in the Supporting Infomation). The experiments show that product formation continues even after full xylose conversion. This observation is attributed to the accumulation of glycoside intermediates,[14] some of which can be subsequently converted into the full range of products.

The formation of major product **1** in methanol and ethanol was tracked in an initial-rate experiment at 160 °C under quasi-steady state conditions as shown in Figure 5. Owing to the initial surplus of substrate, pseudo-first order kinetics were apparent, which resulted in a linear accumulation of product during the short initial period shown in Figure 5 (full kinetic data are provided in Figure S2). Although compound **1** formed with higher selectivity in ethanol (39%) than in methanol (31%) and water (approximately 5%) in the kinetic experiments, the initial rate of formation is lower in ethanol than in methanol. The formation of compound **1** is accompanied by higher rates of conversion of xylose in methanol than in ethanol and a lower rate of conversion in water (Table S3, Supporting Information).

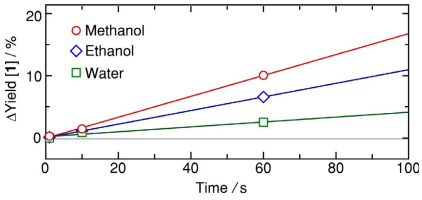

Figure 5. Initial-rate experiments for the formation of product **1** from D-xylose (360 mg), using Sn-Beta (180 mg) at 160 °C and 5 mL of methanol, ethanol, or water; initial rates: 0.85, 0.57 and 0.20 mmol L^{-1} min^{-1}, respectively.

Kinetic profiles underline the complexity of the reaction pathway and suggest that several solvent effects are important. Solvent molecules compete with the substrate for binding to Sn active sites. A weaker binding behavior is expected for alcohols relative to water, leading to better active-site availability for the substrate in alcohols compared to water.[26,27] This rationalization may explain the lower rate of formation of compound **1** and the consequent lower rate of xylose conversion observed in water. For the Sn-Beta-catalyzed conversion of xylose in alcohol, the alcohol enters the catalytic cycle as a nucleophilic reactant. The lower rate of production of compound **1** in ethanol compared to methanol is consistent with previous reports for C4 carbohydrate conversion, which suggests that lower nucleophilicity and steric limitations may direct product selectivity toward the 3,4-dideoxy compound.[9]

In methanol and ethanol the formation of **1**–**6** is continuous during the course of the reaction (Figure S2, Supporting Information). In contrast, the yield of compound **1** in water rises to a maximum and subsequently decreases during the reaction while maintaining a consistent increase of all 3-deoxy and 3,4-dideoxy compounds (**1**–**6**). This finding indicates that some rehydration of compound **1** can occur in water, especially in the presence of accumulating Brønsted acids. Formation of com-

ChemPubSoc Europe

CHEMSUSCHEM Full Papers

pound H-**7** occurs more rapidly in water than formation of compounds Me-**7** and Et-**7** in alcohols (Figure S3). Accumulation of compound **7** in water is accompanied by an increase in formation of compound **7**, indicative of an alteration of the mechanism induced by increased Brønsted acidity. The final levels of furanics decrease slightly from water compared to methanol and ethanol (Figure 3). Observations of a lower carbon balance in water and the discoloring of the reaction mixture also suggest the formation of undetected polymeric species (humins). The distinct selectivity of Sn-Beta-catalyzed xylose conversion in water relative to alcohols can be ascribed to lower reactivity at the Sn active sites owing to competing solvent absorption and to mechanistic effects of Brønsted acid formation. The formation of alkyl lactates is largely suppressed in longer alcohols, consistent with previous studies under conditions that were optimized for lactate formation. Maximum alkyl lactate yields have been reported to decrease from 65% in methanol to approximately 35% in ethanol and 25% in *iso*-propanol.[7] Overall, the beneficial effect of ethanol relative to methanol in the formation of **1**–**3** can be ascribed to the less nucleophilic nature and larger molecular size of ethanol disfavoring side reactions.

Improved yield of chemical building blocks from glucose

The abundance of glucose in biomass is even greater than that of xylose, and glucose is the most abundant carbohydrate in nature. Glucose is available from starch and cellulose, which are both homopolymers composed of glucopyranose subunits. Hexoses are able to form compound **12** (*trans*-2,5,6-trihydroxy-3-hexenoic acid methyl ester; Figure 6a), the C6 analogue of compound **1**, although in lower yields than the analogues obtained from C4 and C5 sugars (Table 1). To substantiate that the solvent effect discussed herein is also applicable to the formation of chemical building blocks from C6 carbohydrates, reactions using glucose as the substrate were performed.

The beneficial effect of ethanol relative to methanol in the formation of compound **12** is also valid for glucose, as can be seen from the NMR spectra of the olefinic region (Figure 6b). The solvent change from methanol to ethanol increases the formation of compound **12** approximately 1.2-fold (from 13.8 to 16.0% under the standard reaction conditions used herein). The formation of the hexono-lactone equivalent of compound **6** also increases, from 16.6 to 19.4%, whereas the formation of alkyl lactate **7** decreases from 31.5 to 12.6%. All of these effects closely follow trends observed for the conversion of xylose and are consistent with previous studies using homogeneous and heterogeneous Sn catalysts for conversion of the less-abundant acyclic C4 carbohydrate erythrulose.[9,10] A shift toward improved selectivity for the formation of commercially interesting 3,4-deoxy esters at the expense of retro-aldol cleavage can be achieved for a series of carbohydrates using a Sn-Beta catalyst in alcohols with a longer chain length than methanol.

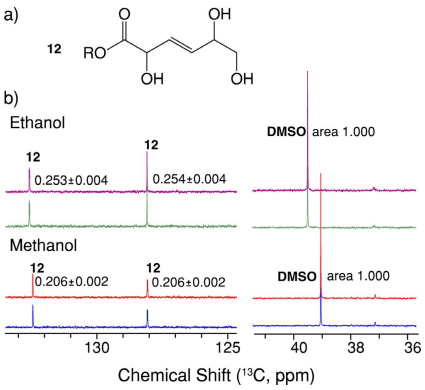

Figure 6. a) Structure of the C6 analogue of compound **1**, *trans*-2,5,6-trihydroxy-3-hexenoic acid methyl ester (**12**). b) Spectral comparison of the areas of the olefinic carbon shifts of compound **12** in ethanol (top) and methanol (bottom) reaction solvents. Duplicate samples are shown in different colors, including the errors of determination of signal areas relative to DMSO as an internal quantification standard.

Conclusions

In conclusion, quantitative ^{13}C NMR was employed for the detection and accurate quantification of previously unknown products in the conversion of abundant C5 and C6 carbohydrates by Sn-Beta, without using reference standard compounds. Identification and quantification are feasible in different solvents, thus permitting the elucidation of solvent effects on reaction selectivity. Exchanging methanol for longer-chain alcohols results in increased yields of C5 3,4-dideoxy esters from 33% in methanol to 42% in ethanol. This increase in yield can be ascribed to the less-nucleophilic and larger ethanol disfavoring competing reactions. The improved yield of C5 3,4-dideoxy esters in ethanol relative to methanol and water correlates with a lower rate of formation, although the pathway forming 3,4-dideoxy acids or esters is assumed to progress under kinetic control.[9] The formation of retro-aldol-derived products is diminished in ethanol and alcohols of longer chain length. Nonetheless, the reaction pathways forming 3-deoxy and 3,4-dideoxy compounds remain viable in various protic solvents.

Simple alcohols have been considered as environmentally preferable solvents and ethanol has been described as preferable to methanol in terms of environmental, health, and safety regulations.[28,29] Hence, the formation of 2,5-dihydroxy-3-pentenoic acid esters in 42% yield and formation of the related 3-deoxy esters in combined yields of nearly 66% from xylose in ethanol is encouraging for the development of environmentally benign processes in a future bio-based chemical industry.

Experimental Section

Reactions were conducted with a Biotage Initiator$^+$ microwave reactor in 5 mL glass reaction vials. Reactions were typically performed with Sn-Beta (180 mg, Si/Sn = 200, hydrothermally synthesized), D-xylose (360 mg), solvent (5 mL) and dimethyl sulfoxide (50 mg) as internal standard.

Catalyst material Sn-Beta was produced according to the synthesis procedure described in the Supporting Information, based on a modification of the procedure described by Valencia and Corma,[30,31] yielding the Sn-Beta catalyst with a Si/Sn ratio of 200. The product composition and structure was confirmed by ICP (inductively coupled plasma; Si/Sn = 200), XRD (*BEA zeolite framework, Figure S4) and N_2-adsorption (see the Supporting Information for details).

To discern effects of solvent upon product composition and pathway usage, each sample was heated to 160 °C for 2 h. Aliquots of 500 μL were taken from each sample, MeOH-d_4 (50 μL; Sigma–Aldrich) was added, and the mixture transferred to a 5 mm NMR tube for immediate analysis. In kinetic experiments, samples in water, methanol, or ethanol were prepared in the same manner detailed above and heated to 160 °C for an allotted time (1 s, 10 s, 1 min, 10 min, 1 h, or 2 h). Samples were rapidly cooled with compressed air and 500 μL aliquots were taken from each sample, mixed with MeOH-d_4 (50 μL), and transferred to 5 mm NMR tubes. All NMR spectra were acquired on an 800 MHz Bruker Avance III NMR spectrometer equipped with a TCI CryoProbe and a SampleJet sample changer. 1D ^{13}C NMR spectra were acquired by sampling 64k complex data points during an acquisition time of 1.36 s, and using an inter-scan recycle delay of 45 s. A pulse sequence with ^{1}H irradiation only applied during signal acquisition was used to minimize distortions of signal integrals by the nuclear Overhauser effect. Protonated ^{13}C carbon atoms were used for quantification and several carbon sites per molecule were used to improve the statistics of the signal area, using integration values from Bruker Topspin 3.5 pl5 (see for example, Figure 6). Standard DQF-COSY, TOCSY, ^{1}H-^{13}C HMBC, standard and edited ^{1}H-^{13}C HSQC, as well as ^{1}H-^{13}C HSQC-TOCSY experiments were employed for compound identification in samples following solvent evaporation overnight in a fume hood and re-dissolution in deuterated solvents. Figure S6 (Supporting Information) demonstrates the accuracy of this method by comparison of a reaction sample with readily available standard compounds. Standard ^{1}H-^{13}C HSQC, edited HSQC, as well as ^{1}H-^{13}C HSQC-TOCSY were used in protic solvents to validate the assignments. All spectra were processed with ample zero filling in all spectral dimensions using Bruker Topspin 3.5 pl5.

Acknowledgements

This work was funded by the Innovation Fund Denmark (case number 5150-00023B) and by Grant 2013 01 0709 of the Carlsberg Foundation. 800 MHz NMR spectra were recorded on the spectrometer of the NMR Center DTU supported by the Villum Foundation.

Conflict of interest

The authors declare no conflict of interest.

Keywords: carbohydrates · green solvents · NMR · solvent effect · tin

[1] Y. Román-Leshkov, J. N. Chheda, J. A. Dumesic, *Science* **2006**, *312*, 1933.
[2] J. B. Binder, R. T. Raines, *J. Am. Chem. Soc.* **2009**, *131*, 1979 – 1985.
[3] P. Gallezot, *Chem. Soc. Rev.* **2012**, *41*, 1538 – 1558.
[4] C. Li, Z. Zhang, Z. K. Zhao, *Tetrahedron Lett.* **2009**, *50*, 5403 – 5405.
[5] A. Corma, S. Iborra, A. Velty, *Chem. Rev.* **2007**, *107*, 2411 – 2502.
[6] E. Taarning, S. Saravanamurugan, M. S. Holm, J. Xiong, R. M. West, C. H. Christensen, *ChemSusChem* **2009**, *2*, 625 – 627.
[7] M. S. Holm, S. Saravanamurugan, E. Taarning, *Science* **2010**, *328*, 602 – 605.
[8] S. Tolborg, I. Sádaba, C. M. Osmundsen, P. Fristrup, M. S. Holm, E. Taarning, *ChemSusChem* **2015**, *8*, 613 – 617.
[9] R. De Clercq, M. Dusselier, C. Christiaens, J. Dijkmans, R. I. Iacobescu, Y. Pontikes, B. F. Sels, *ACS Catal.* **2015**, *5*, 5803 – 5811.
[10] M. Dusselier, P. Van Wouwe, F. de Clippel, J. Dijkmans, D. W. Gammon, B. F. Sels, *ChemCatChem* **2013**, *5*, 569 – 575.
[11] A. Sølvhøj, E. Taarning, R. Madsen, *Green Chem.* **2016**, *18*, 5448 – 5455.
[12] H. S. Chen, A. Wang, H. Sorek, J. D. Lewis, Y. Román-Leshkov, A. Bell, *ChemistrySelect* **2016**, *1*, 4167 – 4172.
[13] S. G. Elliot, C. Andersen, S. Tolborg, S. Meier, I. Sadaba, A. E. Daugaard, E. Taarning, *RSC Adv.* **2017**, *7*, 985 – 996.
[14] S. Tolborg, S. Meier, I. Sádaba, S. G. Elliot, S. K. Kristensen, S. Saravanamurugan, A. Riisager, P. Fristrup, T. Skrydstrup, E. Taarning, *Green Chem.* **2016**, *18*, 3360 – 3369.
[15] S. Saravanamurugan, A. Riisager, E. Taarning, S. Meier, *Chem. Commun.* **2016**, *52*, 12773 – 12776.
[16] S. Saravanamurugan, A. Riisager, E. Taarning, S. Meier, *ChemCatChem* **2016**, *8*, 3107 – 3111.
[17] S. Tolborg, S. Meier, S. Saravanamurugan, P. Fristrup, E. Taarning, I. Sádaba, *ChemSusChem* **2016**, *9*, 3054 – 3061.
[18] E. A. Capanema, M. Y. Balakshin, J. F. Kadla, *J. Agric. Food Chem.* **2004**, *52*, 1850 – 1860.
[19] C. Gaillet, C. Lequart, P. Debeire, J.-M. Nuzillard, *J. Magn. Reson.* **1999**, *139*, 454 – 459.
[20] Ē. Kupce, R. Freeman, G. Wider, K. Wüthrich, *J. Magn. Reson. Ser. A* **1996**, *122*, 81 – 84.
[21] Z. Zhou, R. Kümmerle, X. Qiu, D. Redwine, R. Cong, A. Taha, D. Baugh, B. Winniford, *J. Magn. Reson.* **2007**, *187*, 225 – 233.
[22] M. Weber, C. Hellriegel, A. Rueck, J. Wuethrich, P. Jenks, *J. Pharm. Biomed. Anal.* **2014**, *93*, 102 – 110.
[23] H. Jancke, F. Malz, W. Haesselbarth, *Accredit. Qual. Assur.* **2005**, *10*, 421 – 429.
[24] R. Freeman, H. D. W. Hill, R. Kaptein, *J. Magn. Reson.* **1972**, *7*, 327 – 329.
[25] M. T. Pérez-Prior, J. A. Manso, M. del Pilar García-Santos, E. Calle, J. Casado, *J. Org. Chem.* **2005**, *70*, 420 – 426.
[26] W. N. P. van der Graaff, C. H. L. Tempelman, G. Li, B. Mezari, N. Kosinov, E. A. Pidko, E. J. M. Hensen, *ChemSusChem* **2016**, *9*, 3145 – 3149.
[27] J. R. Christianson, S. Caratzoulas, D. G. Vlachos, *ACS Catal.* **2015**, *5*, 5256 – 5263.
[28] C. Capello, U. Fischer, K. Hungerbuhler, *Green Chem.* **2007**, *9*, 927 – 934.
[29] M. Tobiszewski, J. Namieśnik, F. Pena-Pereira, *Green Chem.* **2017**, *19*, 1034 – 1042.
[30] S. Valencia, A. Corma, (UOP LLC), , **1999** US6306364 B1.
[31] S. Tolborg, A. Katerinopoulou, D. D. Falcone, I. Sádaba, C. M. Osmundsen, R. J. Davis, E. Taarning, P. Fristrup, M. S. Holm, *J. Mater. Chem. A* **2014**, *2*, 20252 – 20262.

Manuscript received: April 7, 2017
Revised manuscript received: June 18, 2017
Accepted manuscript online: June 19, 2017
Version of record online: July 5, 2017

CHEMISTRY & SUSTAINABILITY
CHEMSUSCHEM
ENERGY & MATERIALS

Supporting Information

Quantitative NMR Approach to Optimize the Formation of Chemical Building Blocks from Abundant Carbohydrates

Samuel G. Elliot,[a] Søren Tolborg,[b] Irantzu Sádaba,[b] Esben Taarning,[b] and Sebastian Meier*[a]

cssc_201700587_sm_miscellaneous_information.pdf

Catalyst Synthesis

30.6 g of tetraethyl orthosilicate (Aldrich, 98%) was added to 33.1 g of tetraethylammonium hydroxide (Sigma-Aldrich, 35% in water) under careful stirring (~60 min), and tin(IV) chloride pentahydrate (Aldrich, 98%) dissolved in 2.0 mL of demineralised water was added drop wise. The mixture was then left to stir for several hours. Finally, 3.1 g hydrofluoric acid (Fluka, 47–51%) in 1.6 g of demineralised water was added. The sample was then homogenised and transferred to a Teflon®-container placed in a stainless steel autoclave and incubated at 140 °C for 14 days. The solid was recovered by filtration and washed with demineralised water, followed by drying overnight at 80 °C. The organic template contained within the material was removed by calcination at 550 °C for 6 h (2 °C min^{-1} ramp), yielding the Sn-Beta catalyst with a Si/Sn ratio of 200. The product was confirmed by ICP (Si/Sn = 216), XRD (Figure S4, Primary Phase = *BEA) and N_2-adsorption (S_{BET} = 656 m^2 g^{-1}, $S_{micropore}$ = 425 m^2 g^{-1}, V_{total} = 0.30 mL g^{-1}, $V_{micropore}$ = 0.21 mL g^{-1}).

X-Ray diffraction of the sample was done on a Philips X'Pert diffractometer using Cu-Kα radiation. Elemental analysis was performed using inductively coupled plasma optical emission spectroscopy (ICP-OES) by first fully dissolving the solid sample in a mixture of acids and measuring the resulting liquid on a Varian Vista Perkin Elmer model Optima 3000. Information on the porosity and surface area was obtained by measuring and analysing N_2-adsorption/desorption isotherms of the sample. Surface area was calculated by the BET method and micropore volume by the *t*-plot method using the Autosorb3 software.

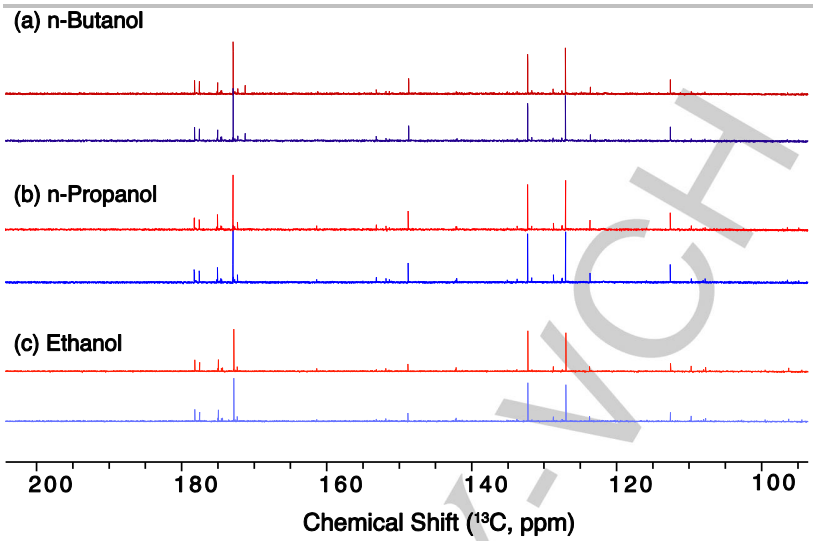

Figure S1. Comparison of experimental duplications for select reactions, demonstrating the reproducibility of the reactions. Large signals at approximately 172, 132 and 127 ppm are produced by *trans*-2,5-dihydroxy-3-pentenoic acid alkyl ester and seen to be of equivalent size.

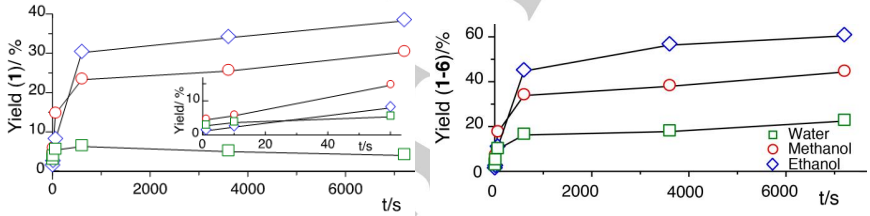

Figure S2. Formation of *trans*-3,4-dideoxy acid and alkyl esters (**1**) in three solvents (left) and cumulative yield of C5 3-deoxy and 3,4-dideoxy acids/esters (**1-6**, right) at 160 °C. In the presence of Brønsted acidity, compound **1** appears to rehydrate and thus decline over time (left) in water, opposite to its formation as a stable product in methanol and ethanol. The inset (left) indicates that **1** forms more slowly in ethanol, while it reaches higher levels than in methanol or water.

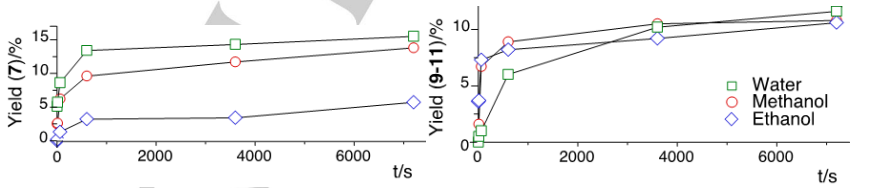

Figure S3. Formation of (alkyl) lactate (**7**) (left) and of furanics (right, sum of furfural and furfural acetals **9-11**) in water, methanol and ethanol at 160 ºC using Sn-Beta catalyst.

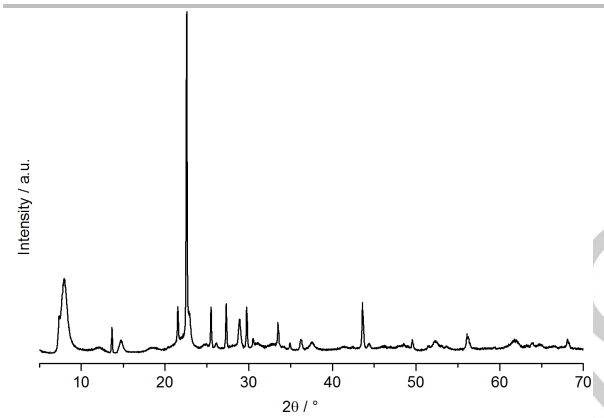

Figure S4. XRD diffractograms of Sn-Beta catalyst.

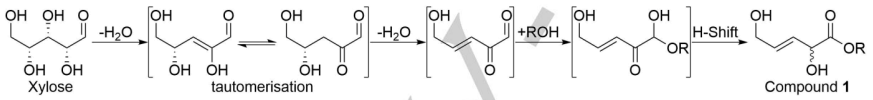

Figure S5. Proposed reaction pathway for the formation of compound **1** from xylose.

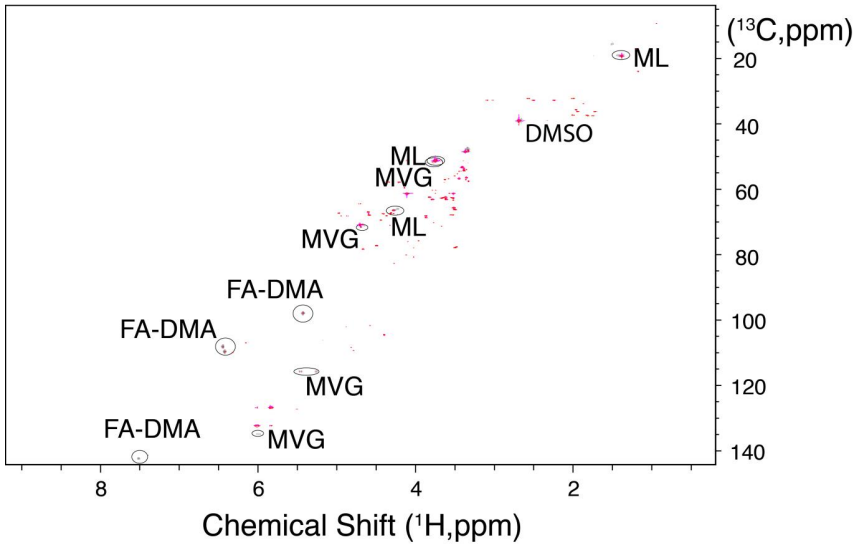

Figure S6. Overlay of ^{1}H-^{13}C HSQC spectra of a reaction mixture (red) and commercial standards of methyl lactate (ML) and methyl vinyl glycolate (MVG) in addition to furfural reacted to its dimethylacetal (FA-DMA) in methanol (reference spectra in grey). Samples contain DMSO as internal standard. This comparison validates the identified compounds in the reaction mixture. Quantifications of the commercial ML and MVG standards were performed, yielding estimated amounts of 8.7 mg ML and 9.6 mg MVG for samples with a weight of 9 and 10 mg respectively. The small differences in the determination may be attributed to residual water in the reference standards.

Table S1. Product distribution of reactions using primary alcohols of varying alkyl chain length.[a]

	3,4-Dideoxy Compounds		3-Deoxy Compounds		Retro-Aldol Compounds		Furanic Compounds		
Solvent	**1**	**2-3**[a]	**4-5**	**6**	**7**	**8**	**9**	**10-11**[b]	Dev.
					C mol%				
Water	2.9	0.7	3.2	10.6	18.2	1.4	12.7	0.0	±0.5
Methanol	30.6	2.5	6.4	7.8	13.8	1.7	1.7	9.1	±0.2
Ethanol	38.6	3.8	9.2	15.1	5.7	1.0	5.7	4.9	±0.4
n-Propanol	34.4	5.5	3.5	10.6	5.6	1.3	9.1	4.8	±0.6
n-Butanol	32.0	3.1	6.0	14.7	4.0	1.3	6.0	2.6	±0.6
iso-Propanol	33.9	3.8	10.1	17.4	2.4	0.9	7.1	1.6	±1.0

Reactions were conducted with 180 mg Sn-Beta^{200}, 360 mg D-xylose, 5 mL solvent and 50 mg dimethyl sulfoxide as internal standard and run at 160°C for 2 h. Compound numbers reference to the compounds in Scheme 1. [a] Combined yield of acyclic and cyclic forms. [b] Combined yields of acetal and hemi-acetal forms.

Table S2. Product distribution of reactions using varying temperatures with ethanol as the solvent.[a]

	3,4-Dideoxy Compounds		3-Deoxy Compounds		Retro-Aldol Compounds		Furanic Compounds		
Temperature	**1**	**2-3**[a]	**4-5**	**6**	**7**	**8**	**9**	**10-11**[b]	Dev.
°C					C mol%				
120	34.7	1.0	5.6	17.1	3.5	3.5	6.3	1.3	±0.8
140	39.5	2.5	8.1	16.2	5.5	5.8	2.7	0.0	±0.6
160	38.6	3.8	9.2	15.1	5.7	4.9	5.7	1.0	±0.4
180	35.8	2.1	13.1	11.3	6.8	6.5	3.0	0.0	±0.6

Reactions were conducted with 180 mg Sn-Beta^{200}, 360 mg D-xylose, 5 mL ethanol and 50 mg dimethyl sulfoxide as internal standard and run for 2 h. Compound numbers reference to the compounds in Scheme 1. [a] Combined yield of acyclic and cyclic forms (see Scheme 1, compounds **2-3**). [b] Combined yields of acetal and hemi-acetal forms.

Table S3. Progression of the reaction mixture composition over time.[a]

Solvent	Time	XYL	XYLU/LYX[a]	Glycosides[b]	3,4-Dideoxy Compounds		3-Deoxy Compounds		Retro-Aldol Compounds		Furanic Compounds		Dev.
					1	**2-3**[c]	**4-5**	**6**	**7**	**8**	**9**	**10-11**[d]	
	s				C mol%								
Water	1	38.2	n.a.	n.a.	3.1	0.0	0.0	0.0	5.1	0.0	0.0	0.0	±0.4
	10	30.2	n.a.	n.a.	4.0	0.0	0.8	0.6	5.7	0.3	0.5	0.0	±0.4
	60	16.8	n.a.	n.a.	5.7	0.0	1.6	3.1	8.6	0.6	1.0	0.0	±0.4
	600	6.6	n.a.	n.a.	6.6	0.4	2.7	7.1	13.4	1.5	6.0	0.0	±0.3
	3600	0.0	n.a.	n.a.	5.3	1.2	3.5	8.3	14.3	1.8	10.2	0.0	±0.3
	7200	0.0	n.a.	n.a.	2.9	0.7	3.2	10.6	18.2	1.4	12.7	0.0	±0.5
Methanol	1	44.9	23.1	12.6	4.8	0.0	0.7	0.0	2.5	0.0	0.0	0.2	±1.2
	10	29.4	23.3	13.2	6.0	0.0	1.3	0.2	2.6	0.0	0.7	0.9	±1.1
	60	4.1	8.7	18.9	14.9	0.1	2.4	0.5	6.2	0.6	2.2	4.5	±0.7
	600	0.0	2.9	9.2	23.6	0.9	6.3	3.6	9.6	0.8	2.6	6.3	±0.7
	3600	0.0	0.1	5.4	25.8	1.1	5.4	6.2	11.7	1.2	3.1	7.4	±0.7
	7200	0.0	n.a.	n.a.	30.6	2.5	6.4	7.8	13.8	1.7	1.7	9.1	±0.2
Ethanol	1	46.6	17.4	3.5	1.6	0.0	0.0	0.0	0.0	0.0	3.6	0.0	±0.6
	10	39.6	17.9	5.3	2.7	0.0	0.0	0.0	0.2	0.0	3.7	0.0	±0.6
	60	13.2	13.6	9.2	8.3	0.0	1.9	1.0	1.3	0.0	7.3	0.0	±0.6
	600	0.0	1.4	6.3	30.5	1.7	8.3	4.8	3.2	0.0	6.2	2.0	±0.8
	3600	0.0	0.2	4.4	34.3	2.0	6.9	13.7	3.4	0.0	7.4	1.8	±0.8
	7200	0.0	n.a.	n.a.	38.6	3.8	9.2	15.1	5.7	1.0	5.7	4.9	±0.4

Reactions were conducted with 180 mg Sn-Beta[200], 360 mg D-xylose, 5 mL solvent and 50 mg dimethyl sulfoxide as internal standard and run at 160°C. Compound numbers reference to the compounds in Scheme 1. [a] Combined yields of xylulose and lyxose (xylose isomerization products). [b] Glycoside formation was quantified using ^{1}H-^{13}C HSQC integration relative to an internal standard calculating ^{1}H-^{13}C HSQC response-factors for pentoses. [c] Combined yield of acyclic and cyclic forms (see Scheme 1, compounds **2-3**). [d] Combined yields of acetal and hemi-acetal forms.

ChemPubSoc Europe

DOI: 10.1002/cctc.201701861

CHEMCATCHEM Full Papers

NMR Spectroscopic Isotope Tracking Reveals Cascade Steps in Carbohydrate Conversion by Tin-Beta

Samuel G. Elliot,[a] Esben Taarning,*[b] Robert Madsen,[a] and Sebastian Meier*[a]

Quantitative isotope tracking studies were used to investigate the reaction pathways that occur for Sn-Beta-catalyzed carbohydrate conversion to various α-hydroxy esters. Experimental insight into the conversion of pentoses was sought (i) by identifying pathways based on isotope patterns in the reaction products and (ii) by probing asymmetric isotope incorporation into products. The results indicate that reaction intermediates remain coordinated to the active site throughout the reaction cascades, regardless of the reaction pathway. A predominant transformation of the C1 carbohydrate position to the C3 position of methyl lactate resembles enzymatic glycolysis. Likewise, the majority of retro-aldol cleavage occurs from the carbohydrate in the ketose form, which again resembles biological glycolysis. In addition, various side-activities are detected in Sn-Beta-catalyzed carbohydrate conversion, which include 5,1-hydride and 1,2-carbon shift of the carbohydrates.

Introduction

The study of carbohydrates as alternative resources to petrochemicals has been intensifying in recent years. Despite this interest, many routes of carbohydrate conversion to useful chemicals are complex and lack fundamental pathway understanding. The overall complexity of carbohydrate conversion in chemocatalytic pathways is reminiscent of the complexity encountered in biochemical pathways. Analytical methods that deal with challenging metabolic reaction systems are, therefore, conceivable additions to the toolbox of biomass research. Recently, we showed that high-field NMR spectroscopy can be used to identify, quantify, and optimize reactants at natural isotope enrichment in biomass conversion.[1] In addition, the use of NMR spectroscopy may provide additional mechanistic insight into reaction cascades through the characterization of isotope distributions in the products.[2–8] Herein, we focus on the Sn-Beta-catalyzed conversion of abundant carbohydrates to methyl lactate (ML) and other α-hydroxy ester coproducts (Figure 1).

The formation of lactate precursors for poly(lactic acid) production using Sn-containing silicate chemocatalysis has been studied intensively since 2009.[9] Subsequent research has illuminated some mechanistic details of the reactions that form ML from trioses and hexoses in methanol solvent. These developments resulted in increasingly feasible methods for tuning reaction selectivity[1,4,10–14] as well as the discovery of new reaction products.[14–20] Most of these new products are α-hydroxy acids such as lactate and some show potential as polymer building blocks.[18,20–23] These bio-monomers include methyl 2,5,6-trihydroxy-3-hexenoate (THM), methyl 2,5-dihydroxy-3-pentenoate (DPM), methyl vinyl glycolate (MVG), and assorted 3-deoxy esters (3DE) and lactones (3DL), the structures of which are shown in Figure 1. Pathways that lead to the formation of these compounds have so far remained less comprehensively studied than those of lactate formation as these products were characterized more recently and because the key C_4–C_6 intermediates are not as easily accessible in pure forms as the analogous C_3 compounds for use as reference standards and prospective reaction substrates.

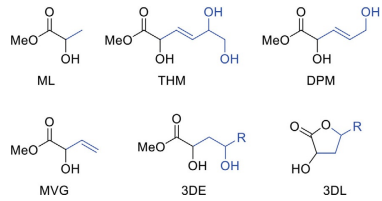

Figure 1. Structures of the products in the Sn-Beta-catalyzed conversion of common carbohydrates, which include ML, THM, DPM, MVG, and assorted 3DE and 3DL. The R group of 3DE and 3DL may be H, CH_2OH, or $CH(OH)$-CH_2OH for tetroses, pentoses, or hexoses, respectively.

In the current study, we use various pentose isotopologues (pentoses with different isotope compositions, that is, different neutron contents) to elucidate mechanistic details in the conversion of carbohydrates to α-hydroxy esters catalyzed by Sn-Beta in methanol. We hypothesized that the products and by-products formed through the same pathway should be identifiable by similar isotope patterns. In addition, the formation of ML through the retro-aldol cleavage of a carbohydrate to dihy-

[a] S. G. Elliot, Prof. R. Madsen, Dr. S. Meier
Department of Chemistry
Technical University of Denmark
Kemitorvet, Bygning 207, 2800 Kgs. Lyngby (Denmark)
E-mail: semei@kemi.dtu.dk

[b] Dr. E. Taarning
Haldor Topsøe A/S
Haldor Topsøes Alle 1, 2800 Kgs. Lyngby (Denmark)
E-mail: esta@topsoe.com

Supporting information and the ORCID identification number(s) for the author(s) of this article can be found under: https://doi.org/10.1002/cctc.201701861.

droxyacetone or glyceraldehyde was reinvestigated. To this end, the symmetry of isotope incorporation was probed for products that might have arisen from symmetric dihydroxyacetone. Such experimental methods that employ isotope tracking should have the prowess to identify consecutive steps in multistep reaction pathways that occur in a concerted manner at the zeolite active sites.

Results and Discussion

Initial experiments were conducted using D-[1-^{13}C]-xylose and uniformly ^{2}H-labeled D-[UL-$^{2}H_6$]-ribose isotopologues (it has been demonstrated previously that the pentose stereochemistry does not affect reaction selectivity).[1] Pentoses were selected because of their inherently asymmetric aldol cleavage reactions that enable the further distinction of product origins. Pentoses and hexoses produce an equivalent set of products,[1,14,19–20] and it is, therefore, reasonable to assume that the mechanistic findings for pentoses can be transferred to the mechanisms of hexose conversion and vice versa.

Methyl lactate

The mechanism of ML formation from trioses has been studied previously for both homogeneous and heterogeneous Sn systems.[3,9,24–26] The mechanism is proposed to consist of five sequential steps: a) enolization, b) dehydration, c) tautomerization, d) (hemi)acetalization, and e) hydride shift (Figure 2). The

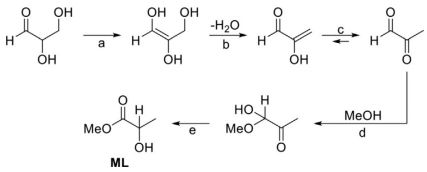

Figure 2. Plausible mechanism for the formation of lactate from trioses from Refs. [3, 9, 24–26]. Either dihydroxyacetone or glyceraldehyde may be employed as starting substrates.

starting substrate may be either a ketose or aldose as isomerization by a 1,2-intramolecular hydride shift will result in a mixture of both forms. Previous studies were conducted using protonated substrates in deuterated solvent and enolization was deduced from deuterium incorporation into the C3-position of ML.[3] A detailed understanding of the process that occurs was sought by the sensitive detection and accurate quantification of hydrogen incorporation from the solvent. In addition, we sought to warrant that intramolecular hydride shifts can be distinguished from exchange with hydrogen atoms from the heterogeneous catalyst.

We used deuterated pentose in protonated solvent to ensure that the substrate and solvent as well as the substrate and catalyst carried different isotopic forms of hydrogen. The resultant isotopologues of lactate were characterized by using NMR spectroscopy at a magnetic field of 18.7 T (800 MHz instrument equipped with cryogenically cooled detection electronics) using a quantitative ^{13}C NMR (qNMR) spectroscopy approach demonstrated previously.[1] The deuterated carbon positions were identified from characteristic chemical shift changes to lower frequency and from characteristic multiplet patterns caused by coupling to quadrupolar ^{2}H nuclei (Figure 3 A). ^{13}C NMR spectra were acquired with recycle delays of 60 s and inverse-gated decoupling to avoid the nuclear Overhauser enhancement of ^{13}C signal intensities for C atoms bound to ^{1}H.

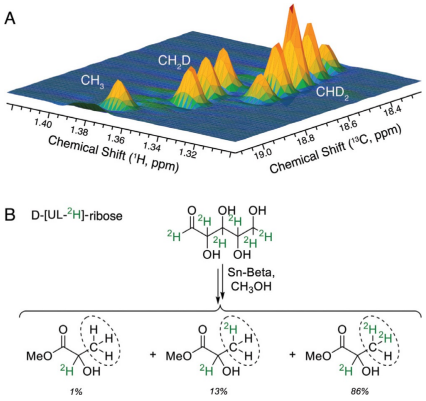

Figure 3. A) Multiplet pattern of the C3-position of ML that results from the incorporation of three, two, and one ^{1}H atoms (from left to right), respectively. B) Fraction of lactate isotopomers produced upon the reaction of D-[UL-$^{2}H_6$]-ribose. Reactions consisted of 36 mg D-[UL-$^{2}H_6$]-ribose, 18 mg Sn-Beta, 500 μL methanol, and 5 mg dimethylsulfoxide (internal standard) heated to 160 °C for 2 h.

The resulting distribution of ML isotopologues from these experiments is shown in Figure 3 B. Most notably, the lack of solvent exchange at the C2-position of lactate supports the hydride shift mechanism in step e (Figure 2), which likely is irreversible, as must be the enolization in step a. The predominant isotopologue (86 %; Figure 3 B) contains a single solvent proton at the C3-position, which is consistent with a reversible tautomerization in step c. The predominance of the singly C3-protonated isotopologue (86 %) over both the doubly (13 %) and triply (1 %) protonated forms indicates that reaction d is significantly faster than the competing reversible tautomerization in step c.

Subsequently, the reaction was repeated using D-[1-^{13}C]-xylose to result in the ^{13}C distributions of ML and MVG shown in Figure 4. The prevalence of ^{13}C incorporation into the C3-position of ML shows that the C3-position of ML originates predominantly from the C1-position of the substrate. This observation was surprising as the formation of a C3 fragment that

ChemPubSoc Europe

CHEMCATCHEM Full Papers

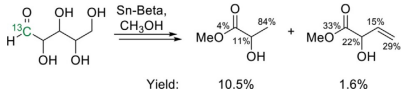

Figure 4. Distribution of ^{13}C in ML and MVG from D-[1-^{13}C]-xylose. Reactions consisted of 36 mg D-[1-^{13}C]-xylose, 18 mg Sn-Beta, 500 µL methanol, and 5 mg dimethylsulfoxide (internal standard) heated to 160 °C for 5 min. Yields were determined by using ^{1}H NMR spectroscopy [mol% carbon].

contains the pentose C1-position could be expected to proceed from a freely formed triose that isomerizes between the aldose and ketose forms. Evidently, such a triose does not emerge in the free form in noteworthy amounts, as this would imply a symmetric ^{13}C distribution in ML as well. We hypothesize that instead of a free triose, the retro-aldol cleavage of a ketose results in an enol bonded covalently to the Sn site (Figure 5B). In this form, the primary alcohol that arises from the

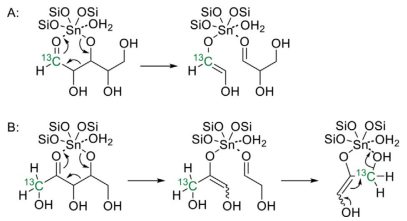

Figure 5. Plausible mechanism for the retro-aldol cleavage of A) [1-^{13}C]-aldopentose and B) [1-^{13}C]-ketopentose to glycolaldehyde and glyceraldehyde.

C1-position of the carbohydrate substrate may coordinate and subsequently dehydrate. In this manner, the labeled C atom is now in the C3-position of ML (Figure 5B). Notably, the conversion of the carbohydrate C1-position to the lactate C3-position is a common feature of chemocatalytic and biocatalytic glycolysis, which results from the coordination or phosphorylation of the carbohydrate C1 site, respectively.[27]

The use of D-[1-^{13}C]-xylose shows 84% ^{13}C label at the C3-position of the ML formed, whereas ^{1}H NMR spectroscopy shows a 10.5% combined yield of all ML isotopomers and 7.4% yield of the ^{13}C3-labeled methyl-[3-^{13}C]-lactate isotopomer, which confirms that this isotopomer covers the majority of the ML formed (Figure S1 in the Supporting Information). These distributions corroborate that the majority of the ML appears to derive from the ketose form (Figure 5B) rather than the aldose (Figure 5A), even if an aldose is used as the substrate. Overall, isotope tracking data suggest that the Sn-Beta-catalyzed ML formation proceeds predominantly from the ketose form in a concerted manner in which retro-aldol fragments remain bound to the active site. Similar isotope distributions with more than 80% ^{13}C label at the C3-position in the ML formed are found for shorter (1 min) or longer (2 h) reaction times.

Upon the retro-aldol cleavage of a ketose or aldose to form ML, an equivalent amount of glycolaldehyde is formed, of which the majority must be unlabeled to correspond to the labeled ML formed. MVG may be formed from the aldol condensation of two glycolaldehyde fragments. As expected, MVG was detected in the mixture and had a much more even distribution of ^{13}C than ML (Figure 4B) with no predominant labeling at any single position.

Methyl 2,5-dihydroxy-3-pentenoate

Recently, it has become clear that various other α-hydroxy esters in addition to ML can be formed in significant amounts under similar catalytic conditions. The most abundant of these longer α-hydroxy esters formed from pentoses is methyl *trans*-2,5-dihydroxy-3-pentenoate (*trans*-DPM), which can be formed in yields above 30%. *trans*-DPM and ML are C_5 and C_3 α-hydroxy esters, respectively, and could be expected to follow similar mechanistic steps in the formation of the α-hydroxy ester functionality. The proposed mechanism for *trans*-DPM formation is expected to differ from that of ML shown in Figure 2 in step c. Here, tautomerization is replaced by an additional dehydration step, after which the pathway can proceed equivalently to steps d and e for ML. To investigate the mechanism for *trans*-DPM formation, we performed an analysis of *trans*-DPM using [UL-$^{2}H_6$]- and [1-^{13}C]-labeled pentoses equivalent to that performed for ML.

Experiments with the deuterated pentose showed less than 4% total solvent proton incorporation into *trans*-DPM, all of which was observed at the C5-position (Figure 6A). Most importantly, this finding excludes the significance of tautomerization to a free 3-deoxyxylosone-type intermediate, which has been suggested previously, in the route to *trans*-DPM.[14,20] The same lack of solvent exchange was observed in the pathway to furfural (Figure S2), which shows that a 3-deoxyxylosone-

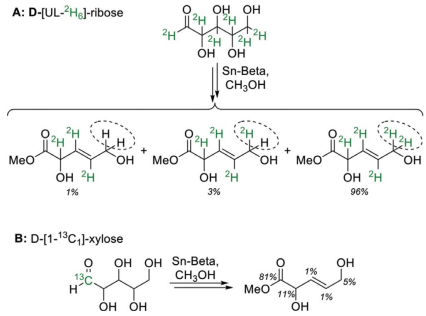

Figure 6. A) Amount of *trans*-DPM produced with the displayed isotopic configuration upon the reaction of D-[UL-$^{2}H_6$]-ribose. B) Distribution of ^{13}C in *trans*-DPM using D-[1-^{13}C]-xylose. Reactions consisted of 36 mg substrate, 18 mg Sn-Beta, 500 µL methanol, and 5 mg dimethylsulfoxide (internal standard) heated to 160 °C for 5 min.

type intermediate was not part of the pathway for Sn-Beta-catalyzed furfural formation.

If we used the [1-^{13}C] pentose substrate, the ^{13}C isotope distributions show a peculiar pattern (Figure 6B). No scrambling of the ^{13}C isotope into the C3- and C4-positions is observed, and these positions retain an isotopic abundance close to the natural isotopic abundance of ^{13}C. In addition, the scrambling of ^{13}C isotope of [1-^{13}C] pentose into the C2- and C5-positions is observed. Such a scrambling of ^{13}C1 to C2 and C5 is consistent with the epimerization of the carbohydrate through a 1,2-carbon shift or isomerization by a 1,5-hydride shift, respectively. Previously, epimerization by 1,2-carbon shifts has been reported for Sn-Beta at lower temperatures, and 1,5-hydride shifts were reported for other catalysts.[13,28,29] In addition, *trans*-DPM is formed as the major isomer in all experiments with negligible formation of the *cis* isomer. The same selectivity is observed for both Sn-Beta and the homogeneous $SnCl_4$ (Figure S3), which excludes spatial confinement as the origin of *cis*/*trans* selectivity.

From these observations we propose a plausible reaction mechanism towards the formation of *trans*-DPM (Figure 7, blue). The C3-position of *trans*-DPM is maintained as an olefinic group throughout. Reversible keto-enol tautomerization of the C3- or C4-positions en route to *trans*-DPM can thus be excluded as no solvent exchange is found at these positions. The formation of a *trans* C2–C3 bond in step c precludes cyclization and leads to a linear pathway to form *trans*-DPM if a *trans* olefinic bond is formed in step e′ as well. The formation of a *cis* olefinic bond in step e′ may enable a cyclic dehydration pathway to furfural, supported by observed furfural isotopologues (Figure S2). Similar to the retro-aldol cleavage of ketose substrates (Figure 5), coordination at C2 elicits most central reaction chemistry in the pathway. Coordination at C2 is vital for hydride shifts in the equilibration of ketose and aldose substrates as well as the dehydration in steps c and e′.

The experimentally observed products 3-deoxy-γ-xylonolactone (3DL) and methyl 3-deoxy-xylonate (3DE) derive from the same pathway (Figure 7, green), whereas *trans*-DPM derives from a different pathway, as witnessed from different patterns of isotope incorporation. Previous experiments identified 3-deoxyglycosone (the glucose analogue of 3DX) in reactions from glucose, and further experiments using a 3-deoxyglycosone substrate indicated that this substrate forms saturated lactones and esters predominantly, which supports steps e and f.[14] A rehydration of *trans*-DPM to 3DE seems unlikely as isolated *trans*-DPM does not react to 3DE under the current reaction conditions (Figure S4).

We hypothesize that the flux of intermediates into the two different pathways, for *trans*-DPM (and possibly furanics) as well as 3DL/3DE, may be influenced by the stereochemistry of step c. Only the formation of a *trans*-2,3-enol favors subsequent 2,4 coordination and dehydration at C4. The formation of a *cis*-enol in step c in Figure 7 (green) will make the simultaneous coordination of the enol and the C4 hydroxyl group less favorable. In such a case, tautomerization to the experimentally observed 3-deoxyxylosone intermediate (3DX) may occur in favor of dehydration, as shown in step d, which leads to the formation of 3DL and 3DE by intra- or intermolecular esterification, respectively. Experiments with commercially available α-hydroxy-γ-butyrolactone showed that under the tested reaction conditions the lactone and the ester equilibrate (Figure S5), which demonstrates that the products 3DL and 3DE and their formation is indistinguishable under the tested reaction conditions.

We considered the stereoselectivity for *trans*-DPM formation and stereoselectivity in the aldose-ketose isomerization by C1–

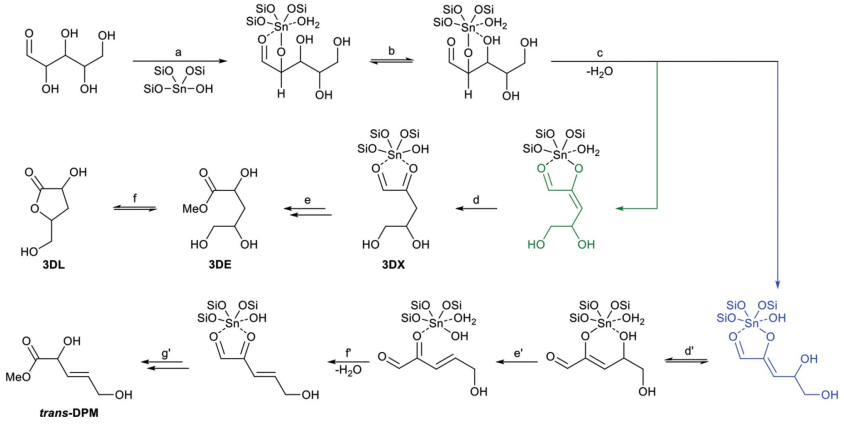

Figure 7. Proposed mechanism for the formation of *trans*-DPM, 3-deoxy-γ-xylonolactone (3DL), and methyl 3-deoxy-xylonate (3DE) from D-xylose. The *cis* precursor to step f′ may also react by alternative pathways to form furfural in addition to the three products displayed.

ChemPubSoc Europe

CHEMCATCHEM Full Papers

C2 hydride shift reported previously[30] and we set out to identify further stereoselective reactions in the pathways shown in Figure 7. Experiments with [UL-$^2H_6$] aldopentose showed additional unanticipated isotope distributions in both 3DL and 3DE. Stereoselectivity was observed for the four potential diastereomers of 3DL with isomerism at C2 and C3 (Figure 8). Although stereoselectivity at the C2-position was low (9% diastereomeric excess (*de*) between xylono- and arabino-lactone forms), stereoselectivity for ^1H incorporation at the C3-position by tautomerization was (46 ± 1)% *de* for these two lactones. The same trend was observed for 3DE with 7% *de* for C2 and 46% *de* for both pairs of C3 diastereoisomers (Figure S6). The almost identical stereoselectivity at C2 and C3 in 3DL and 3DE suggests that the two molecules arise from the same reaction pathway. The high diastereoselectivity of the tautomerizations in this pathway and the high *trans* stereoselectivity in the dehydration pathway (Figure 7) parallel the high stereoselectivity in the hydride shifts of aldose-to-ketose isomerizations. Thus, Sn-Beta catalyzes a variety of stereoselective isomerization and dehydration reactions.

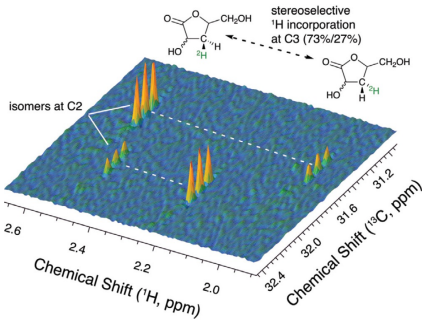

Figure 8. ^1H-^{13}C-HSQC signals for the C3-position of 3DL. The four potential diastereomer products (isomerism at C2 and C3) produced by reaction of enantiomerically pure [UL-$^2H_6$] pentose yield four triplets for CH groups at C3, as splitting by the quadrupolar ^2H was not decoupled.

C5–C1 hydride shift

To elucidate the ability of Sn-Beta to perform a 5,1-hydride shift, [5,5′-$^2H_2$]-arabinose was selected for testing. The reaction of the [5,5′-$^2H_2$]-arabinose showed a final distribution of 80% $^2H_2$ and 20% $^2H^1H$ in the C5-position of *trans*-DPM (Figure 9). Compared with the lower (< 4%) proton incorporation in the uniformly deuterated substrate (Figure 6A) under identical reaction conditions, this finding indicates that intramolecular hydride exchange takes place. A C5–C1 hydride shift as detected previously in Ti-Beta-catalyzed reactions is the most plausible explanation.[29] Analysis of the distribution of ^2H in ML from [5,5′-$^2H_2$]-arabinose showed that the C3-position had 78% $^1H_3$ and 22% $^2H^1H_2$ (Figure S7). This incorporation correlates to the migration of the label from the C5-position to the C1-position as detected from the isotope pattern in *trans*-DPM after a hydride shift for approximately 20% of the molecules (Figure 9). Thus, the use of a [5,5′-$^2H_2$]-labeled pentose underlines that ML originates primarily from the ketose (Figure 5). In addition, the results indicate that a C5–C1 hydride shift occurs in the carbohydrate form, but only for a minority of the carbohydrate substrates.

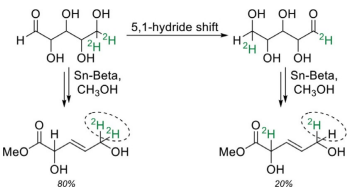

Figure 9. Amount of *trans*-DPM produced with the displayed isotopic configurations upon reaction of a [5,5′-$^2H_2$]-arabinose. Reactions consisted of 36 mg substrate, 18 mg Sn-Beta, 500 µL methanol, and 5 mg dimethylsulfoxide heated to 160 °C for 5 min.

Conclusions

We employed isotope-labeled substrates to track isotope redistribution and solvent exchange in different products formed during chemocatalytic carbohydrate conversion. The experiments showed that ketoses are the primary substrates for retro-aldol cleavage much like enzymatic glycolysis. This finding is consistent with a rapid hydride shift between aldose and ketose under the reaction conditions of α-hydroxy ester formation (≈160 °C). Furthermore, strong binding is observed between substrate and catalyst to result in the regioselective formation of methyl lactate that occurs through the irreversible formation of an enol, which continues in a cascade reaction through to methyl lactate. Analogous conclusions can be drawn for pathways that do not encompass a retro-aldol step. Additionally, experimental data are consistent with the strong coordination of the enol form by the catalyst active site. These pathways include enols formed in the cascade toward methyl *trans*-2,5-dihydroxy-3-pentenoate, 3-deoxy lactones, and 3-deoxy esters, which exhibit little isotope scrambling once the reaction cascade commences. However, our experiments show some atom rearrangement attributed to reactions with unconverted carbohydrates. Sn-Beta was shown to catalyze a 5,1-hydride shift of carbohydrates as well as a 1,2-hydride shift and a Bilik-type 1,2-carbon shift reported previously. We thus find that rich mechanistic information can be derived from the use of quantitative isotope tracking experiments in complex reaction mixtures formed in biomass conversion.

Experimental Section

D-[1-^{13}C]-Xylose (99 at% ^{13}C) was obtained from Sigma–Aldrich. D-[UL-$^2H_6$] and D-[5,5′-$^2H_2$]-arabinose (98 at% ^2H) were obtained from Omicron Chemicals. Reactions were conducted with a Biotage Ini-

tiator+ microwave reactor in 500 μL glass reaction vials. Typically, reactions were conducted with Sn-Beta (18 mg; Si/Sn = 200, hydrothermally synthesized), substrate (36 mg), methanol (500 μL), and dimethylsulfoxide (5 mg) as an internal standard.

The Sn-Beta catalyst was synthesized hydrothermally in accordance with the procedure described by Tolborg et al. with a target Si/Sn ratio of 200.[31] The catalyst structure and composition were confirmed by using inductively coupled plasma optical emission spectroscopy (ICP-OES; 0.9 wt% Sn, Si/Sn = 196), XRD (*BEA framework), and N_2 absorption ($S_{BET} = 540\ m^2 g^{-1}$, $S_{micropore} = 436\ m^2 g^{-1}$, $V_{total} = 0.30\ mL\ g^{-1}$, $V_{micropore} = 0.22\ mL\ g^{-1}$ calculated by the *t*-plot method).

NMR spectroscopic isotope tracking was performed using spectra that were acquired by using an 800 MHz Bruker Avance III NMR spectrometer equipped with a TCI CryoProbe and a SampleJet sample handler. Data were zero-filled to double the number of acquired complex data points before Fourier transformation in all spectral dimensions by using Bruker Topspin 3.5 pl7 software. Quantification was achieved by using qNMR spectroscopic experiments without pulse sequence elements that enhance or suppress signal but with extensive interscan recycle delays. 2D ^{1}H-^{13}C NMR HSQC spectra were used to validate the assignment of the integrated 1D ^{13}C NMR spectra. The incorporation of deuterium was verified from chemical shift changes and multiplet patterns in HSQC spectra, and spectral editing was used to distinguish carbon sites by the number of attached protons (and hence incorporated deuterons; Figures 3 and 8). Quantitative proton decoupled ^{13}C 1D NMR spectra were acquired with recycle delays of 60 s using a pulse sequence that employs inverse-gated decoupling to avoid the nuclear Overhauser enhancement of protonated sites.

Acknowledgements

This work was funded by the Innovation Fund Denmark (case number 5150-00023B). 800 MHz NMR spectra were recorded by using the spectrometer of the NMR center DTU supported by the Villum foundation. We gratefully acknowledge Dr. Søren Tolborg (Haldor Topsøe AS) for his expertise and work in synthesizing the employed Sn-Beta catalyst.

Conflict of interest

The authors declare no conflict of interest.

Keywords: biomass · carbohydrates · heterogeneous catalysis · NMR spectroscopy · reaction mechanisms

[1] S. G. Elliot, S. Tolborg, I. Sádaba, E. Taarning, S. Meier, *ChemSusChem* **2017**, *10*, 2990 – 2996.
[2] R. Bermejo-Deval, M. Orazov, R. Gounder, S.-J. Hwang, M. E. Davis, *ACS Catal.* **2014**, *4*, 2288 – 2297.
[3] P. P. Pescarmona, K. P. Janssen, C. Delaet, C. Stroobants, K. Houthoofd, A. Philippaerts, C. De Jonghe, J. S. Paul, P. A. Jacobs, B. F. Sels, *Green Chem.* **2010**, *12*, 1083 – 1089.
[4] R. Bermejo-Deval, R. S. Assary, E. Nikolla, M. Moliner, Y. Román-Leshkov, S.-J. Hwang, A. Palsdottira, D. Silverman, R. F. Lobo, L. A. Curtiss, M. E. Davis, *Proc. Natl. Acad. Sci. USA* **2012**, *109*, 9727 – 9732.
[5] S. Van de Vyver, C. Odermatt, K. Romero, T. Prasomsri, Y. Román-Leshkov, *ACS Catal.* **2015**, *5*, 972 – 977.
[6] T. R. Carlson, J. Jae, G. W. Huber, *ChemCatChem* **2009**, *1*, 107 – 110.
[7] M. Foston, R. Samuel, A. J. Ragauskas, *Analyst* **2012**, *137*, 3904 – 3909.
[8] H. Ben, G. A. Ferguson, W. Mu, Y. Pu, F. Huang, M. Jarvis, M. Biddy, Y. Deng, A. J. Ragauskas, *Phys. Chem. Chem. Phys.* **2013**, *15*, 19138 – 19142.
[9] E. Taarning, S. Saravanamurugan, M. S. Holm, J. Xiong, R. M. West, C. H. Christensen, *ChemSusChem* **2009**, *2*, 625 – 627.
[10] M. S. Holm, S. Saravanamurugan, E. Taarning, *Science* **2010**, *328*, 602 – 605.
[11] M. Moliner, Y. Román-Leshkov, M. E. Davis, *Proc. Natl. Acad. Sci. USA* **2010**, *107*, 6164 – 6168.
[12] Y. Román-Leshkov, M. Moliner, J. A. Labinger, M. E. Davis, *Angew. Chem. Int. Ed.* **2010**, *49*, 8954 – 8957; *Angew. Chem.* **2010**, *122*, 9138 – 9141.
[13] W. R. Gunther, Y. Wang, Y. Ji, V. K. Michaelis, S. T. Hunt, R. G. Griffin, Y. Román-Leshkov, *Nat. Commun.* **2012**, *3*, 1109.
[14] S. Tolborg, S. Meier, I. Sádaba, S. G. Elliot, S. K. Kristensen, S. Saravanamurugan, A. Riisager, P. Fristrup, T. Skrydstrup, E. Taarning, *Green Chem.* **2016**, *18*, 3360 – 3369.
[15] T. Usui, S. Yanagisawa, M. Ohguchi, M. Yoshino, R. Kawabata, J. Kishimoto, Y. Arai, K. Aida, H. Watanabe, F. Hayase, *Biosci. Biotechnol. Biochem.* **2007**, *71*, 2465 – 2472.
[16] M. S. Holm, Y. J. Pagán-Torres, S. Saravanamurugan, A. Riisager, J. A. Dumesic, E. Taarning, *Green Chem.* **2012**, *14*, 702 – 706.
[17] M. Dusselier, P. Van Wouwe, F. de Clippel, J. Dijkmans, D. W. Gammon, B. F. Sels, *ChemCatChem* **2013**, *5*, 569 – 575.
[18] M. Dusselier, P. Van Wouwe, S. De Smet, R. De Clercq, L. Verbelen, P. Van Puyvelde, F. E. Du Prez, B. F. Sels, *ACS Catal.* **2013**, *3*, 1786 – 1800.
[19] H. S. Chen, A. Wang, H. Sorek, J. D. Lewis, Y. Román-Leshkov, A. Bell, *ChemistrySelect* **2016**, *1*, 4167 – 4172.
[20] S. G. Elliot, C. Andersen, S. Tolborg, S. Meier, I. Sadaba, A. E. Daugaard, E. Taarning, *RSC Adv.* **2017**, *7*, 985 – 996.
[21] K. M. Nampoothiri, N. R. Nair, R. P. John, *Bioresour. Technol.* **2010**, *101*, 8493 – 8501.
[22] E. Castro-Aguirre, F. Iñiguez-Franco, H. Samsudin, X. Fang, R. Auras, *Adv. Drug Delivery Rev.* **2016**, *107*, 333 – 366.
[23] O. Dechy-Cabaret, B. Martin-Vaca, D. Bourissou, *Chem. Rev.* **2004**, *104*, 6147 – 6176.
[24] Y. Hayashi, Y. Sasaki, *Chem. Commun.* **2005**, 2716 – 2718.
[25] P. N. R. Vennestrøm, C. M. Osmundsen, C. H. Christensen, E. Taarning, *Angew. Chem. Int. Ed.* **2011**, *50*, 10502 – 10509; *Angew. Chem.* **2011**, *123*, 10686 – 10694.
[26] L. Li, C. Stroobants, K. Lin, P. A. Jacobs, B. F. Sels, P. P. Pescarmona, *Green Chem.* **2011**, *13*, 1175 – 1181.
[27] A. Bar-Even, A. Flamholz, E. Noor, R. Milo, *Nat. Chem. Biol.* **2012**, *8*, 509 – 517.
[28] M. E. Davis, R. Gounder (Caltech, CA), US2014309415, **2014**.
[29] R. Gounder, M. E. Davis, *ACS Catal.* **2013**, *3*, 1469 – 1476.
[30] S. Saravanamurugan, A. Riisager, E. Taarning, S. Meier, *Chem. Commun.* **2016**, *52*, 12773 – 12776.
[31] S. Tolborg, A. Katerinopoulou, D. D. Falcone, I. Sádaba, C. M. Osmundsen, R. J. Davis, E. Taarning, P. Fristrup, M. S. Holm, *J. Mater. Chem. A* **2014**, *2*, 20252 – 20262.

Manuscript received: November 22, 2017
Revised manuscript received: December 15, 2017
Accepted manuscript online: December 18, 2017
Version of record online: February 19, 2018

Heterogeneous & Homogeneous & Bio- & Nano-
CHEMCATCHEM
CATALYSIS

Supporting Information

NMR Spectroscopic Isotope Tracking Reveals Cascade Steps in Carbohydrate Conversion by Tin-Beta

Samuel G. Elliot,[a] Esben Taarning,*[b] Robert Madsen,[a] and Sebastian Meier*[a]

cctc_201701861_sm_miscellaneous_information.pdf

Supporting Information

69451 Weinheim, Germany

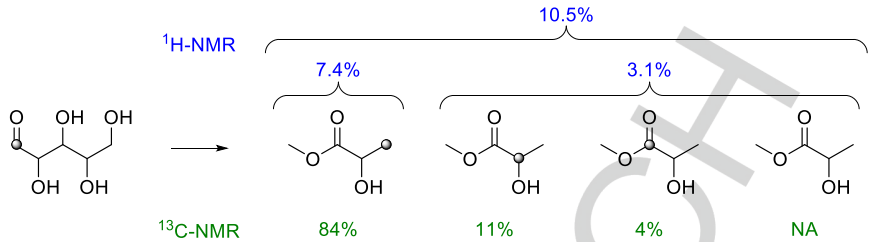

Figure S1. Amount of methyl lactate produced with the displayed isotopic configurations upon reaction of D-[1-^{13}C]-xylose (the ^{13}C atom is highlighted with a grey orb). Total methyl lactate yield and quantitative yields of methyl lactate isotopomers were determined by ^{1}H-NMR and are displayed in blue. Relative yields of the three ^{13}C isotopomers were determined by ^{13}C-NMR and are displayed in green, with the pure ^{12}C isotopomer not detectable by this method. Reactions consisted of 36 mg D-[5,5'-^{2}H$_2$]-arabinose, 18 mg Sn-Beta, 500 µL methanol and 5 mg dimethyl sulfoxide, which were heated to 160°C for 5 min.

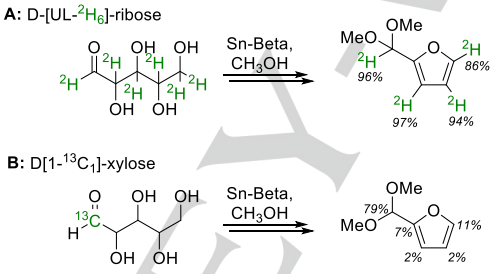

Figure S2. Amount of deuterium remaining at the displayed positions of furfural in its dimethyl acetal form upon reaction of D-[UL-^{2}H$_6$]-ribose (A). Distribution of ^{13}C in furfural in its dimethyl acetal form using D-[1-^{13}C]-xylose (B). Reactions consisted of 36 mg substrate, 18 mg Sn-Beta, 500 µL methanol and 5 mg dimethyl sulfoxide (internal standard), which were heated to 160°C for 5 min.

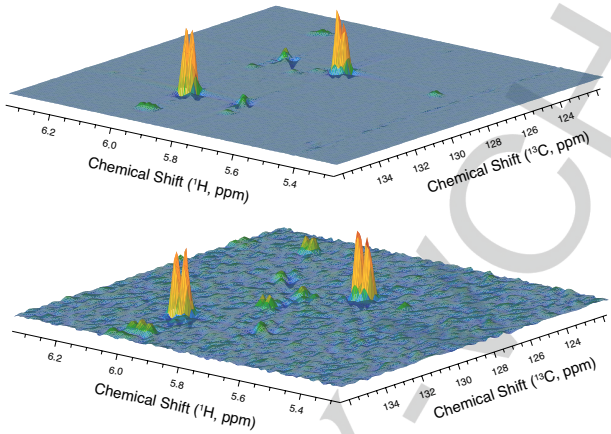

Figure S3. Spectral region containing signals of olefinic groups for a mixture of D-xylose with either Sn-Beta (top) or $SnCl_4$ (bottom) as the catalyst. The spectra show a large formation of *trans*-DPM (C3, ^{1}H = 5.8 ppm, ^{13}C = 126.9 ppm; C4, ^{1}H = 6.0 ppm, ^{13}C = 132.3 ppm), but negligible formation of *cis*-DPM (C3, ^{1}H = 5.5 ppm, ^{13}C = 127.3 ppm; C4, ^{1}H = 5.8 ppm, ^{13}C = 133.7 ppm). 36 mg D-[1-13C]-Xylose, 18 mg Sn-Beta or 0.6 mg $SnCl_4$, 500 µL methanol and 5 mg dimethyl sulfoxide (internal standard), which were heated to 160°C for 5 min.

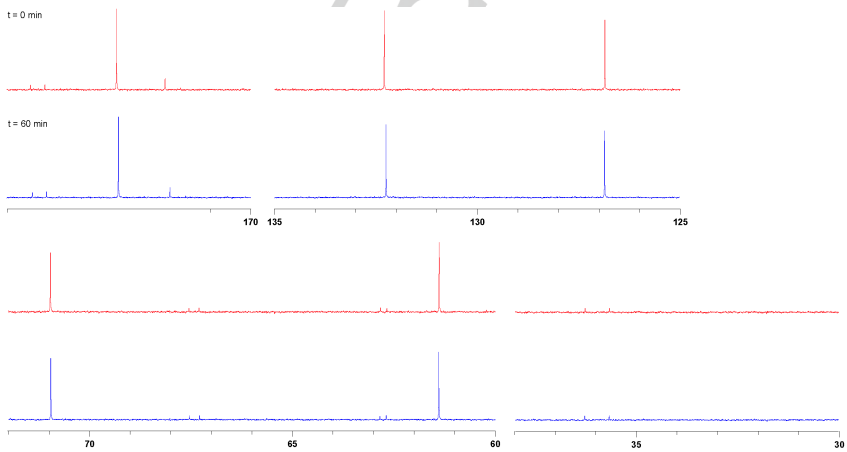

Figure S4. ^{13}C-NMR spectra of methyl *trans*-2,5-dihydroxy-3-pentenoate (*trans*-DPM) reaction, after 0 min and 1 h, showing no change in the reaction mixture. Reactions consisted of 360 mg methyl *trans*-2,5-dihydroxy-3-pentenoate ≥85% purity, 180 mg Sn-Beta (Si/Sn = 150), 100 µL demineralized water, 5 mL methanol and 50 mg dimethyl sulfoxide (internal standard), which were heated to 160°C for 1 h.

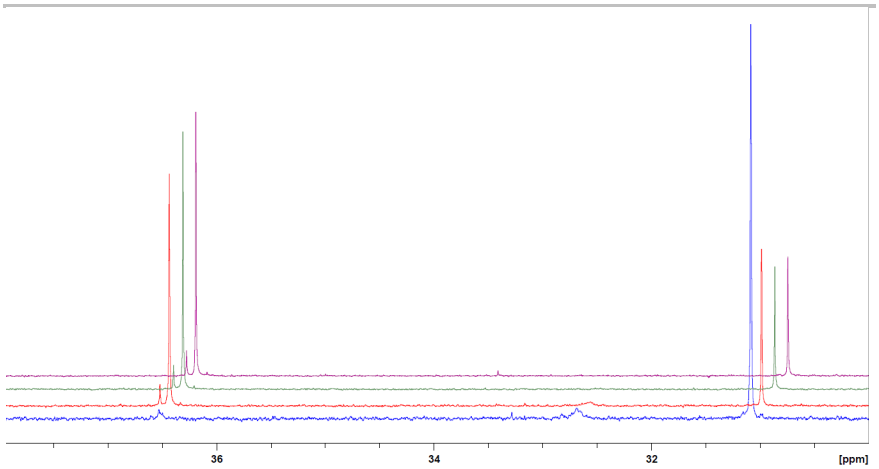

Figure S5. ^{13}C-NMR spectra of α-hydroxy-γ-butyrolactone reaction products, after 0 min, 5 min, 1 h and 2 h, showing both the initial lactone (HBL, 31.1 ppm) and methyl 2,4-dihydroxy butanoate (HBM, 36.5 ppm). Reactions consisted of 36 mg α-hydroxy-γ-butyrolactone, 18 mg Sn-Beta (Si/Sn = 150), 500 µL methanol and 5 mg dimethyl sulfoxide (internal standard), which were heated to 160°C for 5 min, 1h or 2h.

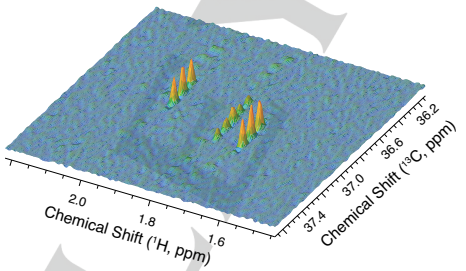

Figure S6. Multiplet pattern of the C3 positions of methyl 3-deoxy-xylonoate (3DE) diastereoisomers resulting from incorporation of one ^{1}H atom, upon reaction of D-[UL-^{2}H$_6$]-ribose. The reaction consisted of 36 mg D-[UL-^{2}H$_6$]-ribose, 18 mg Sn-Beta, 500 µL methanol and 5 mg dimethyl sulfoxide (internal standard), which were heated to 160°C for 5 min.

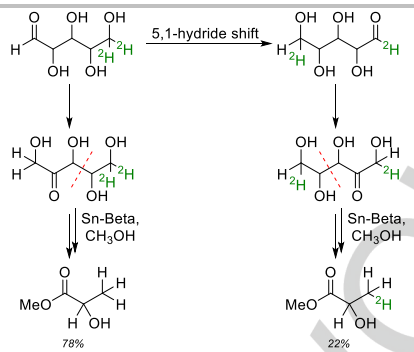

Figure S7. Amount of ML produced with the displayed isotopic configurations upon reaction of D-[5,5'-$^2H_2$]-arabinose. Reactions consisted of 36 mg D-[5,5'-$^2H_2$]-arabinose, 18 mg Sn-Beta, 500 µL methanol and 5 mg dimethyl sulfoxide, which were heated to 160°C for 5 min.

ChemPubSoc Europe

DOI: 10.1002/cssc.201702413

CHEMSUSCHEM Full Papers

Effects of Alkali-Metal Ions and Counter Ions in Sn-Beta-Catalyzed Carbohydrate Conversion

Samuel G. Elliot,[a] Søren Tolborg,[b] Robert Madsen,[a] Esben Taarning,*[b] and Sebastian Meier*[a]

Alkali-metal ions have recently been shown to strongly influence the catalytic behavior of stannosilicates in the conversion of carbohydrates. An effect of having alkali-metal ions present is a pronounced increase in selectivity towards methyl lactate. Mechanistic details of this effect have remained obscure and are herein addressed experimentally through kinetic experiments and isotope tracking. The presence of alkali-metal ions has a differential effect in competing reaction pathways and promotes the rate of carbon–carbon bond breakage of carbohydrate substrates, but decreases the rates of competing dehydration pathways. Further addition of alkali-metal ions inhibits the activity of Sn-Beta in all major reaction pathways. The alkali-metal effects on product distribution and on the rate of product formation are similar, thus pointing to a kinetic reaction control and to irreversible reaction steps in the main pathways. Additionally, an effect of the accompanying basic anions is shown, supposedly facilitating the cation exchange and eliciting a different concentration-dependent effect to that of neutral alkali-metal salts.

Introduction

Chemocatalytic carbohydrate conversion may be achieved by the use of zeolites, which are microporous solid materials widely used in oil refining that are projected to obtain similarly central roles in biomass refining.[1,2] In particular, zeotypes, with elements such as tin instead of aluminum incorporated in the zeolite framework, have been shown to catalyze a range of relevant reactions in the conversion of carbohydrates, including isomerization, dehydration, and retro-aldol cleavage of carbohydrates.[1,3,4] Since carbohydrates comprise approximately 75% of all biomass on Earth, they are attractive as a feedstock for the development of sustainable processes.[5]

Sn-Beta, a tin-containing zeotype (stannosilicate), is a particularly promising heterogeneous catalyst for carbohydrate conversion.[4,6] Sn-Beta is able to catalyze the isomerization and epimerization of carbohydrates under mild reaction conditions (near 100 °C),[7–9] whereas higher temperatures (above 120 °C) facilitate the formation of different α-hydroxy acids/esters and furanic compounds through a combination of retro-aldol cleavage[10–12] or condensation[13] and dehydration reactions.[10,14–18] The major products resulting from conversion of xylose by Sn-Beta above 120 °C are displayed in Scheme 1.

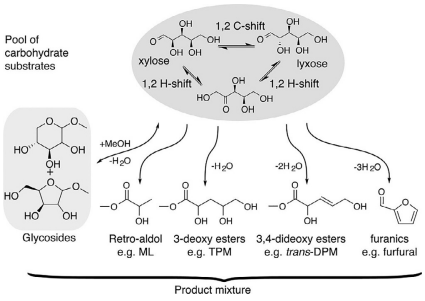

Scheme 1. Competing pathways observed in the conversion of pentoses catalyzed by Sn-Beta in methanol. ML = methyl lactate, TPM = 2,4,5-trihydroxypentanoic acid methyl ester, *trans*-DPM = *trans*-2,5-dihydroxy-3-pentenoic acid methyl ester, furanics = furfural and furfural dimethyl acetal.

Recently, it has been reported that the catalytic performance of stannosilicates can be influenced by the presence of alkali-metal cations.[19] Low millimolar concentrations of alkali-metal ions were found to greatly increase the formation of methyl lactate in methanol (from 30% to 75%) at 160 °C over Sn-Beta.[19,20] At lower temperatures (80 °C), alkali-metal ions have also been reported to promote Sn-Beta-catalyzed epimerization over the isomerization of carbohydrates.[21–23] The effect of alkali-metal ions on zeolite-catalyzed reactions has been more thoroughly studied for reactions with fewer competing pathways than depicted in Scheme 1, using non-carbohydrate substrates. Thus, alkali-metal exchange has been shown to enhance Baeyer–Villiger oxidation by Sn-Beta,[24] but to lower the activity of titanosilicates in epoxidation with H_2O_2.[25,26] These

[a] S. G. Elliot, Prof. R. Madsen, Dr. S. Meier
Department of Chemistry, Technical University of Denmark
Kemitorvet, Bygning 207, 2800 Kgs. Lyngby (Denmark)
E-mail: semei@kemi.dtu.dk

[b] Dr. S. Tolborg, Dr. E. Taarning
Haldor Topsøe A/S
Haldor Topsøes Alle 1, 2800 Kgs. Lyngby (Denmark)
E-mail: esta@topsoe.com

Supporting Information and the ORCID identification number(s) for the author(s) of this article can be found under https://doi.org/10.1002/cssc.201702413.

alkali-metal effects are thought to result from exchange of protons at or in the vicinity of the catalyst active site.[24–26] The detailed nature of the alkali-metal effect in improving methyl lactate yield and carbohydrate epimerization and the correlation between the two effects have hitherto remained unclear.

The current study sets out to systematically study the effect of alkali-metal salts (as demonstrated herein for potassium salts) on the divergent pathways catalyzed by Sn-Beta (Scheme 1). Quantitative high-field NMR spectroscopy was used to distinguish and quantify various reaction products without the need for purification, reference compounds, or instrument calibration.[27] Changes in activity and selectivity of Sn-Beta were thus noninvasively probed by accurate in situ analysis of the resultant reaction mixtures. These assays show that alkali-metal ions promote the activity for methyl lactate formation at moderate concentrations but inhibit all major Sn-Beta-catalyzed pathways at higher concentrations.

Results and Discussion

A variety of potassium salts were initially probed for their impact on the formation of methyl lactate by Sn-Beta. These experiments encompassed the potassium salts of weak and strong acids. The experiments were conducted at mild reaction conditions (120 °C) and with long reaction times (19 h) to ensure full conversion. The potassium salts of weak and strong acids in a concentration range of 0–20 mM K^+ showed distinct effects on the methyl lactate yield (Figure 1). The yields of methyl lactate increased for salts of strong acids and reached a plateau at higher concentrations. In contrast, alkali-metal salts of weak acids (with basic anions) generally show a steeper increase in methyl lactate yield to a well-defined optimum, followed by a subsequent decrease in yield at higher concentrations of the salt.

Mechanistic insights into the observed effect of potassium salts of strong and weak acids were subsequently sought. The effect was analyzed by probing the flux into all major reaction pathways catalyzed by Sn-Beta. The formation of the four major product classes (Scheme 1) and the methyl glycoside byproducts were tracked as initial rate experiments by using quantitative high-resolution NMR spectroscopy to obtain time-resolved kinetic data. These experiments were performed using pentose substrate rather than hexoses at higher temperatures (160 °C), owing to the higher obtained yields of dehydration products and the formation of fewer diastereoisomers when using pentose substrate.[17] Reactions were performed in a microwave reactor and analyzed ex situ with ^{13}C and ^{1}H–^{13}C NMR spectroscopy. The conversion of xylose was tracked in the absence of alkali-metal salt, in the presence of 2 mM KCl, and in the presence of 0.3 mM K_2CO_3. The chosen concentrations are near optimum for methyl lactate formation under these conditions (see the Supporting Information, Tables S1 and S2).[19] In addition, K_2CO_3 concentrations above and below the optimum were also tested (0.1–1 mM).

Initial rate experiments were conducted for only up to two minutes at 160 °C. We observed that xylose was converted very rapidly on this short timescale (Figure S2), although the process had previously been conducted on a timescale of hours.[10] Both substrate and product signals showed initial linear trends with and without alkali-metal salts, indicating that a steady state was achieved (Figure 2 and Figure S3).

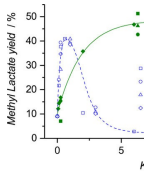

Figure 1. Methyl lactate yield as a function of potassium concentration for various salts of strong acids (filled green symbols) and salts of weak acids (open blue symbols). Reaction conditions: glucose (0.250 g), Sn-Beta (hydrothermally synthesized) (0.100 g), methanol (5 mL) containing up to 20 mM potassium salt, 120 °C, 19 h. Methyl lactate is considered stable under the reaction conditions (Figure S1).

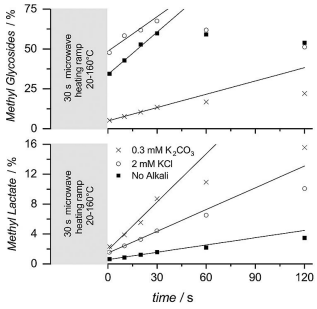

Figure 2. Formation of methyl glycoside and methyl lactate in initial rate experiments. Signal areas were converted into molar yields by a quantitative NMR approach. Reaction mixtures consisted of D-xylose (360 mg), Sn-Beta (PT) (90 mg), methanol (5 mL), and dimethyl sulfoxide (50 mg; internal standard), which were heated from room temperature to 160 °C within 30 seconds (indicated by the grey box) and heated for a given time at 160 °C. Methanol containing no additive, 2 mM KCl, or 0.3 mM K_2CO_3, was used.

The time-resolved experiments show rapid formation of glycosides already during the heating stage, both in the presence of KCl and in the absence of any added salts. In contrast, the rate of glycoside formation is suppressed approximately fourfold for reactions performed at optimum K_2CO_3 concentrations (Figure 2). Thus, alkali-metal salts also exhibit an effect on the formation of methyl glycosides depending on the basicity of the anion, consistent with Fischer glycosylation in the presence of weak Brønsted acidic sites. This effect is also observed for the formation of furanics and is consistent with pathway models suggesting that the formation of furanics encompasses Brønsted acid-catalyzed dehydration. These observations may

ChemPubSoc Europe

CHEMSUSCHEM Full Papers

be explained by neutralization of Brønsted acidity by a basic anion.

Importantly, the initial rate of methyl lactate formation increases both in the presence of K_2CO_3 and of KCl (Figures 2 and 3), demonstrating the positive effect of the alkali-metal cation on the catalytic activity of Sn-Beta towards methyl lactate. A smaller increase is observed in the presence of KCl than in the presence of K_2CO_3. This finding is consistent with both the higher degree of free carbohydrates in the presence of K_2CO_3 (Figure 2), as a result of inhibiting Brønsted acid-catalyzed pathways, and with higher exchange of cations onto the zeotype in the presence of a basic anion.[28,29] Increased rates for the formation of methyl lactate are accompanied by reduced rates for formation of dehydration products (Figure 3). Hence, the change in selectivity is caused by higher activity of retro-aldol cleavage and slightly reduced activity for dehydration pathways.

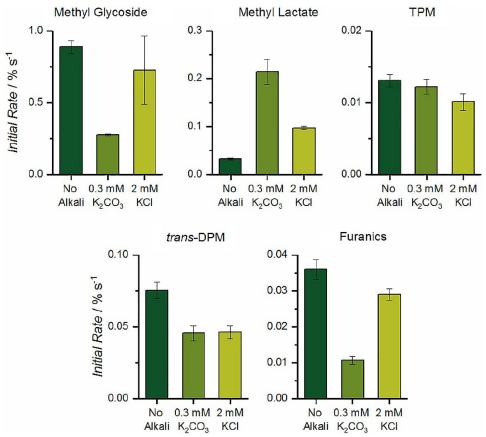

Figure 3. Overview of the effects of KCl and K_2CO_3 on the rates of formation for the designated products. Errors are calculated based on a linear fit of experimental data points.

Subsequently, the reasons for the decline in methyl lactate formation above the optimum concentration of K_2CO_3 were probed. To this end, the initial reaction rates were determined for varying concentrations of K_2CO_3. These rates are consistent with previously reported trends in product distributions for increasing concentrations of K_2CO_3.[16,27] Rates of formation for dehydration products decline upon addition of K_2CO_3, in parallel with a drop in yield of these products upon addition of K_2CO_3. Similarly, the highest rate of methyl lactate formation is found at the K_2CO_3 concentration that also results in the highest yield of methyl lactate (Figure 4). A well-defined optimum for the yield of methyl lactate in the presence of K_2CO_3 results from a deactivation of the catalyst at higher concentrations. Effects of base-catalyzed carbohydrate degradation are secondary and the rate of carbohydrate conversion is reduced in the presence of K_2CO_3, and not increased through possible additional degradation reactions.

Thus, initial rates of conversion indicate that the catalyst kinetically favors dehydration reactions in the absence of added K_2CO_3, but favors the formation of retro-aldol products near 0.3 mM K_2CO_3 prior to deactivation of all reaction pathways by further addition of basic alkali-metal salt. Alkali-metal ions thus promote methyl lactate formation at moderate concentrations but inhibit all major Sn-Beta-catalyzed pathways at higher concentrations. Furthermore, the alkali-metal effect occurs at similar concentrations to those of tin present in the catalyst [K/Sn ratio = 0.31 for an experiment with 0.3 mM K_2CO_3 and Sn-Beta (post-treated, PT) supporting the hypothesis that the alkali-metal cation effect is related to the tin active sites.

In addition to catalyzing the formation of products shown in Figure 4, Sn-Beta had been reported to catalyze carbohydrate epimerization at temperatures near 80 °C.[21–23] For a more complete picture of the alkali-metal effect on Sn-Beta-catalyzed reactions, we therefore also wanted to probe the effect of alkali-metal salt addition on the rate of epimerization. There are two viable mechanisms that can explain the 1,2-carbon shift occurring in the epimerization of carbohydrates: a retro-aldol type mechanism where the shift occurs as a consequence of a retro-aldol/aldol rearrangement (Scheme 2 A) and a Bilik-type mechanism with concerted breakage of the C2–C3 bond and formation of a

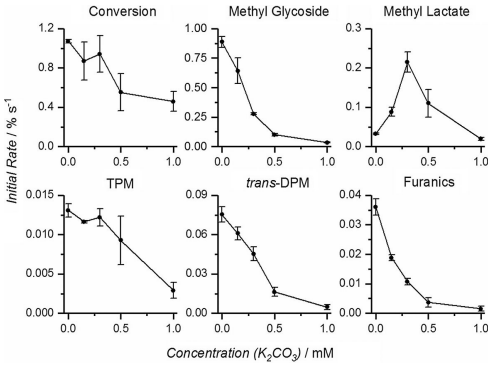

Figure 4. Initial rates of conversion and of formation for different compound classes as a function of K_2CO_3 concentration. Reaction conditions: D-xylose (360 mg), Sn-Beta (PT) (90 mg), methanol (5 mL), and dimethyl sulfoxide (50 mg) at 160 °C. Errors are calculated based on a linear fit of experimental data points.

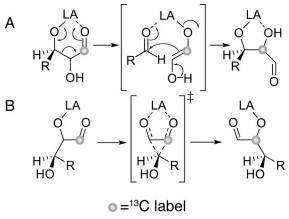

Scheme 2. Comparison of 1,2-carbon shift by a retro-aldol (A) and a Bilik-type (B) cleavage mechanism.[30] The conversion of a ^{13}C-labeled C1 position to a ^{13}C-labeled C2 position is indicated for both cases.

new C1–C3 bond (Scheme 2B). Both suggested reaction mechanisms involve i) breaking of a C=O bond to form a C–O–Sn bond, ii) breaking of a Sn–O bond to form a C=O bond, and iii) breaking of the C2–C3 bond and formation of a new C1–C3 bond.[23,30] Irrespective of which mechanism is responsible for the 1,2-carbon shift, epimerization and retro-aldol cleavage thus share similar reaction steps and a similar effect of alkali-metal ions on both reactions seems possible.

NMR spectroscopy was used to quantitatively measure isotope redistributions and compound yields to correlate the alkali-metal effects both on epimerization and on methyl lactate formation. The 1,2-carbon shift was indirectly probed at high temperatures, which favor the cleavage or dehydration of carbohydrates. To this end, isotopically enriched D-[1-^{13}C$_1$] xylose was converted at 160 °C in methanol by using Sn-Beta under varying concentrations of alkali-metal salts. Isotope scrambling was quantified for all major products after five minutes of reaction.

Experiments conducted with increasing amounts of K_2CO_3 showed that epimerization and retro-aldol cleavage share a similar dependence on alkali-metal concentrations, as expected. The product distributions are depicted in Figure 5A and the fractions of different isotopic isomers of these products are shown in Figure 5B. The product distributions (Figure 5A) in response to varying K_2CO_3 concentrations reflect the trends shown in Figure 4. The ^{13}C label in the product was primarily found at the C1 and C2 positions of all dehydration products, and at the C3 and C2 positions of methyl lactate, as the C1 position of xylose primarily gets converted into C3 of methyl lactate (Figure 5B).[31] All major products showed a comparable trend in the distribution of isotopic isomers with increasing amounts of K_2CO_3. Scrambling increased with K_2CO_3 concentrations for the positions derived from C1 and C2 of xylose up to K_2CO_3 concentrations that provided the optimal methyl lactate yield (0.25 mM K_2CO_3, 0.17 K/Sn). These observations show that the epimerization of carbohydrates by a 1,2-carbon shift[21] also occurs under high-temperature conditions that lead to significant retro-aldol cleavage and dehydration reactions. The relative product distribution of the main product categories shown in Figure 5A, thus stabilizes in the same concentration range of K_2CO_3, where the isotope redistribution due to epimerization (Figure 5B) also stabilizes. Indirect detection of 1,2-carbon shift by stable isotope redistribution thus indicates that moderate alkali-metal exchange accelerates epimerization by Sn-Beta, whereas initial rate experiments show that the same conditions also accelerate the retro-aldol cleavage but impede dehydration by Sn-Beta.

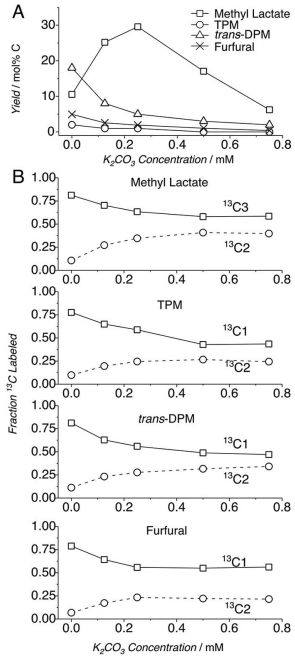

Figure 5. A) Yields of methyl lactate, TPM, *trans*-DPM, and furfural (analyzed in its dimethyl acetal form) at varying alkali-metal concentrations. B) Corresponding ^{13}C distribution at the C1 and C2 positions of methyl lactate, TPM, *trans*-DPM, and furfural dimethyl acetal (see Figure S4 for methyl glycosides). For ML, the C3 position derived from pentose C1 is shown instead of C1. All reactions were conducted with D-[1-^{13}C]-xylose (36 mg), Sn-Beta (HT) (18 mg), methanol (500 μL), and dimethyl sulfoxide (5 mg), which were heated to 160 °C for 5 min. Methanol containing 0 mM, 0.125 mM, 0.25 mM, 0.5 mM and 0.75 mM K_2CO_3, respectively, was used.

Conclusions

We have employed two independent assays to evaluate the role of additives in heterogeneous catalysis. The effects of alkali-metal salts on the activity and selectivity of Sn-Beta-catalyzed carbohydrate conversion were probed. Isotope tracking experiments show that C–C bond breakage in epimerization and retro-aldol reactions is accelerated relative to dehydration reaction pathways in the presence of alkali-metal ions. Epimeri-

ChemPubSoc Europe

CHEMSUSCHEM Full Papers

zation and retro-aldol cleavage display a similar dependence on the alkali-metal ion concentration. Kinetic experiments show that K_2CO_3 and KCl have differential effects on carbohydrate conversion, as K_2CO_3 suppresses Brønsted acid-catalyzed reactions in the formation of methyl glycosides and furanic compounds. Both K_2CO_3 and KCl are activity promoters of retro-aldol cleavage at low alkali-metal concentrations, indicating a modification of the active site by alkali-metal cations. At higher concentrations of alkali-metal salts containing basic anions, all major Sn-Beta-catalyzed pathways are deactivated. Overall, kinetic and isotope data indicate that the alkali-metal effect increases the selectivity for the formation of methyl lactate from carbohydrates by changing the catalyst active site to increase rates of carbon–carbon cleavage and—to a lesser extent—reduce rates of dehydration in kinetically controlled pathways.

Experimental Section

Reactions with isotope-labeled xylose were conducted with a Biotage Initiator+ microwave reactor in 500 μL glass reaction vials. Reactions were typically conducted with 18 mg Sn-Beta (Si/Sn = 200, hydrothermally synthesized), 36 mg [1-$^{13}C_1$]-D-xylose, 500 μL methanol and 5 mg dimethyl sulfoxide as an internal standard. Rate experiments were conducted with a Biotage Initiator+ microwave reactor in 5 mL glass reaction vials. A typical reaction was conducted with 90 mg Sn-Beta (Si/Sn = 150, post-treated), 360 mg D-xylose, 50 mg dimethyl sulfoxide as the internal standard, and 5 mL methanol, as well as alkali-metal salts at concentrations as indicated. Control experiments were conducted in the presence of alkali-metal salts but in the absence of Sn-Beta (see Figure S5).

Hydrothermally synthesized Sn-Beta (Si/Sn = 200) catalyst was prepared according to the procedure reported by Tolborg et al., employing a target Si/Sn ratio of 200.[32] The catalyst structure and composition was confirmed by inductively coupled plasma optical emission spectroscopy (ICP-OES; 0.9 wt% Sn, Si/Sn = 196), X-ray diffraction (XRD; *BEA framework), and N_2 absorption (S_{BET} = 540 $m^2 g^{-1}$, $S_{micropore}$ = 436 $m^2 g^{-1}$, V_{total} = 0.30 $mL g^{-1}$, $V_{micropore}$ = 0.22 $mL g^{-1}$, as calculated by the *t*-plot method). Post-treated Sn-Beta (Si/Sn = 150) catalyst was synthesized by a post-treatment method in accordance with the procedure reported by Hammond et al.[33] The catalyst structure and composition was confirmed by ICP-OES (1.3 wt% Sn, Si/Sn = 152), XRD (*BEA framework) and N_2 absorption (S_{BET} = 688 $m^2 g^{-1}$, $S_{micropore}$ = 555 $m^2 g^{-1}$, V_{total} = 0.43 $mL g^{-1}$, $V_{micropore}$ = 0.22 $mL g^{-1}$, as calculated by the *t*-plot method).

NMR spectra were recorded by using an 800 MHz Bruker Avance III NMR spectrometer equipped with a TCI CryoProbe and a SampleJet sample handler. Quantifications were obtained by qNMR (quantitative NMR) experiments. Response factors in two-dimensional ^1H–^{13}C HSQC NMR spectra were obtained for the analytes of interest by comparison to quantitative, integrated 1D ^{13}C spectra. These quantitative proton-decoupled 1D ^{13}C spectra were acquired with recycle delays of 60 s using a pulse sequence that employs inverse gated decoupling. By employing response factors of ^1H–^{13}C HSQC NMR experiments, far more sensitive spectra (ca. 32 times more sensitive) could be used to accurately and rapidly (20 min NMR experiment time) quantify the main reaction products. The spectra were processed by using Bruker Topspin 3.5 pl7 software using ample zero filling in all spectral dimensions.

Acknowledgements

This work was funded by the Innovation Fund Denmark (case number 5150-00023B). 800 MHz NMR spectra were recorded on the spectrometer of the NMR center at DTU supported by the Villum foundation.

Conflict of interest

The authors declare no conflict of interest.

Keywords: alkali metals · esters · heterogeneous catalysis · kinetics · zeolites

[1] E. Taarning, C. M. Osmundsen, X. Yang, B. Voss, S. I. Andersen, C. H. Christensen, *Energy Environ. Sci.* **2011**, *4*, 793 – 804.
[2] P. A. Jacobs, M. Dusselier, B. F. Sels, *Angew. Chem. Int. Ed.* **2014**, *53*, 8621 – 8626; *Angew. Chem.* **2014**, *126*, 8765 – 8770.
[3] A. Corma, S. Iborra, A. Velty, *Chem. Rev.* **2007**, *107*, 2411 – 2502.
[4] M. J. Climent, A. Corma, S. Iborra, *Green Chem.* **2011**, *13*, 520 – 540.
[5] J. J. Bozell, G. R. Petersen, *Green Chem.* **2010**, *12*, 539 – 554.
[6] R. De Clercq, M. Dusselier, B. F. Sels, *Green Chem.* **2017**, *19*, 5012 – 5040.
[7] E. Taarning, S. Saravanamurugan, M. S. Holm, J. Xiong, R. M. West, C. H. Christensen, *ChemSusChem* **2009**, *2*, 625 – 627.
[8] M. Moliner, Y. Román-Leshkov, M. E. Davis, *Proc. Natl. Acad. Sci. USA* **2010**, *107*, 6164 – 6168.
[9] S. Saravanamurugan, A. Riisager, E. Taarning, S. Meier, *ChemCatChem* **2016**, *8*, 3107 – 3111.
[10] M. S. Holm, S. Saravanamurugan, E. Taarning, *Science* **2010**, *328*, 602 – 605.
[11] F. de Clippel, M. Dusselier, R. Van Rompaey, P. Vanelderen, J. Dijkmans, E. Makshina, L. Giebeler, S. Oswald, G. V. Baron, J. F. M. Denayer, P. P. Pescarmona, P. A. Jacobs, B. F. Sels, *J. Am. Chem. Soc.* **2012**, *134*, 10089 – 10101.
[12] M. Dusselier, P. Van Wouwe, A. Dewaele, E. Makshina, B. F. Sels, *Energy Environ. Sci.* **2013**, *6*, 1415 – 1442.
[13] S. Van de Vyver, C. Odermatt, K. Romero, T. Prasomsri, Y. Román-Leshkov, *ACS Catal.* **2015**, *5*, 972 – 977.
[14] M. Dusselier, P. Van Wouwe, F. de Clippel, J. Dijkmans, D. W. Gammon, B. F. Sels, *ChemCatChem* **2013**, *5*, 569 – 575.
[15] H. S. Chen, A. Wang, H. Sorek, J. D. Lewis, Y. Román-Leshkov, A. Bell, *ChemistrySelect* **2016**, *1*, 4167 – 4172.
[16] S. Tolborg, S. Meier, I. Sádaba, S. G. Elliot, S. K. Kristensen, S. Saravanamurugan, A. Riisager, P. Fristrup, T. Skrydstrup, E. Taarning, *Green Chem.* **2016**, *18*, 3360 – 3369.
[17] S. G. Elliot, C. Andersen, S. Tolborg, S. Meier, I. Sadaba, A. E. Daugaard, E. Taarning, *RSC Adv.* **2017**, *7*, 985 – 996.
[18] E. Nikolla, Y. Román-Leshkov, M. Moliner, M. E. Davis, *ACS Catal.* **2011**, *1*, 408 – 410.
[19] S. Tolborg, I. Sádaba, C. M. Osmundsen, P. Fristrup, M. S. Holm, E. Taarning, *ChemSusChem* **2015**, *8*, 613 – 617.
[20] M. S. Holm, I. Sádaba, S. Tolborg, C. M. Osmundsen, E. Taarning, Patent No. WO2015024875, **2015**.
[21] R. Bermejo-Deval, M. Orazov, R. Gounder, S. J. Hwang, M. E. Davis, *ACS Catal.* **2014**, *4*, 2288 – 2297.
[22] S. Li, T. Josephson, D. G. Vlachos, S. Caratzoulas, *J. Catal.* **2017**, *355*, 11 – 16.
[23] W. R. Gunther, Y. Wang, Y. Ji, V. K. Michaelis, S. T. Hunt, R. G. Griffin, Y. Román-Leshkov, *Nat. Commun.* **2012**, *3*, 1109.
[24] R. Otomo, R. Kosugi, Y. Kamiya, T. Tatsumi, T. Yokoi, *Catal. Sci. Technol.* **2016**, *6*, 2787 – 2795.
[25] T. Tatsumi, K. A. Koyano, Y. Shimizu, *Appl. Catal. A* **2000**, *200*, 125 – 134.
[26] C. B. Khouw, M. E. Davis, *J. Catal.* **1995**, *151*, 77 – 86.
[27] S. G. Elliot, S. Tolborg, I. Sadaba, E. Taarning, S. Meier, *ChemSusChem* **2017**, *10*, 2990 – 2996.
[28] S. M. Ahmed, *Can. J. Chem.* **1966**, *44*, 1663 – 1670.

[29] S. A. Khan, R. Rehma, M. M. Khan, *Waste Manage.* **1995**, *15*, 271 – 282.
[30] W. R. Gunther, PhD. Thesis, Massachusetts Institute of Technology, **2015**.
[31] S. G. Elliot, E. Taarning, R. Madsen, S. Meier, *ChemCatChem* **2018**, *10*, https://doi.org/10.1002/cctc.201701861.
[32] S. Tolborg, A. Katerinopoulou, D. D. Falcone, I. Sadaba, C. M. Osmundsen, R. J. Davis, E. Taarning, P. Fristrup, M. S. Holm, *J. Mater. Chem. A* **2014**, *2*, 20252 – 20262.
[33] C. Hammond, S. Conrad, I. Hermans, *Angew. Chem. Int. Ed.* **2012**, *51*, 11736 – 11739; *Angew. Chem.* **2012**, *124*, 11906 – 11909.

Manuscript received: December 21, 2017
Revised manuscript received: January 29, 2018
Accepted manuscript online: February 26, 2018
Version of record online: March 13, 2018

CHEMISTRY & SUSTAINABILITY
CHEMSUSCHEM
ENERGY & MATERIALS

Supporting Information

Effects of Alkali-Metal Ions and Counter Ions in Sn-Beta-Catalyzed Carbohydrate Conversion

Samuel G. Elliot,[a] Søren Tolborg,[b] Robert Madsen,[a] Esben Taarning,*[b] and Sebastian Meier*[a]

cssc_201702413_sm_miscellaneous_information.pdf

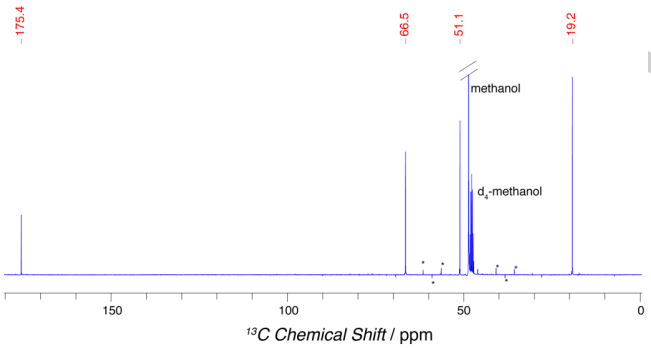

Figure S1. ^{13}C NMR Spectrum after a stability test of methyl lactate. Conditions: 18 mg Sn-Beta (HT), 36 mg DL-methyl lactate and 500 µL methanol reacted at 160 °C for 2 hours. No degradation is observed. The signals around 50 ppm are from the methanol solvent, d4 methanol lock substance and from spectral artefacts with varying phase (strongest artefacts labelled with asterisks). Signals of the intact methyl lactate are labelled by their chemical shift.

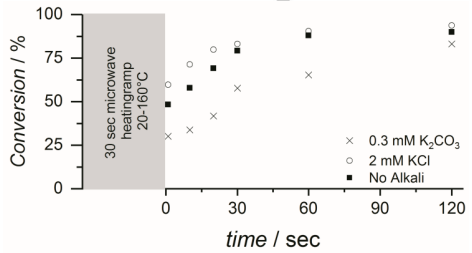

Figure S2. Substrate conversion during the first 2 minutes at 160 °C. 90 mg Sn-Beta (PT), 360 mg D-xylose and 5 mL methanol reacted at 160 °C.

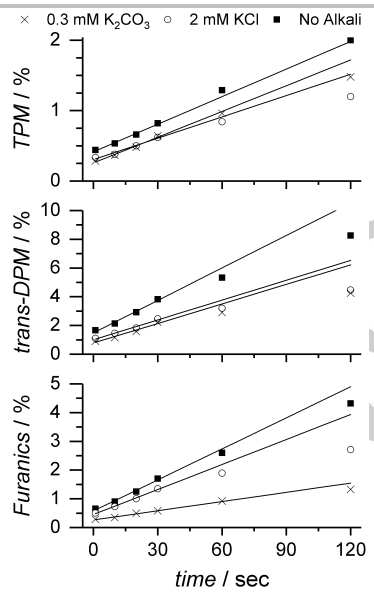

Figure S3. Initial rate experiments of methyl 2,4,5-trihydroxy-pentanoate (TPM, Figure 1, 3-deoxy esters) and methyl 2,5-dihydroxy-3-pentenoate (trans-DPM, Figure 1, 3,4-dideoxy esters). Signal areas were converted to molar yields by a quantitative NMR approach. A particularly large negative effect of the presence of alkali is observed for the rate of formation of *trans*-DPM, and slightly less so for TPM.

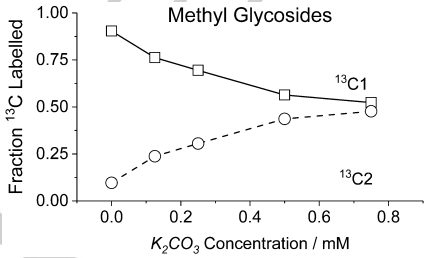

Figure S4. Change in relative ^{1}H-^{13}C HSQC intensities at the C1 and C2 positions for the epimers methyl xyloside and methyl lyxoside in the experiment of Figure 6. The sum of signals for the C1 positions is compared to sum signals at the C2 position. C1-C2 exchange exhibits the same trend in glycosides as for the products of Figure 6. Exact ^{13}C distributions as in the main text Figure 6 were not derived due to the error associated with extensive signal overlap in alcohol regions of the one-dimensional quantitative ^{13}C-NMR spectra.

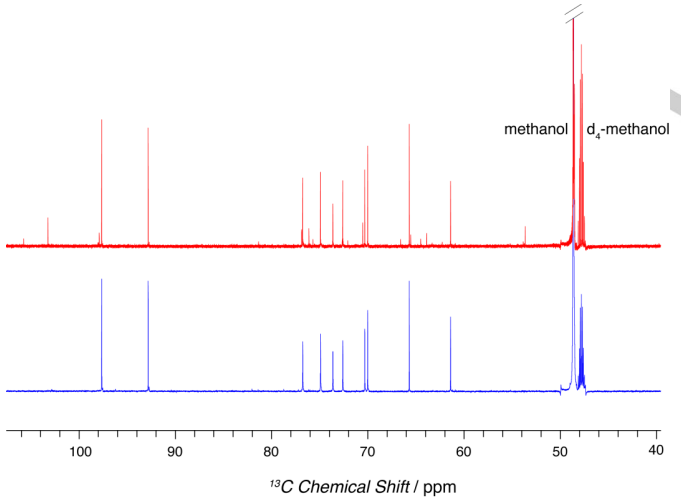

Figure S5. ^{13}C NMR spectra for control experiments of the effect of alkali salts in the absence of Sn-Beta catalyst. Conditions: 0.3 mM K_2CO_3 (red) or 2.0 mM KCl (blue), 360 mg D-xylose, no Sn-Beta, 5 min at 160 °C. Control reaction with KCl shows only alpha/beta-D-xylopyranose, indicative of no conversion. Use of K_2CO_3 shows vastly predominant alpha/beta-D-xylopyranose with minor formation of isomeric carbohydrates.

Table S1. Optimisation of methyl lactate yield from a Sn-Beta(PT) catalyst by addition of K_2CO_3.

	Methyl Lactate Yield	Conversion
	[mol% carbon]	
0.0 mM K_2CO_3	1.14	90.4
0.15 mM K_2CO_3	6.59	74.2
0.3 mM K_2CO_3	10.97	60.3
0.5 mM K_2CO_3	9.42	58.1

Reactions were conducted with 360 mg D-[1-^{13}C]-xylose, 90 mg Sn-Beta (PT), 5 mL methanol and 5 mg dimethyl sulfoxide, which were heated to 120°C for 1 hour. Methanol containing K_2CO_3 was used to obtain the desired concentrations.

Table S2. Optimisation of methyl lactate yield from a Sn-Beta(PT) catalyst by addition of KCl.

	Methyl Lactate Yield	Conversion
	[mol% carbon]	
0.0 mM KCl	7.9	95
0.3 mM KCl	14.7	96
0.6 mM KCl	20.1	96
0.75 mM KCl	20.9	97
1.0 mM KCl	22.9	97
1.5 mM KCl	23.7	97
2.0 mM KCl	25.3	97
3.0 mM KCl	24.4	97
4.7 mM KCl	24.9	97

Reactions were conducted with 360 mg D-[1-^{13}C]-xylose, 90 mg Sn-Beta (PT), 5 mL methanol and 5 mg dimethyl sulfoxide, which were heated to 160°C for 2 hours. Methanol containing KCl was used to obtain the desired concentrations.

Table S3. Yields of major reaction products from Sn-Beta (HF) catalysed conversion of xylose with increasing concentration of alkali ions.

	Furfural*	Methyl lactate	*trans*-DPM	TPM
	Yield [mol% carbon]			
0 mM K_2CO_3	5.0	10.5	17.4	2.7
0.125 mM K_2CO_3	2.6	25.2	8.0	1.6
0.25 mM K_2CO_3	1.9	29.6	5.1	1.1
0.5 mM K_2CO_3	1.0	17.1	2.9	0.7
0.75 mM K_2CO_3	0.4	6.2	1.9	0.4

Reactions were conducted with 36 mg D-[1-^{13}C]-xylose, 18 mg Sn-Beta (HF), 500 µL methanol and 5 mg dimethyl sulfoxide, which were heated to 160°C for 5 min. Methanol containing 0 mM, 0.125 mM, 0.25 mM, 0.5 mM and 0.75 mM K_2CO_3, respectively, was used.*Analysed in its dimethyl acetal form

Topics in Catalysis
https://doi.org/10.1007/s11244-019-01131-y

ORIGINAL PAPER

Response Factors Enable Rapid Quantitative 2D NMR Analysis in Catalytic Biomass Conversion to Renewable Chemicals

Samuel G. Elliot[1] · Irene Tosi[1] · Anders Riisager[1] · Esben Taarning[2] · Sebastian Meier[1]

Abstract
Carbohydrate conversion offers access to a variety of chemicals with diverse functionalities. An accurate analysis of the multiple products in post-reaction material is indispensable for enabling good atom economy in biorefining. A certain need for reconsidering current analytical approaches to chemocatalytic biomass conversion is witnessed by the often poor carbon balances that are reported for carbohydrate conversion processes. Carbohydrate conversion usually includes isomerization and/or dehydration, therefore analytical approaches that are suitable for the distinction and concurrent quantification of isomers are desirable for developing sustainable processes towards known and new chemicals. Quantitative 1D NMR spectroscopy can be used to determine absolute concentrations in the absence of purified reference compounds and can thereafter be used to obtain response factors in other analytical methods resolving the compounds of interest. Here, we show that this approach is applicable for obtaining response factors relative to an internal standard for rapid, highly resolved 2D NMR spectra at natural isotopic abundance. Following calibration, this approach provides a limit of quantification in the order of 0.8 mM within an experiment time of a few minutes. The approach is particularly beneficial for the quantification of compounds at low concentrations, for instance in initial rate experiments, and for the quantification of low populated reaction intermediates.

Keywords Biomass · Catalysis · qNMR · Quantitative analysis · Reference standard · Response factor

1 Introduction

The current trajectories of global population growth and of natural resource consumption are unsustainable, as many natural resources are poised to deplete within the next few generations. Hence, sustainable means of producing known and new chemicals to sustain our materials- and energy-demanding lifestyles are needed. In this shift to alternative industries that rely more on renewables and less on petroleum refining, biomass is a promising feedstock [1, 2]. Biomass conversion offers access to a variety of chemicals with diverse functionalities, for instance through the use of solid acid catalysts such as zeolites [3, 4].

Accurate qualitative and quantitative analysis of the multiple products in post-reaction material is indispensable for the development of biorefinery technology. The conversion of biomass often includes the isomerization or dehydration of carbohydrates [3, 5–10]. Therefore, analytical approaches that are suitable for the distinction and concurrent quantification of isomers (such as monosaccharides and their respective dehydration products) are poised to be particularly valuable for the analysis of biomass conversion products, and thus for aiding sustainable processes towards known and new chemicals. A certain need for reconsidering analytical approaches to chemocatalytic biomass conversion is witnessed by the often poor yields and low carbon balances that are reported for carbohydrate conversion processes, with little effort to identify and quantify the byproduct "dark matter" in the mixture [11].

NMR spectroscopy has been used in qualitative and quantitative analysis for more than five decades [12].

Electronic supplementary material The online version of this article (https://doi.org/10.1007/s11244-019-01131-y) contains supplementary material, which is available to authorized users.

✉ Samuel G. Elliot
sgiel@kemi.dtu.dk

✉ Sebastian Meier
semei@kemi.dtu.dk

[1] Department of Chemistry, Technical University of Denmark, Kemitorvet, 2800 Kgs. Lyngby, Denmark

[2] Haldor Topsøe A/S, Haldor Topsøes Alle 1, 2800 Kgs. Lyngby, Denmark

Published online: 14 January 2019

Recent improvements in instrumentation enable the determination of compound structures also in complex product mixtures [10, 13, 14]. At the same time, the quantitative use of NMR (qNMR) has gained importance in metabolic studies [15–18], natural products research [19, 20], food analysis [21, 22] and pharmaceutical research [18, 23–25]. Compound identification and quantification in mixtures has gained much attention in biocatalysis, while applications in chemocatalysis have so far remained sparse [26–29]. Wider implementation of NMR methodology in chemocatalysis could be attractive, considering that both the substrate (mostly carbohydrates) and the interest in catalyst function and dysfunction bear close resemblance to metabolic and chemocatalytic processes.

Recently, we have shown that quantitative ^{13}C NMR permits the identification of novel chemicals, and optimization of their formation by solvent variation in the stannosilicate catalyzed conversion of carbohydrates [14]. Owing to its superior resolution over ^{1}H NMR, ^{13}C NMR has an important role to play in the analysis of complex mixtures containing chemically similar compounds. This approach permits improved determination of carbon balances and of factors affecting product distribution upon biomass conversion.

Quantitative ^{13}C NMR spectroscopy suffers from mediocre sensitivity due to the low natural abundance and the lower magnetogyric ratio of ^{13}C as compared especially to ^{1}H. The mediocre sensitivity of ^{13}C NMR results in lengthy experiment times that challenge high throughput applications of the methodology. In contrast, faster and more sensitive quantitative ^{1}H NMR methods result in much more congested NMR spectra as the ^{1}H NMR chemical shift range is approximately 20-fold smaller than the ^{13}C chemical shift range. In addition, ^{1}H signals are split into multiplets due to scalar coupling to other protons in the same molecule, thus further congesting the ^{1}H NMR spectrum. Workarounds to these problems can be achieved by indirect detection of ^{13}C signals through highly resolved two-dimensional ^{1}H–^{13}C HSQC spectra, which allow for rapid quantitative analysis of complex post-reaction material when response factors are employed.

2 Results and Discussion

A schematic overview of the rational employed in this study is shown in Scheme 1. ^{1}H–^{13}C HSQC spectra were used for compound quantification upon an initial determination of response factors in the ^{1}H–^{13}C HSQC relative to quantitative ^{13}C NMR spectra. To this end, normalization to a stable internal quantification standard was performed. Two-dimensional ^{1}H–^{13}C HSQC spectra were subsequently optimized for high throughput, achieving a limit of quantification (LOQ) in the order of 0.8 mM with only 5 min of experiment time per sample. When employing a 0.4 M carbohydrate feedstock, this accuracy translates to a LOQ of ≤0.2 mol% carbon. Such high accuracy can be beneficial in various settings, such as initial rate experiments under low conversion or in the tracking of pathway intermediates [26, 27].

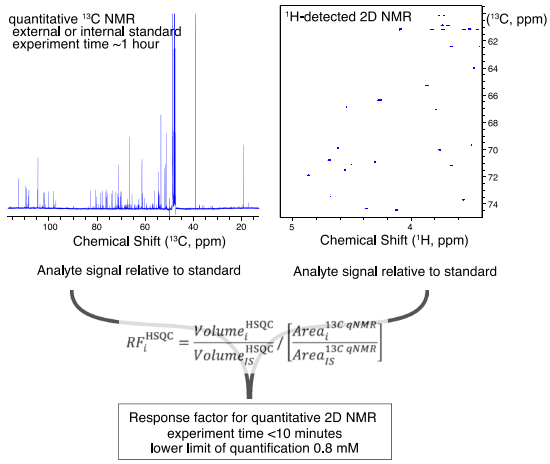

Scheme 1 Strategy for the rapid and accurate quantitative analysis of reaction mixtures using response factors in 2D NMR

2.1 Internal Standards

Internal or external standards are employed in qNMR to obtain highly accurate and precise results [25, 30]. Internal standardization removes many experimental uncertainties and is considered superior to external standardization [30, 31]. The internal standards can be added either prior to biomass conversion or subsequent to the reaction, each approach having advantages and disadvantages. Many biomass reactions are conducted above the boiling point of the solvent, which is typically low in order to expedite subsequent purification steps. Higher reaction temperatures imply possible solvent boil-off with concomitant changes to analyte concentrations, thus arguing for addition of internal standard into the reaction medium prior to the reaction. This approach was therefore employed here.

Special precautions have to be taken in to account for the use of internal standards during the reaction: the standards should not decompose at high temperatures (often between 100 and 200 °C) and should not contain acidic or other functional groups that may affect the reaction system. Prospective qNMR standard substances with Brønsted acidic or basic sites were excluded from the study (for instance the commonly employed standard maleic acid). Beyond being chemically inert, suitable standards yield strong ^{13}C signals at low concentration that do not overlap with alcoholic and olefinic carbon positions that are common in carbohydrate derived products. To this avail, a minimal number of NMR signals are desirable, simplifying analysis and reducing risk of spectral overlap. Strong signals can be warranted by the presence of protonated carbons with relaxation times comparable to those of carbons in the analyte mixture and by symmetric molecules, where several magnetically equivalent carbons contribute the signal. For instance, dimethyl sulfoxide and dimethyl sulfone contain two equivalent carbons, thus doubling signal intensity, while mesitylene contains three sets of three equivalent carbons and 1,4-dioxane contains four equivalent carbons thus increasing the signal intensity (Scheme 2).

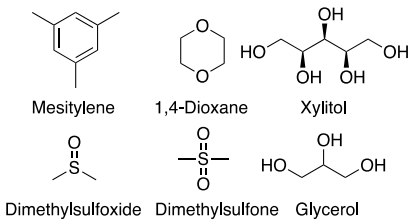

Scheme 2 Structures of selected standard compounds tested herein

In addition, a high boiling point was deemed preferable to ease preparation and reduce risk of material loss during the reaction. Finally, reference compounds should be available in high purity at low cost, be non-hazardous and be miscible with industrially relevant (and especially green) solvents [24, 25]. Based on these considerations, the standards of Scheme 2 and Table 1 were selected.

The miscibility or solubility of the prospective standard compounds was assessed with water, methanol, chloroform and dimethyl sulfoxide as solvents (Supplementary Table S1). Xylitol showed limited solubility in all solvents except water and was not pursued further. In contrast, mesitylene was very poorly miscible with water, but miscible with the other four solvents. Mesitylene, 1,4-dioxane, dimethyl sulfoxide, dimethyl sulfone and glycerol were thus all deemed potentially suitable primary standards for quantitative NMR.

2.2 Reaction Performance

A test reaction was selected to evaluate the stability of internal standards in the presence of Lewis acidic zeolite Sn-Beta. The test reaction was based on previous work within biomass conversion and was comprised of 8 wt% xylose and 2 wt% Sn-Beta zeolite catalyst in methanol [32]. The mixture was reacted at 160 °C for up to 24 h in order to evaluate the stability of internal quantification standards on this timescale. Full conversion was already achieved after 1–2 h. Figure 1 shows the recovery of the standards with reasonable solubility, i.e. mesitylene, 1,4-dioxane, dimethyl sulfoxide (DMSO), dimethyl sulfone ($DMSO_2$) and glycerol. Recovery indicated that all compounds were stable over 2 h under the reaction conditions, while DMSO showed degradation on longer timescales. Dioxane, $DMSO_2$ mesitylene and glycerol thus appeared particularly suitable as internal standards in the presence of Lewis acidic catalysts for prolonged reaction times. For short reaction times, as those required for full

Table 1 Overview of selected internal standards and their performance on conditions 1 and 2

Entry	Internal Standard	B.P. [°C]	Number of NMR signals	
			^{1}H[a]	^{13}C
1	Mesitylene	164	2	3
2	1,4-dioxane	101	1	1
3	Dimethyl sulfoxide	189	1	1
4	Dimethyl sulfone	*107*[b]	1	1
5	Glycerol	290	3	2
6	Xylitol	*94*[b]	4	3

[a]Considering only protons attached to carbon

[b]Melting point

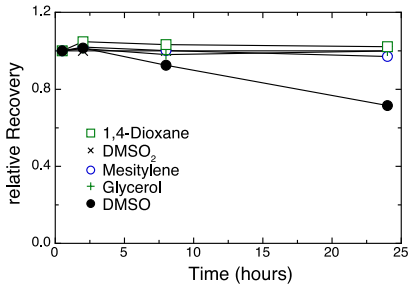

Fig. 1 Stability of internal standards over time. The recovery of NMR signal for five compounds is displayed after 0.5, 2, 8, and 24 h

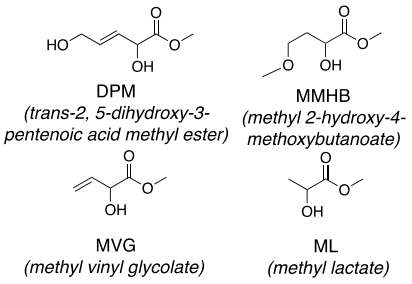

Scheme 3 Selection of major products from Lewis acid catalyzed conversion of xylose, employed for the procedures in this work

conversion in our test reaction, all of the selected reference standards appeared suitable and sufficiently stable as internal standards.

2.3 Determination of 2D NMR Responses Relative to 1D qNMR

Biomass conversion can lead to new chemicals that do not exist as commercial compounds for the determination of response factors in analyses. Quantitative 1D NMR analyses can be used to determine the amounts of chemicals without the need for purified and isolated compounds, as concentrations can be determined relative to a chemically non-identical standard [33]. The signal response in quantitative 1D NMR (e.g. ^{13}C NMR) is proportional to the concentration of atoms generating the signal and is therefore identical even for different compounds. Quantitative 1D NMR spectra have thus previously been used in order to normalize chromatographic analyses in instances where purified and isolated reference compounds are not available [33]. NMR spectroscopy, however, offers an even more versatile toolbox of multi-dimensional spectra with advantageous spectral resolution and sensitivity. ^{1}H–^{13}C HSQC spectra, as are employed here, provide roughly 30-fold higher sensitivity than ^{13}C NMR spectra of same duration and additional resolution due to the acquisition of two spectral dimensions (Supplementary Table S2).

Here, we acquired quantitative ^{13}C NMR spectra and ^{1}H–^{13}C HSQC spectra on a reaction mixture, derived from the aforementioned Sn-Beta catalysed conversion of xylose in methanol at 160 °C. Four products were selected as targets for proof of principle (Scheme 3) only one of which was readily available commercially. The targets all possess secondary alcohols, producing signals within a similar spectral region. Signals in the secondary alcohol region in a ^{1}H–^{13}C HSQC (of 24 min duration) are displayed in Fig. 2. Corresponding reaction products and their chemical shift assignments had previously been identified using various two-dimensional NMR spectra on intact reaction mixtures [10, 14, 32].

Following identification of the signals as in Fig. 2, the signal areas from quantitative ^{13}C NMR spectra can be employed to quantify the target compounds. Provided that the amount of internal standard (IS) is known, a compound i can be quantified using Eq. 1, where N is the number of carbons in the molecule producing the signal, and c_i and c_{IS} are the concentrations of analyte i and internal standard, respectively.

$$\frac{\mathrm{Area}_{\mathrm{i}}^{^{13}CqNMR}/N_{i}^{Carbon}}{\mathrm{Area}_{\mathrm{IS}}^{^{13}CqNMR}/N_{IS}^{Carbon}} = \frac{c_i}{c_{IS}}. \quad (1)$$

Signal areas relative to the internal standard (DMSO) in quantitative ^{13}C NMR spectra (i.e. analyte concentrations)

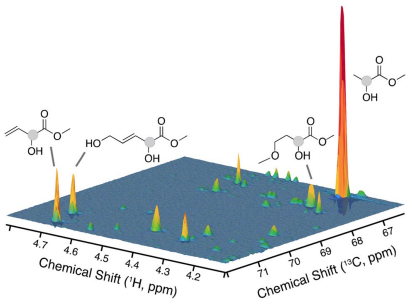

Fig. 2 The hydroxyl region of the ^{1}H–^{13}C HSQC spectra with a selection of identified products indicated

were correlated to the corresponding signal volumes in ^{1}H–^{13}C HSQC spectra, as shown in Fig. 3, yielding compound specific response factors based on the C2–H2 group. The response factor RF_i^{2DNMR} of a selected signal in compound *j* is here defined as:

$$RF_i^{\mathrm{HSQC}} = \frac{Volume_i^{\mathrm{HSQC}}}{Volume_{IS}^{\mathrm{HSQC}}} \Big/ \left[\frac{Area_i^{13C\ qNMR}}{Area_{IS}^{13C\ qNMR}}\right] \quad (2)$$

In plots of HSQC signal volumes versus quantitative ^{13}C NMR signal areas each relative to the standard, the response factors thus simply correspond to the slope. In order to assess the accuracy of response factor determinations, the above-mentioned reaction was conducted for different durations to achieve a variety of concentrations for the target compounds. Linear regressions yielded Pearson correlation coefficients above 0.997 for each of the four displayed determinations (Fig. 3), demonstrating excellent consistency of 1D and 2D NMR quantifications.

By substitution of Eq. 2 into Eq. 1, an equation for determining the concentration by ^{1}H–^{13}C HSQC signal volumes instead of quantitative 1D ^{13}C NMR is obtained:

$$c_i = \frac{\mathrm{Volume}_i^{HSQC}}{\mathrm{Volume}_{\mathrm{IS}}^{HSQC}} \times c_{IS} \times \frac{N_{IS}^{Carbon}}{N_i^{Carbon}} \Big/ RF_i^{HSQC} \quad (3)$$

As ^{1}H–^{13}C HSQC spectra are more sensitive than quantitative ^{13}C NMR spectra, Eq. 3 permits more accurate quantification of the compound *i* and faster determinations than was possible by ^{13}C NMR alone (Table S2 indicates tenfold lower limit of detection at 11-fold faster analyses). Conversion of concentrations to carbon yields requires qualitative knowledge of the chemical identity of compounds *i*. Identification of the compounds can be performed in unpurified reaction mixtures using spectra of reference compounds [10, 34] or through multidimensional assignment spectra recorded with high-field NMR [10, 13, 14].

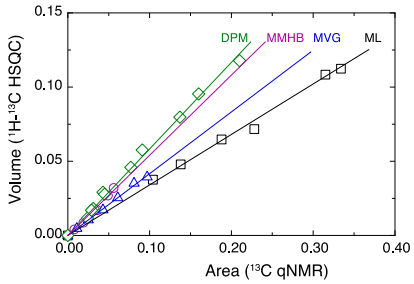

Fig. 3 Correlations between integrals from ^{1}H–^{13}C HSQC normalised to the internal standard (DMSO) integral and quantitative ^{13}C NMR integrals normalised to internal standard. Correlations and linear regressions are shown for four selected products of the Sn-Beta catalysed xylose conversion in methanol

2.4 Variation of Response Factors

Various factors affect the signal response in multidimensional NMR spectra. Magnetization transfer can vary due to variable scalar coupling constants and loss of transverse magnetization during the transfer can likewise vary between molecules. Both of these factors are expected to play very minor roles for the response factors determined in the experiments of Fig. 3. Scalar $^{1}J_{C2H2}$ couplings were determined for α-hydroxy esters and showed a very narrow distribution of couplings constants in the analogous structural motifs (variation between 146.0 and 146.7 Hz, Fig. 4a). Loss of transverse magnetization during the transfer step of few milliseconds in ^{1}H–^{13}C HSQC is likewise expected to be negligible.

The ^{1}H–^{13}C HSQC spectra were recorded with a short inter-scan recycle delay in order to minimize the experiment time of the spectra. Accordingly, response factors show size dependence with higher response for the slightly larger compounds, as longitudinal (T_1) relaxation in these compounds is more complete during the inter-scan delay. The predominant effect of inter-scan T_1 relaxation on differential response factors was probed by acquiring long HSQC spectra with 15 s instead of 1 s inter-scan relaxation delays. Response factors in these experiments were more homogeneous than for experiments using a 1 s recycle delay (Fig. 5). Response factors generally approached a value near 0.33 for longer recycle delays, consistent with the transfer of polarization to carbon from three protons in the DMSO methyl group, but from only one proton in the α-hydroxy ester C2–H2 group. These findings indicate that response factors may be predicted from molecular weight, while the molecular weight of unknown compounds may be estimated from the response factor (Fig. 4b). Alternatively, the response factor for different compounds can be equalised, through suitable adjustments to the 2D NMR experiment, if desired.

2.5 Accelerated Data Acquisition

The results above showed that upon calibration with few samples, responses in ^{1}H–^{13}C HSQC spectra can be used to quantitatively determine mixture composition in biomass conversion with sensitivity and throughput that is superior to the use of quantitative ^{13}C NMR. The use of response factors permits the rapid acquisition of two-dimensional spectra with short inter-scan relaxation delays. Two-dimensional spectra can be further accelerated by recent methodological

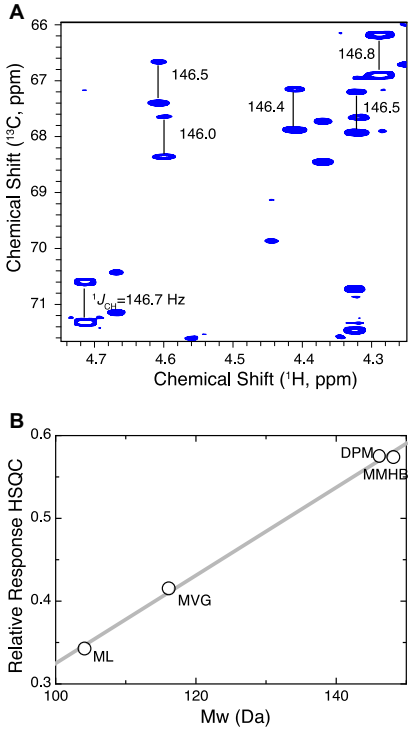

Fig. 4 **a** Contour plot of a ^{1}H–^{13}C-HSQC spectrum recorded without ^{1}H decoupling during the ^{13}C evolution time. Only small variation (and highly similar ^{1}H–^{13}C magnetization transfer efficiency) exists for different α-hydroxy esters. **b** Response factor as a function of molecular weight when using inter-scan recycle delays of 1 s

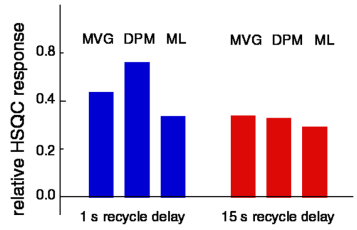

Fig. 5 ^{1}H–^{13}C HSQC response factors for the indicated α-hydroxyesters when using inter-scan recycle delays of 1 s and 15 s, respectively. Complete ^{1}H relaxation leads to more homogeneous response factors near 0.33 relative to DMSO

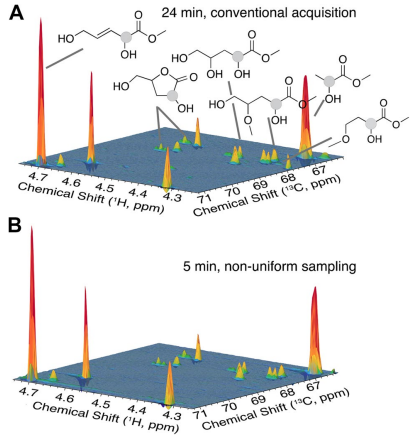

Fig. 6 ^{1}H–^{13}C HSQC spectra obtained by a conventional (**a**) method employing 24 min acquisition time, and a non-uniform sampling method (**b**) using 5 min acquisition time

advances permitting data acquisition through sampling of only a fraction of the data points that were conventionally acquired. Spectra acquired in the conventional manner and through the non-uniform sampling of the ^{13}C dimension are displayed in Fig. 6. The spectrum in Fig. 6b recorded only 20% of the data points that were acquired in Fig. 6a and hence could be acquired in only 5 min.

Spectral quality in the spectrum using non-uniform sampling was still acceptable without any disturbance to signal volumes or introduction of overlapping artefacts. The LOQ was only marginally affected, increasing from 0.75 mM in the regular 24 min experiment to 0.83 mM using non-uniform sampling (Supplementary Table S2). Thus, accurate quantitative determinations can be obtained with minimal sample preparation and within few minutes, a timescale competitive with most other commonly employed analysis methods.

2.6 Validation

To validate the demonstrated methods, a single reference sample of methyl lactate (9.2 mg of 98% nominal

purity, 0.087 mmol) in methanol was prepared in the presence of $DMSO_2$ as internal standard. A quantitative ^{13}C NMR spectrum and a $^{1}H–^{13}C$ HSQC NMR spectrum were recorded to determine the response factor of methyl lactate relative to $DMSO_2$ in the HSQC spectrum. Subsequently, four samples were prepared of varying amounts of methyl lactate. Amounts of methyl lactate were determined by weighing with an analytical balance. Samples were prepared by dissolving the four samples in methanol solution in the presence of $DMSO_2$. Quantitation with $^{1}H–^{13}C$ HSQC NMR was performed using the response factor calculated with a single independent calibration sample and was compared to gravimetric determinations (Fig. 7a) and to quantitation by qNMR (Fig. 7b). Linear regression between HSQC and gravimetric determinations yielded a Pearson correlation coefficient of 0.9995 and a slope of 0.998. Linear regression between HSQC and quantitative ^{13}C NMR determinations yielded a Pearson correlation coefficient of 0.9997 and a slope of 1.016. Overall, comparison of the HSQC determinations using response factors with gravimetric and quantitative NMR determination show excellent consistency.

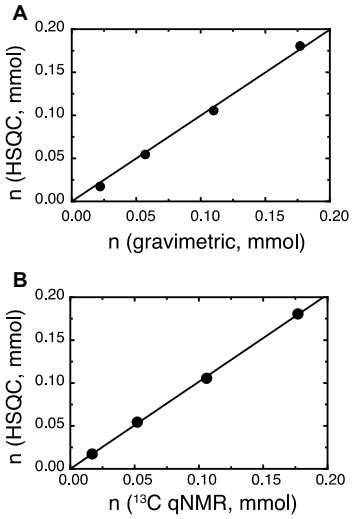

Fig. 7 Comparison of methyl lactate amounts determined by $^{1}H–^{13}C$ HSQC with gravimetric analysis (**a**) and with quantitative ^{13}C NMR analysis (**b**)

3 Conclusion

The cost and atom economy of sustainable processes using biomass substrates depend on the efficient identification, quantification and exploitation of valuable chemicals in the post-reaction material. Where pure reference samples of new chemicals are not commercially available, 1D qNMR is a suitable method for the determination of concentrations, as the same number of nuclei in different chemical compounds produces equivalent signals. Hence, 1D qNMR spectra can be used to determine absolute concentrations in the absence of the purified reference compounds and can thereafter be used to obtain response factors in other analytical methods resolving the compounds of interest.

Here, we have shown that this approach is applicable for obtaining response factors relative to an internal standard for more sensitive and better resolved 2D NMR spectra. Following calibration, these 2D NMR spectra can be used to analyse samples within an experiment time of a few minutes. The higher sensitivity provided by 2D NMR spectra relative to 1D NMR spectra can be particularly beneficial for the identification of compounds at low concentrations, for instance in initial rate experiments, and for the quantification of low populated reaction intermediates.

The approach described herein relies on a correct quantification by 1D qNMR, while the subsequent 2D NMR spectrum merely needs to be acquired in a reproducible manner. The approach is applicable to analytes, where one of the CH groups yields a non-overlapped ^{13}C NMR signal in the reaction mixture. This constraint has not resulted in a practical limitation in the reaction mixtures studied herein. Uncertainties in the acquisition of qNMR reference spectra have been described [31, 35], where internally standardized spectra have less sources of uncertainty than externally standardized spectra [31]. The residual uncertainties that have to be taken into account include weighing uncertainties of the internal standards as well as its purity, including for instance water content, and potential degradation of the internal standards. Notably, these uncertainties in the amount of internal standard will elicit a relative error of determination.

In summary, the referencing of sensitive and rapid quantitative NMR spectra to quantitative one-dimensional spectra permits screening biomass conversion reaction at attractive throughput rates and high chemical detail.

4 Materials and Methods

4.1 Sample Preparation

Test reactions were conducted as previously described [14]. NMR samples were prepared by rapid cooling of the reaction vessel to room temperature, removal of the Sn-Beta catalyst by filtration through a 0.4 µm syringe filter and addition of 50 µl d4-methanol (Sigma Aldrich) as NMR lock substance to 500 µl of the post-reaction material.

4.2 NMR Spectroscopy

All NMR spectra were acquired at 25 °C on a Bruker Avance III 800 MHz NMR instrument equipped with a TCI Cryo-Probe. Quantitative one-dimensional ^{13}C NMR spectra were acquired by acquiring 64 k complex data points of the ^{13}C signal with a spectral width of 239 ppm, thus sampling an acquisition time of 1.36 s for the ^{13}C free induction decay. 128 scans were acquired with an inter-scan recycle delay of 60 s. Inverse gated coupling was applied only during the acquisition period to avoid differential ^{13}C signal enhancements through polarization transfer from ^{1}H to ^{13}C. ^{13}C T_1 relaxation times were probed by the inversion recovery method in order to validate that a recycle delay of 30 s suffices to allow return of the magnetization to its equilibration for quantitative determinations of protonated carbon atoms.

Two-dimensional ^{1}H–^{13}C HSQC spectra were recorded as data matrices of 1024 × 300 complex data points and a spectral width of 9 and 30 ppm in the ^{1}H and ^{13}C dimensions, respectively. An inter-scan recycle delay of 1 s was employed. This experiment sampled the free induction decay for 142 ms in the ^{1}H and for 50 ms in the ^{13}C dimension, respectively. A relatively narrow spectral width in the ^{13}C dimension (55–85 ppm) was employed to rapidly achieve good spectral resolution in the ^{13}C dimension as described previously [21, 36, 37]. Analyte signals and reference compound signals of interest are subject to spectral aliasing if their ^{13}C chemical shifts occur outside the narrow ^{13}C NMR spectral width and appear at observed positions $\delta^{13}C_{obs} = \delta^{13}C \pm n * SW$, where n is an integer and SW is the ^{13}C spectral width of the 2D NMR spectrum. ^{1}H–^{13}C HSQC NMR spectra were acquired within 24 min of experiment time. Non-uniform sampling of the indirect dimension [38] was subsequently used to accelerate data acquisition of the 2D NMR spectra. Spectra of acceptable quality were obtained with sampling of 20% of the data points in the indirect dimension, amounting to a time requirement for acquisition of 2D ^{1}H–^{13}C HSQC spectra on post-reaction samples of 5 min per sample.

A 2D ^{1}H–^{13}C HSQC spectrum without decoupling in the ^{13}C dimension was acquired to probe the variation of $^{1}J_{CH}$ coupling constants at the C2-position of α-hydroxy esters, showing a very narrow distribution of $^{1}J_{CH}$ values (146.0–146.8 Hz) with negligible influence on 2D NMR response factors. A 2D ^{1}H–^{13}C HSQC NMR spectrum with an inter-scan delay of 15 s was recorded to show that ^{1}H T_1 relaxation had a predominant influence on differential response factors for the C-2 positions of different α-hydroxy esters.

4.3 Data Fitting

T_1 relaxation times were determined with the inversion-recovery method for methyl lactate and DPM, representing one of the smallest and one of the largest analytes in the current analysis. Signal areas $A(\tau)$ were recorded as a function of a relaxation delay τ and ^{13}C T_1 relaxation times at the C-2 position of methyl lactate and DPM were determined as:

$$A(\tau) = A(0)\left[1 - 2\left(e^{-\frac{\tau}{T_1}}\right)\right] \quad (4)$$

where $A(0)$ is the the signal area obtained from the Boltzmann magnetization at thermal equilibrium. Data were fit using the program proFit 6.2.9 (QuantumSoft, Zurich, Switzerland). T_1 relaxation times indicate that recycle delays in the order of 30 s correspond to a delay longer than 5 T_1 even for methyl lactate and hence permit the acquisition of quantitative ^{13}C NMR spectra (Supplementary Figure S2).

Acknowledgements This work was funded by the Innovation Fund Denmark (Case Number 5150-00023B). 800 MHz NMR spectra were recorded by using the spectrometer of the NMR center DTU supported by the Villum foundation.

References

1. Cherubini F (2010) The biorefinery concept: Using biomass instead of oil for producing energy and chemicals. Energy Convers Manag 51(7):1412–1421
2. Kokossis AC, Yang A (2010) On the use of systems technologies and a systematic approach for the synthesis and the design of future biorefineries. Comput Chem Eng 34(9):1397–1405
3. Moreau C, Durand R, Razigade S, Duhamet J, Faugeras P, Rivalier P, Ros P, Avignon G (1996) Dehydration of fructose to 5-hydroxymethylfurfural over H-mordenites. Appl Catal A 145(1):211–224
4. Dusselier M, Mascal M, Sels BF (2014) Top chemical opportunities from carbohydrate biomass: a chemist's view of the biorefinery. In: Nicholas KM (ed) Selective catalysis for renewable feedstocks and chemicals. Springer, Cham, pp 1–40
5. Antal MJ, Mok WSL, Richards GN (1990) Mechanism of formation of 5-(hydroxymethyl)-2-furaldehyde from d-fructose and sucrose. Carbohyd Res 199(1):91–109
6. Holm MS, Saravanamurugan S, Taarning E (2010) Conversion of sugars to lactic acid derivatives using heterogeneous zeotype catalysts. Science 328(5978):602–605

7. Moliner M, Roman-Leshkov Y, Davis ME (2010) Tin-containing zeolites are highly active catalysts for the isomerization of glucose in water. Proc Natl Acad Sci USA 107(14):6164–6168
8. Zhao H, Holladay JE, Brown H, Zhang ZC (2007) Metal chlorides in ionic liquid solvents convert sugars to 5-hydroxymethylfurfural. Science 316(5831):1597
9. Choudhary V, Mushrif SH, Ho C, Anderko A, Nikolakis V, Marinkovic NS, Frenkel AI, Sandler SI, Vlachos DG (2013) Insights into the interplay of lewis and brønsted acid catalysts in glucose and fructose conversion to 5-(hydroxymethyl) furfural and levulinic acid in aqueous media. J Am Chem Soc 135(10):3997–4006
10. Tolborg S, Meier S, Sádaba I, Elliot SG, Kristensen SK, Saravanamurugan S, Riisager A, Fristrup P, Skrydstrup T, Taarning E (2016) Tin-containing silicates: identification of a glycolytic pathway via 3-deoxyglucosone. Green Chem 18(11):3360–3369
11. Markley JL, Brüschweiler R, Edison AS, Eghbalnia HR, Powers R, Raftery D, Wishart DS (2017) The future of NMR-based metabolomics. Curr Opin Biotechnol 43:34–40
12. Hollis DP (1963) Quantitative analysis of aspirin, phenacetin, and caffeine mixtures by nuclear magnetic resonance spectrometry. Anal Chem 35(11):1682–1684
13. Forseth RR, Schroeder FC (2011) NMR-spectroscopic analysis of mixtures: from structure to function. Curr Opin Chem Biol 15(1):38–47
14. Elliot SG, Tolborg S, Sádaba I, Taarning E, Meier S (2017) Quantitative NMR approach to optimize the formation of chemical building blocks from abundant carbohydrates. ChemSusChem 10(14):2990–2996
15. Kostidis S, Addie RD, Morreau H, Mayboroda OA, Giera M (2017) Quantitative NMR analysis of intra- and extracellular metabolism of mammalian cells: a tutorial. Anal Chim Acta 980:1–24
16. Lerche MH, Yigit D, Frahm AB, Ardenkjaer-Larsen JH, Malinowski RM, Jensen PR (2018) Stable isotope-resolved analysis with quantitative dissolution dynamic nuclear polarization. Anal Chem 90(1):674–678
17. Mutlib A, Espina R, Atherton J, Wang J, Talaat R, Scatina J, Chandrasekaran A (2012) Alternate strategies to obtain mass balance without the use of radiolabeled compounds: application of quantitative fluorine (19F) nuclear magnetic resonance (NMR) spectroscopy in metabolism studies. Chem Res Toxicol 25(3):572–583
18. Simmler C, Napolitano JG, McAlpine JB, Chen SN, Pauli GF (2014) Universal quantitative NMR analysis of complex natural samples. Curr Opin Biotechnol 25:51–59
19. Sette M, Wechselberger R, Crestini C (2011) Elucidation of lignin structure by quantitative 2D NMR. Chemistry 17(34):9529–9535
20. Yan J, Kiemle D, Liu S (2015) Quantification of xylooligomers in hot water wood extract by ^{1}H-^{13}C heteronuclear single quantum coherence NMR. Carbohydr Polym 117:903–909
21. Bøjstrup M, Petersen BO, Beeren SR, Hindsgaul O, Meier S (2013) Fast and accurate quantitation of glucans in complex mixtures by optimized heteronuclear NMR spectroscopy. Anal Chem 85(18):8802–8808
22. Li X, Hu K (2017) Chapter three—quantitative NMR studies of multiple compound mixtures. In: Webb GA (ed) Annual reports on NMR spectroscopy, vol 90. Academic Press, London, pp 85–143. https://doi.org/10.1016/bs.arnmr.2016.08.001
23. Do NM, Olivier MA, Salisbury JJ, Wager CB (2011) Application of quantitative 19F and 1H NMR for reaction monitoring and in situ yield determinations for an early stage pharmaceutical candidate. Anal Chem 83(22):8766–8771
24. Rundlof T, Mathiasson M, Bekiroglu S, Hakkarainen B, Bowden T, Arvidsson T (2010) Survey and qualification of internal standards for quantification by 1H NMR spectroscopy. J Pharm Biomed Anal 52(5):645–651
25. Rundlof T, McEwen I, Johansson M, Arvidsson T (2014) Use and qualification of primary and secondary standards employed in quantitative (1)H NMR spectroscopy of pharmaceuticals. J Pharm Biomed Anal 93:111–117
26. Elliot SG, Taarning E, Madsen R, Meier S (2018) NMR spectroscopic isotope tracking reveals cascade steps in carbohydrate conversion by tin-beta. ChemCatChem 10(6):1414–1419
27. Elliot SG, Tolborg S, Madsen R, Taarning E, Meier S (2018) Effects of alkali-metal ions and counter ions in Sn-beta-catalyzed carbohydrate conversion. ChemSusChem 11(7):1198–1203
28. Saravanamurugan S, Tosi I, Rasmussen K, Jensen R, Taarning E, Meier S, Riisager A (2017) Facile and benign conversion of sucrose to fructose using zeolites with balanced Brønsted and Lewis acidity. Catal Sci Technol 7:2782–2788
29. Tosi I, Riisager A, Taarning E, Jensen P, Meier S (2018) Kinetic analysis of hexose conversion to methyl lactate by Sn beta: effects of substrate masking and of water. Catal Sci Technol 8:2137–2145
30. Cullen CH, Ray GJ, Szabo CM (2013) A comparison of quantitative nuclear magnetic resonance methods: internal, external, and electronic referencing. Magn Reson Chem MRC 51(11):705–713
31. Le Gresley A, Fardus F, Warren J (2015) Bias and uncertainty in non-ideal qNMR analysis. Crit Rev Anal Chem 45(4):300–310
32. Elliot SG, Andersen C, Tolborg S, Meier S, Sádaba I, Daugaard AE, Taarning E (2017) Synthesis of a novel polyester building block from pentoses by tin-containing silicates. RSC Adv 7(2):985–996
33. Webster GK, Marsden I, Pommerening CA, Tyrakowski CM, Tobias B (2009) Determination of relative response factors for chromatographic investigations using NMR spectrometry. J Pharm Biomed Anal 49(5):1261–1265
34. Petersen BO, Hindsgaul O, Meier S (2014) Profiling of carbohydrate mixtures at unprecedented resolution using high-precision ^{1}H-^{13}C chemical shift measurements and a reference library. Analyst 139(2):401–406
35. Malz F, Jancke H (2005) Validation of quantitative NMR. J Pharm Biomed Anal 38(5):813–823
36. Vitorge B, Jeannerat D (2006) NMR diffusion measurements in complex mixtures using constant-time-HSQC-IDOSY and computer-optimized spectral aliasing for high resolution in the carbon dimension. Anal Chem 78(15):5601–5606
37. Njock GB, Pegnyem DE, Bartholomeusz TA, Christen P, Vitorge B, Nuzillard JM, Shivapurkar R, Foroozandeh M, Jeannerat D (2010) Spectral aliasing: a super zoom for 2D-NMR spectra. Principles and applications. Chimia 64(4):235–240
38. Kazimierczuk K, Orekhov VY (2011) Accelerated NMR spectroscopy by using compressed sensing. Angew Chem Int Ed 50(24):5556–5559

Response Factors Enable Rapid Quantitative 2D NMR Analysis of Biomass Conversion to Renewable Chemicals

Samuel G. Elliot,[1a] Irene Tosi,[1b] Anders Riisager,[1c] Esben Taarning,[2] and Sebastian Meier[1*]

Table S1. Solubility/miscibility and chemical shifts of potential standards.

#	Name	B.P. [°C]	Purity	Solubility/Miscability				NMR signals	
				H_2O	MeOH	$CHCl_3$	DMSO	^{13}C	^{1}H
1	Mesitylene	164	98.0 %	×	✓	✓	✓	137.2, 126.4, 19.9	6.76, 2.24
2	1,4-dioxane	101	99.8 %	✓	✓	✓	✓	66.7	3.67
3	Dimethyl sulfoxide	189	99.8 %	✓	✓	✓	✓	39.0	2.66
4	Dimethyl sulfone	*107* [a]	99.96 %	>1 M	420 mM	850 mM	> 1 M	41.1	3.01
5	Glycerol	290	99 %	✓	✓	✓	✓	72.6, 63.2	3.67, 3.60, 3.54
6	Xylitol	*94* [a]	99 %	>1 M	<50 mM	<50 mM	250 mM	N.A.	N.A.

[a]Melting Point.

Table S2. Performance comparison of different NMR methods.

Method	Acquisition time [h:min]	SINO[1]	LOD[2]		LOQ[3]	
			[mM]	[mol%][4]	[mM]	[mol%][4]
^{13}C NMR	4:26	362	2.4	0.60	7.3	1.8
$^{1}H^{13}C$ HSQC	0:23	3507	0.25	0.062	0.75	0.19
$^{1}H^{13}C$ HSQC	0:05	3179	0.27	0.068	0.83	0.21

[1]Signal to noise ratio compared to a 131 mM DMSO standard. [2]Limit of detection, determined as 3 times the signal to noise ratio. [3]Limit of quantification, determined as 10x the signal to noise ratio. [4]Compared to a 0.4 M xylose reaction solution.

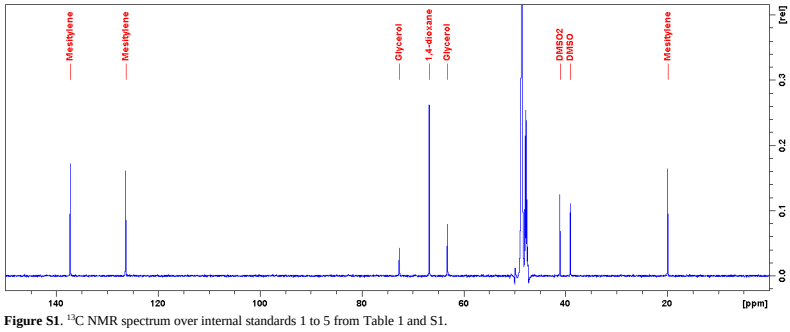

Figure S1. ^{13}C NMR spectrum over internal standards 1 to 5 from Table 1 and S1.

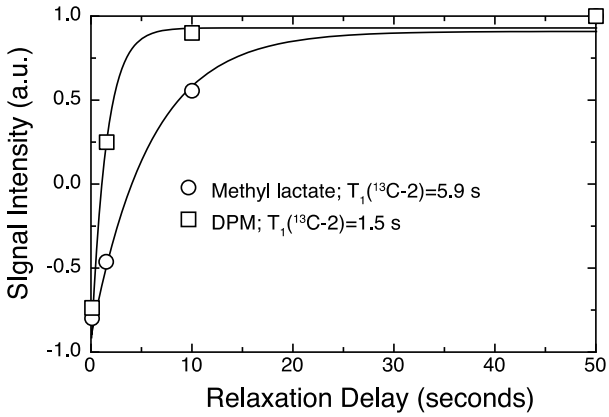

Figure S2. Inversion recovery measurement of spin-lattice relaxation constants T_1^{13C} for the C-2 signals of DPM and methyl lactate.

Topics in Catalysis
https://doi.org/10.1007/s11244-019-01144-7

ORIGINAL PAPER

Uncharted Pathways for $CrCl_3$ Catalyzed Glucose Conversion in Aqueous Solution

Irene Tosi[1] · Samuel G. Elliot[1] · Bo M. Jessen[1] · Anders Riisager[1] · Esben Taarning[2] · Sebastian Meier[1]

Abstract
Innovative processes for converting carbohydrates to materials and fuels form the basis for profitable bio-based economies of the future. For such innovation, approaches that provide detailed structural information would be desirable to detect uncharted chemistries of carbohydrate conversion. Among the most important value-added products accessible though conversion of biomass is 5-hydroxymethylfurfural (HMF), whose market values strongly depends on the quality of the product. Here, we use high-field in situ NMR spectroscopy to shed light on obscure competing reactions of $CrCl_3$-catalyzed carbohydrate conversion to HMF in water. High-field NMR spectroscopy has enormous prowess in distinguishing isomeric and dehydrated products formed from glucose. Previously unidentified compounds were identified with this approach and include anhydrosugars and a variety of branched and linear mono- and disaccharides. Other identified compounds leverage the understanding of the active catalyst species. In addition to providing mechanistic insight, the approaches and findings described herein help to measure and manage carbon balances and product quality in HMF production.

Keywords 2D NMR · Cascade reactions · Catalysis · Chromium trichloride · HMF · Sugars

1 Introduction

A change towards sustainable production of materials and fuels is increasingly imminent. Sustainable production using rapidly renewable resources involves both challenges and opportunities for developing novel catalytic approaches towards the use of resources such as carbohydrates and lignin [1, 2]. The high oxygen content in these substrates as compared to fossil compounds is accompanied by high functionality present in biomass [3]. Such abundant functionality in biomass raises the question, how novel processes can selectively transform the substrate to a product with selected functionality [3].

The most important value-added products accessible from carbohydrates include 5-hydroxymethylfurfural (HMF) [4, 5]. HMF is being investigated by several academic and industrial groups as a promising precursor of polymers, resins, pharmaceuticals, fuel additives and solvents [2]. Depending on its quality, market values in the range of (2–300 USD/kg) have been described [6, 7]. Hence, a production of highly pure compound is desirable for profitability. Processes of production have included transformations of carbohydrates using Lewis acidic salts and water as an obvious green solvent [6]. In addition, water is a more promising option for HMF purification than high-boiling organic solvents or ionic liquids [8–10].

While glucose is the cheaper and hence economically more attractive substrate than fructose, HMF yields from glucose in water have left room for improvement. Such improvement should be based on reliable carbon balances, but reported carbon yields often imply a significant amount of unidentified compounds in the reaction mixtures. The quantity of these compounds would help close the carbon balance of the processes, while their identity would be indicative of reaction mechanisms that are accessible under the given reaction conditions. The nature of byproducts in the

Electronic supplementary material The online version of this article (https://doi.org/10.1007/s11244-019-01144-7) contains supplementary material, which is available to authorized users.

✉ Sebastian Meier
semei@kemi.dtu.dk

[1] Department of Chemistry, Technical University of Denmark, Kemitorvet, 2800-Kgs Lyngby, Denmark

[2] Haldor Topsøe A/S, Haldor Topsøes Alle 1, 2800-Kgs Lyngby, Denmark

Published online: 22 February 2019

reaction mixture also affects purification strategies in order to obtain high quality, high value product [6].

Lewis acidic salts coordinate to the aldehyde group of glucose and thus permit an intramolecular 1,2 hydride transfer that leads to reversible glucose to fructose isomerization. The reversible reaction also leads to the formation of mannose [11–13]. In addition, $CrCl_3$ in water can catalyze 1,5 hydride transfers that convert D-glucose to L-sorbose. Only certain species are suggested to be active for catalysis, most notably $[Cr(H_2O)_5OH]^{2+}$ [10]. Nevertheless, the catalytic reaction remains incompletely understood, as witnessed by poor carbon balances in the conversion and by the detection of unidentifiable carbohydrate byproducts in the conversion [14]. These shortcomings indicate that better understanding of homogeneous Lewis acid catalysis may pave the way to improving both homogeneous and heterogeneous Lewis acid catalysts in carbohydrate conversion [14].

In the current study, we aimed at gaining a comprehensive overview of hitherto unidentified pathways in the conversion of sugars, specifically those that are accessible in the $CrCl_3$-catalyzed conversion of glucose in aqueous solution. Using in situ spectroscopy on the unpurified reaction mixture, we identify various compounds that shed light on the conversions of glucose in aqueous solutions of Lewis-acidic salts (Scheme 1).

2 Results and Discussion

We employed NMR spectroscopy to sense uncharted chemistries in $CrCl_3$-catalyzed glucose conversion. NMR spectroscopy is non-selective and thus permits an unbiased assessment of post-reaction mixture composition. Approaches that are more widely used in metabolic research were adapted, including the use of authentic reference standards, database and literature mining as well as the ability to determine chemical structures in complex samples from high-field NMR data without the knowledge of the analyte sum formula. Two-dimensional assignment spectra were used to identify structural motifs and their arrangement to NMR spin systems in the molecules of the reaction mixture. To this end, multiplicity-edited variants of ^{1}H–^{13}C HSQC and ^{1}H–^{13}C HMBC spectra, as well as ^{1}H–^{1}H TOCSY and ^{1}H–^{1}H COSY spectra were recorded. These approaches identified a variety of unexpected compounds—and hence reaction pathways—in the well-studied reaction. The identification of novel byproducts should aid the measurement and management both of carbon balances and of product quality in Lewis acid catalyzed carbohydrate conversions.

2.1 Detection and Identification of Anhydrosugars in Aqueous Reaction Medium

For structural studies on unpurified reaction mixtures, NMR spectroscopy at high magnetic field (18.7 T magnetic field, 800 MHz ^{1}H Larmor frequency) was employed. The reaction mixture was produced by conversion of 10% (w/v) glucose in the presence of 17 mM $CrCl_3{\cdot}6H_2O$ at 140 °C for 1 h. NMR assignment spectra allowed us to identify the spin systems with chemical shifts shown in Fig. 1. We assigned these spin systems to 1,6-anhydroglucofuranose (AGF) and 1,6-anhydroglucopyranose (AGP). Notably, the intramolecular dehydration products AGF and AGP were formed by reaction in aqueous solvent. Structural assignments to the

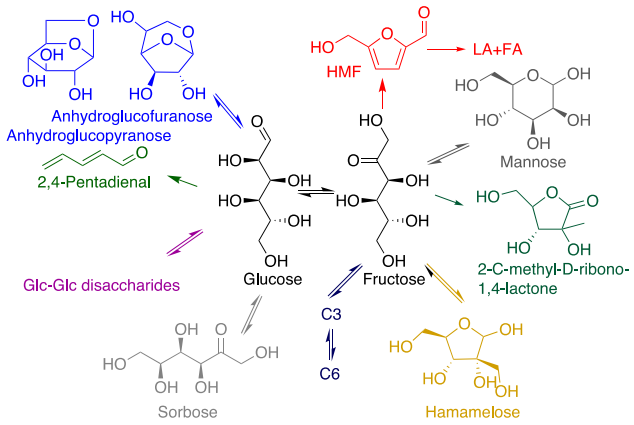

Scheme 1 Reactions of $CrCl_3$-catalyzed glucose conversion in aqueous solution discussed herein

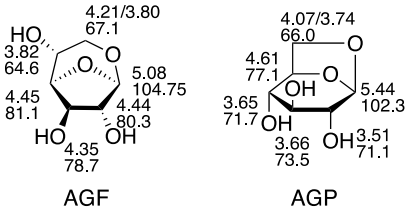

Fig. 1 Structure and chemical shift assignments of 1,6-anhydroglucofuranose (AGF, left) and 1,6-anhydroglucopyranose (AGP, right)

anhydroglucoses were verified by comparison to published values for the purified, non-commercial AGF [15], while the pyranose form was identified by comparison to the spectra of authentic commercial levoglucosan standard. The peak resolving capacity of high-field 2D ^{1}H-^{13}C NMR is above two million signals [16], hence the pattern of CH group signals permits analyte identification with excellent reliability.

The spin system of AGF was identical to a previously reported, unidentified compound (but suspected hexose) from $CrCl_3$-catalyzed glucose conversion in water under identical conditions. The bicyclic structure of the anhydrosugar explains the absence of other tautomers in this compound fractionated from product solutions of the reaction [14]. Anhydroglucoses have previously been reported as potentially reactive byproducts in reaction pathways converting glucose to HMF in non-aqueous media [17–19]. The formation of these compounds as byproducts in aqueous solution on the other hand was less anticipated from computational predictions that suggested formation of these compounds in DMSO but not water [17]. In our experiments, AGF and AGP were detected at similar levels, albeit the substrate for AGP formation (the β-pyranose tautomer of glucose) is much more abundant than the substrate for AGF formation (the β-furanose tautomer of glucose) in aqueous solution. This finding indicates a kinetic preference for the formation of the intramolecular furanoside as compared to the formation of the pyranoside.

We repeated the reaction in DMSO instead of aqueous solvent to verify the higher propensity for formation of anhydroglucose under these conditions. Figure 2a shows a time series of in situ 1D ^{13}C NMR spectra visualizing the faster formation of AGF than of AGP at 110 °C. Subsequently, we added 17% (v/v) water to the product mixture derived in DMSO from the experiment shown in Fig. 2a and followed the hydrolysis of anhydroglucose by in situ NMR spectroscopy at ambient pressure and 95 °C temperature (Fig. 2b). The resultant time courses of AGF and AGP concentrations indicate that AGP was more resilient to

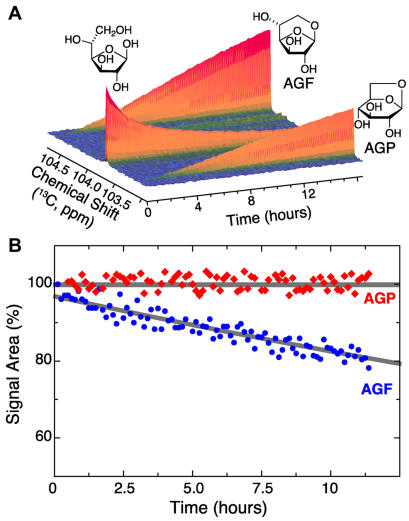

Fig. 2 In situ NMR spectroscopy of AGF and AGP formation in DMSO (**a**) and of AGP and AGF hydrolysis upon addition of 17% (v/v) H_2O (**b**). Lines in (**b**) are a guide to the eye. Reaction conditions: 10% (w/v) glucose at 110 °C, 17 mM $CrCl_3{\cdot}6H_2O$; reaction at 110 °C (**a**) subsequent hydrolysis in 17% H_2O, 83% DMSO, 95 °C (**b**) for the indicated time

hydrolysis than AGF. AGF and especially AGP levels have been found to decrease in post-reaction mixtures upon addition of 17% water to the $CrCl_3$-catalyzed glucose conversion in DMSO. The resilience of AGP to hydrolysis under these conditions indicates that levels are decreased because AGP is hardly formed (rather than being hydrolyzed) in the presence of water [19]. In DMSO without addition of water, AGP and AGF can amount to significant byproducts of HMF (~40% of HMF; see Fig. 1S in the Electronic Supplementary Materials).

2.2 Formation of Intermolecular Acetals

An overview of hemiacetals and acetals that were present in the $CrCl_3$-catalyzed conversion in aqueous solution and in DMSO, respectively, is provided in Fig. 3. Beyond AGF and AGP, the formation of disaccharides could be observed both in aqueous solution and—to a higher degree—in DMSO. Disaccharide formation is the result of intermolecular acetal formation of glucose, while AGF and AGP formation results from intramolecular acetal formation.

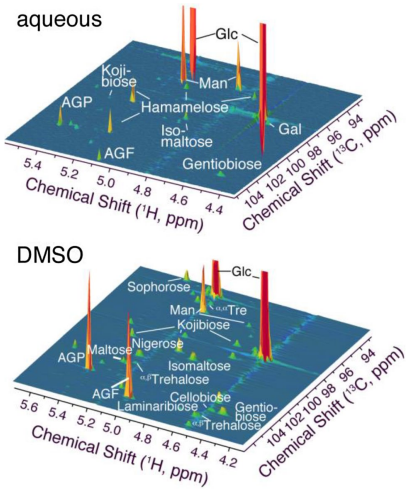

Fig. 3 Surface plot of ^{1}H–^{13}C HSQC spectra on post-reaction samples of glucose conversion in aqueous solution (top) or in DMSO (bottom). Reaction conditions: 10% (w/v) glucose, 17 mM $CrCl_3{\cdot}6H_2O$, 6 mL 90% H_2O/10% D_2O (top) or 99% d6-DMSO/1% DMSO (bottom), 140 °C for 1 h in water and or 30 min in DMSO

Cellobiose has previously attracted some interest as a byproduct in the $CrCl_3$-catalyzed glucose conversion in DMSO [18, 19]. However, cellobiose was here found to be only one of the glucopyranosyl-glucopyranosides formed. The 1–4 linked cellobiose and maltose (4-O-β-D-glucopyranosyl-D-glucose and 4-O-α-D-glucopyranosyl-D-glucose, respectively) were formed in lower amounts than for instance the 1–6 linked disaccharides gentiobiose and isomaltose (6-O-β-D-glucopyranosyl-D-glucose and 6-O-α-D-glucopyranosyl-D-glucose, respectively). Integration of respective signals in the ^{1}H–^{13}C HSQC spectra of Fig. 3 indicated that gentiobiose and isomaltose are formed at levels that are sixfold higher than those of cellobiose and maltose. Furthermore, all other glucopyranosyl-glucopyranosides that can be formed from reaction between two glucoses (trehaloses, kojibiose, sophorose, nigerose and laminaribiose) were detectable. In analogy to the formation of AGF and AGP in aqueous solution, disaccharide formation could also be detected in aqueous medium, albeit at lower levels than in DMSO (Fig. 3). All disaccharide signals were identified by comparison to high-resolution ^{1}H-^{13}C HSQC spectra of authentic standards [20].

2.3 Branched C6-Carbohydrates

Previous mechanistic studies had speculated on the possible presence of branched carbohydrates in aqueous glucose conversion catalyzed by $CrCl_3{\cdot}6H_2O$. In fact, the suspected C6-sugar identified herein as AGF had been assumed to be a branched chain hexose [14].

The signals of the branched chain hexose hamamelose (2-C-(hydroxymethyl)-D-ribose) were herein detected in the post-reaction mixture of glucose conversion by $CrCl_3{\cdot}6H_2O$ in water as indicated in Fig. 3 (top). In solution, hamamelose occurs as an equilibrium of α- and β-furanose and pyranose forms with comparable populations. Hence, hamamelose could be identified by comparison of the ^{1}H–^{13}C HSQC signals to the pattern of tautomer signals from an authentic standard (Fig. 4). In addition to hamamelose, 2-C-(hydroxymethyl)-L-lyxose could be detected in the aqueous reaction mixture, albeit at smaller amounts and predominantly from its pyranose form (Scheme 2). Signals were identical to the 2-C-(hydroxymethyl)-L-lyxose ^{1}H-^{13}C HSQC signals after reacting sorbose with 0.2% (w/v) ammonium heptamolybdate tetrahydrate.

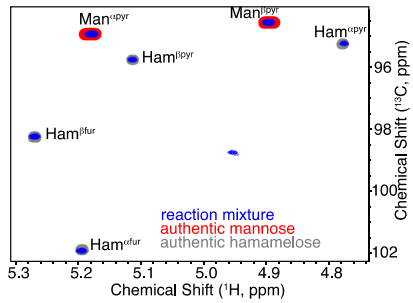

Fig. 4 Spectral region from the ^{1}H–^{13}C HSQC of the reaction mixture displayed in Fig. 3 top. The reaction mixture is displayed in blue, authentic standards of hamamelose and mannose are displayed in red and light grey, respectively. Reaction conditions: 10% (w/v) glucose, 17 mM $CrCl_3{\cdot}6H_2O$, 6 mL 90% H_2O, 10% D_2O, 140 °C for 1 h

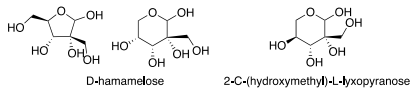

Scheme 2 Branched chain sugars detected upon conversion of glucose with $CrCl_3$

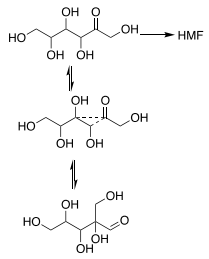

Scheme 3 Plausible mechanism for the conversion of ketoses into branched carbohydrates with a migration of the ketose C1 carbon to 2-hydroxymethyl groups

Hamamelose and 2-C-(hydroxymethyl)-L-lyxose can be formed by Bilik-type carbon shifts from fructose and sorbose, respectively. The Bilik-type carbon shift has been widely described for the direct conversion of glucose to mannose by concurrent C2–C3 bond cleavage and C1–C3 bond formation resulting in an intramolecular C1–C2 carbon shift [21–24]. For ketoses, the concurrent C2–C3 bond cleavage and C2–C4 bond formation leads to the formation of the branched chain ketoses (Scheme 3).

Formation of the branched C6-carbohydrates by a mechanism akin to Scheme 3 was corroborated by using D-[1-^{13}C] glucose as substrate. The ^{13}C label was preferentially incorporated into the 2-hydroxymethyl groups of hamamelose, as expected from the displayed mechanism (see Fig. 2S in the Electronic Supplementary Materials). Alternatively, branched C6-carbohydrates could have been formed by aldol condensation of smaller linear sugars. Branched sugars have thus been discussed as prospective value-added compounds or precursors to value-added chemicals formed from smaller sugars [25]. Due to the reversibility of the Bilik reaction, and the likely irreversibility of fructose dehydration to HMF [17], branched sugars presumably interconvert with their respective ketose forms and serve as off-pathway intermediates for the formation of HMF. Consistent with this interpretation, hamamelose accumulated less in DMSO than in aqueous reaction medium (see e.g., Fig. 3), probably due to the faster competing conversion of fructose to HMF in DMSO. This interpretation agrees with previous reports showing that less fructose exists freely in the reaction system of DMSO as compared to aqueous solutions, as the high dehydration potential of DMSO favors subsequent reaction of fructose to HMF [18].

Both in aqueous solution and in DMSO, the combined amount of carbon that is detected in carbohydrates different from glucose, mannose and fructose is comparable to the level of HMF in the experiments of Fig. 3. Hence, the less canonical pathways of carbohydrate conversion described herein can impact strongly on the carbon balance of the catalyzed reaction.

2.4 Formation of a Variety of C6-Carbohydrates Through Cleavage/Condensation

Ketoses are absent in the hemiacetal spectral region (Fig. 3), but can be conveniently detected in the primary alcohol region of 2D ^{1}H–^{13}C HSQC spectra. Figure 5 displays the primary alcohol spectral region including signals from ketoses and aldoses formed in aqueous solution. As expected, fructose and sorbose were among the ketoses detected in the reaction. Less expected was the presence of smaller amounts of tagatose, the keto-isomer of galactose. In parallel to tagatose, galactose could be detected both from its C1 signal (Fig. 3) and from its C6 signal (Fig. 5) in ^{1}H–^{13}C HSQC spectra. Other C6 sugars such as altrose, idose and allose could be detected by comparison to authentic standards, albeit at low amounts (see Fig. 3S in the Electronic Supplementary Materials). These findings are consistent with the presence of C3 sugars (especially dihydroxyacetone) in the reaction mixture as a possible precursor for the variety of C6 sugars and a likely intermediate in subsequent cleavage/condensation reactions of glucose.

Diverse hexose reaction products have previously been reported when using dedicated retro-aldol and 1,2 carbon shift catalysts for the conversion of aldohexoses [23]. Overall, $CrCl_3$-catalyzed conversion of glucose induces the formation of a diverse ensemble of mono- and disaccharides, branched carbohydrates and anhydrosugars, even though the

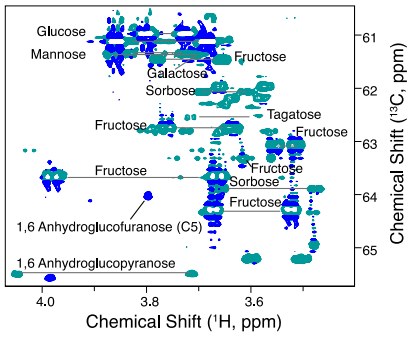

Fig. 5 Spectral region of primary alcohol groups in ^{1}H–^{13}C HSQC, showing ketose signals for fructose, sorbose and tagatose at decreasing amounts, in addition to aldose and anhydrosugars as indicated

formation of these products was not optimized by any means in the current study.

2.5 Dehydration Reactions Different from HMF Formation

Signals outside the spectral region of carbohydrates were evident in NMR spectra of post-reaction mixtures. Such signals included the expected signals from HMF and levulinic acid (see Figs. 4S and 5S in the Electronic Supplementary Materials). The presence of unexpected compounds was evident through the presence of various olefinic, aldehyde or aliphatic hydrogen NMR signals. Figure 6 displays the spin system of byproduct (2E)-2,4-pentadienal in the aqueous reaction mixture. The ^{1}H NMR signals are displayed through their correlations in a ^{1}H–^{1}H TOCSY spectrum. The chemical structure can be determined unambiguously against the reaction mixture background through sequential assignments of a characteristic aldehyde group and four olefinic groups including a terminal CH_2 group. LC–MS analysis confirmed the presence of a compound with the molecular weight of pentadienal in the reaction mixture (see Fig. 6S in the Electronic Supplementary Materials). The chemical identity of the compound was additionally verified through comparison to published chemical shift values [26]. Like anhydrosugars, unsaturated compounds including (2E)-2,4-pentadienal are early intermediates in the pyrolysis of biomass [27]. The formation of such products thus appears accelerated in the presence of catalytic amounts of $CrCl_3$ at 140 °C in aqueous solution.

The presence of unexpected byproducts can hint at the structure of the active catalyst species. In the case of $CrCl_3$ catalysis in water, $[Cr(H_2O)_5OH]^{2+}$ was suggested as the most active Cr(III) species acting as a bifunctional Lewis acid-Brønsted base site [10]. Our aqueous reaction mixture contained a compound most likely representing 2-C-methyl-ribonolactone. A plausible pathway for the formation of this compound is depicted in Scheme 4. The compound is the result of a Lewis acid catalyzed aldose-to-ketose isomerization and subsequent Brønsted base catalyzed benzilic acid rearrangement [28]. Hence, the presence of this compound is consistent with the previously suggested activity of a bifunctional Lewis acid-Brønsted base site. The compound was identified through multiplicity edited ^{1}H–^{13}C HSQC and ^{1}H–^{13}C HMBC spectra identifying a lactone and tertiary alcohol carbon, as well as a secondary alcohol in the vicinity of a methyl group (Fig. 7). Chemical shifts of the compound are strongly indicative of a five-membered ring and are consistent with assignments of the previously characterized purified compound [28].

2.6 Implications for Monitoring Pathways, Carbon Balances and Product Quality

Use of in situ NMR spectroscopy on unpurified reaction mixtures provides a means of detecting and identifying uncharted chemistries in $CrCl_3$-catalyzed glucose conversion. Formation of anhydrosugars and other reactions occurring early in glucose pyrolysis were accelerated in the $CrCl_3$-catalyzed reaction in water at 140 °C. Likewise, branched carbohydrates, disaccharides and carbohydrates formed from subsequent cleavage-condensation reactions

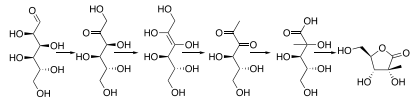

Scheme 4 Plausible pathway towards 2-C-methyl-ribonolactone through isomerization, dehydration and base catalyzed rearrangement [28]

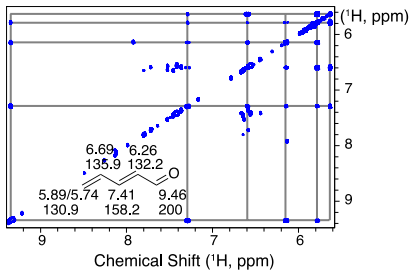

Fig. 6 ^{1}H–^{1}H TOCSY showing the spin system of (2E)-2,4-pentadienal. The assignment of the compound in water is displayed

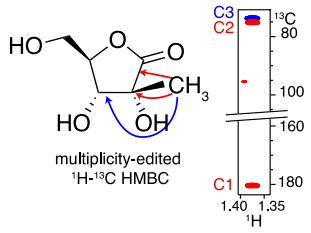

Fig. 7 Structure of 2-C-methyl-ribonolactone and multiplicity edited ^{1}H–^{13}C HMBC showing the connectivities from the methyl protons to quaternary carbons of tertiary alcohol and lactone (red sub-spectrum) and to the CH group of the secondary alcohol C3 (blue sub-spectrum)

could be identified. In addition, a reaction product that could be indicative of the concerted action of Lewis acidic isomerization and Brønsted base catalyzed rearrangement supports the notion that these sites may play a concerted catalytic role. LC–MS was used as a complementary method to validate the presence of compounds with the mass of pentadienal, dehydration products and disaccharides, in addition to HMF (see Fig. 6S in the Electronic Supplementary Materials).

Several pathways and compounds contribute to the carbon balance of the $CrCl_3$-catalyzed reaction in water at 140 °C (Fig. 5S in the Electronic Supplementary Materials, with yields for 15 main compounds and compound classes listed in the figure caption). Unsurprisingly, product distributions are vastly altered when conducting the reaction in DMSO (Figs. 3 and 1S). DMSO stabilizes the acyclic and five-membered furanose structure of fructose relative to the pyranose form [29–31], facilitates dehydration of fructofuranose to HMF and prevents the formation of levulinic acid, while favoring intra- and intermolecular acetal formation of glucose to anhydroglucose and disaccharides, respectively.

Beyond its impact on the carbon balance, the quantitative identification of byproducts has an important role in product purification and hence product quality. Byproduct yields were determined with a lower limit of quantification of ~0.2%, when using 10% (w/v) glucose substrate. As purity and price correlate, validating the purification of highly pure biomass derived compounds is highly desirable for the profitability of future bioeconomies.

3 Conclusion

In conclusion, the methodology and findings described herein identify byproducts without the need for purifying them. Use of high field in situ NMR spectroscopy in conjunction with reference compounds, literature mining and the use of two-dimensional assignment spectra emerges as an attractive approach to identify new reactions in biomass conversion [32, 33]. This approach is particularly promising for identifying hitherto unknown compounds due to the ability to distinguish isomeric compounds, even in the absence of authentic reference standards. Reactivities described herein benefit the understanding of mass balances in HMF formation by providing insight into new classes of byproducts. In addition, the improved mapping of accessible reaction pathways will expedite future identification of impurities and will aid the development of purification strategies towards high-value HMF production from carbohydrates.

4 Experimental Section

4.1 Chemicals

D_2O (99.9 atom % D), d6-DMSO (99.9 atom % D), D-mannose (> 99%), sorbose, tagatose, D-[1-^{13}C] glucose (99 atom % ^{13}C), 1,6-anhydro-β-D-glucopyranose (99%) and ammonium heptamolybdate tetrahydrate (99.98%) were obtained from Sigma–Aldrich. $CrCl_3{\cdot}6H_2O$ (> 96%) was obtained from Merck. Hamamelose was obtained from Carbosynth. In order to detect 2-C-(hydroxymethyl) lyxose signals, sorbose was reacted with 0.2% (w/v) ammonium heptamolybdate tetrahydrate for 2 h at 80 °C and observed NMR signals of 2-C-(hydroxymethyl)-L-lyxose signals were identified in the resultant mixture using previously assigned chemicals shifts for the purified compound [34].

4.2 General Procedure for Catalytic Experiments

Glucose was dissolved to 10% (w/v) in 6 mL of H_2O or DMSO. $CrCl_3{\cdot}6H_2O$ was added to a final concentration of 17 mM. Catalytic experiments were carried out in 15 mL Ace pressure tubes under magnetic stirring at 140 °C for up to 6 h and samples of 500 µl volume were collected after 10, 30, 60, 120, 240 and 360 min. D_2O was added to the aqueous reactions to a final concentration of 10% (v/v). For tracking the fate of D-[1-^{13}C] glucose in aqueous solution, 500 µl of a mixture with standard concentrations (10% D-[1-^{13}C] glucose and 17 mM catalyst) were transferred to a 5 mm NMR sample tube and reaction was tracked in situ at 95 °C overnight in a 600 MHz Bruker Avance III NMR spectrometer equipped with a BBO SmartProbe.

4.3 Assignment NMR Spectra

Assignment spectra of reaction mixtures were recorded at 25 °C on a Bruker Avance III 800 MHz spectrometer equipped with a TCI cryoprobe. NMR spectra included standard and multiplicity edited ^{1}H–^{13}C HSQC, ^{1}H–^{13}C HMBC spectra as well as ^{1}H–^{1}H COSY and ^{1}H–^{1}H TOCSY spectra. Cr(III) lead to some line broadening especially in the ^{1}H dimension. Authentic reference compounds were dissolved to concentrations of 50 mM in D_2O or in d6-DMSO prior to the acquisition of ^{1}H–^{13}C HSQC spectra. All spectra were processed with extensive zero filling in both spectral dimensions using a shifted sine-bell apodization function and analyzed in Bruker Topspin 3.5 pl7. Chemical shifts were referenced relative to the anomeric signal of α-glucopyranose at 5.230 (^{1}H) and 92.990 (^{13}C) ppm [20].

4.4 Data Fitting

^{13}C T_1 relaxation times were measured on reaction mixtures using the inversion-recovery method with recovery delays of 0.1, 1, 5, and 60 s and an inter-scan relaxation delay of 300 s. Spectra were acquired on a Bruker Avance III 800 MHz spectrometer equipped with a TCI cryoprobe. Signal areas were integrated in Bruker Topspin 3.5 pl7 and fitted using proFit 6.2.9 (QuantumSoft, Zurich) as

$$A(\tau) = A(0)\left[1 - 2\left(e^{-\frac{\tau}{T_1}}\right)\right],$$

where $A(0)$ is the signal area derived for the relaxed (Boltzmann equilibrium) spin polarization, τ is the recovery delay and T_1 is the spin–lattice relaxation time. Cr(III) shortened relaxation times to below 1 s for most substrate, solvent and product ^{13}C spins (see Fig. 5S in the Electronic Supplementary Materials). Hence, quantitative ^{13}C spectra, for instance in reaction tracking (Fig. 2), could be acquired with short recycle delays and high sensitivity.

4.5 LC–MS

LC–MS experiments were conducted using a Waters Acquity UPLC system connected to a Waters SQD2 mass spectrometer. The UPLC system contained a quaternary pump, an autosampler, a Waters HILIC column, a temperature-controlled column oven, and a diode array detector. Phase A was 0.1% formic acid (aq) and phase B was acetonitrile/water (95/5, v/v) with 0.1% formic acid. Positive and negative ESI modes were used. Data were acquired, processed and analyzed using the MassLynx version 4.1 software package.

Acknowledgements This work was funded by the Innovation Fund Denmark (Case Number 5150-00023B). 800 MHz NMR spectra were recorded by using the spectrometer of the NMR center DTU supported by the Villum foundation. We gratefully acknowledge Philip Charlie Johansen for technical assistance with LC–MS analyses.

References

1. Davis ME (2015) Heterogeneous catalysis for the conversion of sugars into polymers. Top Catal 58(7):405–409
2. Jang YS, Kim B, Shin JH, Choi YJ, Choi S, Song CW, Lee J, Park HG, Lee SY (2012) Bio-based production of C2–C6 platform chemicals. Biotechnol Bioeng 109(10):2437–2459
3. Shanks BH (2010) Conversion of biorenewable feedstocks: new challenges in heterogeneous catalysis. Ind. Eng. Chem. Res. 49(21):10212–10217
4. Antal MJ, Mok WSL, Richards GN (1990) Mechanism of formation of 5-(hydroxymethyl)-2-furaldehyde from d-fructose and sucrose. Carbohydr Res 199(1):91–109
5. Binder JB, Raines RT (2009) Simple chemical transformation of lignocellulosic biomass into furans for fuels and chemicals. J Am Chem Soc 131(5):1979–1985
6. Yu IKM, Tsang DCW (2017) Conversion of biomass to hydroxymethylfurfural: a review of catalytic systems and underlying mechanisms. Biores Technol 238:716–732
7. Yu IKM, Tsang DCW, Yip ACK, Chen SS, Wang L, Ok YS, Poon CS (2017) Catalytic valorization of starch-rich food waste into hydroxymethylfurfural (HMF): controlling relative kinetics for high productivity. Biores Technol 237:222–230
8. Akien GR, Qi L, Horváth IT (2012) Molecular mapping of the acid catalysed dehydration of fructose. Chem Commun 48(47):5850–5852
9. Hu S, Zhang Z, Song J, Zhou Y, Han B (2009) Efficient conversion of glucose into 5-hydroxymethylfurfural catalyzed by a common Lewis acid $SnCl_4$ in an ionic liquid. Green Chem 11(11):1746–1749
10. Choudhary V, Mushrif SH, Ho C, Anderko A, Nikolakis V, Marinkovic NS, Frenkel AI, Sandler SI, Vlachos DG (2013) Insights into the interplay of Lewis and Bronsted acid catalysts in glucose and fructose conversion to 5-(hydroxymethyl) furfural and levulinic acid in aqueous media. J Am Chem Soc 135(10):3997–4006
11. Roman-Leshkov Y, Moliner M, Labinger JA, Davis ME (2010) Mechanism of glucose isomerization using a solid Lewis acid catalyst in water. Angew Chem 49(47):8954–8957
12. Choudhary V, Pinar AB, Lobo RF, Vlachos DG, Sandler SI (2013) Comparison of homogeneous and heterogeneous catalysts for glucose-to-fructose isomerization in aqueous media. ChemSusChem 6(12):2369–2376
13. Saravanamurugan S, Riisager A, Taarning E, Meier S (2016) Mechanism and stereoselectivity of zeolite-catalysed sugar isomerisation in alcohols. Chem Commun 52(86):12773–12776
14. Nguyen H, Nikolakis V, Vlachos DG (2016) Mechanistic insights into Lewis acid metal salt-catalyzed glucose chemistry in aqueous solution. ACS Catal 6(3):1497–1504
15. Köll P, Angyal SJ (1988) 1H- und 13C-n.m.r.-spektren der 1,6-anhydrohexofuranosen. Carbohydr Res 179:1–5
16. Hertkorn N, Ruecker C, Meringer M, Gugisch R, Frommberger M, Perdue EM, Witt M, Schmitt-Kopplin P (2007) High-precision frequency measurements: indispensable tools at the core of the molecular-level analysis of complex systems. Anal Bioanal Chem 389(5):1311–1327
17. Choudhary V, Burnett RI, Vlachos DG, Sandler SI (2012) Dehydration of glucose to 5-(hydroxymethyl)furfural and anhydroglucose: thermodynamic insights. J Phys Chem C 116(8):5116–5120
18. Jia S, Liu K, Xu Z, Yan P, Xu W, Liu X, Zhang ZC (2014) Reaction media dominated product selectivity in the isomerization of glucose by chromium trichloride: from aqueous to non-aqueous systems. Catal Today 234:83–90
19. Jia S, Xu Z, Zhang ZC (2014) Catalytic conversion of glucose in dimethylsulfoxide/water binary mix with chromium trichloride: role of water on the product distribution. Chem Eng J 254:333–339
20. Petersen BO, Hindsgaul O, Meier S (2014) Profiling of carbohydrate mixtures at unprecedented resolution using high-precision 1H–13C chemical shift measurements and a reference library. Analyst 139(2):401–406
21. Hayes ML, Pennings NJ, Serianni AS, Barker R (1982) Epimerization of aldoses by molybdate involving a novel rearrangement of the carbon skeleton. J Am Chem Soc 104(24):6764–6769
22. Meier S, Karlsson M, Jensen PR (2017) Detecting elusive intermediates in carbohydrate conversion: a dynamic ensemble of acyclic glucose–catalyst complexes. ACS Sustain Chem Eng 5:5571–5577

23. Orazov M, Davis ME (2015) Tandem catalysis for the production of alkyl lactates from ketohexoses at moderate temperatures. Proc Natl Acad Sci 112(38):11777
24. Elliot SG, Taarning E, Madsen R, Meier S (2017) NMR spectroscopic isotope tracking reveals cascade steps in carbohydrate conversion by tin-beta. ChemCatChem 10(6):1414–1419
25. Deneyer A, Tlatli S, Dusselier M, Sels BF (2018) Branching-first: synthesizing C–C skeletal branched biobased chemicals from sugars. ACS Sustain Chem Eng 6(6):7940–7950
26. Sommerwerk S, Heller L, Siewert B, Csuk R (2015) Chemoenzymatic synthesis and cytotoxicity of oenanthotoxin and analogues. Bioorg Med Chem 23(17):5595–5602
27. Heyns K, Stute R, Paulsen H (1966) Bräunungsreaktionen und fragmentierungen von kohlenhydraten. Carbohydr Res 2(2):132–149
28. Hotchkiss DJ, Jenkinson SF, Storer R, Heinz T, Fleet GWJ (2006) Amadori ketoses with calcium hydroxide and the Kiliani reaction on 1-deoxy ketoses: two approaches to the synthesis of saccharinic acids. Tetrahedron Lett 47(3):315–318
29. Kimura H, Nakahara M, Matubayasi N (2013) Solvent effect on pathways and mechanisms for d-fructose conversion to 5-hydroxymethyl-2-furaldehyde: in situ 13C NMR study. J Phys Chem A 117(10):2102–2113
30. Musau RM, Munavu RM (1987) The preparation of 5-hydroxymethyl-2-furaldehyde (HMF) from d-fructose in the presence of DMSO. Biomass 13(1):67–74
31. Hricovíniová Z (2014) Transition-metal-catalyzed transformation of monosaccharides and polysaccharides. In: Ramawat KG, Mérillon J-M (eds) Polysaccharides: bioactivity and biotechnology. Springer, Cham, pp 1–45. https://doi.org/10.1007/978-3-319-03751-6_76-1
32. Tolborg S, Meier S, Sádaba I, Elliot SG, Kristensen SK, Saravanamurugan S, Riisager A, Fristrup P, Skrydstrup T, Taarning E (2016) Tin-containing silicates: identification of a glycolytic pathway via 3-deoxyglucosone. Green Chem 18(11):3360–3369
33. Elliot SG, Tolborg S, Sádaba I, Taarning E, Meier S (2017) Quantitative NMR approach to optimize the formation of chemical building blocks from abundant carbohydrates. ChemSusChem 10(14):2990–2996
34. Hricovíniová-Bíliková Z, Hricovíni M, Petrušová M, Serianni AS, Petruš L (1999) Stereospecific molybdic acid-catalyzed isomerization of 2-hexuloses to branched-chain aldoses. Carbohydr Res 319(1):38–46